Twist-3 Distribution Functions in Single Transverse Spin Asymmetries

Dissertation

der Mathematisch-Naturwissenschaftlichen Fakultät

der Eberhard Karls Universität Tübingen

zur Erlangung des Grades eines

Doktors der Naturwissenschaften

(Dr. rer. nat.)

vorgelegt von

Daniel Marvin Rein

aus Tübingen

Tübingen

2025

Gedruckt mit Genehmigung der Mathematisch-Naturwissenschaftlichen Fakultät der Eberhard Karls Universität Tübingen.

Tag der mündlichen Qualifikation:	16.03.2026
Dekan:	Prof. Dr. Thilo Stehle
1. Berichterstatter:	apl. Prof. Dr. Marc Schlegel
2. Berichterstatter:	Prof. Dr. Werner Vogelsang
3. Berichterstatter:	Prof. Dr. Alessandro Bacchetta

Abstract

Single-spin asymmetries (SSAs) in the scattering of leptons off transversely polarized nucleons are studied across several final states, with a particular focus on single-inclusive processes. Fully analytic expressions for the spin-dependent cross sections are derived within collinear twist-3 factorization. The calculations are performed at next-to-leading order (NLO) accuracy in perturbative Quantum Chromodynamics (pQCD) for single-inclusive hadron production ($\ell N^\uparrow \to hX$), jet production ($\ell N^\uparrow \to \text{jet}X$) and photon production ($\ell N^\uparrow \to \gamma X$). Moreover, the γSIDIS process $\ell N^\uparrow \to \ell'\gamma X$ is also considered, i.e. photon production in semi-inclusive deep inelastic scattering.

Within the employed collinear twist-3 factorization approach, results are expressed in terms of twist-3 multiparton correlation functions, which describe either parton distributions inside a transversely polarized nucleon or fragmentation into an observed hadron. The present analysis focuses exclusively on the former, as only these distribution-type twist-3 functions contribute to the transverse SSA in jet and photon production. For hadron production, twist-3 fragmentation effects would also enter, but are not included here.

For the single-inclusive processes, the results derived in this work establish the validity of collinear twist-3 factorization at one loop. The calculation reflects the typical complexity associated with higher-twist observables, including the appearance of derivative terms of the twist-3 functions. Each process exhibits unique features that render it particularly informative for probing twist-3 multiparton distribution functions. For hadron and jet production, the analytic results confirm that the entire support in the longitudinal momentum fractions x, x' of the qgq distribution functions F^q and G^q is accessed. This is also true for single-inclusive photon production, which introduces additional, less-studied twist-3 distribution functions. The distinctive aspect of the γSIDIS process is its ability to scan the x, x' support of F^q and G^q point-by-point.

To enable numerical predictions, a realistic model for these functions is constructed building on the Sivers transverse-momentum–dependent parton distribution function (TMD) $f_{1T}^{\perp,q}$. Based on this model, an exploratory phenomenological analysis of the transverse SSA is conducted for the kinematics of a future Electron-Ion Collider (EIC), and a comparison is made to HERMES data for single-inclusive pion production ($ep^\uparrow \to \pi^\pm X$). The NLO corrections are found to be significant for both hadron and jet production, and all four processes are shown to be highly sensitive to the functional form of the twist-3 distribution functions F^q and G^q. Furthermore, regions in EIC phase space where the γSIDIS asymmetry $A_{UT}^{\gamma\text{SIDIS}}$ becomes particularly sizeable are identified.

Kurzfassung

Die vorliegende Arbeit untersucht Einfach-Spin-Asymmetrien bei der Streuung von Leptonen an transversal polarisierten Nukleonen für verschiedene Endzustände. Dabei liegt der Fokus insbesondere auf einfach-inklusiven Prozessen. Vollständig analytische Ausdrücke für die spinabhängigen Wirkungsquerschnitte werden innerhalb der kollinearen Twist-3-Faktorisierung hergeleitet. Die Berechnungen erfolgen zur Genauigkeit der nächstführenden Ordnung in der perturbativen Quantenchromodynamik für einfach-inklusive Hadron-Produktion ($\ell N^\uparrow \to hX$), Jet-Produktion ($\ell N^\uparrow \to \text{jet}X$) und Photon-Produktion ($\ell N^\uparrow \to \gamma X$). Darüber hinaus wird auch der γSIDIS-Prozess betrachtet, die Photon-Produktion in semi-inklusiver tief-inelastischer Streuung.

Innerhalb der kollinearen Twist-3-Faktorisierung werden Ergebnisse durch multipartonische Twist-3-Korrelationsfunktionen ausgedrückt. Diese beschreiben entweder die Verteilung von Partonen im transversal polarisierten Nukleon oder die Fragmentation in ein beobachtetes Hadron. Die vorliegende Arbeit behandelt dabei ausschließlich Ersteres, da nur die Verteilungsfunktionen in Twist-3 zu den Spin-Asymmetrien bei der Jet- und Photon-Produktion beitragen. Bei der Produktion von Hadronen würden auch Twist-3-Fragmentationseffekte eine Rolle spielen; diese werden hier jedoch nicht berücksichtigt.

Für die betrachteten einfach-inklusiven Prozesse zeigen die Ergebnisse dieser Arbeit, dass die kollineare Twist-3-Faktorisierung auf Ein-Schleifen-Niveau gültig ist. Dabei zeigt sich auch die typische Komplexität von Rechnungen in höherem Twist, insbesondere durch das Auftreten von Ableitungstermen der Twist-3-Funktionen. Jeder Prozess hat gewisse Eigenheiten, die ihn besonders geeignet machen für die Untersuchung von Verteilungsfunktionen in Twist-3. Die Ergebnisse für Hadron- und Jet-Produktion zeigen, dass der gesamte Träger der qgq-Funktionen F^q, G^q bezüglich der longitudinalen Impulsanteile x, x' abgerufen wird und in die Asymmetrie eingeht. Dies gilt auch für die Photon-Produktion, welche zusätzlich noch weitere, bisher kaum erforschte Twist-3-Verteilungsfunktionen einführt. Ein charakteristischer Aspekt des γSIDIS-Prozesses ist, dass er die Möglichkeit bietet, den x, x'-Träger von F^q und G^q Punkt für Punkt zu untersuchen.

Um numerische Vorhersagen zu ermöglichen, wird ein realistisches Modell dieser Funktionen konstruiert. Es greift zurück auf erste Extraktionen der transversalimpulsabhängigen Partonverteilungsfunktion $f_{1T}^{\perp,q}$ (Sivers-Funktion). Basierend auf diesem Modell wird eine phänomenologische Analyse der Einfach-Spin-Asymmetrie durchgeführt – sowohl für die Kinematik eines zukünftigen Electron-Ion Collider (EIC) als auch zum Vergleich mit HERMES-Daten zur einfach-inklusiven Pion-Produktion ($ep^\uparrow \to \pi^\pm X$). Es zeigt sich, dass die nächstführenden Korrekturen einen signifikanten Einfluss auf die numerischen Ergebnisse für Hadron- und Jet-Produktion haben und dass die Vorhersagen für alle vier Prozesse in hohem Maße von der genauen Form von F^q und G^q abhängen. Des Weiteren werden die Bereiche des EIC-Phasenraums identifiziert, in denen die γSIDIS-Asymmetrie $A_{UT}^{\gamma\text{SIDIS}}$ besonders groß wird.

List of Publications

This work is based on the following list of publications that the author took part in as a collaborator during the time of his Ph.D.

1. **D. Rein**, M. Schlegel, and W. Vogelsang, **Probing the Polarized Photon Content of the Proton in *ep* Collisions at the EIC**, *Phys. Rev. D*, vol. 110, p. 014041, 2024.

   Included in / Relevant to: Chapters 5, 7

2. **D. Rein**, M. Schlegel, P. Tollkühn, and W. Vogelsang, **Transverse Nucleon Single-Spin Asymmetry for Single-Inclusive Hadron and Jet Production at NLO Accuracy**, arXiv: 2503.16119, 2025.

   Included in / Relevant to: Chapters 2 (including figures), 3 (including figures), 4, 6, 7 (including figures), Appendix G(including figures)

3. **D. Rein**, M. Schlegel, P. Tollkühn, and W. Vogelsang, **NLO Corrections and Factorization for Transverse Single-Spin Asymmetries**, arXiv: 2503.16097, 2025.

   Included in / Relevant to: Chapters 3 (including figures), 4, 7 (including figures)

4. M. Harris, J. Marsh, D. Pitonyak, A. Prokudin, J. Putnam, **D. Rein**, and M. Schlegel, **Transverse Single-Spin Asymmetries in γSIDIS as a Direct Probe of Quark-Gluon-Quark Longitudinal Momentum Structure**, *Physics Letters B*, vol. 869, p. 139793, 2025.

   Included in / Relevant to: Chapters 5, 6, 7 (including figures), Appendix G (including figures)

The author carried out, cross-checked and/or verified all analytical results given in each of the publications listed above. The author was actively involved in writing the drafts and corresponding discussions with the collaborators. For the publications 1,2 and 3 the author also independently obtained all of the numerical plots to check and verify the results of other collaborators, or created the plots by himself from scratch. Thus, the author contributed substantially to all of the above publications.

Contents

Chapter 1

Introduction

The concept of spin is omnipresent across modern physics and has been a central topic of research throughout the development of contemporary science. One of the earliest breakthroughs was the Stern–Gerlach experiment in 1922, which provided definitive evidence for angular momentum quantization and the existence of intrinsic spin in quantum mechanics (see Ref.[1] for a recent review). Later, the Dirac equation[2] gave a relativistic formulation of one-particle quantum mechanics and revealed that spin is inherently a relativistic phenomenon and essential for constructing a conserved total angular momentum.

Further theoretical advances led to the development of quantum field theory (QFT), which replaces the one-particle view of the Schrödinger and Dirac equations with a framework based on dynamical quantum fields. QFT is the foundational theory of particle physics and finds applications in many other fields, including statistical physics, solid-state physics, and condensed matter. Among its many successes are first rigorous proofs of the spin-statistics theorem (see, for example, Refs.[3, 4]) and the prediction of the anomalous magnetic moment of the electron (commonly referred to as electron $g-2$, see Ref. [5] for a modern review and Sec. 2.1.3 for further discussion).

Spin also plays a crucial role in high-energy physics and scattering experiments [6]. Although early experiments employed unpolarized beams and targets, it has long been possible to polarize both. The spin of particles in a beam or target can be aligned either parallel (longitudinal polarization) or perpendicular (transverse polarization) to the direction of motion.

Measurements in longitudinally polarized processes, such as those by the European Muon Collaboration (EMC) on the helicity structure function of the proton [7], triggered extensive theoretical and experimental efforts to improve understanding of the proton spin structure [8, 9, 10]. The EMC revealed that only a moderate fraction of the proton spin originates from quarks, in complete contrast to the naive quark model, which attributes the spin entirely to the three valence quarks. This discrepancy led to what became known as the "proton spin crisis"[11]. A review of the current status of this issue can be found in Ref.[12].

The other form of spin alignment is transverse polarization and it has also been accessible in high-energy collision experiments since the 1970s; it is the central focus of this study. A key observable in this context is the single-spin asymmetry (SSA), where exactly one of the involved particles (either in the initial or final state) is transversely polarized, while all others are unpolarized. The SSA is defined as:

$$A_{UT} \;=\; \frac{\sigma^{\uparrow} - \sigma^{\downarrow}}{\sigma^{\uparrow} + \sigma^{\downarrow}}\,, \tag{1.1}$$

where $\sigma^{\uparrow}(\sigma^{\downarrow})$ denotes the cross section for the configuration of spin up (down) of the polarized particle.

SSAs have been measured across a wide variety of processes and experimental facilities, including:

- Pion production at FermiLab [13, 14]
- Pion production at the Brookhaven Alternating Gradient Synchrotron [15]
- Pion, charged hadron, kaon, (anti-)proton and η-meson production at the Relativistic Heavy Ion Collider(RHIC) [16, 17, 18, 19, 20, 21, 22, 23, 24]
- Pion and kaon production at HERMES [25]
- Jet production at RHIC [26, 24]

- Photon production at RHIC [27]
- J/ψ production at RHIC [28]

In practice, experiments often report the analyzing power A_N which accounts for incomplete polarization and potential luminosity imbalances between opposite spin orientations (cf. Ref. [16]):

$$P_{\text{beam}} A_N \;=\; \frac{N^{\uparrow} - R N^{\downarrow}}{N^{\uparrow} + R N^{\downarrow}}\,, \tag{1.2}$$

where $N^{\uparrow}(N^{\downarrow})$ are the event counts for spin-up (down) configurations, P_{beam} gives the beam polarization, and $R = \mathcal{L}^{\uparrow}/\mathcal{L}^{\downarrow}$ is the spin-dependent ratio of luminosities (relevant for polarized beams but not for polarized final states). Although definitions vary slightly across facilities, these quantities can be consistently related to each other to enable comparison between theory and experiment. In this way, one gains insight into the non-perturbative quantities that describe the structure of (or hadronization to) the involved particles.

Theoretically, SSAs are expected to be suppressed in perturbative QCD (pQCD) [29, 30], as the numerator in Eq. (1.1) is power-suppressed compared to the unpolarized cross section in the denominator by the hard scale Q, typically the transverse momentum of the final state particle. This suppression arises because leading-power contributions to the SSA cancel out. The only relevant twist-2 parton distribution function (PDF) for a transversely polarized nucleon is the transversity PDF, which requires a helicity flip for non-zero amplitudes. However, helicity flips are forbidden in massless QCD, as the perturbative quark–gluon–quark vertex conserves helicity. Thus, one expects a power suppression by a factor m_q/Q with small quark masses m_q [29].

Contrary to these expectations, experiments showed an entirely different picture, finding analyzing powers of up to 20% or more for certain $pp^{\uparrow}$ collisions. This sparked tremendous efforts to develop a theory framework that can explain these large asymmetries. One such approach is the collinear twist-3 factorization formalism, which systematically incorporates power-suppressed contributions beyond leading twist.

In this framework, the (operational) *twist* t corresponds to a suppression factor $(\Lambda/Q)^{t-2}$ where Λ is a non-perturbative hadronic scale and Q is a large momentum scale. The leading-power distributions like the aforementioned transversity PDF are of twist-2 ($t = 2$), i.e. they have no suppression factor, while the collinear twist-3 formalism is specifically formulated in terms of power-suppressed quantities of $t = 3$. These quantities can originate from small transverse parton momenta, quark mass effects, or multiparton correlations. They may appear as distribution functions as well as fragmentation functions. In practice, calculations at the twist-3 level are highly involved, requiring the evaluation of many distinct contributions. This is true in particular for the $pp^{\uparrow}$ collisions that were studied in the experiments listed above. Consequently, results are currently limited to leading order (LO) accuracy [31, 32, 33, 34, 35].

To simplify the theoretical setup, lepton–nucleon scattering offers a cleaner alternative: replacing one hadronic participant with a point-like lepton. This motivates the study of the following processes in this work[1]:

- $\ell(l)N^{\uparrow}(P) \to h(P_h)X$, single-inclusive hadron production in the collision of leptons off transversely polarized nucleons [36, 37]
- $\ell(l)N^{\uparrow}(P) \to \text{jet}(P_j)X$, single-inclusive jet production [36, 37]
- $\ell(l)N^{\uparrow}(P) \to \gamma(P_\gamma)X$, single-inclusive photon production (a future publication is planned, the unpolarized case was calculated in Ref. [38])
- $\ell(l)N^{\uparrow}(P) \to \ell'(l')\gamma(P_\gamma)X$, the production of photons in semi-inclusive deep inelastic scattering, called γSIDIS [39]

In the three single-inclusive cases, the final-state lepton is unobserved, and the hard scale is set by the transverse momentum of the observed final-state particle, while for γSIDIS several constraints related to the momentum transfer Q have to be satisfied for a factorized description.

The single-inclusive processes differ fundamentally from typical deep-inelastic scattering (DIS) and its semi-inclusive variant (SIDIS), including γSIDIS. The reason is that the virtuality q^2 of the photon mediating the interaction between lepton and nucleon is not determined by the external momenta. This complicates the kinematics, the momentum flow and consequently the

[1] This thesis is based to a large extent on publications for which the author made a substantial contribution, and the corresponding references are indicated for each of the processes.

entire calculation. This study presents the first next-to-leading order (NLO) results for these single-inclusive processes within the collinear twist-3 formalism. The higher complexity compared to processes with reconstructed q^2 becomes apparent due to the explicit appearance of derivative terms of the involved twist-3 functions. Because of this, the calculations presented in the following chapters are conceptually new. They include novel features that are absent in existing NLO results obtained in the collinear twist-3 formalism, e.g. for DIS ($\ell N^\uparrow \to \ell' X$) [40, 41], SIDIS ($\ell N^\uparrow \to \ell' h X$) [42, 43], Drell-Yan ($pp^\uparrow \to \ell^+\ell^- X$) [44, 45] and hyperon production ($e^+e^- \to \Lambda^\uparrow X$) [46].

The present study explicitly shows the correctness of collinear twist-3 factorization for the selected single-inclusive processes at NLO, with all divergences canceling as expected. For hadron production, existing HERMES data [25] for pions ($ep^\uparrow \to \pi^\pm X$) allows for numerical comparison with the obtained results. Previous studies [47, 48] reveal discrepancies that necessitate full NLO analyses. While the results of this thesis can be seen as the first step in this direction, the twist-3 fragmentation effects would also have to be included, which are not addressed here because they require a different calculational procedure.

Instead, this work focuses exclusively on twist-3 distribution functions. A model is built for the twist-3 qgq functions F^q and G^q in terms of the first transverse moment of the Sivers function $f_{1T}^{\perp,q}$. This enables a first numerical exploration of pion production in both HERMES and projected EIC kinematics, as well as for jet, photon, and γSIDIS processes. The sensitivity of the numerical results to the precise selection of model parameters is generally high, making it a promising opportunity to constrain the model with experimental data.

Importantly, there are no twist-3 fragmentation effects for the latter three processes, so the results presented here constitute the full NLO prediction. Although no experimental data yet exist for these reactions, the phenomenological study presented in this work offers strong motivation for future measurements at the EIC. The processes provide clean access to the twist-3 distribution functions F^q and G^q and probe their full support in longitudinal momentum fractions x, x'. In addition to that, the γSIDIS process even allows a point-by-point scan of these functions in x and x', which is an unprecedented feature.

Ultimately, the goal is to achieve global fits of twist-3 functions at NLO accuracy, incorporating a diverse range of processes and kinematics. While extensive data exist for $pp^\uparrow$ and heavy-ion collisions [13]-[28], corresponding NLO calculations in the collinear twist-3 formalism are still lacking. For the processes covered here, the presented results lay the groundwork for such global analyses when complimented with future experimental data. Overall, the study of transverse spin observables remains a fascinating research area in the coming years from both the theoretical and experimental point of view.

The structure of this thesis is as follows:

- Chapter 2 outlines the theoretical framework and calculational methods.
- Chapters 3–5 present detailed analyses of each single-inclusive process.
- Chapter 6 summarizes all analytical results.
- Chapter 7 provides a comprehensive phenomenological study.
- Chapter 8 concludes with a summary and outlook.

Chapter 2

Formalism

This chapter establishes the general formalism and theory background relevant to this work. It begins with a brief summary of selected theory concepts that provide the foundation of factorization. Next, a precise definition of the single-spin asymmetries (SSAs) considered in the main part of this work is given. Building on this, the extension of factorization to twist-3 and its application to SSAs is discussed in detail, and the calculational procedure is presented using explicit examples.

2.1 Theory Background

Before diving into the actual twist-3 formalism, a summary is provided, highlighting some of the most important theoretical concepts that build its foundation. The section begins with the parton model established in the seventies by Feynman, Bjorken and Paschos, and then gives a brief recap on Quantum Chromodynamics (QCD), with a focus on the Lagrangian of the theory. This is followed by an in-depth discussion of the well-known feature of emerging divergences in next-to-leading order (NLO) perturbative calculations. Different types of divergences as well as the regularization method adopted in this work are reviewed. The section is concluded by a more rigorous refinement of the parton model picture: the so-called factorization theorems. Moreover, a formal definition is given for the parton distribution functions (PDFs) introduced in the parton model. These definitions can then be extended to the twist-3 case.

2.1.1 Parton Model

The description of particle collisions including bound states posed a conceptual challenge in the development of the theoretical tools and methods to compute cross sections for such processes. The issue is that the underlying theory can typically not be solved exactly to find the explicit form of the bound states. This is famously the case for Quantum Chromodynamics (QCD)[1], the theory of quarks carrying a color charge and the corresponding gauge bosons mediating their interactions, the gluons. Quarks and gluons are the building blocks of nucleons and hence of matter in general. The parton model, pioneered by Feynman, Bjorken and Paschos [53, 54, 55], is the first successful approach to this challenge. Although the model is not restricted to this case, the following will focus specifically on nucleons and QCD. The key assumption is that for a high-energy scattering experiment, the nucleon can be thought of as a collection of quasi-free particles – the *partons*. Then, the exchanged gauge boson mediating the interaction would only scatter off a single parton and all other details of the nucleon can be neglected.

To illustrate this idea, consider a generic particle reaction characterized by a hard momentum scale Q. This scale might, for example, represent the momentum transfer in the collision, and "hard" means that it is much larger than a characteristic energy scale Λ of the nucleon, i.e., $Q \gg \Lambda$. The typical length and time scales of such a process are $\sim 1/Q \ll 1$ and hence very small. For example, values above $Q = 100\,\mathrm{GeV}$ are typical for modern accelerator facilities, which translate to a length scale smaller than 0.01 fm, i.e. only a percent of the proton size [56]. Under such conditions, the nucleon appears *flat*, *frozen*, and *unexpected*:

- Flat: Due to relativistic length contraction, the nucleon is compressed strongly in the direction of flight. As the virtual gauge boson "passes through" it, it effectively "sees" only one parton.

[1] In case of QCD certain properties of the bound states can still be predicted by means of so-called lattice methods, see Refs. [49, 50, 51, 52]

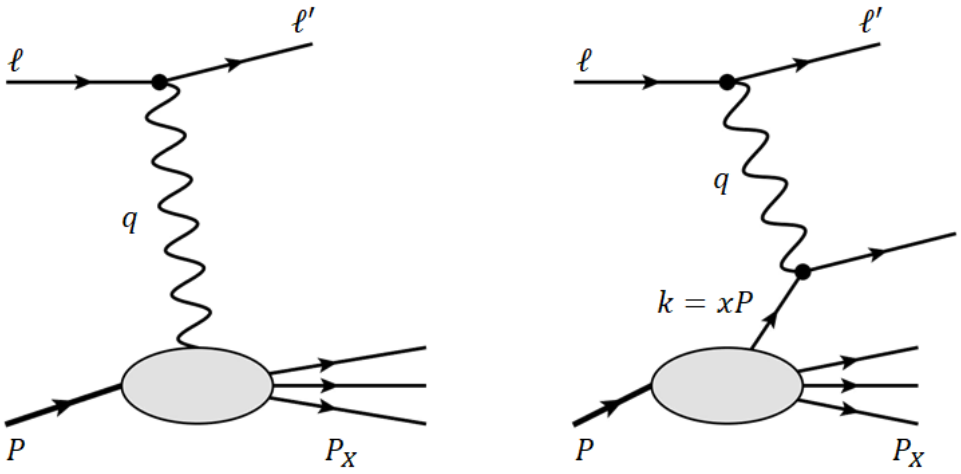

Figure 2.1: Illustration of factorization in the parton model. The scattering off a bound state like the nucleon **(left)** is approximated by the scattering off a single parton from that nucleon **(right)**.

- Frozen: Due to time dilation, the interaction among the nucleon's constituents occurs on a much longer timescale than the scattering off the single parton. Thus, internal interactions can be neglected.
- Unexpected: At high energies, the particles move close to the speed of light, and no information can be exchanged between them before the collision. The scattering occurs without any prior interaction.

These arguments justify the approximation of the model, and the partons are assumed to move collinearly with the nucleon, carrying a fraction x of its momentum. In practice, one computes the cross section $\hat{\sigma}$ for the partonic scattering, weights the result with the probability $f^{i/N}(x)\mathrm{d}x$ to find parton i with momentum xP inside the nucleon N and finally integrates over all momentum fractions x and sums over all parton species i. Schematically this translates into the following expression

$$\sigma \sim \sum_i \int \mathrm{d}x f^{i/N}(x)\hat{\sigma}_i(xP)\,, \tag{2.1}$$

where σ is a generic cross section and the probability density $f^{i/N}(x)$ is a so-called parton distribution function (PDF). PDFs cannot be determined from perturbative calculations since they describe the non-perturbative structure of the nucleon[2]. Importantly, the PDFs are *universal* and do not depend on the specific process being studied. This universality enables one to perform global analyses, where theoretical predictions are fitted to experimental data across a variety of processes and kinematic regions. PDF fitting is an active field and several collaborations regularly publish their updated data sets, see e.g. Refs. [59, 60, 61].

To further illustrate the concept of the parton model via Feynman diagrams consider the deep-inelastic scattering (DIS) process, $\ell(l)N(P) \to \ell'(l')X$, where a lepton scatters off a nucleon. The nucleon might break up into a collection of unobserved final state particles which are simply indicated as X with total momentum P_X. The scattering off the nucleon is indicated by the blob in the left panel of Fig. 2.1, while in the parton model one adopts the point of view of the right panel in Fig. 2.1 where the photon couples to a single quark. In contrast to the nucleon-photon interaction, the quark-photon case only includes elementary degrees of freedom. Thus it can be computed perturbatively using the Feynman rules of the theory. A perturbative expansion is always valid in Quantum Electrodynamics (QED) and, more generally, in the electroweak sector of the standard model, because the couplings are small. The more subtle point is that perturbation theory can also be applied to QCD due to *asymptotic freedom*: the strong coupling $\alpha_s(\mu)$ is a running coupling constant, i.e. it is a function of the scale μ. Asymptotic freedom implies that α_s decreases as μ increases. Therefore, at the hard scale Q of the partonic interaction, $\alpha_s(\mu = Q)$ is small and a perturbative expansion becomes valid. This key feature of QCD was discovered by

[2]Nonetheless there are predictions from lattice QCD, see Refs. [51, 57] and for a very recent study making use of machine-learning techniques Ref. [58]

Gross, Wilczek, and Politzer in the early 1970s [62, 63] and earned them the Nobel Prize in 2004. Conversely, α_s strongly increases at small scales leading to the *confinement* of quarks into colorless bound states called hadrons. The onset of confinement is characterized by the QCD scale Λ_{QCD} and it is the reason why individual quarks or gluons, or any colored state, cannot be observed in isolation.

2.1.2 The QCD Lagrangian

Quantum Chromodynamics (QCD) is a centerpiece to this work, and a brief summary of its formulation is given here. Formally, QCD is a Yang-Mills gauge theory of the special unitary group SU(3) with Dirac fields in the fundamental triplet representation (cf. Ref. [56]). From a less formal and instead more physically motivated point of view, QCD is the theory of quarks and gluons and its Lagrangian is constructed in terms of quark fields $q_{i,a}$ and gluon fields G^α_μ. Quarks, being spin-1/2 fermions, are described by Dirac spinor fields and $i \in \{1,2,3,4\}$ denotes the corresponding spinor index, $a \in \{1,2,3\}$ the color index and $q \in \{u,d,c,s,t,b\}$ (*up, down, charm, strange, top, bottom*) the quark flavor. For the gluon field, $\alpha \in \{1,\ldots,8\}$ denotes the color index in the adjoint representation and $\mu \in \{0,1,2,3\}$[3] the Lorentz vector index. The Lagrangian is constructed by requiring invariance under the simultaneous, local gauge transformation of quark and gluon fields

$$\begin{aligned} q_{i,a}(x) &\rightarrow \left[e^{-ig\omega^\alpha(x)t^\alpha}\right]_{ab} q_{i,b}(x) \equiv U_{ab}(x) q_{i,b}(x) \\ \bar{q}_{i,a}(x) &\rightarrow \bar{q}_{i,b}(x)\left[e^{+ig\omega^\alpha(x)t^\alpha}\right]_{ba} \equiv \bar{q}_{i,b}(x) U^\dagger_{ba}(x) \\ G^\alpha_\mu(x) t^\alpha &\rightarrow \frac{-i}{g} e^{-ig\omega^\alpha(x)t^\alpha} D_\mu e^{+ig\omega^\alpha(x)t^\alpha} \equiv \frac{-i}{g} U(x) D_\mu U^\dagger(x)\,, \end{aligned} \tag{2.2}$$

where $\bar{q} \equiv q^\dagger\gamma^0$ is the adjoint quark field, g is the strong coupling constant, and the $\omega^\alpha(x)$ are real functions of space-time, while the SU(3) generators are denoted as t^α. They are related to the Gell-Mann matrices λ^α by $t^\alpha = \frac{1}{2}\lambda^\alpha$ and they obey the commutation relation $\left[t^\alpha, t^\beta\right] = i f^{\alpha\beta\gamma} t^\gamma$ with the totally antisymmetric structure constants $f^{\alpha\beta\gamma}$. Moreover, the unitary transformation matrix U is introduced and the covariant derivative D is defined by its action on the quark field

$$D_\mu q \equiv \left(\partial_\mu + igt^\alpha G^\alpha_\mu\right) q\,. \tag{2.3}$$

The gluon field strength tensor, required for the kinetic term of the gluons, is defined via a commutator of covariant derivatives

$$F_{\mu\nu} \equiv F^\alpha_{\mu\nu} t^\alpha = \frac{-i}{g}\left[D_\mu, D_\nu\right]\,. \tag{2.4}$$

With these ingredients, the QCD Lagrangian can be written as

$$\mathcal{L}_{\mathrm{QCD}} = \sum_{q=u,d,s,\ldots} \bar{q}\left(i\not{D} - m_q\right) q - \frac{1}{4}\left(F^\alpha_{\mu\nu}\right)^2\,. \tag{2.5}$$

To conclude, a few important remarks on some subtle details are in order:

- Bare quantities: The Lagrangian in 2.5 involves bare, unrenormalized fields, couplings, and masses − unphysical quantities that still contain divergences [56]. They are related to their physical counterparts by *renormalization*, and the basic ideas of this procedure will be discussed in Sec. 2.1.3.

- Quark masses: Gauge invariance does not strictly require that each quark flavor q appears with its own mass m_q, as in Eq. (2.5). More generally, one could allow a mass matrix m in flavor space. However, it is always possible to redefine the quark fields such that this mass matrix becomes diagonal [64], which recovers the above form of the Lagrangian.

- Quantization and gauge fixing: To formulate a quantum field theory, the so far classical fields in Eq. (2.5) must be quantized. This is typically done using the path integral formalism. The procedure requires the inclusion of additional, so-called gauge-fixing terms in the Lagrangian. Faddeev and Popov [65] originally developed this method; a detailed treatment is beyond the scope of this discussion.

[3] or $\mu \in \{0,\ldots,d-1\}$ in dimensional regularization, see Sec. 2.1.3

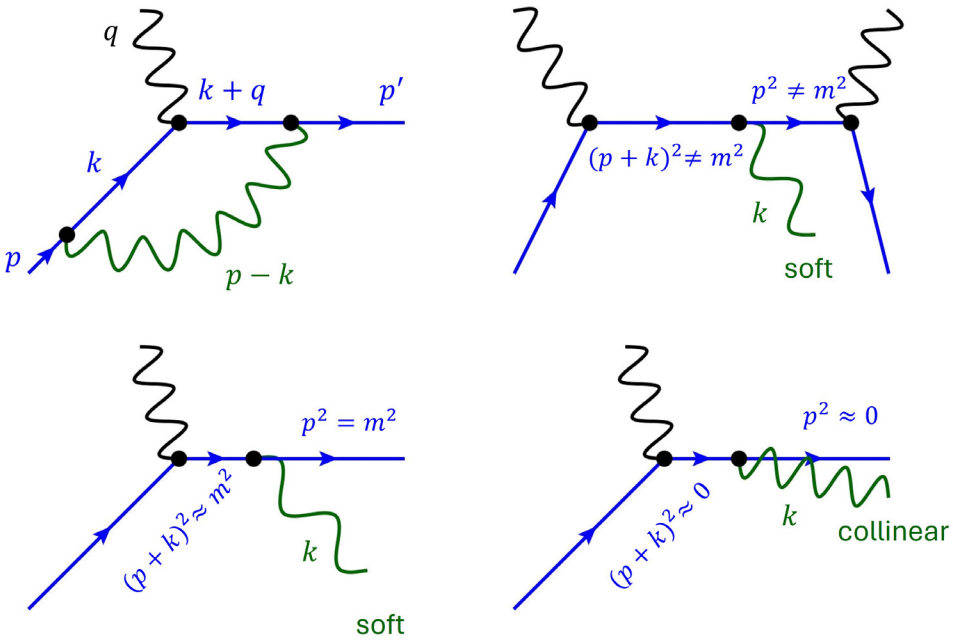

Figure 2.2: Examples of divergent diagrams in a NLO calculation. **(top left):** Virtual UV and IR divergence, **(top right):** Soft emission without a divergence, **(bottom left):** Soft emission divergence, **(bottom right):** Collinear Divergence.

2.1.3 Divergences and Dimensional Regularization

As already elaborated on, the *partonic* scattering cross section can be calculated in a perturbative expansion. It is well-known and discussed in standard texts such as Refs. [56, 66, 67] that, starting at next-to-leading order (NLO), various types of divergent intermediate results arise. The purpose of this subsection is to briefly outline the nature of these divergences and how they can be regularized. The focus will be on the method of dimensional regularization due to 't Hooft and Veltman [68], which is by far the most widely used regularization scheme in practice. Much of the following discussion draws on Ref. [69].

The first question to address is: What new features appear at NLO that lead to divergences? There are two types of NLO contributions: *virtual* loop corrections with unconstrained loop momenta and *real* corrections with an additional real particle in the final state and correspondingly a more involved phase space. Across both types of NLO corrections one distinguishes the following classes of divergences, illustrated by example diagrams in Fig. 2.2

- Ultraviolet (UV) divergences: These arise in loop integrals at infinite loop momentum if the integrand does not fall off sufficiently fast.
- Infrared (IR) divergences: These occur at the opposite end − when the loop momentum goes to zero. This can cause a divergence if the integrand contains a massless propagator.
- Soft divergences: A massless final-state particle, such as a photon or gluon, can lead to a divergence in the phase space integration. This happens in the limit where the particle is emitted with arbitrarily low energy.
- Collinear divergences: In high-energy processes, fermion masses are often neglected. When a massless fermion emits a collinear photon or gluon, its propagator goes on-shell, resulting in a divergence.

Each type of divergence will now be discussed in more detail, starting with the UV divergences encountered in loop diagrams, such as the top-left diagram in Fig. 2.2.

A generic, four-dimensional loop integral at large momentum may take the divergent form

$$I \propto \int \mathrm{d}^4 k \frac{1}{(k^2)^2} \,. \tag{2.6}$$

Here, the integrand falls off too slowly as $k \to \infty$, causing a UV divergence. However, the integral would converge in less than $d = 4$ dimensions. Thus, in dimensional regularization, the integral is

evaluated in a general, continuous number of spacetime dimensions $d < 4$, not restricted to integers. In the end, the limit $d \to 4$ is taken only after divergences have canceled. Crucially, dimensional regularization preserves the symmetries of the theory, such as Lorentz and gauge invariance, which is one of its major strengths. While the concept of non-integer dimensions is not intuitive, it is widely applicable in a straightforward way.

Before examining explicit examples, a few general properties and notational conventions are summarized. An arbitrary d-dimensional integral satisfies the following identities for linearity, scaling and translations ($a, b, c \in \mathbb{C}$)

$$\begin{aligned} \int \mathrm{d}^d k \, (af(k) + bg(k)) &= a \int \mathrm{d}^d k f(k) + b \int \mathrm{d}^d k g(k) \\ \int \mathrm{d}^d k f(ck) &= c^{-d} \int \mathrm{d}^d k f(k) \\ \int \mathrm{d}^d k f(k+q) &= \int \mathrm{d}^d k f(k) \,. \end{aligned} \tag{2.7}$$

In dimensional regularization, momenta become vectors with d components: $k = \left(k^0, k^1, \ldots, k^{d-1}\right)$. The same applies to Lorentz tensors and the metric, which satisfies $g^{\mu\nu} g_{\mu\nu} = d$. It is convenient to write the continuous dimension as $d = 4 - 2\varepsilon$, where $\varepsilon \in \mathbb{R}$ indicates the deviation from the physical limit $d = 4$. To avoid confusion between this ε and the $i\epsilon$ prescription of Feynman propagators, the latter is from now on denoted as $i\delta$.

While vectors and tensors are adapted to d dimensions, the Dirac γ matrices and the identity can be kept 4-dimensional and the standard trace identities remain valid. However, contraction identities change in $4 - 2\varepsilon$ dimensions

$$\begin{aligned} \gamma^\mu \gamma_\mu &= (4 - 2\varepsilon) \mathbb{1} \\ \gamma^\mu \gamma^\nu \gamma_\mu &= -2(1 - \varepsilon) \gamma^\nu \\ \gamma^\mu \gamma^\nu \gamma^\rho \gamma_\mu &= 4 g^{\nu\rho} \mathbb{1} - 2\varepsilon \gamma^\nu \gamma^\rho \\ \gamma^\mu \gamma^\nu \gamma^\rho \gamma^\sigma \gamma_\mu &= -2 \gamma^\sigma \gamma^\rho \gamma^\nu + 2\varepsilon \gamma^\nu \gamma^\rho \gamma^\sigma \,. \end{aligned} \tag{2.8}$$

The fifth gamma matrix γ_5 requires special treatment. The following properties are mutually consistent for $d = 4$, but are not compatible for $d = 4 - 2\varepsilon$ dimensions [70]

$$\begin{aligned} \{\gamma^\mu, \gamma_5\} &= 0 \\ \mathrm{Tr}\left[\gamma_5 \gamma^\mu \gamma^\nu \gamma^\rho \gamma^\sigma\right] &\neq 0 \\ \mathrm{Tr}\left[\gamma_5 \gamma^{\mu_1} \ldots \gamma^{\mu_n}\right] &= \mathrm{Tr}\left[\gamma^{\mu_1} \ldots \gamma^{\mu_n} \gamma_5\right] \,. \end{aligned} \tag{2.9}$$

The original approach of t'Hooft and Veltman, Ref. [68], was to drop the anti-commutation property of γ_5. This aspect of dimensional regularization was later refined by Breitenlohner and Maison, Ref. [71], and received the name *BMHV scheme* (or *HVBM scheme*). Alternative schemes that maintain an anticommuting γ_5 also exist (see Ref. [72]). The BMHV scheme is mathematically consistent to all orders in perturbation theory, though it has its drawbacks for the treatment of chiral gauge theories, such as the electroweak sector of the standard model − this is, however, irrelevant for this work and the BMHV scheme will be used throughout.

The essential idea is that vectors, tensors and also the Dirac matrices γ^μ are split into a 4-dimensional and a $(d-4)$-dimensional part. For example

$$k^\mu = \bar{k}^\mu + \hat{k}^\mu \,, \tag{2.10}$$

where $\bar{k}^\mu$ is the 4-dimensional and $\hat{k}^\mu$ the $(d-4)$-dimensional part of a generic vector k^μ. The two parts life in separate subspaces and thus two arbitrary vectors k^μ, q^μ satisfy

$$\bar{k}^\mu \hat{q}_\mu = 0, \quad k^\mu \bar{q}_\mu = \bar{k}^\mu \bar{q}_\mu, \quad k^\mu \hat{q}_\mu = \hat{k}^\mu \hat{q}_\mu \,. \tag{2.11}$$

The fully antisymmetric levi-civita tensor and γ_5 are defined as purely 4-dimensional objects, i.e. $\gamma_5 = \frac{-i}{4} \epsilon_{\mu\nu\rho\sigma} \bar{\gamma}^\mu \bar{\gamma}^\nu \bar{\gamma}^\rho \bar{\gamma}^\sigma$. The cyclic property of the trace is preserved but γ_5 only anticommutes with the 4-dimensional part of other gamma matrices

$$\{\gamma_5, \bar{\gamma}^\mu\} = 0 \qquad [\gamma_5, \hat{\gamma}^\mu] = 0 \,. \tag{2.12}$$

The calculation of Dirac traces for this work has been performed using the *Tracer* Mathematica package [73], which implements the BMHV scheme.

Finally, dimensional regularization also affects the mass dimensions of fields and couplings. In natural units, the action $S = \int \mathrm{d}^d x \mathcal{L}$ is dimensionless, implying

$$\begin{aligned} \dim(\mathcal{L}) &= d \\ \dim(q) &= \dim(\bar{q}) = \tfrac{d-1}{2} \\ \dim\left(G_\mu^\alpha\right) &= \tfrac{d-2}{2} \\ \dim(g) &= \tfrac{4-d}{2} = \varepsilon \\ \Rightarrow g &\rightarrow \mu^\varepsilon g\,, \end{aligned} \tag{2.13}$$

where the coupling g is redefined to maintain it as dimensionless. Analogously, in QED one redefines $e \rightarrow \mu^\varepsilon e$ for the electric charge.

UV Divergences

The One-Loop Vertex Correction Given the prerequisites outlined above, one can now turn to the explicit calculation of the example shown in the top-left panel of Fig. 2.2, the electron-photon vertex correction in QED. The corresponding Feynman amplitude is given by

$$i\mathcal{M}^\mu \;=\; ie\mu^\varepsilon \bar{u}(p')\Gamma^\mu u(p)\,, \tag{2.14}$$

where u, $\bar{u}$ are (adjoint) spinors and in zeroth order $\Gamma^\mu = \gamma^\mu$. Due to the kinematics, Γ can only depend on q^2. Based on current conservation one can show that it has the following form to all orders in perturbation theory

$$\Gamma^\mu \;=\; F_1(q^2)\gamma^\mu \;+\; F_2(q^2)\frac{i\sigma^{\mu\nu}}{2m}q_\nu\,, \tag{2.15}$$

where F_1, F_2 are so-called form factors, m is the electron mass and one defines $\sigma^{\mu\nu} \equiv \frac{i}{2}[\gamma^\mu, \gamma^\nu]$. In the following, the one-loop correction to Γ^μ will be calculated for the case of an on-shell external photon, i.e. $q^2 = 0$. Applying the familiar Feynman rules one finds

$$\Gamma^\mu \;=\; -ie^2\mu^{2\varepsilon}\int \frac{\mathrm{d}^d k}{(2\pi)^d}\frac{\gamma^\nu\left(\not{k}+\not{q}+m\right)\gamma^\mu\left(\not{k}+m\right)\gamma_\nu}{\left((k+q)^2-m^2\right)\left(k^2-m^2\right)\left((p-k)^2-m_\gamma^2\right)}\,. \tag{2.16}$$

This calculation will contain both UV and IR divergences. To regularize the IR divergence, a fictitious photon mass m_γ is introduced. Note, however, that also the IR divergence can be handled using dimensional regularization, as will be explained below. As a first step to evaluate Eq. (2.16) one can combine the three denominators into just one single denominator by the Feynman parameter method

$$\frac{1}{ABC} \;=\; \int_0^1 \mathrm{d}x\mathrm{d}y\mathrm{d}z\,\delta(x+y+z-1)\frac{2}{\left(Ax+By+Cz\right)^3}\,, \tag{2.17}$$

with A, B, C replaced by the three propagators in Eq. (2.16). Next, one simplifies the resulting expression using the relations $q^2 = p\cdot q = 0$ and $p^2 = m^2$. Subsequently, one introduces $M^2 \equiv (1-z)^2 m^2 + z m_\gamma^2$ and employs a substitution $k \rightarrow k - yq + zp$. This leads to

$$\begin{aligned} \Gamma^\mu \;=\; & -2ie^2\mu^{2\varepsilon}\int_0^1 \mathrm{d}z\int_0^{1-z}\mathrm{d}y\int\frac{\mathrm{d}^d k}{(2\pi)^d}\frac{1}{\left(k^2-M^2\right)^3}\times \\ & \gamma^\nu\left(\not{k}+(1-y)\not{q}+z\not{p}+m\right)\gamma^\mu\left(\not{k}-y\not{q}+z\not{p}+m\right)\gamma_\nu\,. \end{aligned} \tag{2.18}$$

Since the integration over k is symmetric one can discard all linear terms in k in the numerator of Eq. (2.18). One ends up with a quadratic term

$$\Gamma_1^\mu \sim \gamma^\nu \not{k}\gamma^\mu \not{k}\gamma_\nu\,,$$

and a constant term

$$\Gamma_2^\mu \sim \gamma^\nu\left((1-y)\not{q}+z\not{p}+m\right)\gamma^\mu\left(-y\not{q}+z\not{p}+m\right)\gamma_\nu\,.$$

For the quadratic term one can apply an identity from Eq. (2.8) and use the fact that the integrand is independent of y to obtain

$$\Gamma_1^\mu \;=\; 4ie^2\mu^{2\varepsilon}(1-\varepsilon)\gamma_\alpha\gamma^\mu\gamma_\alpha\int_0^1\mathrm{d}z(1-z)\int\frac{\mathrm{d}^d k}{(2\pi)^d}\frac{k^\alpha k^\beta}{(k^2-M^2)^3}\,. \tag{2.19}$$

The tensor integral over k is symmetric under $\alpha \leftrightarrow \beta$ and thus must be proportional to the metric $g^{\alpha\beta}$, hence

$$\int \frac{\mathrm{d}^d k}{(2\pi)^d} \frac{k^\alpha k^\beta}{(k^2 - M^2)^3} = C g^{\alpha\beta} = \frac{g^{\alpha\beta}}{d} \int \frac{\mathrm{d}^d k}{(2\pi)^d} \frac{k^2}{(k^2 - M^2)^3} \,,$$

where the remaining integral can be found in the appendix of Ref. [66]. The resulting parameter integral over z is well-defined for $m_\gamma \to 0$, meaning that there is no IR divergence in this part of the result. Using another identity from Eq. (2.8) one arrives at

$$\Gamma_1^\mu \;=\; \frac{e^2(1-\varepsilon)\Gamma(\varepsilon)}{(4\pi)^2} \left(\frac{m^2}{4\pi\mu^2}\right)^{-\varepsilon} \gamma^\mu \,, \tag{2.20}$$

where $\Gamma(z)$ on the right-hand side of the above result is the Euler Gamma function.

The remaining constant term from the original numerator in Eq. (2.18) has six powers of k in the denominator and only four in the numerator. Thus it is finite and one can already set $\varepsilon = 0$ at this point. Additionally, one can make use of the Dirac equation for the spinors, $\not{p} u(p) = m u(p)$ and $\bar{u}(p')\not{p}' = \bar{u}(p')m$ as well as the fact that the denominator is independent of y. Furthermore, one can also decompose this part into a term $\Gamma_{2a}^\mu \sim \gamma^\mu$ and a term $\Gamma_{2b}^\mu \sim i\sigma^{\mu\nu} q_\nu$. For the former one finds an explicit IR divergence in form of a logarithm of m_γ

$$\Gamma_{2a}^\mu \;=\; \frac{e^2 m^2}{8\pi^2} \gamma^\mu \int_0^1 \mathrm{d}z \frac{(1-z)(1-4z+z^2)}{m^2(1-z)^2 + z m_\gamma^2} \;=\; \frac{e^2}{8\pi^2} \gamma^\mu \left(\log\left(\frac{m_\gamma^2}{m^2}\right) + \frac{5}{2} + \mathcal{O}\left(\frac{m_\gamma}{m}\right)\right) , \tag{2.21}$$

while the latter is free of divergences and has the very compact form

$$\Gamma_{2b}^\mu \;=\; \frac{\alpha}{2\pi} \frac{i\sigma^{\mu\nu} q_\nu}{2m} \,, \tag{2.22}$$

from which one directly concludes that

$$F_2(0) \;=\; \frac{\alpha}{2\pi} \,. \tag{2.23}$$

Anomalous Magnetic Moment This is a famous result with a direct implication for the *anomalous magnetic moment* of the electron. The term "anomalous" is given because it is a deviation from the prediction by the Dirac equation for the *Landé factor* g. The Landé factor describes the relation between the magnetic moment $\boldsymbol{\mu}$ and spin $\boldsymbol{S}$ of a particle of charge q and mass m via

$$\boldsymbol{\mu} \;=\; g \frac{q}{2m} \boldsymbol{S} \,, \tag{2.24}$$

with the Dirac prediction for the electron $g = 2$. One can show that in QED the Landé factor is related to the structure function F_2 by

$$g \;=\; 2(1 + F_2(0)) \;=\; 2\left(1 + \frac{\alpha}{2\pi}\right) \Rightarrow g - 2 \;=\; \frac{\alpha}{\pi} \approx 0.00232 \,. \tag{2.25}$$

This one-loop correction for g was first given by Schwinger, Ref. [74], and constitutes a milestone in the history of QED because it showed for the first time that loop corrections have real physical implications. As indicated in (2.25) it is common to consider just the deviation $g - 2$ from the Dirac prediction, coining the term "electron $g - 2$" for the topic itself. Building on the work of Schwinger, the theoretical predictions for the electron $g - 2$ have reached the order $\mathcal{O}(\alpha^5)$, mainly due to the works of Laporta and Remiddi [75], and later Aoyama, Hayakawa and Kinoshita [76]. For their result, Kinoshita and collaborators computed an astounding 12,672 diagrams. At this level of precision, one also has to include contributions by muons and tauons, by electroweak interactions and also by QCD through the inclusion of quark loops. A modern review of the topic is given in Ref. [5] and the experimental [77, 78, 79] and theoretical [5] values are given in the form $a \equiv (g-2)/2$

$$\begin{aligned} a_e^{\mathrm{EXP}} &= 115\,965\,218\,07.3(2.8) \times 10^{-13} \\ a_e^{\mathrm{SM}} &= 115\,965\,218\,17.8(0.6)(0.4)(0.2)(7.6) \times 10^{-13} \,. \end{aligned} \tag{2.26}$$

The errors given for the standard model prediction a_e^{SM} are the uncertainties of the four- and five-loop QED coefficients, the error on the hadronic contributions and lastly the error on the determination of the electromagnetic fine-structure constant α from measurements of the ^{87}Rb mass [80, 81, 82].

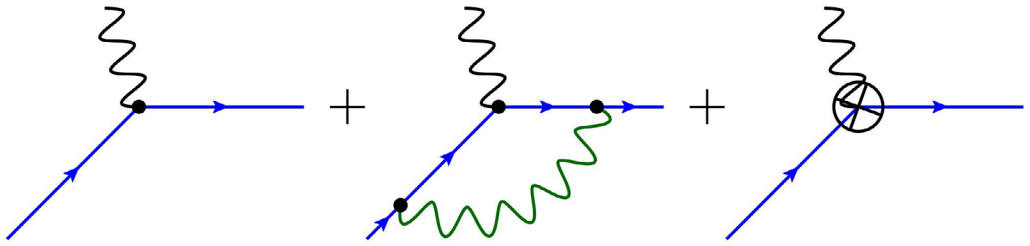

Figure 2.3: Sketch of vertex renormalization at one-loop order. **(left):** zeroth order vertex, **(middle):** NLO virtual correction, **(right):** counter term

Recently, the related muon $g-2$ has attracted a lot of attention because there is an equally precise theoretical prediction up to $\mathcal{O}(\alpha^5)$ in QED, see Ref. [83], which however deviates by 3.7σ from the experimental result obtained at the Brookhaven National Laboratory (BNL) [84]. Such a large deviation could imply physics beyond the standard model, which would undoubtedly be a breakthrough discovery. The largest amount of the theoretical uncertainty originates from QCD effects such as hadronic vacuum polarization (HVP) and hadronic light-by-light (HLbL) diagrams [83]. Due to the low characteristic scale for muon $g-2$, one has to employ non-perturbative methods like dispersion relations or lattice QCD. In the most recent White Paper of the Muon $g-2$ Theory Initiative [85], the collaboration reports on major progress in the determination of the HLbL contribution, including both the data-driven dispersive approach as well as lattice QCD. In particular the inclusion of lattice QCD into the analysis has shifted their recommended theoretical value towards the experimental result, such that the previous tension is no longer present for comparison with the latest experimental average [84, 86, 87, 88, 89, 90]:

$$\begin{aligned} a_\mu^{\text{EXP}} &= 116\,592\,071.5(14.5) \times 10^{-11} \\ a_\mu^{\text{SM}} &= 116\,592\,033(62) \times 10^{-11}\,. \end{aligned} \tag{2.27}$$

Renormalization Back to the calculation of the structure function F_1, one needs to combine all previous results $\propto \gamma^\mu$

$$\gamma^\mu + \Gamma_1^\mu + \Gamma_{2a}^\mu = \left[1 + \frac{\alpha}{4\pi}\left(\frac{1}{\varepsilon} + 4 - \gamma_E - \log\left(\frac{m^2}{4\pi\mu^2}\right) + 2\log\left(\frac{m_\gamma^2}{m^2}\right)\right)\right]\gamma^\mu = F_1(q^2=0)\gamma^\mu\,, \tag{2.28}$$

where the *Euler-Mascheroni constant* γ_E originates from the Taylor expansion of the gamma function $\Gamma(1+\varepsilon) = 1 - \gamma_E\varepsilon + \mathcal{O}(\varepsilon^2)$. For completeness, the general result for $q^2 \neq 0$ reads

$$\begin{aligned} F_1(q^2) &= F_1(0) + \frac{\alpha}{4\pi}\int_0^1 \mathrm{d}x \left[\left(1 - \frac{2m^2 - q^2}{m^2 r(x)}\right)\log\left(r(x)\right)\right. \\ &\qquad \left. + \left(\frac{2m^2 - q^2}{m^2 r(x)} - 2\right)\left(1 + \log\left(\frac{m_\gamma^2}{m^2}\right)\right)\right] \\ F_2(q^2) &= \frac{\alpha}{2\pi}\int_0^1 \mathrm{d}x \frac{1}{r(x)}\,, \end{aligned} \tag{2.29}$$

where $r(x) \equiv 1 - x(1-x)q^2/m^2$. Note that the new term $\propto q^2$ for F_1 only contains an IR divergence but no UV divergence. This is expected due to the very large loop momenta that are considered for the UV divergence: since $k^2 \gg q^2$ it follows that q^2 is negligible and that the divergence is already captured in the simplified case $q^2 = 0$.

Now that the UV divergence has been made explicit, the question is how to interpret it. Clearly, a physical result cannot contain an infinity. In fact, the result in Eq. (2.29) is not yet complete and it misses its corresponding counter term. The reason is that the couplings, masses and fields in the Lagrangian are bare quantities, which themselves contain infinities. Still, one can do calculations using the physical quantities, but then one also needs to consider the corresponding counter terms. As an example, consider the interaction term of the QED Lagrangian

$$\mathcal{L}_{\text{QED}}^{\text{int.}} = e_0 \bar{\psi}_0 \gamma_\mu \psi_0 A_0^\mu\,, \tag{2.30}$$

which is in terms of the bare charge e_0, the bare electron spinors $\bar{\psi}_0, \psi_0$ and the bare photon field A_0^μ. The bare quantities can be related to their physical equivalent by renormalization constants, that are also divergent

$$\begin{aligned} \bar{\psi}, \psi &= Z_2^{-1/2} \bar{\psi}_0, \psi_0 \\ A^\mu &= Z_3^{-1/2} A_0^\mu \\ e &= Z_2 Z_3^{1/2} Z_1^{-1} e_0 \,. \end{aligned} \tag{2.31}$$

This can be plugged into Eq. (2.30); for the procedure of renormalization it is convenient to rewrite it as follows

$$\mathcal{L}_{\text{QED}}^{\text{int.}} \;=\; Z_1 e \bar{\psi} \gamma_\mu \psi A^\mu \;=\; e \bar{\psi} \gamma_\mu \psi A^\mu + (Z_1 - 1) e \bar{\psi} \gamma_\mu \psi A^\mu \,. \tag{2.32}$$

Then, the first term on the rightmost side of the equation can be used to perform perturbation theory, in terms of the physical charge and fields, and the second term generates the counter terms that cancel possible UV divergences. The Lagrangian is still the same as before, nothing has been added or subtracted. It was just reorganized such that all bare quantities are eliminated and calculations can be done entirely in terms of physical quantities. The Feynman rule for the vertex counter term is just the original vertex rule multiplied by the prefactor $Z_1 - 1$. Including all contributions shown in Fig. 2.3, one finds for the renormalized vertex

$$ie\Gamma^\mu_{\text{ren}}(q) \;=\; ie\Gamma^\mu + ie(Z_1 - 1)\gamma^\mu \,. \tag{2.33}$$

To explicitly determine the renormalization constant Z_1, one has to choose a renormalization scheme. As long as the final result is finite, one is free to include an arbitrary constant in Z_1.

A particular choice that is motivated from a physical point of view is the so-called *On-Shell scheme*. One can show that $F_1(0)$ is related to the electric charge e and fixing $F_1^{\text{ren}}(0) = 1$ ensures that the renormalized vertex is described by the physical charge e. This also uniquely fixes Z_1. The On-Shell scheme is well-suited for QED because of its correspondence to the classical theory of electromagnetism: the charges and masses of the theory's elementary degrees of freedom can be measured. Hence, one can always find renormalization conditions that are motivated physically.

This is not the case for QCD where the elementary degrees of freedom cannot be observed individually. Instead one can resort to making the simplest choice possible for the renormalization constants. This is the concept of the *Minimal Subtraction (MS) scheme* where only the ε poles are subtracted and nothing else. In practice, a slight refinement of this idea called the *Modified Minimal Subtraction ($\overline{\text{MS}}$) scheme* is the most commonly used version. In the $\overline{\text{MS}}$ scheme one also subtracts the constants γ_E and $\log 4\pi$, which are universally present in calculations using dimensional regularization. Then, the vertex renormalization constant is given as

$$Z_1^{\overline{\text{MS}}} \;=\; 1 - \frac{\alpha}{4\pi} \frac{S_\varepsilon}{\varepsilon} \;+\; \mathcal{O}(\alpha^2) \,, \tag{2.34}$$

where $S_\varepsilon \equiv (4\pi)^\varepsilon / \Gamma(1-\varepsilon) = 1 - (\gamma_E - \log 4\pi)\varepsilon + \mathcal{O}(\varepsilon^2)$.

The process of eliminating UV divergences by appropriate counterterms is known as *renormalization*. A theory is considered renormalizable if this procedure successfully absorbs all divergences at every order in perturbation theory. There are many more interesting aspects to this topic that would deserve a discussion. This is, however, beyond the scope of this work and the key takeaway here is that both QED and QCD are renormalizable.

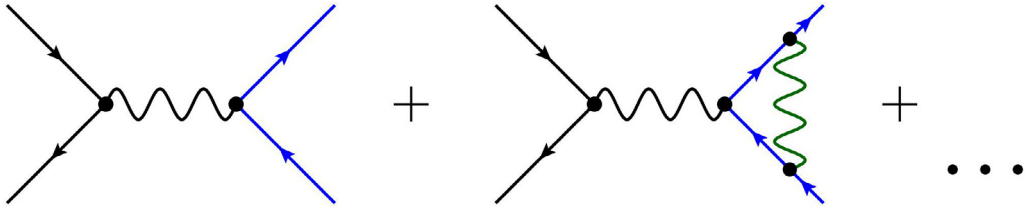

Figure 2.4: Relevant diagrams for the discussion of the IR divergence in the one-loop vertex correction, illustrated for $\mu^-\mu^+ \to e^-e^+$ scattering. **(left):** LO diagram, **(right):** The relevant vertex correction.

IR and Soft Divergences

Even after renormalization, the IR divergence in Eqs. (2.28) and (2.29) remains and must be canceled by some other contribution. It is instructive to isolate the IR divergent part from the renormalized structure function F_1 in the On-Shell scheme as follows

$$\begin{aligned} F_1^{\text{ren}}(q^2) &= f_{\text{IR}}(\beta) \log\left(\frac{m_\gamma^2}{m^2}\right) + \text{IR finite} \\ f_{\text{IR}}(\beta) &= \frac{\alpha}{2\pi}\left[\frac{1+\beta^2}{2\beta}\log\left(\frac{1+\beta}{1-\beta}\right) - 1\right] \\ \beta &= \sqrt{1-\frac{4m^2}{q^2}}; \quad q^2 > 4m^2 \,. \end{aligned} \tag{2.35}$$

Contrary to before, the photon at the vertex is not a real, on-shell particle. Instead, it is virtual and off-shell – its momentum q is fixed by the momenta of the external electrons, implying $q^2 > 4m^2$.

In general, a soft divergence, such as in the bottom-left diagram of Fig. 2.2, cancels such an IR divergence when a physically meaningful, well-defined observable is constructed. Due to subtle details like finite detector resolutions one has to be careful when defining observables to make sure that they are actually measurable. If the observable is indeed well-defined, one can show that IR and soft divergences always cancel. This subsection illustrates this cancellation using the process $\mu^-\mu^+ \to e^-e^+$, based on Ref. [69]. The relevant diagrams up to one-loop order are shown in Fig. 2.4. The order $\mathcal{O}(\alpha)$ correction to the LO cross section is given by the interference of the diagrams in this figure. While additional loop corrections to the LO diagram exist, they are not relevant here because the electron vertex is individually gauge-invariant and physically meaningful. For example, the muon vertex correction must be treated independently: if muons were replaced by quarks, the different charges would prevent combining the two contributions. Since the IR divergent piece of Γ^μ multiplies the basic vertex γ^μ of the LO diagram, one can immediately write down the differential cross section at NLO

$$\frac{\mathrm{d}\sigma}{\mathrm{d}\Omega}\Big|_{\text{LO+virt.}} = \frac{\mathrm{d}\sigma}{\mathrm{d}\Omega}\Big|_{\text{LO}} \times \left(1 + \frac{\alpha}{\pi}\left[\frac{1+\beta^2}{2\beta}\log\left(\frac{1+\beta}{1-\beta}\right) - 1\right]\log\left(\frac{m_\gamma^2}{m^2}\right) + \dots\right), \tag{2.36}$$

where the ellipsis indicates IR finite pieces and other virtual corrections which are immaterial for the present purpose.

The result is manifestly divergent for the limit $m_\gamma \to 0$, which would be problematic for a physical observable. However, the exclusive process $\mu^-\mu^+ \to e^-e^+$ is not measurable in practice: any detector has a finite energy resolution Ξ below which it cannot detect particles. Therefore, if a very soft photon with energy $E_\gamma < \Xi$ is emitted, the final state becomes indistinguishable from the pure e^-e^+ case. Such events are also recorded as $\mu^-\mu^+ \to e^-e^+$, even though the actual process was $\mu^-\mu^+ \to e^-e^+\gamma$.

Hence, this soft photon process must be included to define a physically meaningful observable that will, in the end, be IR finite. To show this explicitly, it suffices to consider photon emission from the electron line as shown in Fig. 2.5 – for the same reason as before one can ignore emissions from the muon line. The fact that the photon is soft ($m_\gamma \approx 0$) will be exploited in several places during the calculation.

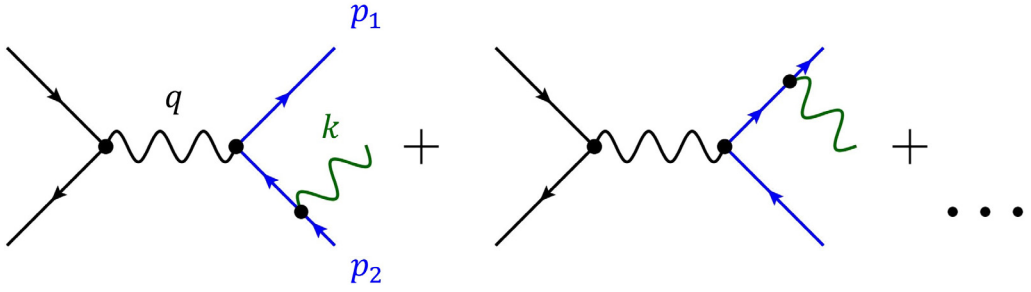

Figure 2.5: Real correction diagrams required for a well-defined observable. The IR divergence in the one-loop electron-photon vertex correction in $\mu^-\mu^+ \to e^-e^+$ scattering is canceled by soft photon emission in $\mu^-\mu^+ \to e^-e^+\gamma$.

An important observation is that the amplitude for each diagram factorizes into a term describing photon emission and the LO amplitude. Intuitively, one can imagine "cutting" the soft photon emission off the diagram, leaving the LO contribution. Because the photon momentum is negligible, the electron (positron) momentum is unchanged by the emission. Making use of the Dirac equation, the total amplitude $i\mathcal{M}_{\text{real}}$ in the soft photon limit is given as

$$i\mathcal{M}_{\text{real}} \;=\; -e\left(\frac{p_1^\mu}{p_1\cdot k}-\frac{p_2^\mu}{p_2\cdot k}\right)\epsilon_\mu^*(k)\times i\mathcal{M}_{\text{LO}}\,, \tag{2.37}$$

where ϵ^* is the polarization vector of the soft final-state photon, and p_1, p_2, k are the momenta of the electron, positron, and photon, respectively (cf. Fig. 2.5). In the e^-e^+ rest frame one has

$$p_1=\begin{pmatrix}E\\ \boldsymbol{p}\end{pmatrix}\,,\quad p_2=\begin{pmatrix}E\\ -\boldsymbol{p}\end{pmatrix}\,,\quad k=\begin{pmatrix}E_\gamma\\ \boldsymbol{k}\end{pmatrix}\,,\quad \cos\theta=\frac{\boldsymbol{p}\cdot\boldsymbol{k}}{|\boldsymbol{p}||\boldsymbol{k}|}\,,\quad \beta=\frac{|\boldsymbol{p}|}{E}=\sqrt{1-\frac{m^2}{E^2}}\,, \tag{2.38}$$

where β is the same as in the last line of Eq. (2.35). Note that for the algebra needed to simplify the squared amplitude, the photon can be considered massless, $m_\gamma = 0$, and thus $E_\gamma = |\boldsymbol{k}|$.

The final step is the integration over the three-particle phase space of electron, positron and photon. One can neglect the photon momentum k compared to the electron and positron momenta p_1, p_2 inside the momentum conserving δ function, i.e. $\delta(p_1+p_2+k-q)\approx\delta(p_1+p_2-q)$. Then the phase space factorizes into the ordinary two-particle phase space and an integral over the photon degrees of freedom

$$\int \mathrm{d}PS_3 \;\approx\; \int \mathrm{d}PS_2 \int \frac{\mathrm{d}^3k}{(2\pi)^3 2E_\gamma} \;=\; \int \mathrm{d}PS_2 \frac{1}{8\pi^2}\int_{-1}^{1}\mathrm{d}\cos\theta\int_{m_\gamma}^{\Xi}\mathrm{d}E_\gamma\, E_\gamma\,. \tag{2.39}$$

Here, the k integral is performed in spherical coordinates and because of the absence of an azimuthal dependence in the squared amplitude, that part of the integral simply yields a factor 2π. The lower bound of the E_γ integral is set to the fictitious photon mass m_γ to regularize the emerging IR divergence and the upper bound reflects that only photons below the resolution Ξ of the detector are considered in the observable. The angular integrals are straightforward to evaluate, leading to the real correction cross section for soft photon emission

$$\frac{\mathrm{d}\sigma}{\mathrm{d}\Omega}\Big|_{E_\gamma<\Xi} \approx \frac{\mathrm{d}\sigma}{\mathrm{d}\Omega}\Big|_{\text{LO}}\times\frac{\alpha}{\pi}\left[\frac{1+\beta^2}{2\beta}\log\left(\frac{1+\beta}{1-\beta}\right)-1\right]\log\left(\frac{\Xi^2}{m_\gamma^2}\right)\,. \tag{2.40}$$

This has the correct form to cancel out m_γ when combined with Eq. (2.36). All in all, the differential cross section for the well-defined observable that has been constructed for muon-muon scattering reads

$$\begin{aligned}\frac{\mathrm{d}\sigma}{\mathrm{d}\Omega}\Big|_{\text{obs}} &= \frac{\mathrm{d}\sigma}{\mathrm{d}\Omega}\Big|_{\text{LO+virt.}} + \frac{\mathrm{d}\sigma}{\mathrm{d}\Omega}\Big|_{E_\gamma<\Xi}\\ &= \frac{\mathrm{d}\sigma}{\mathrm{d}\Omega}\Big|_{\text{LO}}\times\left(1+\frac{\alpha}{\pi}\left[\frac{1+\beta^2}{2\beta}\log\left(\frac{1+\beta}{1-\beta}\right)-1\right]\log\left(\frac{\Xi^2}{m^2}\right)+\dots\right)\,.\end{aligned} \tag{2.41}$$

There is no more dependence on m_γ in the final result, the IR divergence is eliminated! The key is to define a suitable *IR-safe* observable. Note that the same calculations can be repeated for the muon-photon vertex and emission of soft photons from the muon line. In general, defining a suitable observable requires including all final states that are degenerate in energy. The Bloch-Nordsieck Theorem, Ref. [91], then guarantees that virtual and real IR divergences always cancel to yield an IR-safe result.

A crucial point is that this works to all orders in α, and in certain cases only the all-order soft photon result is sensible. To see this, consider the logarithm $\log\left(\Xi^2/m^2\right)$ in the final result Eq. (2.41) of the example calculation above. For a very good detector, the energy resolution is pushed as low as possible and potentially much smaller than the electron mass. This would lead to a large, negative contribution to the cross section which in turn could itself become negative! The fixed-order perturbative expansion fails in such a scenario because $\alpha\log\left(\Xi^2/m^2\right)$ is no longer a small perturbation and one would need to include all orders of this term.

An all-order calculation for the emission of n soft photons is indeed possible and it was first performed by Yennie, Frautschi and Suura [92]. Essential for this calculation is that not all soft photons lead to an IR divergence but only those emitted from a real, on-shell particle. This is sketched in Fig. 2.2. In the top-right diagram, the fermion that emits the photon is off-shell and

thus the propagator with momentum $p+k$ will not hit its pole. In contrast, for the bottom-left diagram one has $p^2 = m^2$ and thus the denominator of the relevant propagator becomes $(p+k)^2 - m^2 = 2p\cdot k \to 0$, i.e. it becomes singular and generates an IR divergence in the limit where all components of the photon momentum k become small. Only diagrams of this type have to be considered when studying the cancellation of IR divergences, which makes the all-order calculation feasible.

Moreover, also the extraction of IR divergences from loop diagrams can be performed to all orders. A further complication for these virtual contributions is that one has to do the renormalization procedure to all orders as well. In the end, one finds that both real and virtual contributions exponentiate and that the same kind of cancellation as in the example calculation for the electron-photon vertex at $\mathcal{O}(\alpha)$ takes place, but now inside the exponent. The generalization of the cross section in Eq. (2.41) with soft photons included to all orders reads

$$\frac{\mathrm{d}\sigma}{\mathrm{d}\Omega}\Big|_{\mathrm{obs}} = \frac{\mathrm{d}\sigma}{\mathrm{d}\Omega}\Big|_{\mathrm{LO}} \times \exp\left(\frac{\alpha}{\pi}\left[\frac{1+\beta^2}{2\beta}\log\left(\frac{1+\beta}{1-\beta}\right) - 1\right]\log\left(\frac{\Xi^2}{m^2}\right) + \dots\right). \tag{2.42}$$

Now, the cross section is always guaranteed to be IR-finite and positive even if the exponent itself might become negative for very small detector resolutions Ξ. In particular, one exactly recovers Eq. (2.41) when expanding the exponential in the above formula to first order in α. While the examples and theorems presented above where all exclusively done in QED, the methods can also be extended to QCD, see Ref. [93]. However, in QCD one also has to consider collinear divergences such as in the bottom-right panel of Fig. 2.2 and then construct IR- and *collinear-safe* observables. This will be discussed below.

First, a brief explanation on how one can handle IR divergences using dimensional regularization is in order. This is the preferred method for higher order calculations as well as QCD because there it quickly becomes cumbersome to keep a non-zero photon (or gluon) mass. To illustrate how dimensional regularization is applied for IR divergences, consider the part Γ^μ_{2a} of the vertex correction from Eq. (2.21), which contains the IR divergence and is given there for $\varepsilon = 0$. For non-zero ε and vanishing photon mass $m_\gamma = 0$ one finds

$$\begin{aligned}\Gamma^\mu_{2a} &= \frac{\alpha}{2\pi}\left(\frac{4\pi\mu^2}{m^2}\right)^\varepsilon \gamma^\mu \int_0^1 \mathrm{d}z (1-4z+z^2)(1-z)^{-1-2\varepsilon} \\ &= \frac{\alpha}{2\pi}\left(\frac{4\pi\mu^2}{m^2}\right)^\varepsilon \gamma^\mu \frac{2-\varepsilon-2\varepsilon^2}{2\varepsilon(1-\varepsilon)(1-2\varepsilon)} = \frac{\alpha}{2\pi}\gamma^\mu\left(\frac{1}{\varepsilon}+\frac{5}{2}+\log\left(\frac{4\pi\mu^2}{m^2}\right)\right) + \mathcal{O}(\varepsilon)\,,\end{aligned} \tag{2.43}$$

which matches Eq. (2.21) up to a logarithm when making the replacement $\frac{1}{\varepsilon} \leftrightarrow \log\left(\frac{m_\gamma^2}{m^2}\right)$. Thus the IR divergence is also regularized in this case, but now in terms of the parameter ε instead of a fictitious mass.

It is noteworthy that unlike UV divergences emerging in the momentum integral and requiring $\varepsilon > 0$, the IR divergence originates from the Feynman parameter integral and requires $\varepsilon < 0$. The different signs for ε in both cases make it necessary to first subtract the UV poles and subsequently employ analytic continuation to $\varepsilon < 0$.

Of course, one also has to work out the phase space integration for the soft photon emission in d dimensions

$$\alpha\int_{m_\gamma}^{\Xi}\frac{dE_\gamma}{E_\gamma} \to \alpha\mu^{2\varepsilon}\int_0^{\Xi}\mathrm{d}E_\gamma\, E_\gamma^{-1-2\varepsilon} = -\frac{\alpha}{2\varepsilon}\left(\frac{\Xi}{\mu}\right)^{-2\varepsilon} = \alpha\left(-\frac{1}{2\varepsilon}+\log\left(\frac{\Xi^2}{\mu^2}\right)\right)+\mathcal{O}(\varepsilon)\,. \tag{2.44}$$

In this way, another $\frac{1}{\varepsilon}$ pole is generated that exactly cancels the pole encountered in (2.43) when combining the virtual and real contributions. Thus, the considered example can be handled also in dimensional regularization and the procedure generalizes to any IR-safe observable.

Collinear Divergences

The last type of divergences is exemplified by the bottom-right diagram in Fig. 2.2. When the center-of-mass energy $\sqrt{s}$ is much larger than the particle masses m_p (i.e. $\sqrt{s} \gg m_p$), one commonly sets $m_p \approx 0$. This is in particular the case in QCD, where computations are typically done with vanishing quark masses. Another reason for this approach is that quark masses are not well defined perturbatively.

In the regime $\sqrt{s} \gg m_p$, also hard emitted photons (or gluons) can cause a divergence. This divergence arises when the photon becomes collinear with the fermion. To get more explicit, one

can go back to the angular integration in the e^-e^+ rest frame, defined by Eq. (2.38), which is part of the phase space in the $\mu^-\mu^+ \to e^-e^+\gamma$ reaction, see Eq. (2.39). One specific integral one would encounter is given by

$$\int_{-1}^{1} \mathrm{d}\cos\theta \frac{1}{(1-\beta\cos\theta)(1+\beta\cos\theta)} \;=\; \frac{1}{\beta}\log\left(\frac{1+\beta}{1-\beta}\right) \;\approx\; \log\left(\frac{s}{m^2}\right)\,, \tag{2.45}$$

where one approximates $\beta = \sqrt{1-4m^2/s} \approx 1 - 2m^2/s$. The explicit logarithm $\log\left(s/m^2\right)$ manifestly shows the mass singularity. It originates from poles inside the integrand. For $m \neq 0$ it is $\beta < 1$ and thus there are no poles inside the integration region for $\cos\theta$. But if $m \to 0$ and consequently $\beta \to 1$, the denominator in the integrand of Eq. (2.45) vanishes for $\theta = 0$, i.e. collinear photon emission from the electron, and for $\theta = \pi$, collinear emission from the positron (see the definition of θ in Eq. (2.38)). So, the collinear limit introduces large logarithms that diverge in the limit $m \to 0$. One can show that they exponentiate, similarly to the logarithms $\log\left(\frac{m_\gamma^2}{m^2}\right)$ in the previous discussion on IR-safety. For the example given there, $\mu^-\mu^+ \to e^-e^+\gamma$, the cross section has the following form in the limit $\sqrt{s} \gg m$

$$\frac{\mathrm{d}\sigma}{\mathrm{d}\Omega}\Big|_{\mathrm{obs}} \;=\; \frac{\mathrm{d}\sigma}{\mathrm{d}\Omega}\Big|_{\mathrm{LO}} \times \exp\left(-\frac{\alpha}{\pi}\left[\log^2\left(\frac{s}{m^2}\right) \;+\; \log\left(\frac{s}{m^2}\right)\log\left(\frac{m^2}{\Xi^2}\right)\right] \;+\; \ldots\right)\,, \tag{2.46}$$

where Ξ again denotes the energy resolution of a given detector and the ellipsis denotes terms unrelated to the collinear divergence. The result contains a so-called *Sudakov Double-Logarithm* $\log^2\left(s/m^2\right)$, a leading-logarithmic enhancement arising from overlapping soft and collinear singularities.

While the expression is IR-safe, it is not yet collinear-safe because the observable only includes soft photons in the final state. This correctly cancels contributions by soft photons in the loop diagrams. However, in a virtual correction, photons with arbitrary energy can become collinear to the electron, i.e. also hard photons which are not accounted for by the allowed soft photon final states. Nevertheless, one can eliminate the mass singularities by summing over all degenerate final states. In general, one has to allow an arbitrary number of massless particles that are moving in the same direction. Kinoshita performed a rigorous treatment of this subject for both QED and QCD, followed by Lee and Nauenberg, cf. Refs [94, 95]. The so-called KLN theorem is named after these three, and it states that it is always possible to define IR- and collinear-safe observables by a suitable combination of final states (and initial states in the case of massive particles in QCD) in a scattering process. The Bloch-Nordsieck theorem is a special case of the KLN theorem for QED.

The simplest example of an IR- and collinear-safe observable would be the total cross section for $\mu^-\mu^+ \to X$ where X is any combination of electrons, positrons and photons, in particular soft and collinear photons. Thus one has the required summation over degenerate final states for the cancellation of divergences. Sterman and Weinberg proposed a more sophisticated observable, see Ref. [96]. They considered the exclusive production of two back-to-back jets of electrons, positrons and photons restricted to cones of a narrow size R (up to a small energy Ξ that is allowed outside the cones to ensure IR-safety). Hard, collinear photons are included for both jets, and thus all mass singularities cancel.

For this work, the most relevant collinear- and IR-safe observables are cross sections with nucleons in the initial state and identified hadrons in the final state. An example is single-inclusive hadron production, $\ell N \to hX$, where X contains an unobserved final-state lepton and any number of hadrons originating either from the nucleon remnants or from the hadronization of particles produced in the hard scattering. Such observables include convolution integrals of the hard partonic scattering cross section with parton distribution functions (PDFs) and fragmentation functions (FFs), schematically

$$\sigma \sim \tilde{f}^q \otimes \tilde{\sigma} \otimes \tilde{D}^q\,. \tag{2.47}$$

Here, the bare PDF $\tilde{f}^q$, the partonic cross section $\tilde{\sigma}$ and the bare FF $\tilde{D}^q$ all contain collinear divergences. However, the divergences are independent of the specific hard scattering process and instead only depend on which nucleons are in the initial state and which hadrons are observed in the final state. Moreover, the $\frac{1}{\varepsilon}$ poles from the partonic cross section exactly match those in the bare PDF and FF. This means that one can define finite, renormalized PDFs f^q and FFs D^q that absorb the divergences of the hard scattering, also yielding a finite partonic cross section $\hat{\sigma}$. As a result, the cross section is given by a convolution of divergence-free quantities,

$$\sigma \sim f^q \otimes \hat{\sigma} \otimes D^q\,, \tag{2.48}$$

and is hence manifestly collinear-safe. This concept is the main idea of so-called factorization theorems and a brief introduction is given in the following Section.

2.1.4 Factorization and Operator Definition for Parton Densities

Factorization The parton model offers a very accessible approach for the description of hadronic observables. However, it is not a derivation but rather an "educated guess" based on strong arguments. Nevertheless, the model can be extended into rigorous factorization theorems, see Ref. [56]. There are several subtle details that would require extensive and lengthy discussion. This is of course beyond the scope of this section and instead only the most important results will be shown. For simplicity, the fragmentation of final state partons into hadrons will not be considered in the following.

In the context of a proper factorization theorem the simple parton model formula in Eq. (2.1) is modified as follows

$$\sigma\left(Q,\dots\right) = \sum_i \left(\hat{\sigma}_i \otimes f^{i/h}\right)\left(Q,\mu,\dots\right) + \mathcal{O}\left(\frac{\Lambda_{\mathrm{QCD}}}{Q}\right) \tag{2.49}$$

where σ denotes a generic observable, $\hat{\sigma}_i$ the partonic scattering cross section including parton species i and $f^{i/N}$ the PDF for parton i inside the nucleon N. As before, Q is the hard momentum scale of the process, which is much larger than the QCD scale, $Q \gg \Lambda_{\mathrm{QCD}}$. The ellipsis indicates the possible dependence on other variables such as possibly a transverse momentum. The symbol $\otimes$ denotes a convolution integral of the partonic cross section with the PDF, typically over the longitudinal momentum fraction x. This is similar to Eq. (2.1), but the convolution could, for example, also include the transverse momentum k_T of the parton in the case of transverse momentum dependent parton distributions (TMDs). A new feature of Eq. (2.49) are the so-called power corrections indicated by $\mathcal{O}\left(\Lambda_{\mathrm{QCD}}/Q\right)$. Although they are power-suppressed they can still be relevant in several kinds of processes.

Evolution Another important difference to the parton model is the explicit dependence of both the partonic scattering and the PDF on a so-called factorization scale μ. This scale sets the boundary between the short-distance and long-distance physics. The former is described by the perturbatively calculable, hard partonic scattering while the latter is described by the non-perturbative PDFs. The generic observable σ, however, does not display μ dependence. Indeed, when including all orders in perturbation theory the factorization scale must cancel out – it is arbitrary and thus cannot be physical. This implies $\frac{\mathrm{d}\sigma}{\mathrm{d}\mu} = 0$ from which one derives so-called evolution equations for the PDFs. One can write them in the schematic form

$$\frac{\mathrm{d}f^{i/N}}{\mathrm{d}\mu} = P \otimes f^{i/N}\,. \tag{2.50}$$

In this equation, P is a perturbatively calculable evolution kernel and $\otimes$ denotes a convolution. In the case of PDFs these evolution equations have been derived by Dokshitzer, Gribov, Lipatov, Altarelli and Parisi, see Refs. [97, 98, 99] for their precise forms. The treatment of evolution is a rich topic on its own but since the focus of this work lies elsewhere the reader is referred to the extensive literature for further details, for example the books [56, 67].

Operator Definition of PDFs From the above discussion it is clear that the parton model constitutes an approximation to a strict field theoretic treatment. Consequently, the picture of parton densities (PDFs) as probability densities does not strictly apply either. The formally correct way to introduce PDFs uses operator matrix elements. These so-called collinear quark-quark correlators, see Refs. [56, 100, 101], are formulated in terms of the dynamical quark fields and the nucleon state. As an example, the unpolarized quark PDF f_1^q of flavor q can be written as

$$f_1^q(x) = \frac{1}{2}\int_{-\infty}^{\infty}\frac{\mathrm{d}\lambda}{2\pi}e^{i\lambda x}\langle P,S|\bar{q}_{i,a}(0)\not{n}_{ij}\mathcal{W}\left[0;\lambda n\right]_{ab}q_{j,b}(\lambda n)|P,S\rangle\,. \tag{2.51}$$

Fig. 2.6 illustrates the momentum flow relevant to this operator definition. Moreover, P is the parent nucleon's momentum and S its spin vector with normalization $S^2 = -1$ and the constraint $P\cdot S = 0$. In this definition, P is approximately light-like, i.e. $P^2 \simeq 0$, and n is another light-like vector satisfying $n^2 = 0$ and $P\cdot n = 1$. Besides these two conditions, n can be chosen arbitrarily and is thus unphysical. Nonetheless, such a vector n is useful to write down the correlator in a Lorentz-invariant way. It turns out that observables can always be written in a form independent of n, and the arbitrariness in the choice of n is thus not a problem.

Between the nucleon states in Eq. (2.51) are the dynamical quark field $q_{j,b}$ and its adjoint $\bar{q}_{i,a}$. Their Spinor indices are denoted $j(i)$ and their color indices $b(a)$. They are linked by a

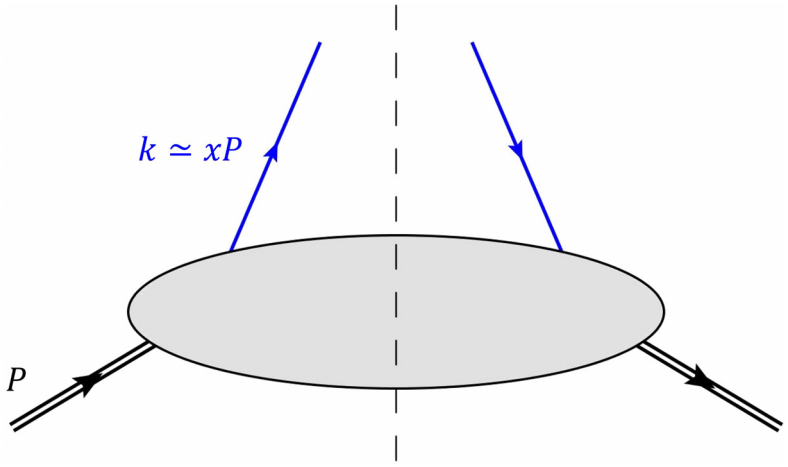

Figure 2.6: Schematic Feynman diagram illustrating the kinematics for the unpolarized quark PDF of flavor q, f_1^q defined in Eq. (2.51), as well as the general quark-quark correlator of flavor q, Φ^q presented in Eq. (2.53).

straight-path Wilson line $\mathcal{W}\left[0;\lambda n\right]_{ab}$ from λn to 0. Note that the two quark fields are evaluated at different space-time coordinates, i.e. at 0 and at λn. Thus they behave differently under a local SU(3) gauge transformation, cf. Eq. (2.2). The transformation law for the Wilson line is derived in App. A, and one finds that it transforms in exactly the right way to render the whole expression gauge invariant[4]

$$\begin{aligned} q_{j,b}(\lambda n) &\rightarrow U_{bd}(\lambda n) q_{j,d}(\lambda n) \\ \bar{q}_{i,a}(0) &\rightarrow \bar{q}_{i,c}(0) U^{\dagger}_{ca}(0) \\ \mathcal{W}\left[0;\lambda n\right]_{ab} &\rightarrow U_{ae}(0) \mathcal{W}\left[0;\lambda n\right]_{ef} U^{\dagger}_{fb}(\lambda n) \end{aligned} \tag{2.52}$$

Furthermore, one recognizes that there is no scale dependence indicated anywhere in Eq. (2.51). This is in contrast to the discussion given at the beginning of this section: proper factorization formulas are formulated in terms of scale-dependent PDFs. The seeming mismatch is explained by the fact that all fields in the definition of Eq. (2.51) are *bare* quantities − they are not the physical ones found in nature. In fact, they contain UV divergences. This applies to Eq. (2.51) for both quark fields q, $\bar{q}$ as well as the gluon fields G^{α}_{μ} and the strong coupling constant g in the definition of the Wilson line. Consequently, the definition of the quark density also contains divergences that must be renormalized. The procedure requires the choice of a specific subtraction scheme, thus introducing the scale dependence, i.e.

$$f_1^q(x) \xrightarrow{ren.} f_1^{q,\overline{\text{MS}}}(x,\mu)\,.$$

So far, the whole discussion is based exclusively on unpolarized processes and the corresponding unpolarized partonic cross sections and PDFs. In the following, it will be shown how one can extend Eq. (2.51) to a more general form also featuring various other types of PDFs. This also includes but is not limited to polarized PDFs. The discussion is mainly based on Refs. [100, 102], while the notation and conventions are following Ref.[101]. The generalization is obtained simply by removing $\not{n}$ from Eq. (2.51), since $\not{n}$ acts like a projector that singles out just the unpolarized PDF. The relevant momentum flow is again shown in Fig. 2.6. This leads to the definition of the quark-quark correlator Φ^q of flavor q

$$\Phi^q_{ij}\left(x;n,P,S\right) = \int_{-\infty}^{\infty} \frac{\mathrm{d}\lambda}{2\pi} e^{i\lambda x} \langle P,S|\bar{q}_j(0)\mathcal{W}\left[0;\lambda n\right] q_i(\lambda n)|P,S\rangle\,, \tag{2.53}$$

where the dependence on the auxiliary light-cone vector n as well as the nucleon momentum P and its spin S has been indicated explicitly. While one cannot exactly calculate the correlator Φ^q, one can parametrize it in terms of suitable structures. To do so, one analyzes its behavior under hermitian conjugation, parity and time-reversal. This gives consistency conditions that constrain which structures could possibly appear in the parametrization. The behavior of matrix elements

[4]for this reason, Wilson lines are also commonly called *gauge links*

and fields under these discrete transformations as well as the consistency conditions for Φ^q are discussed in App. B. One finds

$$\begin{aligned}
\left[(\Phi^q)^\dagger\right]_{ij} &= \left(\gamma^0\right)_{ik} \Phi^q_{kl} \left(\gamma^0\right)_{lj} \\
\Phi^q_{ij}\left(x; n, P, S\right) &= \left(\gamma^0\right)_{ik} \Phi^q_{kl} \left(x; \bar{n}, \bar{P}, -\bar{S}\right) \left(\gamma^0\right)_{lj} \\
\left(\Phi^q_{ij}\right)^*\left(x; n, P, S\right) &= \left(-i\gamma_5 C\right)_{ik} \Phi^q_{kl} \left(x; \bar{n}, \bar{P}, \bar{S}\right) \left(-i\gamma_5 C\right)_{lj} ,
\end{aligned} \tag{2.54}$$

Combining all of these constraints, one can write down the parametrization for the quark-quark correlator Φ^q, following the conventions of Ref. [101]

$$\begin{aligned}
\Phi^q(x) &= \frac{1}{2}\left(\not{P} f_1^q(x) + M e^q(x) - M(S\cdot n)\not{P}\gamma_5 g_1^q(x) + \frac{1}{2}M^2(S\cdot n)\left[\not{P},\not{n}\right]\gamma_5 h_L^q(x) \right. \\
&\quad - \frac{1}{2}\left[\not{P},\not{S}\right]\gamma_5 h_1^q(x) - M\left(\not{S} - (S\cdot n)\not{P}\right)\gamma_5 g_T^q(x) + M^2 \not{n} f_3^q(x) \\
&\quad \left. - M^3 (S\cdot n)\not{n}\gamma_5 g_3^q(x) + \frac{M^2}{2}\left[\not{S} - (S\cdot n)\not{P}, \not{n}\right]\gamma_5 h_3^q(x)\right) ,
\end{aligned} \tag{2.55}$$

where the nucleon mass is denoted by M. The nine distribution functions in Eq. (2.55) are all of order $\mathcal{O}(1)$ such that the relative size of the different structures in the parametrization is entirely given in terms of the factors of M and P. To further illustrate this point, it is convenient to slightly rewrite the above equation. One can introduce the auxiliary vectors $n_+ \equiv \frac{1}{P^+}P$ and $n_- \equiv P^+ n$ as well as the nucleon helicity $\lambda \equiv M(S\cdot n)$ and the transverse component of the spin vector $S_T \equiv S - (S\cdot n)P$. Reordering the terms then yields

$$\begin{aligned}
\frac{\Phi^q(x)}{P^+} &= \frac{1}{2}\left(\not{n}_+ f_1^q(x) - \lambda \not{n}_+ \gamma_5 g_1^q(x) - \frac{1}{2}\left[\not{n}_+, \not{S}_T\right]\gamma_5 h_1^q(x)\right) \\
&\quad + \frac{M}{2P^+}\left(e^q(x) + \frac{\lambda}{2}\left[\not{n}_+, \not{n}_-\right]\gamma_5 h_L^q(x) - \not{S}_T \gamma_5 g_T^q(x)\right) \\
&\quad + \frac{M^2}{2(P^+)^2}\left(\not{n}_- f_3^q(x) - \lambda \not{n}_- \gamma_5 g_3^q(x) + \frac{1}{2}\left[\not{S}_T, \not{n}_-\right]\gamma_5 h_3^q\right) ,
\end{aligned} \tag{2.56}$$

which matches the form given in Ref. [100]. The advantage of Eq. (2.56) is that it makes explicit the suppression of the distribution functions in the second and third lines by powers of M/P^+. One defines the (operational) *twist* t of a suppression factor $\left(\Lambda/P^+\right)^{t-2}$, where Λ is a characteristic hadronic momentum scale. One identifies $\Lambda = M$ and thus counts the first line of Eq. (2.56) as twist-2 ($t = 2$), the second as twist-3 ($t = 3$) and the third as twist-4 ($t = 4$). The twist-2 functions f_1^q, g_1^q h_1^q are the unpolarized, helicity and transversity PDFs. They can be interpreted as probability densities just like in the parton model. The higher-twist distribution functions, however, lack such a probabilistic interpretation (cf. Ref. [101]).

Nonetheless, all distribution functions have the same support property, namely $-1 < x < 1$. Negative arguments correspond to the anti-quark counterparts that can be obtained via charge conjugation of Φ^q. One finds the following relations (including functions up to twist-3) for the C-even functions

$$\begin{aligned}
f_1^{\bar{q}}(x) &= -f_1^q(-x) \\
h_1^{\bar{q}}(x) &= -h_1^q(-x) \\
h_L^{\bar{q}}(x) &= -h_L^q(-x) ,
\end{aligned} \tag{2.57}$$

and the C-odd functions

$$\begin{aligned}
g_1^{\bar{q}}(x) &= g_1^q(-x) \\
g_T^{\bar{q}}(x) &= g_T^q(-x) \\
e^{\bar{q}}(x) &= e^q(-x) .
\end{aligned} \tag{2.58}$$

The quark–quark correlator's role in collinear twist-3 factorization is summarized as follows. Functions from the second line of Eq. (2.56) and their corresponding *intrinsic* contributions to an observable, see Ref. [101], have to be considered in general. They do, however, not enter the observables studied here. Two other twist-3 effects do matter: kinematical contributions from correlators with nonzero quark transverse momentum k_T, and dynamical contributions from correlators containing a third field, such as the gluonic field strength $F^{n\rho} \equiv n_\mu F^{\mu\rho}$. Their definitions

and parametrizations are provided in App. C. Of particular relevance is the *quark-gluon-quark correlator*, which is also given here since it will be referred to regularly throughout this work

$$\begin{aligned}\Phi_F^{q,\rho}(x,x') &= \int_{-\infty}^{\infty}\tfrac{\mathrm{d}\lambda}{2\pi}\int_{-\infty}^{\infty}\tfrac{\mathrm{d}\mu}{2\pi}\,\mathrm{e}^{i\lambda x'}\mathrm{e}^{i\mu(x-x')}\,\langle P,S|\,\bar q(0)\;ig\,F^{n\rho}(\mu n)\;q(\lambda n)\,|P,S\rangle \\ &= \frac{1}{2}M\,i\epsilon^{Pn\rho S}\,\not{P}\,F^q(x,x') - \frac{1}{2}M\,S_T^\rho\,\not{P}\gamma_5\,G^q(x,x') + \dots\,. \end{aligned} \tag{2.59}$$

Along with two quark fields $\bar q$, q familiar from Eq. (2.53), this correlator contains the gluonic field strength tensor $F^{n\rho}\equiv n_\mu F^{\mu\rho}$ and is parametrized in terms of the qgq functions F^q, G^q. These functions depend on two longitudinal momentum fractions x, x' and are accompanied by other twist-3 functions. These other functions, however, are simply indicated by the ellipsis in (2.59), since they do not enter the studied observables. Again, the vector n is light-like, $n^2=0$, and normalized by the condition $P\cdot n=1$ but otherwise arbitrary and thus unphysical. Also in the collinear twist-3 case, all arbitrariness of n will eventually cancel out in an observable. To show this explicitly, however, is more involved than for twist-2, see Ref. [101]. Moreover, the Wilson lines required for gauge invariance of the matrix element are not shown for brevity. One also defines $\epsilon^{Pn\rho S}\equiv P_\mu n_\nu S_\sigma\epsilon^{\mu\nu\rho\sigma}$ where ϵ is the totally anti-symmetric tensor of sign convention $\epsilon^{0123}=+1$. Note that the transverse part a_T^μ of any vector a^μ is defined via a transverse projector:

$$a_T^\mu\equiv g_T^{\mu\nu}a_\nu\,,\quad \text{where}\quad g_T^{\mu\nu}\equiv g^{\mu\nu}-P^\mu n^\nu - P^\nu n^\mu\,. \tag{2.60}$$

Lastly, the letter F in Φ_F^q indicates that the correlator is defined using a field strength tensor F instead of a covariant derivative D, cf. Ref. [102]. Similarly, the functions F^q, G^q are sometimes also given the subscript FT, where the additional T indicates transverse polarization. Nevertheless, throughout this work these extra subscripts will be dropped in favor of an easier notation and better readability.

2.2 Spin Asymmetry

To set the stage for the main part of this work, the key observable is defined: the transverse single-spin asymmetry (SSA). It is commonly studied in the context of spin phenomena in high-energy physics. For a generic particle collision, such as in a collider experiment, the SSA can be defined as

$$A_{UT}\equiv\frac{\sigma\left(\boldsymbol{S_T}\right)-\sigma\left(-\boldsymbol{S_T}\right)}{\sigma\left(\boldsymbol{S_T}\right)+\sigma\left(-\boldsymbol{S_T}\right)}\,. \tag{2.61}$$

Here, $\sigma(\boldsymbol{S}_T)$ is the transverse-spin-dependent cross section and $\boldsymbol{S}_T$ the spin vector of the transversely (T) polarized particle. The subscript UT indicates that the other involved particles are *unpolarized* (U). The transversely polarized cross section in the numerator of (2.61) is given by the difference of the cross sections with flipped spin, while the unpolarized counterpart in the denominator is given as the sum. To be more precise, the generic σ is a short-hand for a differential cross section. For example, in case of single-inclusive hadron production, $\ell(l)N^\uparrow(P)\to h(P_h)X$ (external momenta indicated in brackets), it would stand for $E_h\frac{\mathrm{d}\sigma}{\mathrm{d}^3\boldsymbol{P_h}}(\boldsymbol{S_T})$.

A related observable that is also commonly considered in experiments is the *right-left asymmetry* A_{RL}, which will be studied in the phenomenological analyses of Ch. 7. The beam direction and the transverse spin vector $\boldsymbol{S}_T$ define a plane, and one simply counts the events with particles detected to either the right or left side of this plane to compute the asymmetry. In terms of the azimuthal angle ϕ of the observed final state particle and the azimuthal angle ϕ_S of the spin vector $\boldsymbol{S}_T$, the right-left asymmetry is given as

$$A_{RL}=\frac{\int_{\phi_s+\pi}^{\phi_s+2\pi}\mathrm{d}\phi\,\sigma\left(\phi,\phi_s\right)-\int_{\phi_s}^{\phi_s+\pi}\mathrm{d}\phi\,\sigma\left(\phi,\phi_s\right)}{\int_0^{2\pi}\mathrm{d}\phi\,\sigma\left(\phi,\phi_s\right)}\,. \tag{2.62}$$

This type of asymmetry will be thoroughly analyzed in the numerics Chapter, Ch. 7.

Note that other quantities, such as a $\sin\left(\phi-\phi_s\right)$ weighted cross section, are also used in practice.

2.3 The Transverse SSA at Leading Order (LO)

Now that the foundation is laid out, one can turn to centerpiece of this study: the calculation of SSAs in the collinear twist-3 approach. The formalism is an extension on the collinear factorization

discussed in Sec. 2.1.4 for unpolarized or longitudinally polarized processes and some aspects of the twist-3 case have already been hinted at. Collinear twist-3 factorization is commonly used in the description of transverse-spin observables in single-inclusive hard processes, see Refs. [32, 103, 104]. This section starts the general discussion, with the process of single-inclusive hadron production, $\ell(l)N^\uparrow(P) \to h(P_h)X$, as an illustrative example. By reviewing the known leading order (LO) result, the basic methods and concepts are introduced. The proceeding sections follow up on this by showing the necessary steps to extend the calculation to next-to-leading order (NLO).

The kinematics of the hadron production process are defined as follows. The momenta of the lepton, the nucleon and the produced hadron are labeled as l^μ, P^μ and P_h^μ. Their masses will be denoted as m_ℓ, M and M_h, respectively. The scattering process is assumed to happen on an energy scale much larger than these masses. Hence, one negelcts m_ℓ, M and M_h wherever possible and treats the momenta as light-like vectors $\ell^2 \simeq 0$, $P^2 \simeq 0$, $P_h^2 \simeq 0$. Moreover, one introduces the nucleon spin vector S^μ with the normalization $S^2 = -1$ and the constraint $P \cdot S = 0$. The *hadronic* Mandelstam variables for this process are defined as $s = (l+P)^2 \simeq 2l \cdot P$, $t = (P - P_h)^2 \simeq -2P \cdot P_h$ and $u = (l - P_h)^2 \simeq -2l \cdot P_h$. Note that $s + t + u > 0$ for the single-inclusive reactions considered in this work.

The application of the general formalism to single-inclusive lepton-nucleon scattering has been discussed in a variety of publications, for example in Refs. [40, 41, 47, 105, 106, 107, 108, 109]. The procedure will be presented step by step using schematic expressions, more details are reserved for a separate chapter on $\ell N^\uparrow \to hX$.

The collinear twist-3 approach makes use of multiparton correlators like in Eq. (2.59) to describe the soft physics of the interaction. Such correlators have been discussed exhaustively in the literature, for example in [101, 110, 111], and App. C gives an overview of the most important aspects and definitions. The above references introduce terminology often used in the context of collinear twist-3 factorization:

- Contributions to a SSA generated by an expansion of two-parton correlators in a transverse momentum $k_T \ll 1$, such as (C.1), (C.3), are called *kinematical* twist-3 contributions
- Three-parton correlators like (2.59) generate so-called *dynamical* twist-3 contributions. The label "dynamical" is given because of the third dynamical field in the matrix elements
- *intrinsic* contributions are generated by the twist-3 functions in the parametrization of the ordinary quark-quark correlator, Eq. (2.53). But, they do not enter any observable in this work

Refs. [47, 101] already calculated the SSA (2.61) in the collinear twist-3 formalism to LO accuracy. Particularly important is the discussion in Ref. [101] on the role of the light-cone vector n^μ, which is unphysical and enters the calculations via the soft matrix elements in (2.59) and App.C. Since n^μ is not unambiguously defined, physical observables such as cross sections or SSAs must not depend on a particular choice. For the leading-twist fragmentation functions in Eqs. (C.14), (C.15), or the photon-in-lepton distribution (C.20) this usually is not an issue. The arbitrary light-cone vectors featured in their respective definitions are actually not present in the relevant terms of their parametrizations. Hence, they do not even enter the calculation. On the other hand, things become more complicated for subleading twist-3 matrix elements such as (2.59). Establishing the independence of n^μ for the full result is a rather complex task in the twist-3 calculation beyond LO, but also provides a good check on the correctness of the results. In fact, in Ref. [101] the LO result for $\ell N^\uparrow \to hX$ is computed for an arbitrary n. In contrast, the present work uses a fixed choice for n,

$$n^\mu = -\tfrac{2}{t} P_h^\mu \,. \tag{2.63}$$

This avoids the computation of additional terms in intermediate steps, that will eventually cancel out. With the fixed vector n^μ one can repeat the LO calculation and recover the result of [101] (see Eq. (67) therein). Extended to $d = 4 - 2\varepsilon$ space-time dimensions, it reads

$$\begin{aligned} E_h \frac{\mathrm{d}\sigma_{\mathrm{LO}}}{\mathrm{d}^{d-1}\mathbf{P}_h}(S) \;&=\; \sigma_0(S) \int_{v_0}^{v_1} \mathrm{d}v \int_{x_0}^{1} \tfrac{\mathrm{d}w}{w}\, \hat{\sigma}_{\mathrm{LO}}(v,w,\varepsilon) \sum_q e_q^2 \left[\left(F^q - x\,(F^q)'\right)(x,x)\, z^{2\varepsilon} D_1^q(z) \right] \\ &\quad + h_1^q \otimes \Im[\hat{H}_{FU}^q]. \end{aligned} \tag{2.64}$$

Equation (2.64) employs a Lorentz-invariant, nucleon-spin-dependent prefactor $\sigma_0(S)$. It appears frequently below and is given as

$$\sigma_0(S) = \left(\frac{2\alpha_{\mathrm{em}}^2}{s(-u)} \right) \left(\frac{4\pi\, M\, \epsilon^{lPP_hS}}{s\,(-u)} \right) . \tag{2.65}$$

There is an explicit factor of the nucleon mass M, leading to a typical (twist-3) power suppression. In other words, if the transverse momentum of the detected hadron is large, the factor $\sigma_0(S)$ dilutes the SSA in (2.61). The integration in Eq. (2.64) is carried out using the dimensionless combinations v, w of the hadronic Mandelstam variables s, t, u. Along with the integration boundaries they are given by

$$x = \frac{x_0}{w}, \quad z = \frac{1-v_1}{1-v}, \quad x_0(v) = \frac{1-v}{v}\frac{u}{t}, \quad v_0 = \frac{u}{t+u}, \quad v_1 = \frac{s+t}{s}. \tag{2.66}$$

In terms of these new variables v and w, the LO hard partonic function $\hat{\sigma}_{\mathrm{LO}}$ reads

$$\hat{\sigma}_{\mathrm{LO}}(v, w, \varepsilon) = \frac{1 + v^2 - \varepsilon(1-v)^2}{(1-v)^4}\,\delta(1-w)\,. \tag{2.67}$$

Eq. (2.64) is identical to Eq. (67) of Ref. [101] if a transformation according to Eq. (2.66) is performed, along with setting $\varepsilon = 0$.

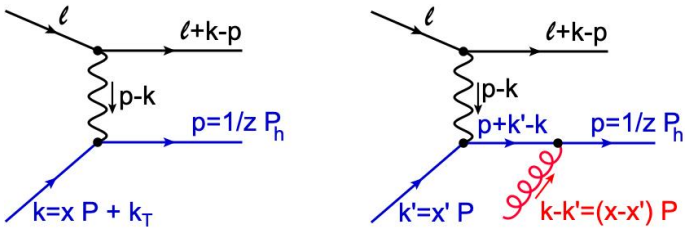

Figure 2.7: LO Feynman diagrams contributing to Eq. (2.64). **Left:** *Kinematical* twist-3 contribution, **Right:** *Dynamical* twist-3 contribution.

Two kinds of multiparton correlation effects contribute to the LO result in Eq. (2.64):

- Twist-3 distribution functions of the initial state nucleon such as the qgq function F^q, alongside the twist-2 quark fragmentation function D_1^q (definitions in (2.59) and (C.14)). This work will entirely focus on these twist-3 distributions of the initial nucleon; the derivation and discussion of the corresponding contributions to the spin-dependent cross section at NLO are the centerpiece of this study

- Twist-3 fragmentation functions of the final state hadronization process, indicated in (2.64) by the $h_1 \otimes \Im[\hat{H}_{FU}]$ term. This term features the leading-twist *transversity* quark distribution h_1 and the imaginary part of a qgq fragmentation function $\hat{H}_{FU}$ (see Ref. [101]). Although such contributions may constitute a numerically large part of the SSA (2.61), they are disregarded in this work, i.e. one sets $\Im[\hat{H}_{FU}] = 0$. First, because the computational procedure is entirely different from the twist-3 distribution effects highlighted below. And second, for jet (see Ch. 4) and photon production (see Ch. 5), twist-3 fragmentation effects do not enter and the presented derivations constitute the complete NLO result

Keeping in mind that only the effects due to multiparton *distributions* in the nucleon are considered, one can further examine the LO formula in Eq. (2.64). The function F^q is probed for the special configuration $x' = x$ of quark and gluon momentum fractions. This corresponds to a situation where an additional soft gluon with vanishing longitudinal momentum is attached to the hard part of the process (see Ref. [101]). Hence $F^q(x, x)$ is called a *soft-gluon pole* matrix element (SGP). In the literature, it is also known as the *Efremov-Teryaev-Qiu-Sterman* (ETQS) matrix element [31, 32, 103, 112, 113]. Note that the ETQS-matrix element enters (2.64) along with a *derivative term* $F'(x, x) = \frac{\mathrm{d}}{\mathrm{d}x}F(x, x)$ as a combination $(1 - x\frac{\mathrm{d}}{\mathrm{d}x})F(x, x)$.

Ref. [101] shows that there are two kinds twist-3 distribution effects to consider for (2.64): the *kinematical* twist-3 contributions from quark-quark correlations (C.1) through the Sivers function $f_{1T}^{\perp(1),q}$, and the *dynamical* twist-3 contributions from quark-gluon-quark correlations (2.59). The corresponding diagrams are shown in Fig. 2.7.

The kinematical effects are computed keeping a non-zero transverse momentum k_T for the incoming parton momenta, as indicated on the left in Fig. 2.7. First, one needs to integrate out all δ-function containing k_T. Then, one Taylor-expands to first order around $k_T = 0$. In this way, the k_T-dependence is shifted from the hard part to the Sivers function, giving rise to its *first transverse moment* $f_{1T}^{\perp(1),q}$. This method has been used at LO in Ref. [101], and the calculations below extend it to NLO.

The right diagram in Fig. 2.7 generates the *dynamical* twist-3 effects at LO. One must compute the interference of such an amplitude's imaginary part with the real part of another amplitude to

obtain a non-vanishing result. For the mentioned diagram in Fig. 2.7 a quark propagator gives rise to the necessary imaginary part:

$$\frac{1}{(p+k'-k)^2+i\delta} = \frac{1}{(-t/z)(x'-x+i\delta)} = \frac{-z}{t}\left(\frac{\mathcal{P}}{x'-x} - i\pi\delta(x'-x)\right). \tag{2.68}$$

The real part of the propagator is given by Cauchy's principal value $\mathcal{P}/(x'-x)$, but it does not contribute to the SSA. On the other hand, the δ-function comes with the required imaginary unit i and fixes the momentum fraction $x'=x$ such that one obtains the SGP function $F^q(x,x)$.

In Ref. [101] it is explained how one needs to combine the kinematical and dynamical effects, using the following identity

$$f_{1T}^{\perp(1),q}(x) = +\pi F^q(x,x)\,. \tag{2.69}$$

This equation relates the first transverse moment of the Sivers function $f_{1T}^{\perp(1),q}$ and the SGP function $F^q(x,x)$ to each other. The relation was first derived in Ref. [114] and it is pivotal for this work. For processes such as semi-inclusive deep inelastic scattering (SIDIS) with one hadron in the initial and one hadron in the final state respectively, one uses the + sign as indicated in (2.69). For Drell-Yan-like processes with two initial hadrons one needs a − sign instead. Eq. (2.69) serves as a bridge between the kinematical and dynamical twist-3 effects.

Although the relation's validity has been questioned in Ref. [115], it is absolutely essential for the collinear twist-3 formalism. The LO formula (2.64) is independent of the unphysical vector n^μ from Eqs. (2.59), (C.1) only after kinematical and dynamical contributions are summed via Eq. (2.69).

Additionally, one finds that the relation is also required to ensure color gauge invariance. To check this, a parameter κ is included in the metric tensor of gluonic polarization sums and propagators:

$$-g^{\mu\nu} \to -d^{\mu\nu}(k,n) \equiv -\left(g^{\mu\nu} - \kappa\,\frac{k^\mu n^\nu + k^\nu n^\mu}{k\cdot n + i\delta}\right), \tag{2.70}$$

where k denotes the relevant momentum of the sum or propagator. The specific gauge is then given by the choice of the parameter κ, i.e. $\kappa=0$ for Feynman and $\kappa=1$ for light-cone gauge. One finds that, at NLO, kinematical and SGP contributions do indeed both display a κ-dependence. The parameter κ only vanishes after Eq. (2.69) is applied to combine the two contributions. This again underlines how essential Eq.(2.69) is for the collinear twist-3 approach.

It is noteworthy that there is an alternative method to compute the SGP contributions to a SSA at NLO. It is based on Ward-Takahashi identities and yields equivalent results, see Ref. [116].

2.4 Setup of the NLO Calculation

The discussion above establishes the expression for the spin–dependent cross section within collinear twist-3 factorization at leading order (LO). A few points are worth highlighting before turning to the next stage of the calculation:

- **Combining Kinematical and Dynamical Effects:** It is essential to tie together kinematical contributions by the first transverse–moment of the Sivers function $f_{1T}^{\perp(1),q}$ and dynamical soft-gluon pole contributions $\propto F^q(x,x)$. This is achieved by employing the identity

  $$f_{1T}^{\perp(1),q}(x) = \pi F^q(x,x)\,.$$

  Only then results are independent of the auxiliary light–cone vector n^μ and the gauge parameter κ introduced in (2.70). This relation is therefore indispensable for the collinear twist-3 formalism. At NLO, the function F^q will also enter at different configurations of x, x' along with the other qgq function G^q

- **Power Suppression:** The prefactor $\sigma_0(S) \propto M$ in Eq. (2.65) shows explicitly that the single-spin asymmetry (SSA) is a genuine twist-3 observable: at large hadron transverse momentum the nucleon mass M suppresses the polarized cross section relative to the unpolarized one. The same prefactor is present at NLO.

- **Fragmentation Effects:** While the term $h_1 \otimes \Im[\hat{H}_{FU}]$ in Eq. (2.64) representing twist-3 qgq fragmentation contributions can be numerically sizeable, this work concentrates on the initial-state (distribution) mechanism. For single-inclusive jet and photon production no fragmentation-related twist-3 effects enter. Consequently, the following discussion assumes $\Im[\hat{H}_{FU}] = 0$.

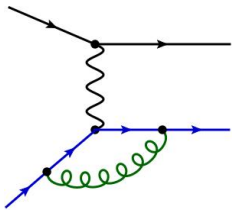

Figure 2.8: Diagram for the virtual vertex correction contributing to the kinematical part at NLO. External momenta are the same as in Fig. 2.7 (left). One needs the interference of this diagram with the LO diagram in Fig. 2.7 (left), and also the mirrored case.

These insights from the LO picture prepare the ground for the next step: incorporating NLO corrections. At NLO, virtual loop and real-emission diagrams enter, singularities must be regularized and eventually cancel, and the factorization of twist-3 matrix elements can be tested beyond tree level. The following section will therefore develop the main concepts for the NLO calculation. This work will cover the processes of single-inclusive hadron production $\ell N^\uparrow \to hX$, jet production $\ell N^\uparrow \to \text{jet}X$ and photon production $\ell N^\uparrow \to \gamma X$. Each of these will be discussed in detail in a designated chapter. The general strategy, however, is the same for all three reactions and will be presented in the following. To better illustrate the important concepts, example expressions for the case of $\ell N^\uparrow \to hX$ will be used.

2.4.1 Kinematical Twist-3 at NLO

First, some special features of kinematical twist-3 contributions at NLO are highlighted. Consider a partonic hard factor $\hat{\sigma}(k, p, l, l', r)$ that is a function of the external momenta of the initial (l) and final ($l' = l + k - p - r$) lepton and the quark (k, p). The momentum r can either be a loop momentum in case of virtual corrections, as in Fig. 2.8. Or it can be the momentum of an undetected final state parton, for example a gluon, as in the real-gluon-emission diagrams of Fig. 2.9.

To start the calculation, one employs an approximation to the parton momenta. For the final state parton, only hadronization via the leading-twist fragmentation functions $D_1^{h/(q,g)}(z)$ is considered. Thus, the corresponding parton momentum is approximated by $p^\mu \simeq 1/z\, P_h^\mu$.

For the initial quark momentum k^μ one must also capture the subleading-twist kinematical effects. The left diagram of Fig. 2.7 indicates that one must adjust the usual parton model approximation and include a finite transverse momentum k_T^μ. Optionally, one may choose to include a term $\propto k_T^2$, which allows one to keep $k^2 = 0$. This simplifies several intermediate steps of the calculation, and the kinematical approximation then reads

$$k^\mu \simeq x\, P^\mu - \tfrac{k_T^2}{2x}\, n^\mu + k_T^\mu \,. \tag{2.71}$$

First, the case of a single fragmenting quark in the final state is discussed. In addition to the LO diagram (Fig. 2.7 left) this also includes the NLO virtual QCD vertex correction, see Fig. 2.8. The order in which integrations and k_T-expansions are performed is crucial. It is essential that one keeps $k_T \neq 0$ in the virtual loop diagrams and integrates out all k_T-dependent δ-functions as a first step. Only afterwards one can proceed with the expansion up to linear order in k_T. If one does not follow this order and first expands in k_T, the result is ambiguous and can be incorrect.

To illustrate this point, consider the NLO vertex correction in Fig. 2.8. Suppressing the fragmentation function and z-integration, one can write the following expression for the result of the loop integration

$$\begin{aligned}
&\int \tfrac{\mathrm{d}x}{x} \int \mathrm{d}^{d-2}k_T\, \delta\left(\hat{s} + \hat{t} + \hat{u} + 2l_T \cdot k_T\right)\, (\sigma_0 + l_T \cdot k_T\, \sigma_1)\, (\hat{s}, \hat{t}, \hat{u}, \varepsilon)\, \epsilon^{P n k_T S_T}\, f_{1T}^{\perp,q}(x, k_T^2) \\
\to\quad & \int_{x_0}^\infty \tfrac{\mathrm{d}w}{w} \int \mathrm{d}^{d-2}k_T\, \delta\left(\tfrac{1}{w} - (1-\chi)\right)\, (\sigma_0 + l_T \cdot k_T\, \sigma_1)\, (v, w, \varepsilon)\, \epsilon^{P n k_T S_T}\, f_{1T}^{\perp,q}(\tfrac{x_0}{w}, k_T^2) \\
\to\quad & \int \mathrm{d}^{d-2}k_T\, w_0\, (\sigma_0 + l_T \cdot k_T\, \sigma_1)\, (v, w_0, \varepsilon)\, \epsilon^{P n k_T S_T}\, f_{1T}^{\perp,q}(\tfrac{x_0}{w_0}, k_T^2) \,.
\end{aligned} \tag{2.72}$$

Here, the loop correction (to all orders in ε) is denoted as $\sigma_0 + l_T \cdot k_T\, \sigma_1$. It enters with a δ-function that is also encountered at LO. Because of the eventual Taylor expansion, only linear terms in k_T are kept for the loop correction and the δ-function. Conveniently, $k_T \cdot l_T$ is the only non-vanishing scalar product of external momenta with k_T. This is due to the explicit choice made in Eq. (2.63) for the light-cone vector n^μ, which determines the transverse direction via the projector $g_T^{\mu\nu}$ in (2.60).

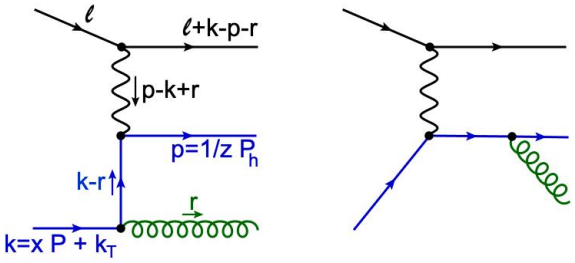

Figure 2.9: Diagrams that generate the kinematical twist-3 effects at NLO for the real-gluon emission channel $qg \to q$. One needs the squared modulus of the sum of these diagrams.

From the first to the second line of (2.72), the integration variable is transformed as before, i.e. $x \to x_0/w$. The short-hand $\chi = \frac{2\,t\,(l_T \cdot k_T)}{s\,u\,(1-v)}$ allows to write the argument of the δ-function in a compact way. The δ-function is then used to carry out the w-integration from the second to the third line, fixing $w = w_0 \equiv 1/(1-\chi)$. An implicit dependence of (2.72) on k_T remains through w_0 and χ. One must keep this dependence in mind when Taylor-expanding the integrand to first order in k_T. After the expansion, the first transverse moment of the Sivers function is generated as follows

$$\int \mathrm{d}^{d-2}k_T k_T^\rho k_T^\sigma \, f_{1T}^{\perp,q}(x,k_T^2) = -M^2\, g_T^{\rho\sigma}\, f_{1T}^{\perp(1),q}(x)\,. \tag{2.73}$$

Eventually, Eq.(2.72) simplifies to

$$\begin{aligned}&\left(\sigma_1(v,w,\varepsilon) + \frac{2t\,\partial_w(w\,\sigma_0)(v,w,\varepsilon)}{su(1-v)}\right)\Bigg|_{w=1} f_{1T}^{\perp(1),q}(x_0)\\ &\quad + \left(\frac{2t}{su(1-v)}\,\sigma_0(v,w,\varepsilon)\right)\Bigg|_{w=1}\left(-x_0\,\left(f_{1T}^{\perp(1),q}\right)'(x_0)\right)\,.\end{aligned} \tag{2.74}$$

Notably, a derivative term $\propto \left(f_{1T}^{\perp(1),q}\right)'$ enters the above expansion.

Next, the real-gluon-emission corrections of Fig. 2.9 are discussed. Here, the argument r in the partonic factor $\hat\sigma(k,p,l,l',r)$ denotes the momentum of an undetected final state gluon. Because of this additional particle in the final state, the phase space integration becomes more complicated compared to leading order. Similar to the case of virtual corrections discussed above, the order of the next steps is important: One could try to immediately expand $\hat\sigma(k,p,l,l',r)$ in k_T and then perform the phase space integration. However, this would cause inconsistencies and possibly wrong results. The other option is to do the phase space integral first while keeping $k_T \neq 0$ throughout. Then one obtains a unique result for the integrated cross section $\hat\sigma(k,p,l,\varepsilon)$ (l', r integrated out).

The phase space integral and the corresponding integrated cross section are given as

$$\hat\sigma(k,p,l,\varepsilon) \sim \frac{\mu^{2\varepsilon}}{(2\pi)^{d-1}} \int \mathrm{d}^d l' \delta^+\left((l')^2\right) \int \mathrm{d}^d r \delta^+\left(r^2\right) \delta^{(d)}\left(k+l-l'-p-r\right) \hat\sigma(k,p,l,l',r,\varepsilon)\,, \tag{2.75}$$

which can be simplified in a suitable reference frame. Imposing the condition $\boldsymbol{k}+\boldsymbol{l}-\boldsymbol{p}=\boldsymbol{0}$ corresponds to a partonic reference frame and it enables one to carry out all integrations except for two angles ϕ and θ. In this frame, one finds for the momenta l' and r

$$l' = k+l-p-r; \qquad r = \frac{1}{2}\sqrt{\hat s+\hat t+\hat u+2k_T\cdot l_T}\,(1,\ldots,\sin\theta\cos\phi,\sin\theta\sin\phi,\cos\theta)\,, \tag{2.76}$$

where one again encounters $k_T \cdot l_T$ as the only scalar product of external momenta with k_T, due to the choice for n^μ, see Eq. (2.63). Making use of the δ-functions and the conveniently chosen reference frame, the phase space integral can be brought into the form

$$\hat\sigma(k,p,l,\varepsilon) \sim \frac{S_\varepsilon \Gamma^2(1-\varepsilon)}{4(2\pi)^3\Gamma(1-2\varepsilon)}\left(\frac{\hat s+\hat t+\hat u+2k_T\cdot l_T}{\mu^2}\right)^{-\varepsilon}\int_0^\pi \mathrm{d}\phi \sin^{-2\varepsilon}\phi \int_0^\pi \mathrm{d}\theta \sin^{1-2\varepsilon}\theta\,\hat\sigma(\phi,\theta,\varepsilon)\,, \tag{2.77}$$

with $S_\varepsilon \equiv \frac{(4\pi)^\varepsilon}{\Gamma(1-\varepsilon)}$. The remaining angular integration will be needed to all orders in ε, as will be explained below. Refs. [117, 118, 119] provide the necessary tools to perform these all-order calculations. It turns out that, ahead of expanding around $\varepsilon = 0$, one has to do the Taylor expansion in k_T.

The fact that one has to be careful with the order of the expansions in k_T and ε is due to a unique feature that appears at NLO for twist-3 observables. Keeping $k_T \neq 0$ throughout the phase space integration one finds (schematically) the following formula for the kinematical twist-3 contribution:

$$\int \frac{\mathrm{d}z}{z^2} \int \frac{\mathrm{d}x}{x} \int \mathrm{d}^{d-2}k_T \, \frac{\hat{\sigma}(\hat{s},\hat{t},\hat{u},k_T\cdot l_T,\mu,\varepsilon,\kappa)}{(\hat{s}+\hat{t}+\hat{u}+2\,k_T\cdot l_T)^{1+2\varepsilon}} \, \epsilon^{Pnk_TS_T} \, f_{1T}^{\perp,q}(x,k_T^2)\, D_1^q(z)\,, \tag{2.78}$$

where the partonic Mandelstam variables $\hat{s} = (l + x\,P)^2 = x\,s$, $\hat{t} = (x\,P - P_h/z)^2 = \frac{x}{z}t$, $\hat{u} = (l - P_h/z)^2 = u/z$ have been introduced. Note that also the gauge parameter κ (see (2.70)) explicitly appears in $\hat{\sigma}$, so (2.78) by itself is not gauge invariant at NLO. However, leading-twist observables as well as the twist-3 observable considered here eventually turn out to be independent of κ. For the case of leading twist this is immediately apparent, since all terms proportional to κ are also proportional to k_T, and $k_T = 0$. The gauge dependence also vanishes in case of the twist-3 calculation: After combining kinematical and SGP parts via Eq. 2.69, κ cancels out exactly; this will also be discussed in Sec. 3.2.

In addition, an explicit denominator $(\hat{s}+\hat{t}+\hat{u}+2\,k_T\cdot l_T)^{1+2\varepsilon}$ has been extracted which, for $k_T = 0$ (leading twist), typically displays a soft singularity at $\hat{s}+\hat{t}+\hat{u} = 0$. Here, one needs to Taylor-expand the factor

$$\frac{\hat{\sigma}(\hat{s},\hat{t},\hat{u},k_T\cdot l_T,\mu,\varepsilon,\kappa)}{(\hat{s}+\hat{t}+\hat{u}+2\,k_T\cdot l_T)^{1+2\varepsilon}}$$

up to first order in k_T, and the first transverse moment of the Sivers function is again generated via Eq. (2.73). Explicitly, one finds the following expansion

$$\frac{-2(1+2\varepsilon)\,l_{T\sigma}\hat{\sigma}(\hat{s},\hat{t},\hat{u},\mu,\varepsilon)}{(\hat{s}+\hat{t}+\hat{u})^{2+2\varepsilon}} + \frac{l_{T\sigma}\left(\frac{\partial\hat{\sigma}}{\partial(k_T\cdot l_T)}\right)(\hat{s},\hat{t},\hat{u},\mu,\varepsilon,\kappa)}{(\hat{s}+\hat{t}+\hat{u})^{1+2\varepsilon}}\,,$$

and subsequently applies the change of variables $z = \frac{1-v_1}{1-v}$, $x = \frac{x_0}{w}$, discussed in Sec. 2.3. Omitting the v-integration as well as the FF D_1^q, one can write Eq. (2.78) as follows:

$$\int_{x_0}^1 \frac{\mathrm{d}w}{w} \left(\frac{\sigma_1(v,w,\varepsilon)\, f_{1T}^{\perp(1)}\left(\frac{x_0}{w}\right)}{(1-w)^{2+2\varepsilon}} + \frac{\sigma_2(v,w,\varepsilon,\kappa)\, f_{1T}^{\perp(1)}\left(\frac{x_0}{w}\right)}{(1-w)^{1+2\varepsilon}} \right). \tag{2.79}$$

Similar expressions to the second term $\propto 1/(1-w)^{1+2\varepsilon}$ are also commonly encountered in leading-twist calculations. Such terms have a soft singularity for $w \to 1$ that must be regularized via the following formula:

$$\frac{1}{(1-w)^{1+\varepsilon}} = -\frac{1}{\varepsilon}\delta(1-w) + \frac{1}{(1-w)_+} - \varepsilon \left(\frac{\log(1-w)}{1-w}\right)_+ + \mathcal{O}(\varepsilon^2)\,, \tag{2.80}$$

where one can also replace $\varepsilon \to 2\varepsilon$ if necessary. This expansion introduces the so-called plus-distributions, which are defined via an integral with a suitable test function:

$$\begin{aligned} \int_z^1 \frac{\mathrm{d}w}{w} \frac{f(w)}{(1-w)_+} &= \int_z^1 \mathrm{d}w\, \frac{\frac{1}{w}f(w) - f(1)}{1-w} + f(1)\,\log(1-z) \\ \int_z^1 \frac{\mathrm{d}w}{w} \left(\frac{\log(1-w)}{1-w}\right)_+ f(w) &= \int_z^1 \mathrm{d}w \left[\frac{\log(1-w)}{1-w}\left(\frac{1}{w}f(w) - f(1)\right)\right] + \frac{f(1)}{2}\log^2(1-z)\,. \end{aligned} \tag{2.81}$$

In the end, one finds that virtual contributions cancel the $\frac{1}{\varepsilon}$ pole introduced by the expansion in Eq. (2.80), ensuring IR-safety.

The first term in (2.79) is $\propto 1/(1-w)^{2+2\varepsilon}$, meaning that the term causing the soft singularity enters with a higher power. Consequently, the expansion in (2.80) does not apply. The higher power is a result of the k_T-expansion and thus a new, genuine twist-3 feature. Based on integration by parts, a method to deal with these more singular terms is developed in App. E. Integration by parts also introduces a derivative term $(f_{1T}^{\perp(1)})' = \pi(F^q)'$. Thus, both virtual and real corrections for the kinematical twist-3 effects generate derivative terms.

To summarize the concepts discussed so far, it is pivotal to perform the various steps for the calculation of the kinematical part at NLO in the correct order:

1. Perform all integrations (to all orders in ε) such that no δ functions including the transverse momentum k_T remain

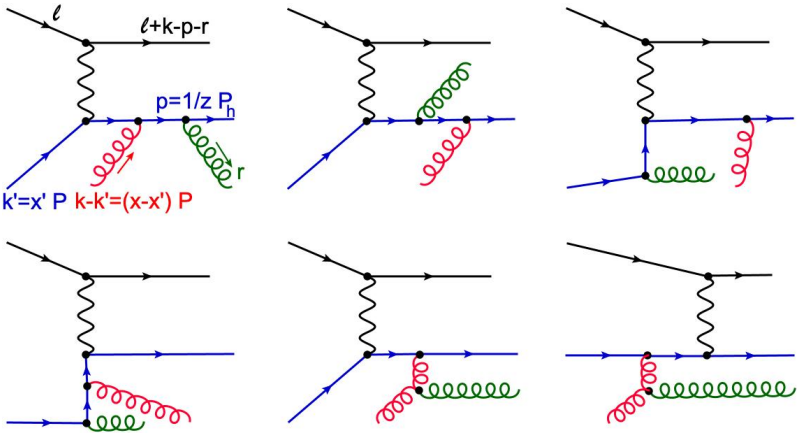

Figure 2.10: $qg \to q$ channel diagrams that give the dynamical contribution at NLO. One needs the interference of these diagrams with the ones in Fig. 2.9, at $k_T = 0$.

2. Taylor expand the resulting expression to first order in k_T and apply Eq. (2.73) to get the first moment of the Sivers function $f_{1T}^{\perp(1),q}$
3. Apply Eq. (2.80) to terms $\propto 1/(1-w)^{1+2\varepsilon}$. Additionally, there are terms $\propto 1/(1-w)^{2+2\varepsilon}$ that need to be treated using the methods of App. E.1.
4. Eventually, one can expand the result around $\varepsilon = 0$

2.4.2 Dynamical Twist-3 at NLO

Next is the computation of QCD corrections to the LO diagram on the right of Fig. 2.7, generated by dynamical twist-3 effects. Special features and observations at NLO are discussed as well as the general strategy for the calculation of dynamical twist-3 effects at NLO. The radiation of an unobserved gluon will serve as an illustrative example (see diagrams in Fig. 2.10). As discussed in Sec. 2.3, the SSA requires an imaginary part in the hard scattering amplitudes. The only source of this imaginary part at LO is the propagator (2.68), meaning that the LO formula (2.64) is entirely given in terms of a SGP contribution $\propto F(x,x)$. As will be demonstrated below, there are various other sources of imaginary parts at NLO:

Integral contribution: To start, consider the following general form of dynamical twist-3 contributions at NLO

$$\int \frac{\mathrm{d}z}{z^2} \int \mathrm{d}x \int_{x-1}^{1} \mathrm{d}x' \frac{i}{x'-x} \left[\hat{\sigma}^1(x,x',z)\, F^q(x,x') + \hat{\sigma}^5(x,x',z)\, G^q(x,x') \right] D_1^q(z) + \text{c.c.}\,. \quad (2.82)$$

This formula is specific to real-gluon-emission corrections to the leading order, given by the diagrams in Fig. 2.10. Since this partonic channel features quark-gluon (qg) correlations in the initial nucleon as well as the fragmentation of a quark (q) into the observed final-state hadron, it is referred to as $qg \to q$ channel below. Unlike the LO case, cf. (2.64), both qgq functions F^q and G^q enter at NLO.

The generic partonic factors $\hat{\sigma}^{1,5}$ are given by the interference of Feynman amplitudes: On the one hand, an amplitude $\mathcal{M}_{qg}$ with an initial-state quark *and* a gluon (see Fig. 2.10), and on the other hand, an amplitude $\mathcal{M}_q$ with a single quark in the initial state (as in Fig. 2.9, but with $k_T = 0$). The formula (2.82) explicitly factors out an imaginary unit i such that the numerator of the partonic factors $\hat{\sigma}^{1,5}$ is real. Since the complex conjugate c.c. is added in (2.82), another imaginary unit must appear in $\hat{\sigma}^{1,5}$ for a non-zero contribution. This is where the small imaginary parts $i\delta$ in the denominators of Feynman propagators become important, and the decomposition of such a propagator in real and imaginary parts is given in Eq. (2.68).

At NLO, however, one also encounters certain propagators where the procedure of Eq. (2.68) leads to problems in the subsequent phase space integration. An example for such a propagator found in the $qg \to q$ channel is given by

$$\frac{i}{(p-k+k'+r)^2 + i\delta}.$$

Here, the partonic momenta are approximated as in the right diagram of Fig. 2.7, namely $k \simeq x\,P$, $k' \simeq x'\,P$ and $p \simeq P_h/z$. Furthermore, r refers to the momentum of the unobserved final-state gluon. Following Eq. (2.68), one would decompose this propagator as follows:

$$\frac{1}{(p-k+k'+r)^2+i\delta} = \underset{\ldots}{\mathcal{P}} - \frac{i\,\pi}{2k\cdot r-\hat{t}}\,\delta\left(\zeta - \frac{\hat{s}+\hat{u}-2l\cdot r}{2k\cdot r-\hat{t}}\right), \tag{2.83}$$

where $\zeta \equiv \frac{x'}{x}$ is introduced for convenience. Using the δ-function would fix x' to a r-dependent quantity, i.e. $x' = x'(r)$. Consequently, this r-dependence would also implicitly enter $F(x,x')$ and $G(x,x')$ in Eq. (2.82). Since both functions F and G are essentially unknown, performing the subsequent phase space integration over r^μ would become rather complicated. This is especially true for the computation of the all-order-in-ε result. Of course, it is formally possible to do a Taylor expansion in x' of F^q and G^q. But then one also runs into several difficulties.

Instead, the approach used in this work is to keep the causal $i\delta$ in Eq. (2.83) small but finite. Then, one can perform the phase space integration *before* the x'-integral. In this case, imaginary parts are not generated by a propagator decomposition as in (2.83). Consequently, x' is not set to a fixed value but can vary within the integration boundaries in (2.82). Hence, such contributions will be referred to as *integral contributions* in the following. For the integral contributions, the imaginary parts emerge after phase space integration via the appearance of complex-valued logarithms, for example:

$$\begin{aligned}
\log\left(\frac{1-(B^2+C^2)/\left(A+i\delta\right)^2}{(1-B/(A+i\delta))^2}\right) &= \log\left|\frac{1-(B^2+C^2)/A^2}{(1-B/A)^2}\right| \\
&\quad + i\pi\,\theta(1-\zeta)\theta(\zeta)\,\mathrm{sgn}\left(\zeta - \tfrac{-\hat{u}}{\hat{s}+\hat{t}}\right) \\
\text{with}: \quad A &= -((1-\zeta)\hat{s}+\zeta\hat{t}+\hat{u})/4 \\
B &= A + \zeta\frac{\hat{t}}{2} + \frac{\hat{t}\hat{u}}{2(\hat{s}+\hat{t})} \\
C &= \frac{\sqrt{\hat{s}\hat{t}\hat{u}(\hat{s}+\hat{t}+\hat{u})}}{2(\hat{s}+\hat{t})},
\end{aligned} \tag{2.84}$$

Here, θ denotes the Heaviside step function and sgn the sign function. The logarithm in (2.84) produces an imaginary part for $0<\zeta<1$, corresponding to $0<x'<x$. This applies to all complex logarithms resulting from the phase space integration.

Since the calculation is performed in $d = 4-2\varepsilon$ dimensions, soft and/or collinear singularities appear in the form of $\frac{1}{\varepsilon}$ poles. However, the aforementioned logarithms like (2.84) only show up at order $\mathcal{O}(\varepsilon^0)$, i.e. they are not accompanied by any $\frac{1}{\varepsilon}$ poles. In this way one arrives at a result of the following form for the integral contributions to the $qg \to q$ channel:

$$\begin{aligned}
\int_{v_0}^{v_1}\mathrm{d}v\int_{x_0}^{1}\frac{\mathrm{d}w}{w}\int_0^1\mathrm{d}\zeta\;\Big[&\tilde{\sigma}^1(v,w,\zeta)\,F^q\left(\tfrac{x_0}{w},\zeta\tfrac{x_0}{w}\right) \\
&+\tilde{\sigma}^5(v,w,\zeta)\,G^q\left(\tfrac{x_0}{w},\zeta\tfrac{x_0}{w}\right)\Big]\;D_1^q\left(\tfrac{1-v_1}{1-v}\right),
\end{aligned} \tag{2.85}$$

where the integration variables x and z are substituted by v and w as before. The partonic functions $\tilde{\sigma}^{1,5}$ are finite for $d\to 4$ and depend neither on external kinematical variables s, t, u, nor on the renormalization scale μ.

Notably, $\tilde{\sigma}^{1,5}$ have discontinuities due to the sign functions from the complex logarithms as in Eq. (2.84). This alone would keep the integrability of Eq. (2.85) intact. However, one finds that there are singularities at $\zeta=0$, $\zeta=1$ and $\zeta=w$ in the integrands ($f_{1,2,3}$ are some generic functions independent of ζ):

$$\begin{aligned}
\tilde{\sigma}^{1,5}(v,w,\zeta) &\xrightarrow{\zeta\to 1} \frac{f_1(v,w)}{(1-\zeta)^2}, \\
\tilde{\sigma}^{1,5}(v,w,\zeta) &\xrightarrow{\zeta\to 0} \frac{f_2(v,w)}{\zeta^2}, \\
\tilde{\sigma}^{1,5}(v,w,\zeta) &\xrightarrow{\zeta\to w} \frac{f_3(v,w)}{(w-\zeta)^2}.
\end{aligned} \tag{2.86}$$

This behavior immediately indicates that the ζ-integral in (2.85) diverges.

One must regularize the divergent contributions in terms of ε to combine and eventually cancel them with divergences from other sources. It is instructive to first consider the simpler example of a partonic factor $\tilde{\sigma}^0(v,w,\zeta) \xrightarrow{\zeta\to 1} f_0(v,w)/(1-\zeta)$. The basic idea is to move the problematic denominator to the qgq functions F^q, G^q and then add and subtract suitable terms to the numerator. Let $\tilde{\sigma}^0(\zeta) \equiv \hat{\sigma}^0_{\text{int}}(\zeta)/(1-\zeta)$ with a finite partonic function $\hat{\sigma}^0_{\text{int}}$, such that the divergent behavior is explicitly factored out. Then one can write

$$\begin{aligned}\tilde{\sigma}^0(\zeta)F\left(\tfrac{x_0}{w},\zeta\tfrac{x_0}{w}\right) = \hat{\sigma}^0_{\text{int}}(\zeta)\frac{F\left(\frac{x_0}{w},\zeta\frac{x_0}{w}\right)}{1-\zeta} &= \hat{\sigma}^0_{\text{int}}(\zeta)\left(\underbrace{\frac{F\left(\frac{x_0}{w},\zeta\frac{x_0}{w}\right)-F\left(\frac{x_0}{w},\frac{x_0}{w}\right)}{1-\zeta}}_{F_{\text{int}}}+\frac{F\left(\frac{x_0}{w},\frac{x_0}{w}\right)}{1-\zeta}\right)\\ &\equiv \hat{\sigma}^0_{\text{int}}(\zeta)F_{\text{int}}\left(x_0,w,\zeta\right)+\tilde{\sigma}^0(\zeta)F\left(\tfrac{x_0}{w},\tfrac{x_0}{w}\right), \qquad (2.87)\end{aligned}$$

where effectively a zero in the form $0 = F\left(\frac{x_0}{w},\frac{x_0}{w}\right) - F\left(\frac{x_0}{w},\frac{x_0}{w}\right)$ has been added to the numerator. The first term in the second line contains an integrable combination F_{int} of the function F and the finite partonic function $\hat{\sigma}^0_{\text{int}}$. Thus, it is integrable over the whole range $0 \le \zeta \le 1$ and would constitute the result for the integral contribution.

The partonic factor $\tilde{\sigma}^0$ in the second term is still divergent, but it is now accompanied by the qgq function $F^q\left(\frac{x_0}{w},\frac{x_0}{w}\right)$ which is independent of ζ and hence independent of x'. Thus, one can go back to the stage before the phase space integration, where one still has the propagator (2.83). Now, one can simply apply the δ-function to fix x' which is not a problem anymore because x' does not enter the argument of F^q and, consequently, F^q remains independent of the gluon momentum r. Then, the phase space integral over r can be carried out analytically to all orders in ε. The original divergence in ζ will now show up as a $\frac{1}{\varepsilon}$ pole. Effectively, the divergence for $\zeta \to 1$ from the integral contribution is shifted to a divergence for $\varepsilon \to 0$ in a pole contribution, in this case a soft-gluon pole contribution. These pole contributions originating from adding and subtracting terms in an intermediate step will be referred to as *subtraction terms* in the following. Importantly, "subtraction" in this context is not related to a subtraction as part of the renormalization procedure.

Going back from the simplified example to the partonic factors in the $qg \to q$ channel, the concept can be applied as follows: based on the singular structure (2.86), one may redefine the partonic functions as

$$\hat{\sigma}^{1,5}_{\text{Int}}(v,w,\zeta) \equiv \zeta^2(1-\zeta)^2(w-\zeta)^2\,\tilde{\sigma}^{1,5}(v,w,\zeta)\,. \qquad (2.88)$$

Indeed, the new partonic functions $\hat{\sigma}^{1,5}_{\text{Int}}$ are now well-behaved and integrable. The factor $\zeta^2(1-\zeta)^2(w-\zeta)^2$ and accordingly the divergent behavior is moved to the qgq functions in (2.85) as follows:

$$(F,G)\left(\tfrac{x_0}{w},\zeta\tfrac{x_0}{w}\right) \to \frac{(F,G)\left(\frac{x_0}{w},\zeta\frac{x_0}{w}\right)}{\zeta^2(1-\zeta)^2(w-\zeta)^2}. \qquad (2.89)$$

Next, one needs to add and subtract suitable terms from the numerator, namely Taylor expansions of $(F,G)\left(\frac{x_0}{w},\zeta\frac{x_0}{w}\right)$ around the three poles up to the linear term in ζ. The integrable combinations of the qgq functions then read

$$\begin{aligned}F^{qg\to q}_{\text{Int}}(x_0,w,\zeta) \equiv\ & \frac{1}{\zeta^2(1-\zeta)^2(w-\zeta)^2}\Big[F^q\left(\tfrac{x_0}{w},\zeta\tfrac{x_0}{w}\right)\\ &+\frac{\zeta^2(1-\zeta)^2}{(1-w)^3w^3}\left(\left(5w^2+2\zeta-3w-4w\zeta\right)F^q\left(\tfrac{x_0}{w},x_0\right)+(w-\zeta)(1-w)\,x_0\left(\partial_2F^q\right)\left(\tfrac{x_0}{w},x_0\right)\right)\\ &-\frac{\zeta^2(w-\zeta)^2}{(1-w)^3}\left(\left(5-4\zeta-3w+2w\zeta\right)F^q\left(\tfrac{x_0}{w},\tfrac{x_0}{w}\right)-\frac{1}{2}(1-\zeta)(1-w)\,\tfrac{x_0}{w}\left(F^q\right)'\left(\tfrac{x_0}{w},\tfrac{x_0}{w}\right)\right)\\ &-\frac{(w-\zeta)^2(1-\zeta)^2}{w^3}\left(\left(2\zeta+w+2w\zeta\right)F^q\left(\tfrac{x_0}{w},0\right)+\zeta\,x_0\left(\partial_2F^q\right)\left(\tfrac{x_0}{w},0\right)\right)\Big], \qquad (2.90)\end{aligned}$$

and

$$
\begin{aligned}
G_{\rm Int}^{qg\to q}(x_0,w,\zeta) \;\equiv\; & \frac{1}{\zeta^2(1-\zeta)^2(w-\zeta)^2}\Big[G^q\left(\tfrac{x_0}{w},\zeta\tfrac{x_0}{w}\right)\\
&+\frac{\zeta^2(1-\zeta)^2}{(1-w)^3w^3}\left((5w^2+2\zeta-3w-4w\zeta)\,G^q\left(\tfrac{x_0}{w},x_0\right)+(w-\zeta)(1-w)\,x_0\,(\partial_2 G^q)\left(\tfrac{x_0}{w},x_0\right)\right)\\
&+\frac{\zeta^2(w-\zeta)^2(1-\zeta)}{(1-w)^2}\,\tfrac{x_0}{w}\,(\partial_2 G^q)\left(\tfrac{x_0}{w},\tfrac{x_0}{w}\right)\\
&-\frac{(w-\zeta)^2(1-\zeta)^2}{w^3}\left((2\zeta+w+2w\zeta)\,G^q\left(\tfrac{x_0}{w},0\right)+\zeta\,x_0\,(\partial_2 G^q)\left(\tfrac{x_0}{w},0\right)\right)\Big]\,. \qquad (2.91)
\end{aligned}
$$

Although it is not apparent at first glance, both modified functions $(F,G)_{\rm Int}^{qg\to q}$ in Eqs. (2.90),(2.91) are integrable over $0\le\zeta\le 1$ and $x_0\le w\le 1$. Consequently, one arrives at a well-defined, convergent result for the *integral contributions* to the $qg\to q$ channel, which can be written as

$$
\begin{aligned}
\int_{v_0}^{v_1}\mathrm{d}v\int_{x_0}^1\frac{\mathrm{d}w}{w}\int_0^1\mathrm{d}\zeta\;\Big[&\hat\sigma^1_{\rm Int}(v,w,\zeta)\,F_{\rm Int}^{qg\to q}(x_0,w,\zeta)\\
&+\hat\sigma^5_{\rm Int}(v,w,\zeta)\,G_{\rm Int}^{qg\to q}(x_0,w,\zeta)\Big]\;D_1^q\left(\tfrac{1-v_1}{1-v}\right)\,. \qquad (2.92)
\end{aligned}
$$

It is interesting to note that the procedure described above to regularize the divergences in the ζ-integral can also be applied in slightly modified ways. It is noteworthy that terms $\propto C_F$ in $\tilde\sigma^{1,5}(v,w,\zeta)$ are less divergent around the three ζ-poles. In particular, there is no divergence around $\zeta=w$. Thus, it would suffice to factor out lower powers of $1-\zeta$, ζ and $w-\zeta$. This would in turn lead to different expressions for $F_{\rm int}^{qg\to q}$ and $G_{\rm int}^{qg\to q}$ than those in Eqs. 2.90 and 2.91. Moreover, the subsequent parts of the calculation discussed below would also be different.

Pole contributions: One must of course add back the subtraction terms from Eqs. (2.90),(2.91), i.e. all terms beside $(F,G)\left(\frac{x_0}{w},\zeta\frac{x_0}{w}\right)$. Like in the simplified example above, the variable ζ does not enter the qgq functions F,G for the subtraction terms, and these functions are only evaluated at certain, special configurations of their arguments x,x':

- Soft-gluon pole (SGP): The function $F\left(\frac{x_0}{w},\frac{x_0}{w}\right)$ and its derivative term in the third line of (2.90) are evaluated on the $x=x'$ diagonal. This configuration is already familiar from the LO result (2.64) as well as the kinematical twist-3 part in Sec. 2.4.1 (Eqs. (2.79),(2.74) with Eq. (2.69)). Physically, $x'=x$ means that the initial-state gluon (see for example Fig. (2.10)) has vanishing longitudinal momentum, i.e. it is a soft gluon. For the other qgq function G only a derivative term enters the third line of Eq. (2.91) since $G\left(\frac{x_0}{w},\frac{x_0}{w}\right)=0$.
- Soft-fermion pole (SFP): The functions $F\left(\frac{x_0}{w},0\right)$, $G\left(\frac{x_0}{w},0\right)$ are encountered in the fourth lines of Eqs. (2.90),(2.91), alongside their derivatives. Physically, $x'=0$ means that an initial quark enters a partonic amplitude (e.g. in the right diagram of Fig. 2.7) with zero longitudinal momentum, hence the name soft-fermion pole.
- Hard pole (HP): The functions $F\left(\frac{x_0}{w},x_0\right)$, $G\left(\frac{x_0}{w},x_0\right)$ appear in the second lines of Eqs. (2.90), (2.91). They are referred to as *hard poles* (HP) because neither the quark nor the gluon entering the partonic amplitude are soft.

The HP, SGP and SFP subtraction terms can be calculated as explained for the simplified example, see Eq. (2.87): Since the qgq functions F and G are independent of the integration variable ζ (or $x\prime$), one can go back to Eq. (2.82), at the stage before the phase space integration. Because of the independence of ζ for the functions F,G, the decomposition (2.86) can be used without any problems. Thus, the δ-function fixes $\zeta=\frac{\hat s+\hat u-2l\cdot r}{2k\cdot r-\hat t}$ in the partonic cross section $\hat\sigma$ as well as the prefactors of the subtraction terms (2.90),(2.91). Afterwards, the phase space integration can be performed to all orders in ε for all subtraction terms. This is the key advantage of the procedure.

The HP functions $F\left(\frac{x_0}{w},x_0\right)$, $G\left(\frac{x_0}{w},x_0\right)$ only enter via the subtraction terms (2.90),(2.91). In the $qg\to q$ channel, the gluon emission causes collinear singularities in the form of $\frac{1}{\varepsilon}$ poles. These poles are canceled by the corresponding HP term in the renormalization formula (2.100) (third and fifth line), which will be discussed in more detail below.

The SGP- and SFP-contributions, on the other hand, are also generated *directly* from Feynman propagators in the partonic amplitudes,

$$
\frac{1}{(r-k+k')^2+i\delta}=\frac{1}{(2k\cdot r)(\zeta-1+i\delta)}=\frac{1}{2k\cdot r}\left(\frac{\mathcal{P}}{\zeta-1}-i\pi\,\delta(\zeta-1)\right)\,, \qquad (2.93)
$$

along with (2.68) for the direct SGP-contribution, and

$$\frac{1}{(k'-r)^2+i\delta} = \frac{1}{(2k\cdot r)(-\zeta+i\delta)} = -\frac{1}{2k\cdot r}\left(\frac{\mathcal{P}}{\zeta}+i\pi\,\delta(\zeta)\right), \tag{2.94}$$

for the direct SFP-contribution. In the end, one must add the direct SGP- and SFP-contributions to the respective contributions from the subtraction terms. More details will be given below.

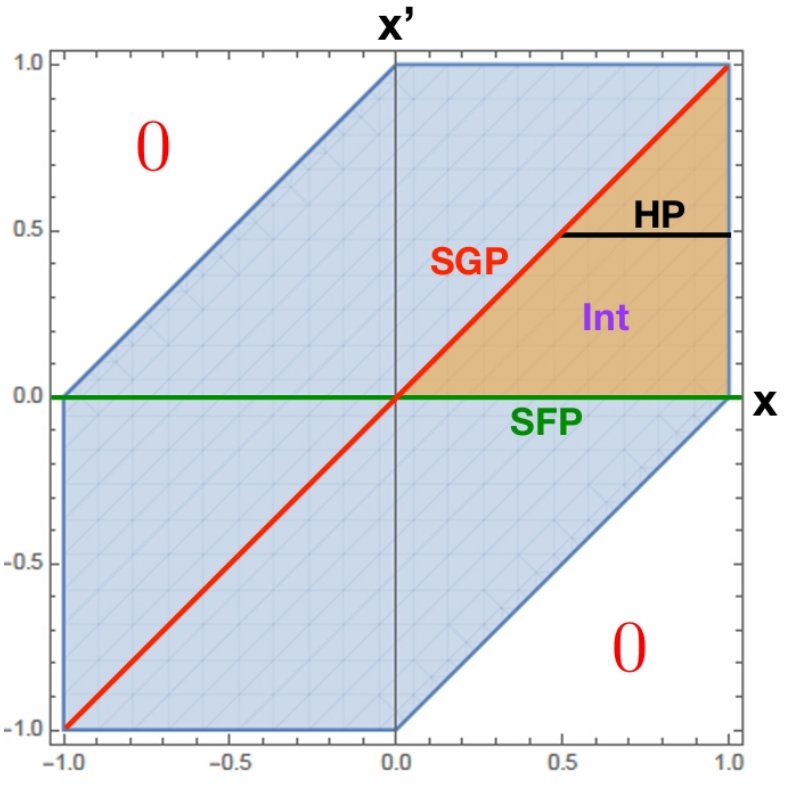

Figure 2.11: Region of support in momentum fractions x, x' of the qgq functions F^q, G^q. The parts probed by the different contributions are indicated by "int" for the integral contributions and "HP", "SGP" and "SFP" for the hard, soft-gluon and soft-fermion poles respectively

The different contributions encountered in this section are depicted in Fig. 2.11, where the corresponding regions of the support in longitudinal momentum fractions x, x' of the qgq functions F^q, G^q are indicated. Although only the colored triangle is probed directly, one needs to keep in mind the symmetry properties of the qgq functions, namely $F^q(x,x') = +F^q(x',x)$ and $G^q(x,x') = -G^q(x',x)$. Thus, one also gains access to the region that is obtained from reflecting the colored triangle about the SGP ($x = x'$) diagonal. Additionally, the behavior under charge conjugation, i.e. $F^{\bar{q}}(x,x') = F^q(-x,-x')$ and $G^{\bar{q}}(x,x') = G^q(-x,-x')$, implies that one can also reflect about the origin because the same support region is probed for antiquarks as for quarks. As will be discussed in the corresponding sections in Ch. 3, the production channels $qq \to q$ (Sec. 3.3) and $qq \to q'$ (Sec. 3.4) feature the qgq functions at different arguments and thus acces the top-left and bottom-right regions in Fig. 2.11. Thus, combining all channels, the full support in x, x' is accessed at NLO.

2.4.3 Photon-in-Lepton Contribution at NLO

For processes like $\ell N \to hX$, collinear singularities at NLO can also be caused by the unobserved final-state lepton, if it is assumed to be massless. This is because the phase space integral contains a configuration where final- and initial-state lepton momenta are collinear. In such a configuration, a quasi-real photon is exchanged between lepton and nucleon and the corresponding photon propagator goes on-shell, causing a divergence. In dimensional regularization, this leads to a $\frac{1}{\varepsilon}$ pole. This happens independently of whether one considers a polarized or unpolarized process. Ref. [120] discusses how one can deal with this issue, choosing either of the following two options:

- Keep a non-zero lepton mass m_ℓ throughout and expand the result around $m_\ell = 0$, only keeping the $\log(m_\ell)$-terms and those of order $\mathcal{O}(m_\ell^0)$
- Work out the NLO contribution for $m_\ell = 0$ and regulate the collinear singularity through dimensional regularization. The singularity is then canceled by a so-called *Weizsäcker-Williams contribution*, generated by the photon-in-lepton density $f_1^{\gamma/\ell}$, see Eq. (C.20)

In the first approach, it becomes more complicated to carry out the phase space integration. Even more so for an all-order-in-ε result (see App. E). Regardless of this disadvantage, the finite lepton mass regulates the aforementioned collinear singularity. In the end, one can expand around $m_\ell = 0$ and a generic partonic factor takes the form (see [120]):

$$\hat{\sigma}_{\mathrm{NLO}}(v, w, m_\ell, \mu) = \hat{\sigma}_{\log}(v, w, \mu)\, \log\left(\tfrac{s}{m_\ell^2}\right) + \hat{\sigma}_0(v, w, \mu) + \mathcal{O}\left(m_\ell^2\, \log\left(m_\ell^2\right)\right) . \tag{2.95}$$

The logarithm in this expression might become rather large and require resummation because of the small lepton mass in its argument. However, this is beyond the scope of this work.

In the second approach one needs to include contributions from quasi-real photons as partons within the lepton, described by $f_1^{\gamma/\ell}$, see Eq. (C.20). Following Ref. [120] and in particular Eq. (23) therein, one makes the following factorization ansatz. For the kinematical twist-3 contributions to the transversely polarized cross section one has

$$\begin{aligned} E_h \frac{\mathrm{d}\sigma_{\mathrm{kin}}^{\mathrm{real}\,\gamma}}{\mathrm{d}\mathbf{P}_h} \quad \propto \quad & \int \frac{\mathrm{d}z}{z^2} \int \mathrm{d}y \int \mathrm{d}x\, \delta\left(y + \tfrac{\hat{t}}{\hat{s}+\hat{u}}\right)\, f_{1,\mathrm{bare}}^{\gamma/\ell}(y)\, D_1^q(z)\, \times \\ & \left[f_{1T}^{\perp(1),q}(x)\, \hat{\sigma}_{\mathrm{kin}}^{\mathrm{real}\,\gamma}(y, x, z)\right] , \end{aligned} \tag{2.96}$$

and for the dynamical contributions,

$$\begin{aligned} E_h \frac{\mathrm{d}\sigma_{\mathrm{dyn}}^{\mathrm{real}\,\gamma}}{\mathrm{d}\mathbf{P}_h} \quad \propto \quad & \int \frac{\mathrm{d}z}{z^2} \int \mathrm{d}y \int \mathrm{d}x \int_{x-1}^{1} \mathrm{d}x'\, \delta\left(y + \tfrac{\hat{t}}{\hat{s}+\hat{u}}\right)\, f_{1,\mathrm{bare}}^{\gamma/\ell}(y)\, D_1^q(z)\, \times \\ & \left[F^q(x, x')\, \hat{\sigma}_{\mathrm{dyn},1}^{\mathrm{real}\,\gamma}(y, x, x', z) + G^q(x, x')\, \hat{\sigma}_{\mathrm{dyn},5}^{\mathrm{real}\,\gamma}(y, x, x', z)\right] . \end{aligned} \tag{2.97}$$

The partonic factors in these formulas are constructed from slightly modified versions of the NLO Feynman diagrams discussed above: the lepton lines are removed and the exchanged virtual photon becomes real with collinear momentum $q^\mu = y\, l^\mu$, where l^μ is the initial lepton's momentum. The partonic factors are of the order $\mathcal{O}(\alpha_{\mathrm{em}}\alpha_s)$ and because of the much simpler phase space, their calculation is straightforward. As before, the necessary imaginary parts for the dynamical contribution (2.97) are generated by propagator poles. Here, only SGP and SFP terms appear due to the absence of propagators like in Eq. (2.83).

Since the renormalized photon-in-lepton distribution $f_1^{\gamma/\ell,\overline{\mathrm{MS}}}(x, \mu)$ in (C.23) is of order $\mathcal{O}(\alpha_{\mathrm{em}})$, the contributions (2.96) and (2.97) are of the order $\mathcal{O}(\alpha_{\mathrm{em}}^2\alpha_s)$. Thus, they can be matched to the other NLO corrections from real-gluon radiation discussed above. In this way, the collinear $\frac{1}{\varepsilon}$ pole of the photon-in-lepton contributions indeed cancels for each partonic channel, providing a good consistency check for the calculation. Moreover, after one combines "partonic photon" and other NLO corrections, the artificial factorization scale μ in (C.23) is canceled. Finally, one arrives at the same conclusion as in Ref. [120]: one exactly recovers the expansion around $m_\ell = 0$ given in Eq. (2.95), meaning that both approaches yield identical results.

2.5 Renormalization of Multiparton Correlation Functions

The *bare* collinear correlation functions, for example in App. C, still contain ultraviolet (UV) divergences. In dimensional regularization, these UV divergences appear as $\frac{1}{\varepsilon}$ poles in a perturbative calculation at order $\mathcal{O}(\alpha_s)$ in the strong coupling constant. Through the process of renormalization, for example using the popular $\overline{\mathrm{MS}}$-scheme, such poles are systemically removed. Although the method is well established for twist-2 matrix elements[5], the renormalization of bare twist-3 functions such as those given in App. C is more complicated since the corresponding splitting kernels are more involved. The necessary formulas for the twist-3 correlation functions will be presented below. This includes the renormalization of the bare qgq function in the soft-gluon pole (SGP) configuration $F_{\mathrm{bare}}^q(x, x)$ as well as the bare $q\gamma q$ functions in the soft-fermion pole

[5] the corresponding $\overline{\mathrm{MS}}$-renormalization equations for the fragmentation functions are given in App. C.5

(SFP) configurations $F^q_{\gamma,\text{bare}}(0,x), G^q_{\gamma,\text{bare}}(0,x)$ and $F^q_{\gamma,\text{bare}}(-x,0), G^q_{\gamma,\text{bare}}(-x,0)$. The former are required for single-inclusive hadron and jet production, while the latter play an important role for photon production.

2.5.1 Renormalization of the Bare qgq Function

The required renormalization formula for the bare SGP function $F^q_{\text{bare}}(x,x)$ is found from the literature, see Ref. [121]. One can read off the relevant splitting function for $F(x,x)$ from the corresponding LO evolution equation given there. Ref. [121] explicitly shows only the non-singlet case in Eq. (43). However, each individual quark flavor q also gets a contribution from the triple-gluon correlation functions $N(x,x'), O(x,x')$[6]. This contribution is independent of the quark flavor q and is thus canceled out in the non-singlet case $q-q'$. The triple-gluon part is given explicitly in Eq. (107) of Ref. [122]. Note that this reference misses some other terms, though, as elaborated on in Ref. [121]. One arrives at the following renormalization formula

$$\begin{aligned}
F^q_{\text{bare}}(x,x,\mu) \;=\;& F^{q,\overline{\text{MS}}}(x,x,\mu) + \frac{\alpha_s(\mu)}{2\pi}\frac{S_\varepsilon}{\varepsilon}\times \\
&\int_x^1 \frac{\mathrm{d}w}{w}\Big[P_{qq}(w)\,F^{q,\overline{\text{MS}}}\left(\tfrac{x}{w},\tfrac{x}{w},\mu\right) \\
&+\frac{N_c}{2}\left(\frac{1+w}{(1-w)_+}F^{q,\overline{\text{MS}}}\left(\tfrac{x}{w},x,\mu\right) - \frac{1+w^2}{(1-w)_+}F^{q,\overline{\text{MS}}}\left(\tfrac{x}{w},\tfrac{x}{w},\mu\right)\right) \\
&+\frac{N_c}{2}\,G^{q,\overline{\text{MS}}}\left(\tfrac{x}{w},x,\mu\right) - N_c\,F^{q,\overline{\text{MS}}}(x,x,\mu)\;\delta(1-w) \\
&+\frac{1}{2N_c}\left((1-2w)\,F^{q,\overline{\text{MS}}}\left(-\tfrac{1-w}{w}x,x,\mu\right) + G^{q,\overline{\text{MS}}}\left(-\tfrac{1-w}{w}x,x,\mu\right)\right) \\
&+2P_{qg}(w)\frac{w}{x}\left(\left(N^{\overline{\text{MS}}}+O^{\overline{\text{MS}}}\right)\left(\tfrac{x}{w},\tfrac{x}{w},\mu\right) - \left(N^{\overline{\text{MS}}}-O^{\overline{\text{MS}}}\right)\left(\tfrac{x}{w},0,\mu\right)\right)\Big] + \mathcal{O}\left(\alpha_s^2\right),
\end{aligned} \tag{2.98}$$

where the renormalization/factorization scale μ is introduced as well as $S_\varepsilon = (4\pi)^\varepsilon/\Gamma(1-\varepsilon)$, a convenient prefactor consistent with the $\overline{\text{MS}}$-scheme at NLO. P_{qq} and P_{qg} are the well-known LO $q\to q$ and $g\to q$ splitting functions (with $C_F = \frac{N_c^2-1}{2N_c} = \frac{4}{3}$ for $N_c=3$, and $T_R = \frac{1}{2}$),

$$\begin{aligned}
P_{qq}(w) &= C_F\left[\frac{1+w^2}{(1-w)_+} + \frac{3}{2}\delta(1-w)\right], \\
P_{qg}(w) &= T_R\left[w^2+(1-w)^2\right].
\end{aligned} \tag{2.99}$$

The numerous different contributions to Eq. (2.98) can be broken down as follows

- The SGP function $F^{q,\overline{\text{MS}}}\left(\frac{x}{w},\frac{x}{w},\mu\right)$ in the second line of (2.98) is generated by quark-quark splitting. Such a term is familiar from the twist-2 PDFs and a similar term is also found in the splitting kernel for the $q\gamma q$ functions below
- The third line of (2.98) includes contributions of the vector-type function F that are $\propto N_c$. They come with a + distribution and one has both a HP configuration $F^{q,\overline{\text{MS}}}\left(\frac{x}{w},x,\mu\right)$ as well as SGP configuration $F^{q,\overline{\text{MS}}}\left(\frac{x}{w},\frac{x}{w},\mu\right)$
- In the fourth line of (2.98) one encounters further contributions $\propto N_c$. These include a non-distributional HP configuration $G^{q,\overline{\text{MS}}}\left(\frac{x}{w},x,\mu\right)$ as well as a SGP contribution $F^{q,\overline{\text{MS}}}(x,x,\mu)$ accompanied b a δ function
- The fifth line of (2.98) is suppressed by an overall factor $\frac{1}{2N_c}$. It includes another type of HP configurations, namely $F^{q,\overline{\text{MS}}}\left(-\frac{1-w}{w}x,x,\mu\right)$ and $G^{q,\overline{\text{MS}}}\left(-\frac{1-w}{w}x,x,\mu\right)$. Notably, these feature a negative first argument and correspond to quark-antiquark-gluon ($q\bar{q}g$) correlations
- Finally, the triple-gluon functions $\left(N^{\overline{\text{MS}}},O^{\overline{\text{MS}}}\right)\left(\frac{x}{w},\frac{x}{w},\mu\right)$ and $\left(N^{\overline{\text{MS}}},O^{\overline{\text{MS}}}\right)\left(\frac{x}{w},0,\mu\right)$ are featured in the last line of (2.98). They enter with the quark-gluon splitting function P_{qg}. Again, these terms are independent of the considered flavor for F^q_{bare} and thus absent in the non-singlet evolution equation

[6] for a definition see Eqs. (C.11) and (C.12)

In addition to the ETQS matrix element $F(x,x)$, the leading order formula (2.64) also includes a contribution from the derivative term $F' = \frac{\mathrm{d}}{\mathrm{d}x}F$. The two terms enter via the combination $\left(1 - x\frac{\mathrm{d}}{\mathrm{d}x}\right) F(x,x)$. Hence, the following $\overline{\mathrm{MS}}$-subtraction is needed

$$
\begin{aligned}
\left(1 - x\tfrac{\mathrm{d}}{\mathrm{d}x}\right) F^q_{\mathrm{bare}}(x,x,\mu) \;&=\; \left(1 - x\tfrac{\mathrm{d}}{\mathrm{d}x}\right) F^{q,\overline{\mathrm{MS}}}(x,x,\mu) + \frac{\alpha_s(\mu)}{2\pi}\frac{S_\varepsilon}{\varepsilon} \times \\
&\int_x^1 \frac{\mathrm{d}w}{w}\left[P_{qq}(w)\left(F^{q,\overline{\mathrm{MS}}} - \frac{x}{w}\left(F^{q,\overline{\mathrm{MS}}}\right)'\right)\left(\tfrac{x}{w},\tfrac{x}{w},\mu\right)\right. \\
&+\frac{N_c}{2}\frac{1+w}{(1-w)_+}\left(F^{q,\overline{\mathrm{MS}}} - \frac{x}{w}\left(\partial_1 F^{q,\overline{\mathrm{MS}}}\right) - x\left(\partial_2 F^{q,\overline{\mathrm{MS}}}\right)\right)\left(\tfrac{x}{w},x,\mu\right) \\
&-\frac{N_c}{2}\frac{1+w^2}{(1-w)_+}\left(F^{q,\overline{\mathrm{MS}}} - \frac{x}{w}\left(F^{q,\overline{\mathrm{MS}}}\right)'\right)\left(\tfrac{x}{w},\tfrac{x}{w},\mu\right) \\
&+\frac{N_c}{2}\left(G^{q,\overline{\mathrm{MS}}} - \frac{x}{w}\left(\partial_1 G^{q,\overline{\mathrm{MS}}}\right) - x\left(\partial_2 G^{q,\overline{\mathrm{MS}}}\right)\right)\left(\tfrac{x}{w},x,\mu\right) \\
&-N_c\left(F^{q,\overline{\mathrm{MS}}} - x\left(F^{q,\overline{\mathrm{MS}}}\right)'\right)(x,x,\mu)\,\delta(1-w) \\
&+\frac{1}{2N_c}\left(F^{q,\overline{\mathrm{MS}}}\left(-\tfrac{1-w}{w}x,x,\mu\right) - \delta(1-w)\,F^{q,\overline{\mathrm{MS}}}(0,x,\mu)\right) \\
&+\frac{1}{2N_c}\left(G^{q,\overline{\mathrm{MS}}}\left(-\tfrac{1-w}{w}x,x,\mu\right) + \delta(1-w)\,G^{q,\overline{\mathrm{MS}}}(0,x,\mu)\right) \\
&-\frac{1}{2N_c}\left((1-2w)\,x\left[\partial_1 F^{q,\overline{\mathrm{MS}}} + \partial_2 F^{q,\overline{\mathrm{MS}}}\right]\left(-\tfrac{1-w}{w}x,x,\mu\right)\right) \\
&-\frac{1}{2N_c}\left(x\left[\partial_1 G^{q,\overline{\mathrm{MS}}} + \partial_2 G^{q,\overline{\mathrm{MS}}}\right]\left(-\tfrac{1-w}{w}x,x,\mu\right)\right) \\
&+\left(1-2w^2+\delta(1-w)\right)\times \\
&\left.\frac{w}{x}\left(\left(N^{\overline{\mathrm{MS}}} + O^{\overline{\mathrm{MS}}}\right)\left(\tfrac{x}{w},\tfrac{x}{w},\mu\right) - \left(N^{\overline{\mathrm{MS}}} - O^{\overline{\mathrm{MS}}}\right)\left(\tfrac{x}{w},0,\mu\right)\right)\right] + \mathcal{O}\left(\alpha_s^2\right)\,,
\end{aligned}
\tag{2.100}
$$

where a shorthand is used for the derivatives with respect to the first (second) argument of the correlation functions, $(\partial_1(\partial_2)(F,G))\,(x,x')$. The notation is defined in Eq. C.6. Note that integration by parts is applied for terms with a derivative of N or O. The even larger number of different contributions to the renormalization formula (2.100) can be broken down in a similar way as for Eq. (2.98) above. Note that the x-derivative can not only act directly on the integrand but also on the lower integration boundary in (2.98). This generates additional boundary terms which are accompanied by a $\delta(1-w)$ in (2.100).

2.5.2 Renormalization of the Bare $q\gamma q$ Functions

Eq. (2.100) provides the only twist-3 renormalization needed for single-inclusive hadron production, $\ell N^\uparrow \to hX$. On the other hand, photon production, $\ell N^\uparrow \to \gamma X$, requires several other formulas. The process features an interference channel that contains $q\gamma q$ functions defined in Eq. (C.7) and $g\gamma g$ functions defined in Eq. (C.8), which have quite involved splitting kernels as well. To the best of the author's knowledge, these results are not available in the literature; the derivation for $q\gamma q$ follows below. To be more precise, one needs renormalization for a $q\bar{q}\gamma$ configuration. This means that a quark and antiquark emitted from the nucleon participate in the partonic scattering process on one side of the final state cut and only an emitted photon on the other side of the cut. Consequently, the distribution functions enter as $F^q_\gamma(x'-x,x')$ and $G^q_\gamma(x'-x,x')$. Notably, this is a different combination of x, x' in their arguments compared to the hadron production case. The splitting kernel receives contributions from three types of mixing, namely with:

1. The qgq functions F^q, G^q
2. Themselves, the $q\gamma q$ functions F^q_γ, G^q_γ
3. The $g\gamma g$ functions O^1_γ, O^2_γ

Mixing of $q\gamma q$ with qgq

Starting with the qgq part of the splitting kernel, the relevant Feynman diagrams are shown in Fig. 2.12. Let $\mathcal{A}$ denote the amplitude of the left-hand side of the final-state cut and $\mathcal{B}$ of the

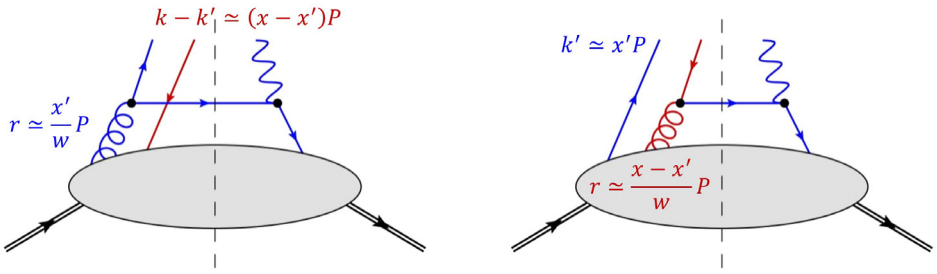

Figure 2.12: Feynman diagrams required for the splitting kernel of the $q\gamma q$ functions. These diagrams contribute to the mixing of $q\gamma q$ with qgq functions.

right-hand side for a given diagram. Then, the contribution to the renormalization formula from that diagram is schematically given by

$$\int \frac{\mathrm{d}^d k}{(2\pi)^d}\delta(k\cdot n - x)\int \frac{\mathrm{d}^d k'}{(2\pi)^d}\delta(k'\cdot n - x')\int \frac{\mathrm{d}^d q}{(2\pi)^{d-1}}\delta^+(q^2)\sum_X (2\pi)^d \delta^{(d)}(k+q-(P-P_X))\mathcal{A}\mathcal{B}^* \,. \tag{2.101}$$

The momentum q of the quark line going through the cut is restricted by a delta function $\delta^+(q^2) = \theta(q\cdot n)\delta(q^2)$, alongside a Heaviside step function.

For the right diagram of Fig. 2.12 one employs the collinear approximation $k' \approx x'P$ for the quark and $r \approx \xi P$ for the gluon. Demanding that the antiquark (drawn in red in Fig. 2.12) is collinear to the gluon and takes a fraction w of its momentum, one finds $\xi = \frac{x-x'}{w}$. Similarly, for the left diagram the correct approximations are $k - k' \approx (x - x')P$ and $r \approx \frac{x'}{w}P$.

Next, the functions F_γ^q, G_γ^q can be projected out from their corresponding correlator $\Phi_\gamma^{q,\rho}$ via

$$\begin{aligned} F_\gamma^q &= \frac{i}{2M}\epsilon_\rho{}^{PnS}\,\mathrm{Tr}\left[\not{n}\Phi_\gamma^{q,\rho}\right] \\ G_\gamma^q &= \frac{1}{2M}\left(S_T\right)_\rho \mathrm{Tr}\left[\gamma_5\not{n}\Phi_\gamma^{q,\rho}\right] \,. \end{aligned} \tag{2.102}$$

Subsequently, one can carry out the algebra for the Dirac traces, which can be done in $d = 4$ dimensions. The reason is that one only needs to extract the $\frac{1}{\varepsilon}$ pole in the end. The $\mathcal{O}(\varepsilon)$ corrections that one would get from calculating the traces for non-zero ε are irrelevant. The resulting expression will still contain an integral over the transverse component k_T of the quark momentum, which has to be done in $d = 4 - 2\varepsilon$ dimensions since it is the origin of the $\frac{1}{\varepsilon}$ pole. Notably, one will encounter terms $\propto (k_T\cdot S_T)^2$ in the integrand, which can be handled using the identity

$$\int \mathrm{d}^{d-2}k_T\,(k_T\cdot S_T)^2\, f\left(k_T^2\right) = \int \mathrm{d}^{d-2}k_T\left(\frac{-k_T^2}{d-2}\right) f\left(k_T^2\right) \,. \tag{2.103}$$

This is equivalent to a replacement $(k_T\cdot S_T)^2 \to -k_T^2/2 + \mathcal{O}(\varepsilon)$ inside the integrand. Afterwards, one is left with just one integral, namely

$$\begin{aligned} \int \frac{\mathrm{d}^{d-2}k_T}{(2\pi)^{d-2}k_T^2} &= -\frac{\Omega(d-2)}{(2\pi)^{d-2}}\int_0^\infty \mathrm{d}|\boldsymbol{k_T}|\,|\boldsymbol{k_T}|^{d-5} \\ &= -\frac{2\pi^{1-\varepsilon}}{\Gamma(1-\varepsilon)(2\pi)^{2-2\varepsilon}}\left(\underbrace{\int_0^\mu \mathrm{d}k\,k^{-1-2\varepsilon_{\mathrm{IR}}}}_{\text{IR part}} + \underbrace{\int_\mu^\infty \mathrm{d}k\,k^{-1-2\varepsilon_{\mathrm{UV}}}}_{\text{UV part}}\right) \\ &\xrightarrow{\text{UV limit}} -\frac{S_\varepsilon}{2\pi}\frac{\mu^{-2\varepsilon}}{2\varepsilon} \,, \end{aligned} \tag{2.104}$$

where $\Omega(d) = 2\pi^{d/2}/\Gamma(d/2)$ is the solid angle in d dimensions and $S_\varepsilon \equiv (4\pi)^\varepsilon/\Gamma(1-\varepsilon)$ is a convenient constant for $\overline{\mathrm{MS}}$ subtraction. The crucial point is that only the UV part is kept. The IR part, however, is not considered for renormalization and it is not well-defined in a perturbative

context. Putting everything together one obtains

$$
\begin{aligned}
F^q_{\gamma,\text{bare}}(x'-x,x',\mu) \;=\;& F^{q,\overline{\text{MS}}}_\gamma(x'-x,x',\mu) \,+\, \frac{\alpha_{em}}{2\pi}\frac{S_\varepsilon}{2\varepsilon}e_q\int\frac{\mathrm{d}w}{w}\frac{\theta\left(\frac{1-w}{w}(x-x')\right)}{x-x'(1-w)}\times \\
&\Big[\left(x\left(w-(1-w)^2\right)+x'(1-w)(1-2w)\right)F^{q,\overline{\text{MS}}}\left(x'+\tfrac{x-x'}{w},x',\mu\right) \\
&+\left(x'(1-w)-x\left(w+(1-w)^2\right)\right)G^{q,\overline{\text{MS}}}\left(x'+\tfrac{x-x'}{w},x',\mu\right)\Big] \\
&+\frac{\alpha_{em}}{2\pi}\frac{S_\varepsilon}{2\varepsilon}e_q\int\frac{\mathrm{d}w}{w}\frac{\theta\left(\frac{1-w}{w}x'\right)}{xw+x'(1-w)}\times \\
&\Big[\left(xw^2-x'(1-w)(1-2w)\right)F^{q,\overline{\text{MS}}}\left(x'-x,x'-x-\tfrac{x'}{w},\mu\right) \\
&+\left(xw^2+x'(1-w)\right)G^{q,\overline{\text{MS}}}\left(x'-x,x'-x-\tfrac{x'}{w},\mu\right)\Big]\,+\,\ldots
\end{aligned}
\tag{2.105}
$$

$$
\begin{aligned}
G^q_{\gamma,\text{bare}}(x'-x,x',\mu) \;=\;& G^{q,\overline{\text{MS}}}_\gamma(x'-x,x',\mu) \,+\, \frac{\alpha_{em}}{2\pi}\frac{S_\varepsilon}{2\varepsilon}e_q\int\frac{\mathrm{d}w}{w}\frac{\theta\left(\frac{1-w}{w}(x-x')\right)}{x-x'(1-w)}\times \\
&\Big[\left(x'(1-w)-x\left(w+(1-w)^2\right)\right)F^{q,\overline{\text{MS}}}\left(x'+\tfrac{x-x'}{w},x',\mu\right) \\
&+\left(x\left(w-(1-w)^2\right)+x'(1-w)(1-2w)\right)G^{q,\overline{\text{MS}}}\left(x'+\tfrac{x-x'}{w},x',\mu\right)\Big] \\
&+\frac{\alpha_{em}}{2\pi}\frac{S_\varepsilon}{2\varepsilon}e_q\int\frac{\mathrm{d}w}{w}\frac{\theta\left(\frac{1-w}{w}x'\right)}{xw+x'(1-w)}\times \\
&\Big[\left(xw^2+x'(1-w)\right)F^{q,\overline{\text{MS}}}\left(x'-x,x'-x-\tfrac{x'}{w},\mu\right) \\
&+\left(xw^2-x'(1-w)(1-2w)\right)G^{q,\overline{\text{MS}}}\left(x'-x,x'-x-\tfrac{x'}{w},\mu\right)\Big]\,+\,\ldots\,,
\end{aligned}
\tag{2.107}
$$

for the vector-type $q\gamma q$ function F^q_γ. Analogously, the result for the axial-vector-type function G^q_γ reads

where the ellipsis indicates higher order terms of the splitting kernel as well as the contributions for mixing with $q\gamma q$ and $g\gamma g$ functions. The expressions are rather lengthy but they share a lot of similarities and can be broken down as follows

- The first integrals in (2.105) and (2.107) are generated by the diagram on the right of Fig. 2.12. They feature the qgq functions $F^{q,\overline{\text{MS}}}\left(x'+\frac{x-x'}{w},x',\mu\right)$ and $G^{q,\overline{\text{MS}}}\left(x'+\frac{x-x'}{w},x',\mu\right)$, which are evaluated at positive arguments. For $x'=x$, a SGP contribution $F^{q,\overline{\text{MS}}}(x,x,\mu)$ is generated, while $G^{q,\overline{\text{MS}}}$ vanishes in this case
- The second integrals in the above formulas are generated by the diagram on the left of 2.12 and feature $\left(F^{q,\overline{\text{MS}}},G^{q,\overline{\text{MS}}}\right)\left(x'-x,x'-x-\frac{x'}{w},\mu\right)$. The arguments are negative for $0<x'<x$ and thus one can interpret these as antiquark contributions. For $x'=x$, antiquark SFP configurations $\left(F^{\bar q,\overline{\text{MS}}},G^{\bar q,\overline{\text{MS}}}\right)\left(\frac{x}{w},0,\mu\right)$ are generated

In the actual calculation (see Ch. 5), one only needs the two SFP configurations of $x'=x$ and $x'=0$. For the former case one finds the following simplified formulas

$$
\begin{aligned}
F^q_{\gamma,\text{bare}}(0,x,\mu) \;=\;& F^{q,\overline{\text{MS}}}_\gamma(0,x,\mu) \,+\, \frac{\alpha_{em}}{2\pi}\frac{S_\varepsilon}{2\varepsilon}e_qF^{q,\overline{\text{MS}}}(x,x,\mu) \,+\, \frac{\alpha_{em}}{2\pi}\frac{S_\varepsilon}{2\varepsilon}e_q\int_x^1\frac{\mathrm{d}w}{w}\times \\
&\Big[\left(w-(1-w)^2\right)F^{q,\overline{\text{MS}}}\left(-\tfrac{x}{w},0,\mu\right)-\left(w+(1-w)^2\right)G^{q,\overline{\text{MS}}}\left(-\tfrac{x}{w},0,\mu\right)\Big]\,+\,\ldots \\
G^q_{\gamma,\text{bare}}(0,x,\mu) \;=\;& G^{q,\overline{\text{MS}}}_\gamma(0,x,\mu) \,-\, \frac{\alpha_{em}}{2\pi}\frac{S_\varepsilon}{2\varepsilon}e_qF^{q,\overline{\text{MS}}}(x,x,\mu) \,+\, \frac{\alpha_{em}}{2\pi}\frac{S_\varepsilon}{2\varepsilon}e_q\int_x^1\frac{\mathrm{d}w}{w}\times \\
&\Big[\left(w+(1-w)^2\right)F^{q,\overline{\text{MS}}}\left(-\tfrac{x}{w},0,\mu\right)-\left(w-(1-w)^2\right)G^{q,\overline{\text{MS}}}\left(-\tfrac{x}{w},0,\mu\right)\Big]\,+\,\ldots\,,
\end{aligned}
\tag{2.108}
$$

where the qgq functions for quark q at negative arguments can be related to the corresponding function for antiquark $\bar q$ via $F^q(-x,-x')=F^{\bar q}(x,x')$ and $G^q(-x,-x')=G^{\bar q}(x,x')$. The second case of SFP functions, i.e. $F_\gamma(-x,0),G_\gamma(-x,0)$, can be obtained from Eqs. (2.105) and (2.107) by setting $x'=0$ or alternatively from Eq. (2.108) by replacing $x\to-x$ as well as using the symmetry of F^q,F^q_γ and the antisymmetry of G^q,G^q_γ under interchange of their arguments. Both approaches are consistent with each other, which provides a small check on the correctness of the derivation.

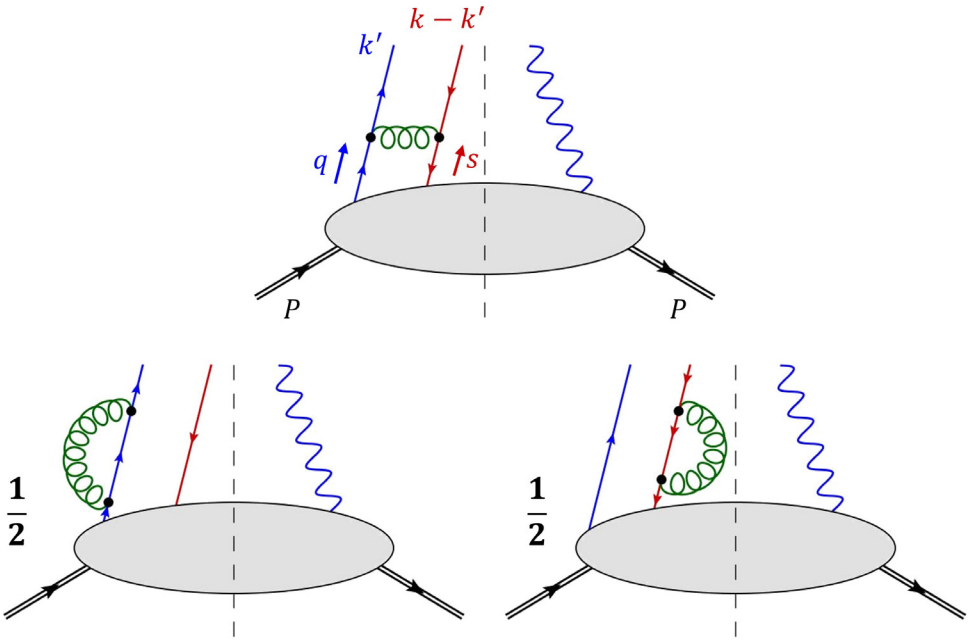

Figure 2.13: Feynman diagrams required for the splitting kernel of the $q\gamma q$ functions. These diagrams contribute to the mixing of $q\gamma q$ functions with themselves.

Mixing of $q\gamma q$ with $q\gamma q$

The second part of the $q\gamma q$ splitting kernel describes their self-mixing; the relevant Feynman diagrams are shown in Fig. 2.13. Note the important factors of 1/2 for the (anti-)quark self-energy diagrams in the bottom of Fig. 2.13. They originate from the Z_2 renormalization factor of the quark propagator and their appearance is well known from the derivation of evolution equations of the ordinary twist-2 PDFs, see for example Ref. [123]. Notably, the contribution from the diagrams of Fig. 2.13 to the correlator $\Phi_\gamma^{q,\rho}(x'-x,x')$ has a different schematic form than Eq. (2.101). The reason is that there is no longer a quark line crossing the final state cut and consequently one has

$$\int \frac{\mathrm{d}^d k}{(2\pi)^d}\delta(k\cdot n - x)\int \frac{\mathrm{d}^d k'}{(2\pi)^d}\delta(k'\cdot n - x')\sum_X (2\pi)^d \delta^{(d)}(k-(P-P_X))\mathcal{A}\mathcal{B}^* \,. \tag{2.109}$$

Top Diagram Consider first the top diagram in Fig. 2.13 and apply the collinear approximation $q \approx \xi P$, $k \approx xP$. Unlike the qgq calculation, ξ cannot be fixed immediately for the terms below. Moreover, there is no on-shell condition for any particle crossing the final state cut in this diagram. Consequently, there is one less δ function available than before and one more integral to be evaluated. Applying Eq. (2.102) to project out F_γ^q, G_γ^q from the corresponding correlator leads to the intermediate result

$$\begin{aligned}
F_\gamma^q(x'-x,x') &= \frac{-i}{2}\alpha_s C_F \int \mathrm{d}\xi \int \frac{\mathrm{d}^{d-2}k'_T}{(2\pi)^{d-2}}\int_{-\infty}^{\infty}\frac{\mathrm{d}b'}{2\pi} F_\gamma^q(\xi-x,\xi)\,\times \\
&\qquad \frac{g_\perp^{\lambda\eta}(\xi P-k')\mathrm{Tr}\left[\not{n}\not{k}'\gamma_\lambda \not{P}\gamma_\eta\left(\not{k}'-x\not{P}\right)\right]}{\left((\xi P-k')^2+i\delta\right)\left((k')^2+i\delta\right)\left((k'-xP)^2+i\delta\right)} \\
G_\gamma^q(x'-x,x') &= \frac{-i}{2}\alpha_s C_F \int \mathrm{d}\xi \int \frac{\mathrm{d}^{d-2}k'_T}{(2\pi)^{d-2}}\int_{-\infty}^{\infty}\frac{\mathrm{d}b'}{2\pi} G_\gamma^q(\xi-x,\xi)\,\times \\
&\qquad \frac{g_\perp^{\lambda\eta}(\xi P-k')\mathrm{Tr}\left[\gamma_5\not{n}\not{k}'\gamma_\lambda \not{P}\gamma_5\gamma_\eta\left(\not{k}'-x\not{P}\right)\right]}{\left((\xi P-k')^2+i\delta\right)\left((k')^2+i\delta\right)\left((k'-xP)^2+i\delta\right)},
\end{aligned} \tag{2.110}$$

with the quark momentum k' given by the decomposition $k' = x'P + b'n + k'_T$. Furthermore, the transverse projector of momentum p is defined as $g_\perp^{\mu\nu}(p) = g^{\mu\nu} - (p_\mu n_\nu + p_\nu n_\mu)/(p\cdot n)$.

One must explicitly keep the causal imaginary part in the Feynman propagators, denoted here as $i\delta$, since the next step is to use contour integration for the b' integral. In the end, one is again

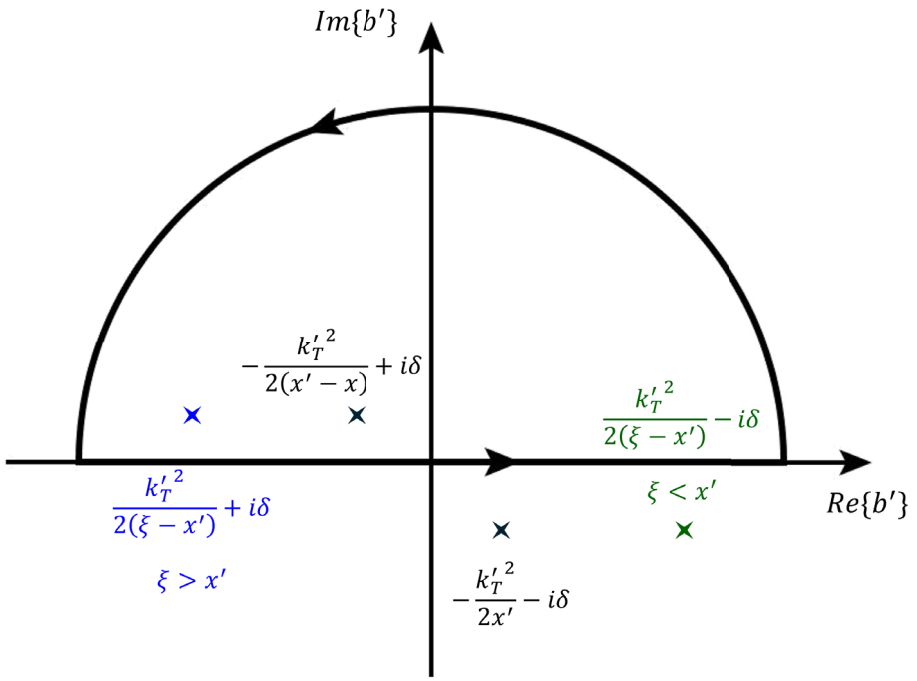

Figure 2.14: Sketch of the integration contour for the b' integrals in Eq. (2.110) including the position of all poles for $0 < x' < x$. One has to distinguish between the cases $\xi > x'$ and $\xi < x'$ shown in blue and green respectively.

interested in the SFP configurations $x' = x$ and $x' = 0$ and hence it is practical to assume $0 < x' < x$ to determine the position of the poles in the complex b'-plane. A sketch of the integration contour including the position of all poles is shown in Fig. 2.14. One must separate the cases $\xi > x'$ (displayed in blue), where two poles are inside the contour, and $\xi < x'$ (displayed in green), where only one pole is inside the contour. Computing the necessary residues is straightforward and one obtains the following schematic form for both F_γ^q and G_γ^q

$$F_\gamma^q\left(x'-x,x'\right) \propto \int_{-1+x}^{1} \mathrm{d}\xi \left(\int \frac{\mathrm{d}^{d-2}k_T'}{(2\pi)^{d-2}\left(k_T'\right)^2} \right) F_\gamma^q(\xi-x,\xi)\left(\theta(\xi-x')A(x,x',\xi)+B(x,x',\xi)\right) , \tag{2.111}$$

where the boundaries on the ξ integral follow directly from the support properties of $F_\gamma^q(\xi-x,\xi)$ and θ denotes the Heaviside step function. The k_T' integral is the same as before, see Eq. (2.104), and generates a $\frac{1}{\varepsilon}$ pole.

According to the step function, one splits up the ξ integral into one part over the interval $(-1+x, x')$ and a second part over the interval $(x', 1)$. For the former one employs the substitution $\xi = x - \frac{x-x'}{w}$ and for the latter $\xi = \frac{x'}{w}$. These substitutions may not seem intuitive. They can, however, be motivated physically: assume the collinear approximation $k \approx xP, k' \approx x'P$. Furthermore, assume that the quark of momentum k' participating in the hard scattering is collinear to the quark emitted from the nucleon with momentum q. Denoting the momentum fraction as w, i.e. $k' = wq$ one finds $k' = wq = x'P \Rightarrow \xi = \frac{x'}{w}$. Analogously, if the antiquark with momentum $k - k'$ is collinear to the emitted antiquark from the nucleon with momentum s and takes a fraction w of its momentum, then one has $k - k' = ws = (x - x')P \Rightarrow \xi = x - \frac{x-x'}{w}$. Using these substitutions, one finds for the contribution of the top diagram in Fig. 2.13

$$\begin{aligned}
F_\gamma^q\left(x'-x,x'\right) &= \frac{\alpha_s}{2\pi}\frac{S_\varepsilon}{\varepsilon}C_F\left(\int_{x-x'}^{1}\frac{\mathrm{d}w}{w}\frac{x-x'(1-w)}{x(1-w)}F_\gamma^q\left(\tfrac{x'-x}{w},x-\tfrac{x-x'}{w}\right)\right. \\
&\quad \left. +\int_{x'}^{1}\frac{\mathrm{d}w}{w}\frac{xw+x'(1-w)}{x(1-w)}F_\gamma^q\left(\tfrac{x'}{w}-x,\tfrac{x'}{w}\right)\right)+\dots \\
G_\gamma^q\left(x'-x,x'\right) &= \frac{\alpha_s}{2\pi}\frac{S_\varepsilon}{\varepsilon}C_F\left(\int_{x-x'}^{1}\frac{\mathrm{d}w}{w}\frac{x-x'(1-w)}{x(1-w)}G_\gamma^q\left(\tfrac{x'-x}{w},x-\tfrac{x-x'}{w}\right)\right. \\
&\quad \left. +\int_{x'}^{1}\frac{\mathrm{d}w}{w}\frac{xw+x'(1-w)}{x(1-w)}G_\gamma^q\left(\tfrac{x'}{w}-x,\tfrac{x'}{w}\right)\right)+\dots ,
\end{aligned} \tag{2.112}$$

where the ellipsis indicates the contributions by other diagrams as well as higher order terms. Interestingly, the formulas for F_γ^q and G_γ^q are of identical form.

Self-Energy Diagrams Moving on with the two self-energy diagrams at the bottom of Fig. 2.13, it turns out that they both give the same contribution. So, in the following, only the computation of the bottom-left diagram is discussed. It is noteworthy that these kinds of diagrams are in fact familiar from the derivation of evolution kernels of ordinary twist-2 PDFs, see Ref. [123]. Here, a direct and explicit approach will be shown for their evaluation. One starts again with the schematic form of Eq. (2.109) but, in contrast to before, one does not apply any collinear approximation just yet. Labeling the momentum of the gluon in the loop as r (the green gluon line in Fig. 2.13, bottom left), one has to deal with the following loop integral

$$\mathcal{J}(k') \equiv \int \frac{\mathrm{d}^d r}{(2\pi)^d} \frac{\not{k}' \gamma_\lambda \left(\not{k}' - \not{r}\right) \gamma_\eta g_\perp^{\lambda\eta}(r)}{(r^2 + i\delta)\left((k')^2 + i\delta\right)\left((r-k')^2 + i\delta\right)}\,, \tag{2.113}$$

where again the transverse projector $g_\perp$ appears because of the choice of light-cone gauge, cf. App. D. Since this projector is now in terms of the loop momentum r one also has to explicitly include the $i\delta$ shown in the definition of Eq. (2.70). Another consequence is that a non-quadratic denominator enters the integral. For this specific part one cannot apply the Feynman parameter method, cf. Eq. (2.17), and contour integration will be used instead. Thus, one first splits up the loop integral according to the two terms in $g_\perp$. While doing so, one can already apply an identity from Eq. (2.8) for a first small simplification

$$\begin{aligned}\mathcal{J}(k') \;=\; & \int \frac{\mathrm{d}^d r}{(2\pi)^d} \frac{-2(1-\varepsilon)\not{k}'\left(\not{k}' - \not{r}\right)}{(r^2 + i\delta)\left((k')^2 + i\delta\right)\left((r-k')^2 + i\delta\right)} \\ & - \int \frac{\mathrm{d}^d r}{(2\pi)^d} \frac{\not{k}'\not{r}\left(\not{k}' - \not{r}\right)\not{n} + \not{k}'\not{n}\left(\not{k}' - \not{r}\right)\not{r}}{(r^2 + i\delta)\left((k')^2 + i\delta\right)\left((r-k')^2 + i\delta\right)(r\cdot n + i\delta)} \equiv \mathcal{J}_1(k') - \mathcal{J}_2(k')\,.\end{aligned} \tag{2.114}$$

Here, the first integral $\mathcal{J}_1(k')$ only contains quadratic denominators and the Feynman parameter method can be applied. Then, because the integral of an antisymmetric integrand vanishes, one is left with $\not{k}'\not{k}' = (k')^2$ in the numerator, which cancels the corresponding denominator and one can subsequently set $(k')^2 = 0$. After a Wick rotation of the remaining r integral it can be handled in much the same way as previously the k_T integral in Eq. (2.104), also discarding its IR part. As a result one finds a rather compact expression

$$\mathcal{J}_1(k') \;=\; \frac{-i}{(4\pi)^2}\mu^{-2\varepsilon}\frac{S_\varepsilon}{\varepsilon}\,. \tag{2.115}$$

For the second integral, one first rewrites the numerator in a suitable way

$$\not{k}'\not{r}\left(\not{k}' - \not{r}\right)\not{n} + \not{k}'\not{n}\left(\not{k}' - \not{r}\right)\not{r} = -2(k')^2\, n\cdot r - \left(r^2 + (r-k')^2 - (k')^2\right)\not{k}'\not{n} + 2x'\not{k}'\not{r}\,, \tag{2.116}$$

where the anti-commutation relations of the gamma matrices were used, as well as $k'\cdot n = x'$.

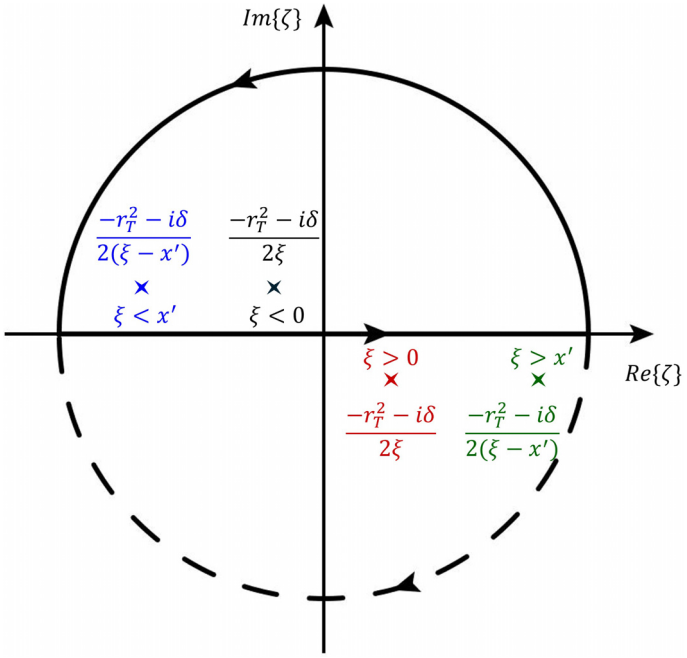

Figure 2.15: Sketch of the integration contour for the ζ integral in Eq. (2.120), including the position of all poles for $0 < x' < x$. Only the case $0 < \xi < x'$ gives a non-zero contribution and corresponds to the poles marked in red and blue.

Subsequently, one can further separate the integral accordingly

$$\begin{aligned}
\mathcal{J}_2(k') &= \not{k}'\not{n}\int \frac{\mathrm{d}^d r}{(2\pi)^d}\frac{1}{(r^2+i\delta)\left((r-k')^2+i\delta\right)(r\cdot n+i\delta)} \\
&\quad + \frac{-\not{k}'\not{n}}{\left((k')^2+i\delta\right)}\left(\int \frac{\mathrm{d}^d r}{(2\pi)^d}\frac{r^2}{(r^2+i\delta)\left((r-k')^2+i\delta\right)(r\cdot n+i\delta)}\right. \\
&\qquad \left. + \int \frac{\mathrm{d}^d r}{(2\pi)^d}\frac{(r-k')^2}{(r^2+i\delta)\left((r-k')^2+i\delta\right)(r\cdot n+i\delta)}\right) \\
&\quad - 2\int \frac{\mathrm{d}^d r}{(2\pi)^d}\frac{r\cdot n}{(r^2+i\delta)\left((r-k')^2+i\delta\right)(r\cdot n+i\delta)} \\
&\quad + \frac{2x'\not{k}'}{\left((k')^2+i\delta\right)}\gamma_\alpha\int \frac{\mathrm{d}^d r}{(2\pi)^d}\frac{r^\alpha}{(r^2+i\delta)\left((r-k')^2+i\delta\right)(r\cdot n+i\delta)} \\
&= \not{k}'\not{n}\mathcal{J}_{2,1}(k') - \frac{\not{k}'\not{n}}{\left((k')^2+i\delta\right)}\left(\mathcal{J}_{2,2}(k')+\mathcal{J}_{2,3}(k')\right) \\
&\quad - 2\mathcal{J}_{2,4}(k') + \frac{2x'\not{k}'}{\left((k')^2+i\delta\right)}\gamma_\alpha\mathcal{J}^\alpha_{2,5}(k')\,. \qquad (2.117)
\end{aligned}$$

Again, explicit factors of $(k')^2$ are canceled against the term $(k')^2 + i\delta$ in the denominator where possible. It is convenient to also decompose $\mathcal{J}^\alpha_{2,5}$ as much as possible. Notice that its integrand only contains k' and n such that in general it must be of the form $\mathcal{J}^\alpha_{2,5} = A(k')^\alpha + Bn^\alpha$. By contracting both sides of this ansatz with k'_α and n_α one finds expressions for the coefficients A, B. They are given in terms of the other integrals in the decomposition (2.117)

$$A = \frac{\mathcal{J}_{2,4}}{x'}, \quad B = \frac{1}{x'}\left(\frac{(k')^2}{2}\mathcal{J}_{2,1} + \frac{\mathcal{J}_{2,2}}{2} - \frac{\mathcal{J}_{2,3}}{2} - \frac{(k')^2}{x'}\mathcal{J}_{2,4}\right). \qquad (2.118)$$

Plugging this back into Eq. (2.117) leads to a considerable simplification

$$\mathcal{J}_2\left(k'\right) \,=\, 2\not{k}'\not{n}\left(\mathcal{J}_{2,1} - \frac{\mathcal{J}_{2,3}}{\left(k'\right)^2 + i\delta} - \frac{\mathcal{J}_{2,4}}{x'}\right). \tag{2.119}$$

The next thing to note is that $\mathcal{J}_{2,3}$ vanishes as $\delta \to 0$ since the integrand becomes antisymmetric. Thus, only $\mathcal{J}_{2,1}$ and $\mathcal{J}_{2,4}$ remain. Both can be evaluated using the same strategy. The loop momentum r is decomposed as $r^\mu = \xi P^\mu + \zeta n^\mu + r_T^\mu$ and the ζ integral is computed using the residue theorem. One can set $k' = x'P$ right away because of the absence of $\left(k'\right)^2$ in the denominators and after a bit of simplification one finds

$$\mathcal{J}_{2,1} - \frac{\mathcal{J}_{2,4}}{x'} \,=\, \int_{-\infty}^{\infty}\frac{\mathrm{d}\xi}{2\pi}\frac{1-\frac{\xi}{x'}}{\xi+i\delta}\int\frac{\mathrm{d}^{d-2}r_T}{(2\pi)^{d-2}}\frac{i}{4\xi(\xi-x')}\int_{-\infty}^{\infty}\frac{\mathrm{d}\zeta}{2\pi i}\frac{1}{\left(\zeta-\frac{-r_T^2-i\delta}{2\xi}\right)\left(\zeta-\frac{-r_T^2-i\delta}{2(\xi-x')}\right)}. \tag{2.120}$$

While the residues of the two poles are easy to compute, one has to take some care in determining the positions of the poles in the complex ζ plane, which is sketched in Fig 2.15. The pole structure depends on whether $\xi > 0$ or $\xi < 0$ and whether $\xi > x'$ or $\xi < x'$. From the fact that one could close the semi-circle contour in either the upper or lower half-plane it is apparent that the poles must be located on opposite sides of the real axis. Since the end result is needed in particular for $x' = x$ and $x' = 0$, i.e. the SFP configurations, it is pragmatic to work with $0 < x' < x$. Then it follows that $0 < \xi < x'$ is the only region with a non-vanishing contribution. After application of the residue theorem and some simplification, the r_T integral is the same as in Eq. (2.104). Employing a substitution $\xi = x'\alpha$ one arrives at the result

$$\mathcal{J}_{2,1} - \frac{\mathcal{J}_{2,4}}{x'} \,=\, \frac{-i}{(4\pi)^2}\mu^{-2\varepsilon}\frac{S_\varepsilon}{\varepsilon}\left(-\frac{1}{x'}\int_0^1\frac{1-\alpha}{\alpha+i\delta}\mathrm{d}\alpha\right) \,=\, -\frac{\mathcal{J}_1}{x'}\int_0^1\frac{1-\alpha}{\alpha+i\delta}\mathrm{d}\alpha\,, \tag{2.121}$$

with the loop integral $\mathcal{J}_1$ of Eq. (2.115). Lastly, after projecting out F_γ^q, G_γ^q from the corresponding correlator as previously, carrying out the remaining Dirac traces and simplifying the result while making a small substitution $\alpha \to 1-\alpha$ one finds the following contribution from each of the bottom diagrams in Fig. 2.13 to the $q\gamma q$ splitting kernel

$$\begin{aligned}
F_\gamma^q\left(x'-x,x'\right) &= -\frac{\alpha_s}{2\pi}C_F\frac{S_\varepsilon}{\varepsilon}F_\gamma^q\left(x'-x,x'\right)\left(-\frac{3}{2}+2\int_0^1\frac{\mathrm{d}\alpha}{1-\alpha+i\delta}\right)+\dots \\
G_\gamma^q\left(x'-x,x'\right) &= -\frac{\alpha_s}{2\pi}C_F\frac{S_\varepsilon}{\varepsilon}G_\gamma^q\left(x'-x,x'\right)\left(-\frac{3}{2}+2\int_0^1\frac{\mathrm{d}\alpha}{1-\alpha+i\delta}\right)+\dots\,,
\end{aligned} \tag{2.122}$$

where the ellipsis indicates contributions from other diagrams and higher order terms, as before. Now, one can combine the contributions from the top diagram of Fig. 2.13, given in Eq. (2.112), and the bottom diagrams, given in Eq. (2.122). The key observation is that the divergences of the integrals for $w, \alpha \to 1$ exactly cancel each other and one can combine terms to form plus-distributions. For this step it is useful to split the α integrals from the bottom diagrams as follows

$$\begin{aligned}
\int_0^1\frac{\mathrm{d}\alpha}{1-\alpha+i\delta} &= \int_0^{x-x'}\frac{\mathrm{d}\alpha}{1-\alpha}+\int_{x-x'}^1\frac{\mathrm{d}\alpha}{1-\alpha+i\delta} = -\log\left(1-(x-x')\right)+\int_{x-x'}^1\frac{\mathrm{d}w}{1-w+i\delta} \\
\int_0^1\frac{\mathrm{d}\alpha}{1-\alpha+i\delta} &= \int_0^{x'}\frac{\mathrm{d}\alpha}{1-\alpha}+\int_{x'}^1\frac{\mathrm{d}\alpha}{1-\alpha+i\delta} = -\log\left(1-x'\right)+\int_{x'}^1\frac{\mathrm{d}w}{1-w+i\delta}\,,
\end{aligned} \tag{2.123}$$

which then leads to plus-distributions $1/(1-w)_+$ defined as in Eq. (2.81). Finally, one arrives at the following formulas for the $q\gamma q \to q\gamma q$ splitting kernel. The result for the vector-type $q\gamma q$ function $F^q_{\gamma,\mathrm{bare}}$ reads

$$\begin{aligned}
F^q_{\gamma,\mathrm{bare}}\left(x'-x,x',\mu\right) &= F_\gamma^{q,\overline{\mathrm{MS}}}\left(x'-x,x',\mu\right)+\frac{\alpha_s}{2\pi}\frac{S_\varepsilon}{\varepsilon}C_F\left(\frac{3}{2}F_\gamma^{q,\overline{\mathrm{MS}}}\left(x'-x,x',\mu\right)\right. \\
&\quad+\int_{x-x'}^1\frac{\mathrm{d}w}{w}\frac{x-x'(1-w)}{x(1-w)_+}F_\gamma^{q,\overline{\mathrm{MS}}}\left(\tfrac{x'-x}{w},x-\tfrac{x-x'}{w},\mu\right) \\
&\quad\left.+\int_{x'}^1\frac{\mathrm{d}w}{w}\frac{xw+x'(1-w)}{x(1-w)_+}F_\gamma^{q,\overline{\mathrm{MS}}}\left(\tfrac{x'}{w}-x,\tfrac{x'}{w},\mu\right)\right)+\dots\,.
\end{aligned} \tag{2.124}$$

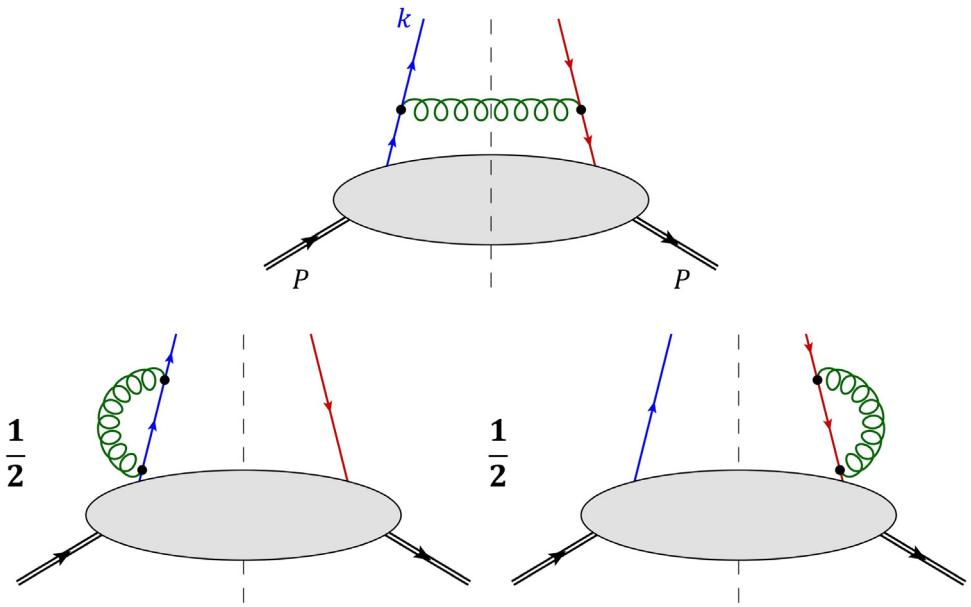

Figure 2.16: Feynman diagrams required for the qq-splitting kernel of the ordinary twist-2 PDFs.

Interestingly, the formula for the axial-vector-type function $G^q_{\gamma,\text{bare}}$ has identical shape

$$\begin{aligned} G^q_{\gamma,\text{bare}}(x'-x,x',\mu) &= G^{q,\overline{\text{MS}}}_\gamma(x'-x,x',\mu) + \frac{\alpha_s}{2\pi}\frac{S_\varepsilon}{\varepsilon}C_F\left(\frac{3}{2}G^{q,\overline{\text{MS}}}_\gamma(x'-x,x',\mu)\right. \\ &+ \int_{x-x'}^1 \frac{\mathrm{d}w}{w}\frac{x-x'(1-w)}{x(1-w)_+}G^{q,\overline{\text{MS}}}_\gamma\left(\tfrac{x'-x}{w},x-\tfrac{x-x'}{w},\mu\right) \\ &\left.+ \int_{x'}^1 \frac{\mathrm{d}w}{w}\frac{xw+x'(1-w)}{x(1-w)_+}G^{q,\overline{\text{MS}}}_\gamma\left(\tfrac{x'}{w}-x,\tfrac{x'}{w},\mu\right)\right) + \ldots . \end{aligned} \tag{2.125}$$

The origins of the different terms in the above equations are briefly recapped as follows

- The $q\gamma q$ functions $\left(F^{q,\overline{\text{MS}}}_\gamma, G^{q,\overline{\text{MS}}}_\gamma\right)(x'-x,x',\mu)$ in the first lines of Eqs. (2.124), (2.125) are generated exclusively by the self-energy diagrams at the bottom of Fig. 2.13. They are accompanied by a factor $\frac{3}{2}$ which is reminiscent of the quark-quark splitting function P_{qq}
- The integrals in the second lines are obtained by combining the first terms in the result (2.112) of the top diagram in Fig. 2.13 with terms from the self-energy diagrams where the α integral is split according to the first line in Eq. (2.123). This contribution features the $q\gamma q$ functions $\left(F^{q,\overline{\text{MS}}}_\gamma, G^{q,\overline{\text{MS}}}_\gamma\right)\left(\frac{x'-x}{w},x-\frac{x-x'}{w},\mu\right)$. In the $x'=x$ configuration, the arguments of these functions become independent of w and the remaining integral vanishes
- The last lines in (2.124), (2.125) combine the second terms in (2.112) with terms generated by using the second line in (2.123). The $q\gamma q$ functions $\left(F^{q,\overline{\text{MS}}}_\gamma, G^{q,\overline{\text{MS}}}_\gamma\right)\left(\frac{x'}{w}-x,\frac{x'}{w},\mu\right)$ are featured in this contribution. For the case $x'=x$, the integrand simplifies to a plus-distribution, and one can combine the first and last lines into the quark-quark splitting function P_{qq} defined in (2.99)

Specializing to the SFP configuration $x'=x$ one finds the somewhat simpler results

$$\begin{aligned} F^q_{\gamma,\text{bare}}(0,x,\mu) &= F^{q,\overline{\text{MS}}}_\gamma(0,x,\mu) + \frac{\alpha_s}{2\pi}\frac{S_\varepsilon}{\varepsilon}\int_x^1\frac{\mathrm{d}w}{w}P_{qq}(w)F^{q,\overline{\text{MS}}}_\gamma\left(x\tfrac{1-w}{w},\tfrac{x}{w},\mu\right)+\ldots \\ G^q_{\gamma,\text{bare}}(0,x,\mu) &= G^{q,\overline{\text{MS}}}_\gamma(0,x,\mu) + \frac{\alpha_s}{2\pi}\frac{S_\varepsilon}{\varepsilon}\int_x^1\frac{\mathrm{d}w}{w}P_{qq}(w)G^{q,\overline{\text{MS}}}_\gamma\left(x\tfrac{1-w}{w},\tfrac{x}{w},\mu\right)+\ldots \end{aligned} \tag{2.126}$$

The other SFP configuration $x'=0$ can be obtained in two equivalent ways. Either by setting $x'=0$ in Eqs. (2.124), (2.125) or by letting $x\to -x$ in Eq. (2.126) and using the symmetry properties of F^q_γ, G^q_γ under exchange of their arguments. Both approaches give the same result,

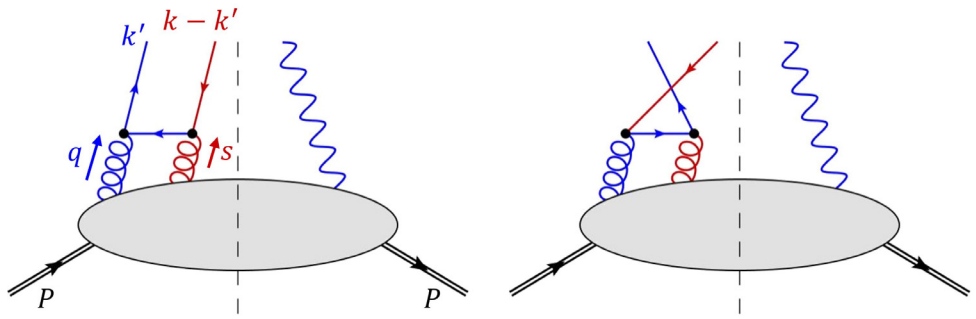

Figure 2.17: Feynman diagrams required for the splitting kernel of the $q\gamma q$ functions. These diagrams contribute to the mixing of $q\gamma q$ with $g\gamma g$ functions.

which can be seen as a small consistency check on the derivation. Additionally, one could have anticipated the appearance of the quark-quark splitting function P_{qq} because of the strong similarity of the diagrams in Fig. 2.13 for the $q\gamma q$ functions and those in Fig. 2.16 for the ordinary twist-2 PDFs. The photon is merely a spectator in the $q\gamma q$ case and it is thus not surprising to find a very similar result as for the PDFs. This further solidifies the correctness of the above derivation.

Mixing of $q\gamma q$ with $g\gamma g$

The last element needed for the renormalization of F_γ^q and G_γ^q is their mixing with the $g\gamma g$ functions defined in Eq. (C.26). The relevant diagrams are shown in Fig. 2.17. Again, there is no particle line crossing the final state cut. Thus, the calculational procedure is very similar to that presented in the previous subsection, with the schematic expression shown in Eq. (2.109) as starting point. Moreover, one also applies a collinear approximation in the form $k \approx xP$, $q \approx \xi P$ with q denoting the momentum of the gluon shown in blue in Fig. 2.17. This is followed by employing Eq. (2.102) to get expressions for F_γ^q, G_γ^q, leading to the intermediate result

$$
\begin{aligned}
F_\gamma^q\left(x'-x,x'\right) &= \alpha_s \int \frac{\mathrm{d}\xi}{\xi(\xi-x)} \int \frac{\mathrm{d}^{d-2}k'_T}{(2\pi)^{d-2}} \int \frac{\mathrm{d}b'}{2\pi i} \epsilon_\rho{}^{PnS} \times \\
&\quad \left[g_T^{\mu\nu}\epsilon^{\rho PnS} O_\gamma^1(\xi,\xi-x) + g_T^{\nu\rho}\epsilon^{\mu PnS} O_\gamma^2(\xi,\xi-x) + g_T^{\rho\mu}\epsilon^{\nu PnS} O_\gamma^2(\xi-x,\xi)\right] \times \\
&\quad \frac{\mathrm{Tr}\left[\not{n}\not{k}'\gamma_\nu\left(\not{k}'-\xi\not{P}\right)\gamma_\mu\left(\not{k}'-x\not{P}\right)\right]}{\left((k')^2+i\delta\right)\left((k'-\xi P)^2+i\delta\right)\left((k'-xP)^2+i\delta\right)} \\
G_\gamma^q\left(x'-x,x'\right) &= \alpha_s \int \frac{\mathrm{d}\xi}{\xi(\xi-x)} \int \frac{\mathrm{d}^{d-2}k'_T}{(2\pi)^{d-2}} \int \frac{\mathrm{d}b'}{2\pi i} \left(S_T\right)_\rho \times \\
&\quad \left[g_T^{\mu\nu}\epsilon^{\rho PnS} O_\gamma^1(\xi,\xi-x) + g_T^{\nu\rho}\epsilon^{\mu PnS} O_\gamma^2(\xi,\xi-x) + g_T^{\rho\mu}\epsilon^{\nu PnS} O_\gamma^2(\xi-x,\xi)\right] \times \\
&\quad \frac{-i\mathrm{Tr}\left[\gamma_5\not{n}\not{k}'\gamma_\nu\left(\not{k}'-\xi\not{P}\right)\gamma_\mu\left(\not{k}'-x\not{P}\right)\right]}{\left((k')^2+i\delta\right)\left((k'-\xi P)^2+i\delta\right)\left((k'-xP)^2+i\delta\right)},
\end{aligned}
\tag{2.127}
$$

where O_γ^1, O_γ^2 are the $g\gamma g$ functions defined in Eq. (C.26) and a decomposition of the quark momentum, $k' = x'P + b'n + k'_T$ is used. Furthermore, the transverse projector $g_T^{\mu\nu} = g^{\mu\nu} - (P^\mu n^\nu + P^\nu n^\mu)$ is also present. After evaluating the Dirac traces in the above equation one can solve the b' integrals therein using contour integration. A sketch of the contour and the pole structure is shown in Fig. 2.14. To determine the position of the poles it is of course essential to keep the causal $i\delta$ in the Feynman propagators.

Additionally, it is assumed that $0 < x' < x$. This is motivated by the fact that one eventually needs only the SFP configurations $x' = x$ and $x' = 0$ for the calculation of the Interference channel in $\ell N^\uparrow \to \gamma X$. Computing the necessary residues is straightforward, but one has to distinguish the cases $\xi > x'$ (shown in blue in Fig. 2.14) and $\xi < x'$ (in green) and also deal with terms $\propto (k_T \cdot S_T)^2$. Fortunately, the handling of such terms is already covered by Eq. (2.103), i.e. via replacing $(k_T \cdot S_T)^2 \to -k_T^2/2 + \mathcal{O}(\varepsilon)$, which leads again to the k_T integral of Eq. (2.104). Finally,

one is left with the following schematic form for F_γ^q

$$F_\gamma^q\left(x'-x,x'\right) = \frac{\alpha_s}{2\pi}\frac{S_\varepsilon}{\varepsilon}\int_{-1+x}^{1}\mathrm{d}\xi\left(\theta(\xi-x')A(x,x',\xi)+B(x,x',\xi)\right)O_\gamma^1(\xi,\xi-x) + \ldots\,, \tag{2.128}$$

where the ellipsis is a placeholder for the terms accompanying $O_\gamma^2(\xi,\xi-x)$ and $O_\gamma^2(\xi-x,\xi)$, which have the same structure. The schematic form for G_γ^q is completely analogous. As implied by the Heaviside step function $\theta(\xi-x')$, the integrals are split into a part covering the interval $(-1+x,x')$ and another part covering $(x',1)$.

The procedure for the computation related to the right diagram in Fig. 2.17 is completely analogous. The only difference arises in the distinction of cases for the contour integration. There, one has to separate the cases $\xi < x-x'$ and $\xi > x-x'$. Consequently, one finds a slightly modified schematic result for this diagram

$$F_\gamma^q\left(x'-x,x'\right) = \frac{\alpha_s}{2\pi}\frac{S_\varepsilon}{\varepsilon}\int_{-1+x}^{1}\mathrm{d}\xi\left(\theta(x-x'-\xi)C(x,x',\xi)+D(x,x',\xi)\right)O_\gamma^1(\xi,\xi-x) + \ldots\,, \tag{2.129}$$

As a final step for the left diagram in Fig. 2.17, one applies the same substitutions for ξ as for the top diagram in Fig. 2.13, discussed in the previous subsection. The two substitutions used for the integrals in Eq. (2.128) can be summarized as:

1. **Interval $(-1+x, x')$:** the antiquark of momentum $k-k'$ takes fraction w of the gluon momentum s (shown in red) $\Rightarrow \xi = x - \frac{x-x'}{w}$
2. **Interval $(x', 1)$:** the quark of momentum k' takes fraction w of the gluon momentum q (shown in blue) $\Rightarrow \xi = \frac{x'}{w}$

For the right diagram in Fig. 2.17, on the other hand, one needs to employ different substitutions for ξ. The two substitutions applied to the integrals in Eq. (2.129) are given as:

1. **Interval $(-1+x, x-x')$:** the quark of momentum k' takes fraction w of the gluon momentum s (shown in red) $\Rightarrow \xi = x - \frac{x'}{w}$
2. **Interval $(x-x', 1)$:** the antiquark of momentum $k-k'$ takes fraction w of the gluon momentum q (shown in blue) $\Rightarrow \xi = \frac{x-x'}{w}$

Some simplification using the symmetry properties given in (C.29) leads to the final result

$$\begin{aligned}
F_{\gamma,\mathrm{bare}}^q\left(x'-x,x',\mu\right) = {} & F_\gamma^{q,\overline{\mathrm{MS}}}\left(x'-x,x',\mu\right) + \frac{\alpha_s}{2\pi}\frac{S_\varepsilon}{\varepsilon}\int_{x-x'}^{1}\frac{\mathrm{d}w}{w}2w\frac{x(1-w)-x'(1-2w)}{x(x'-x(1-w))}\times \\
& \left(2O_\gamma^{1,\overline{\mathrm{MS}}}\left(x-\tfrac{x-x'}{w},\tfrac{x'-x}{w},\mu\right)+O_\gamma^{2,\overline{\mathrm{MS}}}\left(x-\tfrac{x-x'}{w},\tfrac{x'-x}{w},\mu\right)+O_\gamma^{2,\overline{\mathrm{MS}}}\left(\tfrac{x'-x}{w},x-\tfrac{x-x'}{w},\mu\right)\right) \\
& +\frac{\alpha_s}{2\pi}\frac{S_\varepsilon}{\varepsilon}\int_{x'}^{1}\frac{\mathrm{d}w}{w}2w\frac{xw+x'(1-2w)}{x(x'-xw)}\times \\
& \left(2O_\gamma^{1,\overline{\mathrm{MS}}}\left(\tfrac{x'}{w},\tfrac{x'}{w}-x,\mu\right)+O_\gamma^{2,\overline{\mathrm{MS}}}\left(\tfrac{x'}{w},\tfrac{x'}{w}-x,\mu\right)+O_\gamma^{2,\overline{\mathrm{MS}}}\left(\tfrac{x'}{w}-x,\tfrac{x'}{w},\mu\right)\right)+\ldots\,,
\end{aligned} \tag{2.130}$$

for the $q\gamma q$ function $F_{\gamma,\mathrm{bare}}^q$. The corresponding result for $G_{\gamma,\mathrm{bare}}^q$ is given by

$$\begin{aligned}
G_{\gamma,\mathrm{bare}}^q\left(x'-x,x',\mu\right) = {} & G_\gamma^{q,\overline{\mathrm{MS}}}\left(x'-x,x',\mu\right) + \frac{\alpha_s}{2\pi}\frac{S_\varepsilon}{\varepsilon}\int_{x-x'}^{1}\frac{\mathrm{d}w}{w}\frac{2w}{x}\times \\
& \left(O_\gamma^{2,\overline{\mathrm{MS}}}\left(\tfrac{x'-x}{w},x-\tfrac{x-x'}{w},\mu\right)-O_\gamma^{2,\overline{\mathrm{MS}}}\left(x-\tfrac{x-x'}{w},\tfrac{x'-x}{w},\mu\right)\right) \\
& +\frac{\alpha_s}{2\pi}\frac{S_\varepsilon}{\varepsilon}\int_{x'}^{1}\frac{\mathrm{d}w}{w}\frac{2w}{x}\left(O_\gamma^{2,\overline{\mathrm{MS}}}\left(\tfrac{x'}{w},\tfrac{x'}{w}-x,\mu\right)-O_\gamma^{2,\overline{\mathrm{MS}}}\left(\tfrac{x'}{w}-x,\tfrac{x'}{w},\mu\right)\right) \\
& +\ldots\,,
\end{aligned} \tag{2.131}$$

where the ellipsis indicates higher order terms or the contributions by other diagrams. The two formulas above can be broken down into the individual contributions of the diagrams in Fig. 2.17

- The first integrals $\int_{x-x'}^{1}$ in Eqs. (2.130), (2.131) combine contributions from the left diagram in Fig. 2.17 corresponding to $\xi = x - \frac{x-x'}{w}$ with contributions from the right diagram corresponding to $\xi = \frac{x-x'}{w}$. These integrals feature (anti-)symmetric combinations of $O_\gamma^{1,\overline{\rm MS}}, O_\gamma^{2,\overline{\rm MS}}$ at arguments $x - \frac{x-x'}{w}$ and $\frac{x'-x}{w}$. For $x' = x$, the $g\gamma g$ functions are independent of w and the integrals become trivial
- Contributions from the left diagram in Fig. 2.17 for $\xi = \frac{x'}{w}$ and from the right diagram for $\xi = x - \frac{x'}{w}$ combine into the second integrals $\int_{x'}^{1}$ in (2.130), (2.131). There, (anti-)symmetric combinations of $O_\gamma^{1,\overline{\rm MS}}, O_\gamma^{2,\overline{\rm MS}}$ at arguments $\frac{x'}{w}$ and $\frac{x'}{w} - x$ are featured. In the case $x' = x$, the integrals do simplify, but the $g\gamma g$ functions retain their w-dependence

Once more, the special case of the SFP configuration $x' = x$ is also given explicitly, while the other SFP $x' = 0$ can be obtained either directly from Eqs. (2.130), (2.131) or through symmetry of the following formulas

$$\begin{aligned}
F^q_{\gamma,\rm bare}(0,x,\mu) &= F^{q,\overline{\rm MS}}_\gamma(0,x,\mu) + \frac{\alpha_s}{\pi}\frac{S_\varepsilon}{x\varepsilon}\Big(2O^{1,\overline{\rm MS}}_\gamma(x,0,\mu) + O^{2,\overline{\rm MS}}_\gamma(x,0,\mu) + O^{2,\overline{\rm MS}}_\gamma(0,x,\mu)\Big) \\
&+\frac{\alpha_s}{2\pi}\frac{S_\varepsilon}{\varepsilon}\int_x^1 \frac{{\rm d}w}{w}\frac{2w}{x}\Big(2O^{1,\overline{\rm MS}}_\gamma\left(\tfrac{x}{w}, x\tfrac{1-w}{w},\mu\right) + O^{2,\overline{\rm MS}}_\gamma\left(\tfrac{x}{w}, x\tfrac{1-w}{w},\mu\right) + O^{2,\overline{\rm MS}}_\gamma\left(x\tfrac{1-w}{w}, \tfrac{x}{w},\mu\right)\Big) + \dots \\
G^q_{\gamma,\rm bare}(0,x,\mu) &= G^{q,\overline{\rm MS}}_\gamma(0,x,\mu) + \frac{\alpha_s}{\pi}\frac{S_\varepsilon}{x\varepsilon}\Big(O^{2,\overline{\rm MS}}_\gamma(0,x,\mu) - O^{2,\overline{\rm MS}}_\gamma(x,0,\mu)\Big) \\
&\quad+\frac{\alpha_s}{2\pi}\frac{S_\varepsilon}{\varepsilon}\int_x^1 \frac{{\rm d}w}{w}\frac{2w}{x}\Big(O^{2,\overline{\rm MS}}_\gamma\left(\tfrac{x}{w}, x\tfrac{1-w}{w},\mu\right) - O^{2,\overline{\rm MS}}_\gamma\left(x\tfrac{1-w}{w}, \tfrac{x}{w},\mu\right)\Big) + \dots . \qquad (2.132)
\end{aligned}$$

This concludes the derivation of the $q\gamma q$ splitting kernels. All required twist-3 renormalization formulas are now established. The hard-scattering calculations in the following chapters exhibit the same collinear divergences, which are thus canceled by renormalization, leaving the spin-dependent cross sections finite. In other words, collinear twist-3 factorization does indeed hold for the considered observables.

Chapter 3

Single-Inclusive Hadron Production $\ell N^{\uparrow} \to hX$

3.1 Channel $qg \to q$: Virtual Corrections

After establishing the overall setup, attention now turns to the individual channels, beginning with the virtual corrections to the LO diagrams. As alluded to in the previous chapter, the *kinematical* twist-3 contributions are generated by the first moment of the Sivers function $f_{1T}^{\perp(1),q}$. The LO is represented by the left diagram of Fig. 2.7 and the corresponding NLO virtual correction is shown in Fig. 2.8; this quark–photon vertex correction is the only virtual contribution relevant for the kinematical twist-3 effects. The computational procedure is described in Sec. 2.4.1 (see Eqs. (2.72), (2.74)) and can be performed to all orders in ε. The NLO result from Fig. 2.8 can be considered gauge invariant because the gauge parameter κ from Eq. (2.70) exactly cancels in the final results. The choice for the light-cone vector n^μ in Eq. (2.63) greatly simplifies the loop integration because the transverse momentum l_T of the initial lepton remains as the single non-vanishing transverse component of the external momenta. Notably, only the color factor C_F appears in the vertex correction of Fig. 2.8.

Because the modified gluon propagator of Eq. (2.70) introduces denominators that are not purely quadratic in the momentum, the loop integrals are handled as follows. First, perform a Sudakov-type decomposition of the loop momentum,

$$r^\mu = (r \cdot P)\, n^\mu + (r \cdot n)\, P^\mu + r_T^\mu \,,$$

with the transverse component defined by Eq. (2.60). Next, separate the integration into light-cone and transverse components (in $d-2 = 2-2\varepsilon$ dimensions) and first evaluate the $r \cdot P$ component by contour integration. With the light-cone vector of Eq. (2.63), the transverse integrals can be carried out analytically to all orders in ε; the remaining component $r \cdot n$ is then also integrated analytically.

The virtual corrections to the LO *dynamical* twist-3 contribution, shown in the right diagram of Fig. 2.7, require more involved calculations. These corrections comprise three box diagrams (Fig. 3.1), four vertex diagrams (Fig. 3.2), and one self-energy diagram (Fig. 3.3). The external momenta in all of these diagrams are the same as in the right of Fig. 2.7. The various loops yield three distinct color factors. For example, the left box diagram of Fig. 3.1 carries the factor $\frac{N_c}{2}$ due to the three-gluon vertex, the middle box is proportional to $C_F - \frac{N_c}{2}$, and the right box to just C_F. Altogether, only two independent color factors remain, C_F and $\frac{N_c}{2}$, which are combined in the

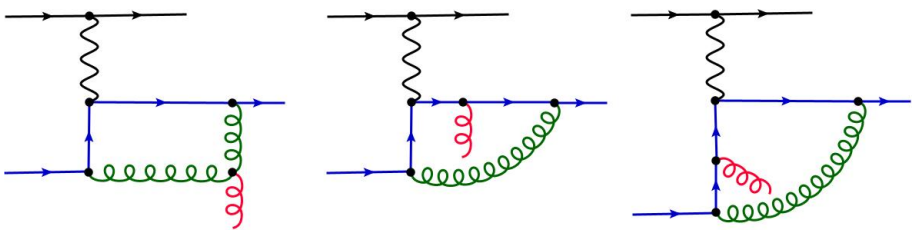

Figure 3.1: Box diagrams of the NLO virtual corrections to the dynamical twist-3 contribution. These diagrams come in interference with the LO diagram in Fig. 2.7 (left), with $k_T = 0$.

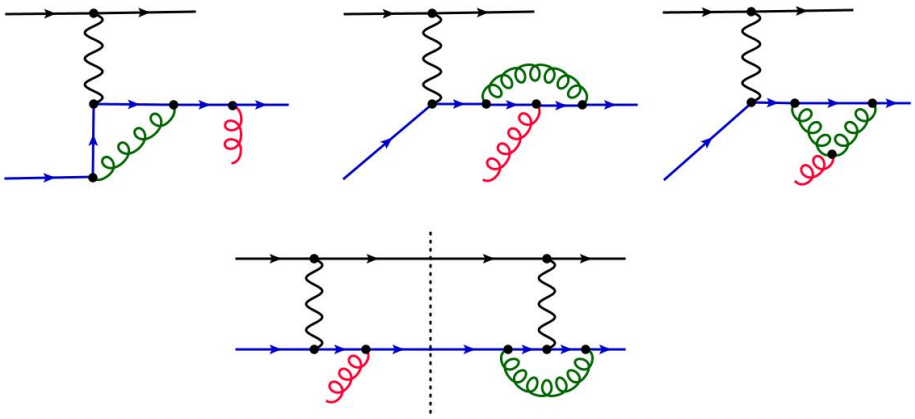

Figure 3.2: Vertex correction diagrams of the NLO virtual corrections to the dynamical twist-3 contribution. The upper diagrams come in interference with the LO diagram in Fig. 2.7 (left), with $k_T = 0$. The lower diagram is the interference of the LO dynamical twist-3 diagram of Fig. 2.7 (right) and the vertex correction in Fig. 2.8, with $k_T = 0$.

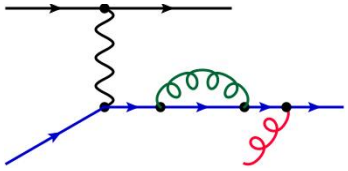

Figure 3.3: Self-energy diagram of the NLO virtual corrections to the dynamical twist-3 contribution. This diagram comes in interference with the LO diagram in Fig. 2.7 (left), with $k_T = 0$.

final result. The corrections to kinematical and dynamical twist-3 effects are eventually combined using Eq. (2.69).

The two-body phase space of the virtual corrections is more restricted than in the real-emission case. Consequently, the factorization formula for the dynamical twist-3 contributions (Eq. (2.82)) simplifies; the x-integration can be carried out directly using the δ-function $\delta(x - x_0) \propto \delta(1 - w)$.

As discussed earlier, a non-zero imaginary part must arise for the diagrams of Figs. 3.1, 3.2, and 3.3 in order to yield a non-zero result for Eq. (2.82). At LO such an imaginary part originates from the quark-propagator decomposition of Eq. (2.68), which produces a $\delta(x - x')$ and thus fixes $x' = x = x_0$. Such propagators are also present for the virtual NLO corrections, generating the familiar soft-gluon-pole (SGP) contribution associated with the ETQS matrix element $F(x_0, x_0)$. No soft-fermion or hard poles are produced because of the restricted phase space.

Additionally, loop integrals can also develop imaginary parts in certain regions of the x'-integration of Eq. (2.82), an effect known from other calculations such as the transverse SSA in two-photon exchange DIS [40, 41, 105, 124].

For $x' > x = x_0$, the left and middle box diagrams of Fig. 3.1, the upper vertex corrections of Fig. 3.2, and the self-energy diagram of Fig. 3.3 generate such terms. Although x remains fixed at x_0, x' must be integrated from x_0 to 1. With the substitution $x' = \frac{x_0}{w}$ and the symmetry properties of the qgq functions (Eq. (C.5)), the resulting expression,

$$\int_{v_0}^{v_1} \mathrm{d}v \int_{x_0}^{1} \frac{\mathrm{d}w}{w} D_1^q\left(\tfrac{1-v_1}{1-v}\right) \Big[\hat{\sigma}_1^{\Im, x'>x}\left(x = x_0, x' = \tfrac{x_0}{w}, \varepsilon\right) F^q\left(\tfrac{x_0}{w}, x_0\right) + \hat{\sigma}_5^{\Im, x'>x}\left(x = x_0, x' = \tfrac{x_0}{w}, \varepsilon\right) G^q\left(\tfrac{x_0}{w}, x_0\right)\Big] , \tag{3.1}$$

has the same structure as the hard-pole subtraction terms in Eqs. (2.90) and (2.91). Including this contribution is essential to cancel all collinear $\frac{1}{\varepsilon}$ poles.

Another non-zero imaginary part arises in the region $x' < 0$ from the middle and right box diagrams of Fig. 3.1. Changing variables to $x' = -\frac{1-w}{w} x_0$ and again using the symmetries of

Eq. (C.5) leads to

$$\int_{v_0}^{v_1}\mathrm{d}v\int_{x_0}^{1}\frac{\mathrm{d}w}{w}\,D_1^q\left(\tfrac{1-v_1}{1-v}\right)\,\Big[\hat{\sigma}_1^{\Im,x'<0}\left(x_0,-\tfrac{1-w}{w}x_0,\varepsilon\right)\,F^q\left(-\tfrac{1-w}{w}x_0,x_0\right) \\ +\hat{\sigma}_5^{\Im,x'<0}\left(x_0,-\tfrac{1-w}{w}x_0,\varepsilon\right)\,G^q\left(-\tfrac{1-w}{w}x_0,x_0\right)\Big]\,. \tag{3.2}$$

which probes the qgq functions at negative arguments. This structure matches the hard-pole terms of the $qq\to q$ channel, where the relevant twist-3 matrix elements correspond to $q\bar{q}g$ correlations. The contribution of Eq. (3.2) is again required to cancel the $\frac{1}{\varepsilon}$ poles in that channel. More details of this cancellation are given later in Sec. 3.3.

Despite the many loop diagrams, the complete virtual correction assumes the compact form

$$\begin{aligned}E_h\frac{\mathrm{d}\sigma_{\mathrm{NLO,\,virt}}}{\mathrm{d}^{d-1}\mathbf{P}_h} &= \sigma_0(S)\,\frac{\alpha_s}{2\pi}\int_{v_0}^{v_1}\mathrm{d}v\int_{x_0}^{1}\frac{\mathrm{d}w}{w}\sum_q e_q^2\left(\tfrac{1-v_1}{1-v}\right)^{2\varepsilon}\,D_1^q\left(\tfrac{1-v_1}{1-v}\right)\times\\ &\quad[\hat{\sigma}_{\mathrm{virt,SGP}}(v,w,\chi_\mu,\varepsilon)\,\left((1+\varepsilon)\,F^q-x_0\,(F^q)'\right)(x_0,x_0)\\ &\quad+\hat{\sigma}_{\mathrm{virt},\Im,\mathrm{x}'>\mathrm{x}}(v,w,\chi_\mu,\varepsilon)\,\left(F^q+G^q\right)\left(\tfrac{x_0}{w},x_0\right)\\ &\quad+\hat{\sigma}_{\mathrm{virt},\Im,\mathrm{x}'<0}(v,w,\chi_\mu,\varepsilon)\,\left(F^q+G^q\right)\left(-\tfrac{1-w}{w}x_0,x_0\right)\,]\,.\end{aligned} \tag{3.3}$$

With the short-hand notation $\chi_\mu\equiv\frac{s\,u}{t\,\mu^2}$ and

$$A(v,\chi_\mu,\varepsilon)\equiv\frac{\Gamma^2(1-\varepsilon)}{\Gamma(1-2\varepsilon)}\chi_\mu^{-\varepsilon}(1-v)^{-2\varepsilon}v^{\varepsilon}\,,$$

the partonic factors can be given to all orders in ε

$$\begin{aligned}\hat{\sigma}_{\mathrm{virt,SGP}}(v,w,\chi_\mu,\varepsilon) &= C_F\,S_\varepsilon\,\frac{\pi\varepsilon}{\sin(\pi\varepsilon)}A(v,\chi_\mu,\varepsilon)\,\hat{\sigma}_{\mathrm{LO}}(v,w,\varepsilon)\,\frac{-(2-\varepsilon+2\varepsilon^2)}{\varepsilon^2\,(1-2\varepsilon)},\\ \hat{\sigma}_{\mathrm{virt},\Im,\mathrm{x}'>\mathrm{x}}(v,w,\chi_\mu,\varepsilon) &= S_\varepsilon\,A(v,\chi_\mu,\varepsilon)\frac{v(1+v)}{(1-v)^4}\,\frac{w^{1+\varepsilon}}{(1-w)^{1+\varepsilon}}\,\frac{N_c(1-\varepsilon-\varepsilon^2)+C_F\,\varepsilon(1+\varepsilon)}{(1-\varepsilon)(1-2\varepsilon)},\\ \hat{\sigma}_{\mathrm{virt},\Im,\mathrm{x}'<0}(v,w,\chi_\mu,\varepsilon) &= S_\varepsilon\,A(v,\chi_\mu,\varepsilon)\frac{v(1+v)}{(1-v)^4}\,\frac{w^{1+\varepsilon}}{(1-w)^{\varepsilon}}\,\frac{(2\,C_F-N_c)(1-\varepsilon-\varepsilon^2)}{\varepsilon\,(1-\varepsilon)(1-2\varepsilon)}.\end{aligned} \tag{3.4}$$

The virtual SGP coefficient $\hat{\sigma}_{\mathrm{virt,SGP}}$ depends only on C_F, even though several contributing loops individually also contain N_c. Taking the sum, all N_c-dependent terms cancel. Moreover, $\hat{\sigma}_{\mathrm{virt,SGP}}$ is proportional to the LO partonic factor $\hat{\sigma}_{\mathrm{LO}}$ of Eq. (2.67). Expanding the remaining prefactor,

$$\frac{-(2-\varepsilon+2\varepsilon^2)}{\varepsilon^2\,(1-2\varepsilon)}=-\frac{2}{\varepsilon^2}-\frac{3}{\varepsilon}-8+\mathcal{O}(\varepsilon)\,,$$

reveals soft and collinear divergences identical to those in the unpolarized cross section (cf. Eq. (8) of Ref. [120]). This is familiar from observations in polarized SIDIS [125]. The double pole $-\frac{2}{\varepsilon^2}$ cancels once the real and virtual NLO corrections are combined.

3.2 Channel $qg\to q$: Real Corrections

This section analyzes features arising in the calculation of real-gluon–emission corrections. Because the $qg\to q$ channel served as an illustrative example of the general computational strategy in Sec. 2.4, the focus will be on the more specific aspects of this channel.

The relevant NLO Feynman diagrams for the *kinematical* twist-3 contributions, generated by the first moment of the Sivers function $f_{1T}^{\perp(1),q}$, are displayed in Fig. 2.9. These kinematical contributions combine with the corresponding SGP terms through Eq. (2.69). As elaborated on in Sec. 2.4, the kinematical real-gluon-emission contributions are gauge–dependent: the gauge parameter κ of Eq. (2.70) appears explicitly. This gauge dependence cancels only when the kinematical and SGP pieces are added.

The NLO Feynman diagrams for the *dynamical* twist-3 contributions are shown in Fig. 2.10. The procedure for evaluating these contributions follows Sec. 2.4: first one treats the integral contributions in Eq. (2.92), which generates the *subtraction* terms in Eqs. (2.90), (2.91). These include hard-pole (HP), soft-gluon-pole (SGP) and soft-fermion-pole (SFP) pieces. The latter two must subsequently be combined with their *direct* counterparts.

A technical feature specific to the HP as well as the direct and subtraction SGP contributions plays an essential role in this calculation: in addition to factors $1/(1-w)^{1+\varepsilon}$, that one also commonly encounters in leading-twist observables, further factors such as $1/(1-w)^{2+\varepsilon}$ and $1/(1-w)^{3+\varepsilon}$ occur. The latter are even more singular in the limit $w \to 1$. For example, a generic HP or SGP function $\sigma(v,w,\varepsilon)$ can be decomposed as follows:

$$\sigma(v,w,\varepsilon) \;=\; \frac{\sigma_3(v,\varepsilon)}{(1-w)^{3+\varepsilon}} + \frac{\sigma_2(v,\varepsilon)}{(1-w)^{2+\varepsilon}} + \frac{\sigma_1(v,\varepsilon)}{(1-w)^{1+\varepsilon}} + \sigma_{\rm reg}(v,w,\varepsilon)\,, \tag{3.5}$$

where the remainder $\sigma_{\rm reg}$ is integrable over $x_0 < w < 1$. For the term $1/(1-w)^{1+\varepsilon}$ one can use the familiar decomposition in Eq. (2.80). The other terms, $1/(1-w)^{2+\varepsilon}$ and $1/(1-w)^{3+\varepsilon}$, are handled through analytic continuation and integration-by-parts identities described in App. E, producing various derivatives of the qgq functions $F(x,x')$ and $G(x,x')$ in the final result.

3.2.1 Hard Poles

The subtraction HP contributions generated from (2.90),(2.91) contain the HP configurations $(F,G)\left(\frac{x_0}{w},x_0\right)$ of the qgq functions as well as the derivative terms $-x_0\partial_2(F,G)\left(\frac{x_0}{w},x_0\right)$[1]. The former feature singular factors up to $1/(1-w)^{3+\varepsilon}$, the latter only up to $1/(1-w)^{2+\varepsilon}$. After applying the integration-by-parts identities of App. E, the result contains various derivative terms. Schematically, one has

$$\begin{aligned}
(F,G)\left(\tfrac{x_0}{w},x_0\right) \quad &\xrightarrow{\text{App. } E} \quad \begin{cases} (F,G)\left(\frac{x_0}{w},x_0\right) \\ -x_0\partial_1(F,G)\left(\frac{x_0}{w},x_0\right) \\ x_0^2\partial_1^2(F,G)\left(\frac{x_0}{w},x_0\right) \end{cases} \\
-x_0\partial_2(F,G)\left(\tfrac{x_0}{w},x_0\right) \quad &\xrightarrow{\text{App. } E} \quad \begin{cases} -x_0\partial_2(F,G)\left(\frac{x_0}{w},x_0\right) \\ x_0^2\partial_1\partial_2(F,G)\left(\frac{x_0}{w},x_0\right) \end{cases} .
\end{aligned} \tag{3.6}$$

At this stage, the HP terms are combined with the $\overline{\rm MS}$ renormalization contributions given in the third line of Eq. (2.100) as well as with the HP piece of the virtual corrections $\propto \hat{\sigma}_{\rm virt,\Im,x'>x}$ in the third line of Eq. (3.3). Integration by parts is performed on derivative terms containing $-x_0\partial_1(F,G)\left(\frac{x_0}{w},x_0\right)$ or $x_0^2\partial_1^2(F,G)\left(\frac{x_0}{w},x_0\right)$, i.e. for terms that only include derivatives with respect to the first argument. This is done when the accompanying partonic factors are regular, but not for distributional terms such as $1/(1-w)_+$, $\left(\frac{\log(1-w)}{1-w}\right)_+$, or $\delta(1-w)$. Useful identities for these integrations by parts are listed in App. E.

All $\frac{1}{\varepsilon}$ poles cancel except those coming with $\delta(1-w)$; these cancel later against the SGP terms. The cancellation concerns only contributions with the color factor N_c, whereas C_F terms show no $\frac{1}{\varepsilon}$ poles. The explicit HP result is presented in Eq. (6.8).

3.2.2 Soft-Gluon Poles

Direct SGP contributions arise when propagators such as Eqs. (2.68) and (2.93) hit their poles. Schematically, one can write these contributions in the following form

$$\int {\rm d}x'\, i\left[\frac{\sigma_2(x)}{(x'-x)(x'-x+i\delta)} + \frac{\sigma_1(x,x')}{x'-x+i\delta}\right] F(x,x') + \text{c.c.}\,. \tag{3.7}$$

The second term fixes $x'=x$ and projects out the ETQS function $F(x,x)$. The first term, proportional to $\delta(x'-x)/(x'-x)$, is replaced by $-\frac{\rm d}{{\rm d}x'}\delta(x'-x)$ and integrated by parts, producing a derivative of $F(x,x)$. The expression then reduces to

$$\frac{2\pi}{x}\,\sigma_2(x)\,(x\,(\partial_2 F)(x,x)) + 2\pi\,\sigma_1(x,x)\,F(x,x)\,. \tag{3.8}$$

The evaluation of the partonic functions σ_1 and σ_2 follows the lines described above for the HP contributions, with technical details again given in App. E.

A complete cancellation of $\frac{1}{\varepsilon}$ poles occurs. The process is particularly involved for terms coming with $\delta(1-w)$, which can originate from the $1/(1-w)^{1+\varepsilon}$ expansion (2.80) as well as from the boundary terms generated by integration by parts in the HP sector.

[1] The notation for the partial derivatives of the functions F,G is defined Eq. (C.6)

Cancellation of poles for the N_c terms: For the second derivative $F''(x,x)$, there are only $\frac{1}{\varepsilon}$ poles accompanied by $\delta(1-w)$. They cancel once SGP and HP terms are combined.

For the first derivative $-x_0F'(x,x)$, cancellation of the $\delta(1-w)$ poles requires inclusion of the direct SGP terms, SGP and HP subtraction terms generated through Eqs.(2.90),(2.91), and the renormalization term in the last line of Eq. (2.100). After these additions, all poles accompanied by the plus distribution $1/(1-w)_+$ also cancel, and the remaining $\frac{1}{\varepsilon}$ pole is regular in w; it is integrated by parts and merged with the regular non-derivative terms multiplying $F(x,x)$. To complete the cancellation of all $\frac{1}{\varepsilon}$ poles for $F(x,x)$ (without derivative) one has to include two further contributions: first, the virtual HP correction $\hat{\sigma}_{\mathrm{virt},\Im,x'>\mathrm{x}}$ contains a factor $1/(1-w)^{1+\varepsilon}$ that generates a $\delta(1-w)$ upon expansion via (2.80). At $w=1$ the HP contribution effectively becomes a SGP contribution that must be included for the cancellation of all $\frac{1}{\varepsilon}$ poles. Second, one must also include the Weizsäcker-Williams (WW) contributions by the photon-in-lepton PDF $f_1^{\gamma/\ell}$. Then, one finally arrives at finite result for $\varepsilon \to 0$

Cancellation of poles for the C_F terms: The C_F part of the SGP corrections is more involved because it also contains *kinematical* twist-3 contributions. These are essential to cancel all $\frac{1}{\varepsilon}$ poles and also for color-gauge invariance. Here too, all poles cancel once the following pieces are all included

- Kinematical twist-3 terms − they become SGP contributions upon application of Eq. (2.69)
- Direct SGP contributions from propagator poles such as in (2.68) and (2.93)
- Subtraction SGP contributions generated from Eqs. (2.90),(2.91)
- SGP terms in the renormalization of the ETQS function $F(x,x)$, see Eq. (2.100)
- The renormalization of the twist-2 fragmentation function D_1^q, see Eq. (C.17)
- The WW contributions by the photon-in-lepton density $f_1^{\gamma/\ell}$, see Sec. 2.4.3
- The imaginary as well as SGP parts of the loop diagrams $\hat{\sigma}_{\mathrm{virt},\Im,x'>x}$ and $\hat{\sigma}_{\mathrm{virt,SGP}}$, see Eq. (3.4)

The final analytic NLO expressions for the SGP contributions, valid in $d=4$, are shown in Eq. (6.6).

As in the HP sector, all regular non-distributional terms accompanying derivative contributions are integrated by parts so that only $\delta(1-w)$ and plus-distributions remain. Identities used for these manipulations are summarized in App. E.

3.2.3 Soft-Fermion Poles

The $qg \to q$ channel also receives soft-fermion-pole contributions. These arise both from the SFP subtraction terms in Eqs. (2.90), (2.91) and from propagators in the diagrams of Fig. 2.10 whose poles generate an imaginary SFP part, see Eq. (2.94). An additional WW piece is generated by the photon-in-lepton mechanism of Eq. (2.97) (Sec. 2.4.3). The partonic cross sections accompanying $(F,G)\left(\frac{x_0}{w},0\right)$ and their derivatives $-x_0\partial_2(F,G)\left(\frac{x_0}{w},0\right)$ are straightforward to evaluate, with no complications in the soft limit $w \to 1$. Because of this simplicity the SFP factors can be expanded directly in ε. The derivative SFP terms $-x_0\partial_2(F,G)\left(\frac{x_0}{w},0\right)$ originate solely from the SFP subtraction terms and are finite for $\varepsilon \to 0$.

A residual collinear $\frac{1}{\varepsilon}$ pole remains even after adding the SFP subtraction, direct SFP, and WW terms, indicating that there must be additional contributions for $(F,G)\left(\frac{x_0}{w},0\right)$. Indeed, the $qq \to q$ channel, which will be discussed in the next section, produces terms proportional to the same SFP matrix elements. Combining these with the $qg \to q$ SFP contributions removes the last $\frac{1}{\varepsilon}$ poles and yields finite SFP cross sections.[2]

Since SFP renormalization terms appear neither in Eq. (2.100) nor in the LO cross section (2.64), the SFP sector is independent of the renormalization scale μ, though it retains a dependence on the lepton mass m_ℓ through the WW contribution. Eq. (6.6) presents the final SFP results.

3.3 Channel $qq \to q$

The twist-3 calculation for the $qq \to q$ channel parallels the procedure in Sec. 3.2 for the $qg \to q$ channel. Figs. 3.4 and 3.5 show the corresponding Feynman diagrams. It turns out that neither

[2] A similar inter-channel cancellation of SFP contributions was observed in Ref. [126] for SIDIS.

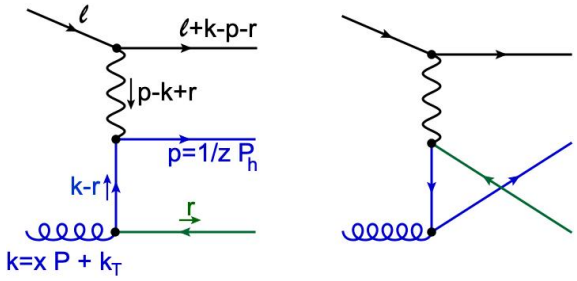

Figure 3.4: NLO real-emission diagrams with a gluon in the initial state. These diagrams come in interference with several other diagrams for various channels. $\boldsymbol{qq \to q}$ **:** interference with the diagrams in Fig. 3.5, with $k_T = 0$, $\boldsymbol{qq \to q'}$ **:** interference with the diagrams in Fig. 3.6, with $k_T = 0$, $\boldsymbol{gg \to q}$ **:** interference with themselves (kinematical part) and interference with the diagrams in Fig. 3.7 (with $k_T = 0$, dynamical part).

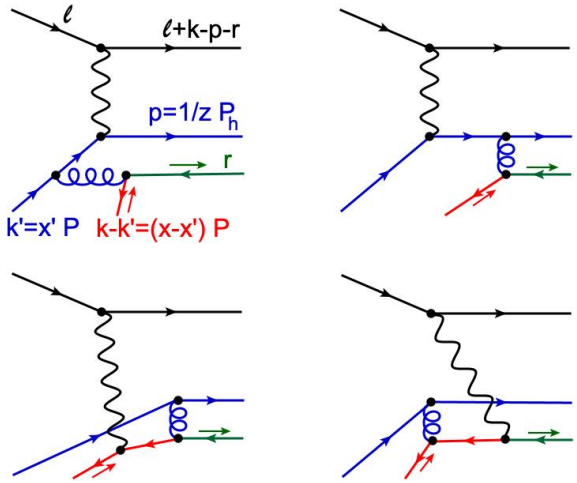

Figure 3.5: NLO diagrams with a quark-antiquark pair in the initial state contributing to the dynamical twist-3 part of the $qq \to q$ channel. These diagrams come in interference with the diagrams in Fig. 3.4, with $k_T = 0$.

kinematical twist-3 nor SGP contributions appear in this channel. Soft divergences in the limit $w \to 1$ can be handled simply by means of Eq. (2.80).

This channel displays several symmetries for an exchange of quark-antiquark in the initial and final states. As a consequence, it suffices to calculate the interference of the diagrams in Fig. 3.5 with those in Fig. 3.4 only. This corresponds to a quark-antiquark-gluon ($q\bar{q}g$) correlation in the initial state and quark fragmentation in the final state, hence labeled $q\bar{q} \to q$. However, all other channels such as $q\bar{q} \to \bar{q}$, $\bar{q}q \to q$, and $\bar{q}q \to \bar{q}$ are directly related to the $q\bar{q} \to q$ channel by the aforementioned symmetries. Therefore, this channel simply obtains the label $qq \to q$.

The hadronic matrix element entering the factorized description of the $qq \to q$ channel is the quark-gluon-quark correlator (2.59). But, contrary to before, it is now evaluated at different light-cone fractions, namely as $\Phi^{q,\rho}_{F,ij}(x'-x,x')$. The reason is the aforementioned $q\bar{q}g$ configuration featured by this channel: antiquark and gluon switch roles compared to the $qg \to q$ channel. This flip results in different arguments for the qgq functions, specifically $x \to x'-x$. Thus, the factorization formula of Eq. (2.82) for the $qg \to q$ channel has to be adjusted in the following way

$$\int \frac{\mathrm{d}z}{z^2} \int \mathrm{d}x \int_{x-1}^{1} \mathrm{d}x' \, \frac{i}{x} \, \Big[\, \hat{\sigma}^{qq\to q,1}(x,x',z)\, F^q(x'-x,x') + \hat{\sigma}^{qq\to q,5}(x,x',z)\, G^q(x'-x,x') \, \Big] \, D_1^q(z) + \text{c.c.}. \tag{3.9}$$

The partonic factors $\hat{\sigma}^{qq\to q,1,5}(x,x',z)$ are obtained as interference of the diagrams of Figs. 3.4 and 3.5. Their color factor is $C_F - N_c/2 = -\frac{1}{2N_c}$, meaning that the $qq \to q$ channel is suppressed by a factor $1/N_c^2$ compared to the $qg \to q$ channel.

Interestingly, the upper and lower diagrams of Fig. 3.5 form two independent classes of interference effects, since the virtual photon couples to either the quark or the antiquark respectively;

one may treat the two cases separately, and splits the partonic functions in (3.9) accordingly,

$$\hat{\sigma}^{q\bar{q}\to q,1,5}(x,x',z) \;=\; -\frac{1}{2N_c}\left[\hat{\sigma}_1^{q\bar{q}\to q,1,5}(x,x',z)+\hat{\sigma}_2^{q\bar{q}\to q,1,5}(x,x',z)\right], \tag{3.10}$$

where $\hat{\sigma}_{1,2}$ in (3.10) refer to the interferences of the upper/lower two diagrams in Fig. 3.5 with those in Fig. 3.4, respectively. The symmetries mentioned above are given in terms of a substitution $x' \to x - x'$ in (3.9). They allow to restrict oneself to the $q\bar{q} \to q$ configuration of Fig. 3.5, and they read explicitly:

$$\begin{aligned}
\hat{\sigma}_{1,2}^{q\bar{q}\to q,1}(x,x',z) &= \hat{\sigma}_{2,1}^{q\bar{q}\to \bar{q},1}(x,x-x',z) = \hat{\sigma}_{2,1}^{\bar{q}q\to q,1}(x,x-x',z)\,,\\
\hat{\sigma}_{1,2}^{q\bar{q}\to q,5}(x,x',z) &= -\hat{\sigma}_{2,1}^{q\bar{q}\to \bar{q},5}(x,x-x',z) = -\hat{\sigma}_{2,1}^{\bar{q}q\to q,5}(x,x-x',z)\,.
\end{aligned} \tag{3.11}$$

The computational procedure for the two interference effects $\hat{\sigma}_1^{qq\to q}$ and $\hat{\sigma}_2^{qq\to q}$ differs. Starting with the integral contributions, as described in Sec. 2.4.2, will demonstrate this feature. Analogous to the $qg \to q$ channel, the partonic factors contain poles at the endpoints $\zeta = 0, \zeta = 1$ as well as in between at $\zeta = w$. To regularize these poles and render the integral contributions finite, one can apply the same strategy as before, laid out in the paragraph following Eq. (2.86). In the present case, the partonic functions $\hat{\sigma}_{(1,2)}$ for the two interference effects carry different ζ-poles; they are modified as follows:

$$\begin{aligned}
\hat{\sigma}_{1,\mathrm{Int}}^{qq\to q,1,5}(v,w,\zeta) &\equiv \zeta\,(w-\zeta)^2\,\hat{\sigma}_1^{qq\to q,1,5}(v,w,\zeta)\,,\\
\hat{\sigma}_{2,\mathrm{Int}}^{qq\to q,1,5}(v,w,\zeta) &\equiv (1-\zeta)\,\hat{\sigma}_2^{qq\to q,1,5}(v,w,\zeta)\,.
\end{aligned} \tag{3.12}$$

Now, $\hat{\sigma}_{1,2,\mathrm{Int}}^{qq\to q,1,5}(v,w,\zeta)$ are well-behaved and integrable. The prefactors are shifted to the correlation functions $F, G\left(-(1-\zeta)\,\frac{x_0}{w}, \zeta\,\frac{x_0}{w}\right)$. Subsequently, the poles are regularized by adding and subtracting suitable terms from the numerator. Similar to the $qg \to q$ channel, cf. Eqs. (2.90),(2.91), this leads to integrable combinations of the qgq functions $F_{\mathrm{Int},1/2}^{qq\to q}, G_{\mathrm{Int},1/2}^{qq\to q}$; They are given as

$$\begin{aligned}
F_{\mathrm{Int},1}^{qq\to q}(x_0,w,\zeta) \;\equiv\; & \frac{1}{\zeta\,(w-\zeta)^2}\left[F^q\left(-(1-\zeta)\,\tfrac{x_0}{w}, \zeta\,\tfrac{x_0}{w}\right) - \frac{\zeta\,(2w-\zeta)}{w^2}\,F^q\left(-\tfrac{1-w}{w}x_0, x_0\right)\right.\\
& \left. -\frac{\zeta\,(\zeta-w)}{w^2}\,x_0\left[\partial_1 F^q + \partial_2 F^q\right]\left(-\tfrac{1-w}{w}x_0, x_0\right) - \frac{(w-\zeta)^2}{w^2}\,F^q\left(-\tfrac{x_0}{w}, 0\right)\right],
\end{aligned} \tag{3.13}$$

$$\begin{aligned}
G_{\mathrm{Int},1}^{qq\to q}(x_0,w,\zeta) \;\equiv\; & \frac{1}{\zeta\,(w-\zeta)^2}\left[G^q\left(-(1-\zeta)\,\tfrac{x_0}{w}, \zeta\,\tfrac{x_0}{w}\right) - \frac{\zeta\,(2w-\zeta)}{w^2}\,G^q\left(-\tfrac{1-w}{w}x_0, x_0\right)\right.\\
& \left. -\frac{\zeta\,(\zeta-w)}{w^2}\,x_0\left[\partial_1 G^q + \partial_2 G^q\right]\left(-\tfrac{1-w}{w}x_0, x_0\right) - \frac{(w-\zeta)^2}{w^2}\,G^q\left(-\tfrac{x_0}{w}, 0\right)\right],
\end{aligned} \tag{3.14}$$

and

$$F_{\mathrm{Int},2}^{qq\to q}(x_0,w,\zeta) \;\equiv\; \frac{1}{1-\zeta}\left[F^q\left(-(1-\zeta)\,\tfrac{x_0}{w}, \zeta\,\tfrac{x_0}{w}\right) - F^q\left(0, \tfrac{x_0}{w}\right)\right], \tag{3.15}$$

$$G_{\mathrm{Int},2}^{qq\to q}(x_0,w,\zeta) \;\equiv\; \frac{1}{1-\zeta}\left[G^q\left(-(1-\zeta)\,\tfrac{x_0}{w}, \zeta\,\tfrac{x_0}{w}\right) - G^q\left(0, \tfrac{x_0}{w}\right)\right]. \tag{3.16}$$

Through this procedure, the following types of subtraction terms are introduced

- The upper diagrams in Fig. 3.5 introduce HP subtraction terms $\propto (F,G)\left(-\frac{1-w}{w}x_0, x_0\right)$ via Eqs. (3.13), (3.14). Furthermore, also the derivative terms $-x_0\,(\partial_1+\partial_2)\,(F,G)\left(-\frac{1-w}{w}x_0, x_0\right)$ are generated. There are no other sources of HP terms in this channel.
- The other subtraction terms in (3.13), (3.14) are $\propto (F^q, G^q)\left(-\frac{x_0}{w}, 0\right) = (F^{\bar{q}}, G^{\bar{q}})\left(\frac{x_0}{w}, 0\right)$, i.e. they are antiquark SFP contributions. They must be combined with direct SFP contributions, as will be discussed below
- The lower diagrams in Fig. 3.5 only generate SFP subtraction $\propto (F,G)\left(0, \frac{x_0}{w}\right)$ via Eqs. (3.15) and (3.16). They must also be combined with direct SFP contributions. Subsequently, they must be added to the SFP pieces from the $qg \to q$ channel to cancel all $\frac{1}{\varepsilon}$ poles, see the discussion below

Given this overview, the computation of the various contributions will now be discussed one by one in more detail, with the first one being the *hard pole* contributions. These contributions can be calculated as in Sec. 3.2. The limit of $w \to 1$ is less complicated, though, since one only encounters terms $\propto 1/(1-w)^{1+2\varepsilon}$ after phase space integration. Hence, one can simply apply Eq. (2.80). Note that for the HP contribution one does not need to include any photon-in-lepton terms (see Sec. 2.4.3).

Furthermore, one only needs $\overline{\text{MS}}$-renormalization terms for the SGP matrix element $F(x,x)$, but not for the quark FF D_1^q. The relevant pieces are given in the last four lines of Eq. (2.100). Finally, one must also include the virtual contribution of $\hat{\sigma}_{\text{virt},\Im,\text{x}'<0}$, see Eqs. (3.3), (3.4). After adding all terms, the NLO result for the HP contribution to the $qq \to q$ channel becomes finite and well-defined.

Next, the subtraction and *direct* antiquark SFPs need to be combined. The latter emerge from a propagator hitting its pole similar to (2.94). Interestingly, the subtraction terms and the direct contribution originate from different classes of interference effects: subtraction terms from class 1 (upper diagrams in Fig. 3.5) and direct contributions from class 2 (lower diagrams). This again reflects the intricate interplay of seemingly unrelated dynamical twist-3 terms at NLO. Eventually, the $\frac{1}{\varepsilon}$ poles cancel once the SFPs $F, G(-\frac{x_0}{w}, 0)$ from the photon-in-lepton mechanism are added.

Similarly, the subtraction SFP contributions $F, G(0, \frac{x_0}{w})$ from Eqs. (3.15),(3.16) should be combined with direct SFPs in $\hat{\sigma}_1^{qq\to q,1,5}(v,w,\zeta)$ rather than in $\hat{\sigma}_2^{qq\to q,1,5}(v,w,\zeta)$. Moreover, one has to add the corresponding SFP from the photon-in-lepton contribution. As already alluded to in Sec. 3.2.3, the SFP contributions of the $qg \to q$ and $qq \to q$ channels must be combined to cancel the last remaining $\frac{1}{\varepsilon}$ poles. Also recall that the final NLO SFP result is assigned to the $qg \to q$ channel.

The analytical formulas for the $qq \to q$ channel are shown explicitly in Eq. (6.9).

3.4 Channel $qq \to q'$

The calculation for the $qq \to q'$ channel resembles that for $qq \to q$. The main difference is that the flavors of the fragmenting final-state quark and the initial quark–antiquark pair are not necessarily the same. Additionally, since the color factor for this channel is $T_R = \frac{1}{2}$, it is only suppressed by $\mathcal{O}(1/N_c)$ relative to the $qg \to q$ channel, rather than by $\mathcal{O}\left(1/N_c^2\right)$ like the $qq \to q$ channel. Nonetheless, in Ch. 7 it will turn out that this channel generally gives a negligible contribution to the numerical results.

The interference of the two diagrams in Fig. 3.6 with those in Fig. 3.4 generates the partonic functions for this channel. It contributes solely because quark and antiquark fragmentation into the observed hadron differ; in contrast, it vanishes for jet production. It may, however, gain importance when heavy quarks are involved, for example in D-meson production.

The $qq \to q'$ channel is "stand-alone" in the sense that it is finite and well behaved by itself. No $\overline{\text{MS}}$ counterterms from neither the LO soft-gluon-pole (SGP) matrix elements nor the quark fragmentation function are required to cancel collinear singularities. However, photon-in-lepton contributions generating logarithms of the form $\log\left(\frac{s\,u}{m_\ell^2\,t}\right)$ must be included.

Technically, the computation proceeds exactly as in the previous section for the $qq \to q$ channel. There is an antisymmetry property of the partonic functions when the fragmenting final-state quark is replaced by an antiquark:

$$\hat{\sigma}^{q\bar{q}\to q',1,5}(x,x',z) \;=\; -\hat{\sigma}^{q\bar{q}\to \bar{q}',1,5}(x,x',z)\,. \tag{3.17}$$

As a result, the $qq \to q'$ contribution enters with the difference of quark- and antiquark fragmentation functions in the final NLO formulas.

Further symmetry properties reflect the exchange of quark and antiquark in the initial state:

$$\begin{aligned}
\hat{\sigma}^{q\bar{q}\to q',1}(x,x',z) &= -\hat{\sigma}^{q\bar{q}\to q',1}(x,x-x',z)\,,\\
\hat{\sigma}^{q\bar{q}\to q',5}(x,x',z) &= +\hat{\sigma}^{q\bar{q}\to q',5}(x,x-x',z)\,.
\end{aligned} \tag{3.18}$$

These relations ensure that the qgq functions also enter as differences $F^{q-\bar{q}}, G^{q-\bar{q}}$ of their quark and antiquark components.

The methods for calculating the integral contributions to this channel remain the same as before. One finds that the partonic functions carry a divergent denominator $\frac{1}{\zeta(1-\zeta)}$. This denominator is moved to the qgq-functions, and subsequently one subtracts suitable SFP terms; this leads to the

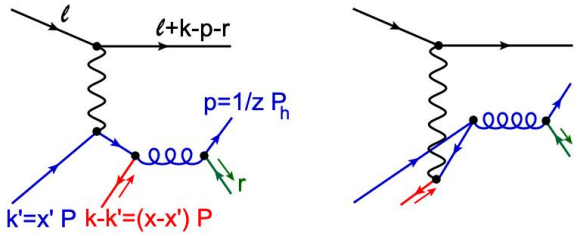

Figure 3.6: NLO diagrams contributing to the $qq \to q'$ channel's dynamical twist-3 part. These diagrams come in interference with the diagrams in Fig. 3.4, with $k_T = 0$.

definitions

$$F_{\text{Int}}^{qq\to q'}(x_0,w,\zeta) \equiv \frac{F^q\left(-(1-\zeta)\,\frac{x_0}{w},\zeta\,\frac{x_0}{w}\right)-\zeta\,F^q\left(0,\frac{x_0}{w}\right)-(1-\zeta)\,F^q\left(-\frac{x_0}{w},0\right)}{\zeta(1-\zeta)}\,, \tag{3.19}$$

$$G_{\text{Int}}^{qq\to q'}(x_0,w,\zeta) \equiv \frac{G^q\left(-(1-\zeta)\,\frac{x_0}{w},\zeta\,\frac{x_0}{w}\right)-\zeta\,G^q\left(0,\frac{x_0}{w}\right)-(1-\zeta)\,G^q\left(-\frac{x_0}{w},0\right)}{\zeta(1-\zeta)}\,. \tag{3.20}$$

These two combinations yield finite, well-behaved integral contributions.

Turning to the soft-fermion pole (SFP) terms, Eqs. (3.19),(3.20) reveal two types of SFPs that appear as subtraction terms. Together with photon-in-lepton SFPs, these exhaust all sources of SFPs for this channel. Unlike the $qq \to q$ channel, there are no direct SFP contributions. Both types of SFPs, $(F^q, G^q)\left(0,\frac{x_0}{w}\right)$ and $(F^q, G^q)\left(-\frac{x_0}{w},0\right)$, can be related to each other via charge conjugation. Thus, one may interpret them as corresponding quark and antiquark distributions. Combined with the symmetry properties (3.17),(3.18), this feature causes the channel to be driven by the difference of quark- and antiquark correlations.

Explicit analytical results for this channel are presented in Eq. (6.14).

3.5 Channel $qg \to g$

The $qg \to g$ channel is computed in a similar way as the $qg \to q$ case described earlier. The partonic factors originate from

- an interference of the diagrams in Fig. 2.9 among themselves (kinematical twist-3 contribution, with non-zero k_T), and
- an interference of the diagrams in Figs. 2.9 (with $k_T = 0$) and 2.10 (dynamical twist-3 contribution).

Here, however, the observed hadron arises from fragmentation of the final-state gluon rather than the quark. This requires exchanging the external quark and gluon momenta in the diagrams of Figs. 2.9 and 2.10, i.e. $r^\mu \leftrightarrow p^\mu$. This exchange alters the momentum flow and therefore the analytic expressions. The factorization formula for this channel involves the gluon fragmentation function D_1^g (Eq. (C.15)) instead of the quark fragmentation function D_1^q. Because D_1^g enters for the first time at NLO, the only $\overline{\text{MS}}$-renormalization needed to cancel collinear singularities is that of the quark fragmentation function in Eq. (C.17).

The technical procedure parallels the $qg \to q$ calculation but is less involved for two reasons: first, the behavior in the $w \to 1$ limit is simpler and second, no hard-pole (HP) contributions occur. A notable feature is that the C_F component of the direct soft-gluon-pole (SGP) contributions cancels exactly against the corresponding kinematical twist-3 term. Consequently, the surviving direct SGP terms are proportional only to the color factor N_c, reflecting a non-Abelian QCD effect.

In Addition to the direct contributions, one also gets SGP subtraction terms from the integral contributions. They come with both color factors C_F and N_c. For the integral contribution, the partonic functions are again handled as described below Eq. (2.82): they share a singular denominator $\frac{1}{\zeta(1-\zeta)^2}$ that is shifted from the partonic factors to the qgq functions. Then, one subtracts SGP and SFP terms to ensure integrability, leading to the following finite combinations:

$$F_{\text{Int}}^{qg\to g}(x_0,w,\zeta) \equiv \frac{1}{\zeta\,(1-\zeta)^2}\Big[F^q\left(\tfrac{x_0}{w},\zeta\,\tfrac{x_0}{w}\right)-\zeta(2-\zeta)\,F^q\left(\tfrac{x_0}{w},\tfrac{x_0}{w}\right)+\tfrac{\zeta\,(1-\zeta)}{2\,w}\,x_0\,\left(F^q\right)'\left(\tfrac{x_0}{w},\tfrac{x_0}{w}\right) -(1-\zeta)^2\,F^q\left(\tfrac{x_0}{w},0\right)\Big]\,, \tag{3.21}$$

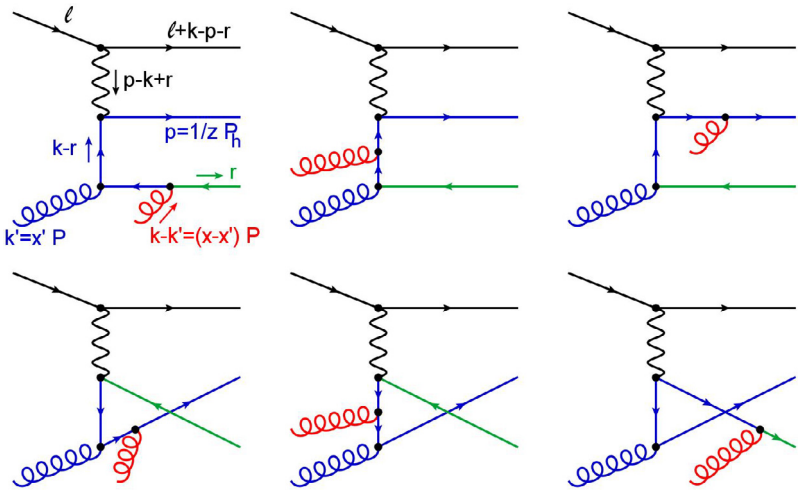

Figure 3.7: NLO diagrams contributing to the $gg \to q'$ channel's dynamical twist-3 part. These diagrams come in interference with the diagrams in Fig. 3.4, with $k_T = 0$.

$$G_{\text{Int}}^{qg\to g}(x_0, w, \zeta) \equiv \frac{1}{\zeta\,(1-\zeta)^2}\left[G^q\left(\tfrac{x_0}{w}, \zeta\,\tfrac{x_0}{w}\right) + \tfrac{\zeta\,(1-\zeta)}{w}\,x_0\,\left(\partial_2 G^q\right)\left(\tfrac{x_0}{w}, \tfrac{x_0}{w}\right) - (1-\zeta)^2\,G^q\left(\tfrac{x_0}{w}, 0\right)\right]. \tag{3.22}$$

Adding the SGP subtraction terms from these expressions to the direct SGP contribution (proportional to N_c) as well as including both the photon-in-lepton terms and the renormalization of D_1^q in Eq. (C.17) (proportional to C_F) yields a finite SGP partonic cross section. One can apply integration by parts to the derivative terms to simplify the results, which is straightforward since no plus-distributions or delta functions accompany these derivatives.

Finally, one must combine the SFP pieces from the subtraction terms in Eqs. (3.21) and (3.22) with the direct SFP and photon-in-lepton SFP contributions. The collinear poles cancel completely, leaving a well-defined finite result.

The explicit analytical expressions for the $qg \to g$ channel are given in Eq. (6.18).

3.6 Channel $gg \to q$

Lastly, this section highlights key features of the remaining channel $gg \to q$. This process involves gluon–gluon correlations inside the transversely polarized nucleon and quark fragmentation in the final state. Unlike the $qg \to q$ and $qg \to g$ channels, where the kinematical twist-3 effects arise from the first moment of the Sivers function alone, here, two kinematical distributions contribute at NLO: $G_T^{(1)}$ and $\Delta H_T^{(1)}$ (see Eq. (C.3)). The respective kinematical twist-3 terms are obtained from the interference of the diagrams in Fig. 3.4 with themselves, for non-zero transverse momentum k_T.

For the dynamical twist-3 effects, one evaluates the interference of the diagrams in Fig. 3.7 with those in Fig. 3.4 (with $k_T = 0$). Both the symmetric $d^{\alpha\beta\gamma}$ and antisymmetric $f^{\alpha\beta\gamma}$ SU(3) structure constants appear, so the factorized description involves both triple-gluon correlators defined in Eqs. (C.11) and (C.12). Thus, the schematic form of the dynamical contribution is

$$\int \frac{\mathrm{d}z}{z^2} \int \mathrm{d}x \int \mathrm{d}x' \frac{i}{xx'(x-x')} \left[\hat{\sigma}^f_{\sigma\tau\rho}(x, x', z)\, N_F^{\sigma\tau\rho}(x, x') + \hat{\sigma}^d_{\sigma\tau\rho}(x, x', z)\, O_F^{\sigma\tau\rho}(x, x')\right] D_1^q(z) + \text{c.c.}\,. \tag{3.23}$$

where the partonic functions $\hat{\sigma}^{f,d}_{\sigma\tau\rho}$ are generated by the diagrams of Fig. 3.7. A remarkable simplification emerges at this point: these diagrams contain no propagators of the type (2.83), the usual source of logarithms with negative arguments (cf. Eq. (2.84)) that generate imaginary parts. Their absence implies that there are no integral contributions in the $gg \to q$ channel and therefore no subtraction terms as in Eq. (2.90). This makes $gg \to q$ the only partonic channel at NLO where the transverse SSA originates exclusively from propagator poles.

The hard factors $\hat{\sigma}^{f,d}$ exhibit such propagator poles at $x' = x$ (previously called soft-gluon pole) and at $x' = 0$ (previously called soft-fermion pole). Because only gluons from the nucleon enter the hard scattering, both cases correspond to a gluon carrying vanishing longitudinal momentum. Furthermore, the triple-gluon correlators N_F and O_F (Eqs. (C.11), (C.12)) are expressed in terms

of combinations of

$$(N,O)(x,x')\,,\quad (N,O)(x,x-x')\quad \text{and}\quad (N,O)(x',x'-x)\,.$$

Consequently, the propagator poles cannot be tied to a unique region of the support of N and O. Therefore, the identification as soft-gluon or soft-fermion poles is not adequate and will not be used for this channel.

Decomposing the propagators into a principal value and a δ-function (as in Eq. (2.68)) and using the explicit factor $i/\left[xx'(x-x')\right]$ in Eq. (3.23) yields terms proportional to "δ-function over its argument". As in Eq. (3.7), these can be rewritten as derivatives of δ-functions,

$$\frac{\delta\left(x'-x\right)}{x'-x}=-\frac{\mathrm{d}}{\mathrm{d}x'}\delta\left(x'-x\right),\qquad \frac{\delta\left(x'\right)}{x'}=-\frac{\mathrm{d}}{\mathrm{d}x'}\delta\left(x'\right)$$

Subsequently, integration by parts produces derivative terms of N,O at several arguments. Using the symmetry relations (C.13), the resulting expressions depend only on

$$(N,O)(x,x),\quad (N,O)(x,0),\quad \frac{\mathrm{d}}{\mathrm{d}x}(N,O)(x,x),\quad \frac{\mathrm{d}}{\mathrm{d}x}(N,O)(x,0)\,.$$

Unlike the other channels, here the calculations were carried out with a general light-like vector n^μ, parameterized as in Eq. (59) of Ref. [101], introducing two free parameters. Following the method of that reference, the dependence on these parameters and hence on the choice of n^μ cancels only if kinematical and dynamical twist-3 effects are properly related. The necessary relations for the gluonic kinematical functions $G_T^{(1)}$ and $\Delta H_T^{(1)}$ are given in Eqs. (13),(14) of Ref. [110] for $d=4$ − going to $d=4-2\varepsilon$ dimensions they need to be extended as follows

$$\begin{aligned} G_T^{(1)}(x) &= 4\pi\left(N(x,x)-(1+\varepsilon)N(x,0)\right),\\ \Delta H_T^{(1)}(x) &= -8\pi(1-\varepsilon)N(x,0). \end{aligned}\tag{3.24}$$

Finally, one needs to add the relevant term from the renormalization formula of the SGP function $F^q(x,x)$, given in the last two lines of Eq. (2.100). Furthermore, the photon-in-lepton contributions to this channel must be included. Then, all collinear $\frac{1}{\varepsilon}$ poles cancel, leading to a finite and well-behaved result. Integration-by-parts identities (Eq. (E.9)) are useful in demonstrating these cancellations.

An intriguing outcome, presented in the final results in Eq. (6.23), is that the partonic hard-scattering factors accompanying the triple-gluon functions $(N,O)(x,x)$ coincide, whereas those multiplying $(N,O)(x,0)$ differ only by an overall sign.

Chapter 4

Single-Inclusive Jet Production $\ell N^{\uparrow} \to \mathrm{jet} X$

Having established the NLO analytic formulas for single-inclusive hadron production in Sec. 2.3 and Ch. 3, one can adapt them to single-inclusive jet production, $\ell(l) + N^{\uparrow}(P) \to \mathrm{jet}(P_j) + X$. For jets, no fragmentation functions are involved, and in particular there are no twist-3 fragmentation effects. This means that, contrary to hadron production, the derivation given below gives the *complete* result at NLO accuracy. Furthermore, the presence of less non-perturbative objects makes it easier to extract the unknown twist-3 distribution functions F^q, G^q from fits to future experimental data. The first step to go from hadrons to jets is to replace the quark and gluon fragmentation functions (FFs) by δ-functions:

$$D_1^{h/(q,g)}\left(\tfrac{1-v_1}{1-v},\mu\right) \to \delta\left(1-\tfrac{1-v_1}{1-v}\right) = (1-v_1)\,\delta(v-v_1). \tag{4.1}$$

This simple procedure works for the LO contribution (2.64), but is not sufficient at NLO. The reason is that final-state collinear divergences cancel for a jet cross section. For the hadron case, however, collinear singularities had to be subtracted from the hard partonic cross sections, and canceled by renormalization of the FFs. As was shown in Refs. [127, 128, 129], at NLO it is relatively straightforward to account for this mismatch when the produced jet is relatively narrow.

4.1 Jet Definitions

To start the discussion, one first needs to specify in detail how the jet is defined. It is customary to introduce a radius R that sets the size of the jet. For the so-called cone algorithms, see for example Ref. [130], a particle a of pseudorapidity η_a and azimuth ϕ_a is defined as inside the jet j if it is inside the circle of radius R centered around the jet's counterparts η_j and ϕ_j

$$R_{aj}^2 = (\eta_a - \eta_j)^2 + (\phi_a - \phi_j)^2 \le R^2\,. \tag{4.2}$$

Here the jet four-momentum P_j is defined as the sum of all particle momenta p_a inside the jet. For the cone algorithms, the jet can also be defined geometrically, as a cone of half-opening angle δ. Particle a is counted as inside the cone if the angle θ_{aj} between its three-momentum $\boldsymbol{p}_a$ and the jet's three-momentum $\boldsymbol{P}_j$ is smaller than the half-opening angle, $\theta_{aj} < \delta$. As was shown in Ref. [131], both definitions can be connected for $R, \delta \ll 1$ using the relation

$$R = \delta \cosh(\eta_j)\,. \tag{4.3}$$

Another class of jet algorithms are the k_T-type algorithms, cf. Ref. [132]. In addition to pseudorapidity η_a and azimuth ϕ_a they also take into account the transverse momentum $k_{a,T}$ of a particle a in the definition of the jet. As a starting point one defines the set of all particles in the final state and computes the following *distances*

$$\begin{aligned} d_{ab} &\equiv \min\left((k_{a,T})^{2p}, (k_{b,T})^{2p}\right)\frac{R_{ab}^2}{R^2} \\ d_{aB} &= (k_{a,T})^{2p} \\ R_{ab}^2 &= (\eta_a-\eta_b)^2 + (\phi_a-\phi_b)^2\,, \end{aligned} \tag{4.4}$$

where d_{ab} is the distance between the particles a, b and d_{aB} the distance between the particle a and the initial beam. The algorithm then proceeds iteratively and starts out by finding the smallest distance. If it is a d_{ab} the particles a, b are combined into a single jet j by taking the sum of the four-momenta, $P_j = p_a + p_b$[1]. If it is a d_{aB}, then particle a becomes a jet j and is removed from the set of final-state objects. The distances are recalculated (now possibly also between jets and particles) and the procedure is repeated until the set of final-state objects (particles or jets) is empty. The parameter p in Eq. (4.4) distinguishes different cases of k_T algorithms,

- $p = 1$: Inclusive k_T algorithm
- $p = 0$: Inclusive Cambridge/Aachen algorithm
- $p = -1$: Anti-k_T algorithm

For the present work, results are always given for k_T-type algorithms. As will be shown below, at NLO and working in a suitable approximation, it does not matter which kind of k_T algorithm is chosen, i.e. which value of p is specified.

4.2 Small Cone Approximation

If the jet radius R is small, $R \ll 1$, one can systematically derive analytical matching terms that translate from the collinear-subtracted single-parton cross sections to a jet cross section [127, 128, 129]. This is called the *small-cone approximation (SCA)* (or sometimes narrow-jet approximation, NJA) and actually turns out to be rather accurate also at larger values of R, even out to $R \sim 0.7$. The SCA has already been used to obtain the jet counterparts of the unpolarized and longitudinally polarized NLO single-hadron cross sections in Refs. [120, 133]. It results in additional contributions to the NLO partonic cross sections that depend on the jet definition and its radius R. Applying the SCA to the present calculation, one finds that the jet-specific terms for the transversely polarized cross section are different from the ones obtained for the unpolarized and longitudinally polarized cross sections in [120, 133]. To explain the origin of this deviation, some details of the computation are presented in the following.

The general strategy is applicable to any partonic hard scattering process $ab(c) \to jkl$. This could be, for example, the $qg \to q$ channel's kinematical part $\ell q \to \ell qg$ or its dynamical part $\ell qg \to \ell qg$ (with a third particle c in the initial state). As discussed above, the first step is to replace the FF $D_1^q(z) \to \delta(1-z)$, which describes the case where just the final state quark of momentum p forms the jet of momentum P_j alone, i.e. $p = P_j$.

Of course, also the final state gluon of momentum r could be inside the jet, in which case the jet momentum would be given as the sum of the two parton momenta $P_j = p + r$. This case is, however, not included when adapting the single-hadron cross section via (4.1). There, the jet momentum is always given by $P_j = p$ no matter the direction in which the gluon is radiated. So, the gluon could be inside the cone geometrically while not actually being counted as part of the jet. The partonic cross section for this situation will be denoted as $\sigma_{q(g)}$ in the following. Or, vice versa, the gluon could form the jet and the quark be inside it but not be counted as part of the jet − this will correspond to $\sigma_{g(q)}$ below. There is an elegant way to reconcile this issue without repeating the calculation as a whole: Subtract the contributions $\sigma_{q(g)}$, $\sigma_{g(q)}$ for the two situations described above and then add back σ_{qg}, the contribution for quark and gluon forming the jet together. The jet cross section σ_j is then given schematically as

$$\sigma_j = \big(\sigma_q - \sigma_{q(g)}\big) + \big(\sigma_g - \sigma_{g(q)}\big) + \sigma_{qg}\,, \tag{4.5}$$

where $\sigma_q(\sigma_g)$ are the inclusive quark (gluon) cross sections adapted from the single-hadron results (see Secs. 3.2 and 3.5), i.e. with FFs replaced by δ-functions according to Eq. (4.1). In the SCA, $\sigma_{q(g)}(R)$, $\sigma_{g(q)}(R)$ and $\sigma_{qg}(R)$ can be computed analytically. They depend on the jet radius R and in the case of $\sigma_{qg}(R)$ also on the specific choice of jet-algorithm, which will be a k_T-type algorithm in this work. For the channels $qq \to q$ and $gg \to q$ the replacement of the quark FF by a δ-function is already sufficient and they do not receive any R-dependent contributions in the SCA. Furthermore, the channel $qq \to q'$ vanishes identically since it is given in terms of the difference of quark and antiquark FFs, which both get replaced by the same δ-function and thus cancel. Hence, the former quark fragmentation channel $qg \to q$ and the former gluon fragmentation channel $qg \to g$ are the only ones to consider here.

[1] this way of combining particles into a jet corresponds to the widely used E-recombination scheme, cf. Ref. [130]

As discussed in Refs. [127, 128, 129] the SCA corresponds to an expansion around vanishing jet radius $R = 0$ and the partonic cross sections take on the general form $\mathcal{A}\log(R) + \mathcal{B} + \mathcal{O}(R^2)$. In the following, the most important steps to extract the coefficients $\mathcal{A}$ and $\mathcal{B}$ for the partonic cross sections $\sigma_{q(g)}$, $\sigma_{g(q)}$ and σ_{qg} are briefly summarized.

4.2.1 Former Quark and Gluon Fragmentation Channels

Starting with the case of former quark fragmentation $\sigma_{q(g)}$, the first thing to note is that this cross section is independent of the choice for the jet algorithm since the jet is formed by a single parton. Hence, for simplicity the following discussion is given for a cone algorithm.

Moving on, one needs to distinguish between two useful reference frames:

- The center-of-mass system (c.m.s.) of the initial lepton and nucleon. In this frame the relevant four-momenta can be parametrized as follows

$$\begin{aligned} l &= \frac{\sqrt{s}}{2}(1,\ldots,0,1) \\ P &= \frac{\sqrt{s}}{2}(1,\ldots,0,-1) \\ P_j &= P_{j,T}(\cosh\eta_j,\ldots,\cos\phi_j,\sin\phi_j,\sinh\eta_j) \\ r &= r^0(1,\ldots,\sin\theta_r\cos\phi_r,\sin\theta_r\sin\phi_r,\cos\theta_r)\ . \end{aligned} \tag{4.6}$$

  Note that the jet radius R as well as the half-opening angle δ are defined with respect to this frame. Also, the relation of Eq. (4.3) between R and δ, see Ref. [131], is derived for this frame only. One can express the *jet* Mandelstam variables $s = (l+P)^2 \simeq 2l\cdot P$, $t = (P - P_j)^2 \simeq -2P\cdot P_j$ and $u = (l - P_j)^2 \simeq -2l\cdot P_j$ in terms of the jet's transverse momentum $P_{j,T}$ and its pseudorapidity η_j, which will prove useful in what follows. The relations read

$$\begin{aligned} t &= -P_{j,T}\sqrt{s}\,e^{+\eta_j} \qquad u = -P_{j,T}\sqrt{s}\,e^{-\eta_j} \\ P_{j,T} &= \sqrt{\frac{tu}{s}} \qquad \cosh\eta_j = \frac{-t-u}{2\sqrt{tu}}\,. \end{aligned} \tag{4.7}$$

- The "partonic" frame. It is defined by the condition $\boldsymbol{k}+\boldsymbol{l}-\boldsymbol{p}=\boldsymbol{0}$, where l is the lepton momentum, k is given in Eq. (2.71) and corresponds to the sum of initial parton momenta, and p is the final-state-quark momentum. The partonic frame is used for the phase space integration, see Eq. (2.77), as well as for the following discussion. A convenient parametrization is given by

$$\begin{aligned} l &= l^0(1,\ldots,\sin\psi,\cos\psi) \\ k &= k^0(1,\ldots,-\sin\psi',\cos\psi') \\ p &= p^0(1,\ldots,0,1) \\ r &= r^0(1,\ldots,\sin\theta\cos\phi,\sin\theta\sin\phi,\cos\theta)\ , \end{aligned} \tag{4.8}$$

  with some angles ψ, ψ'. The energy components can be expressed in terms of the *partonic* Mandelstam variables $\hat{s} = (l + x\,P)^2 = x\,s$, $\hat{t} = (x\,P - P_j)^2 = xt$, $\hat{u} = (l - P_j)^2 = u$ as well as the scalar product $k_T \cdot l_T$. They are given up to terms of order $\mathcal{O}\left(k_T^2\right)$ as

$$\begin{aligned} l^0 &= \frac{\hat{s}+\hat{u}+2k_T\cdot l_T}{2\sqrt{\hat{s}+\hat{t}+\hat{u}+2k_T\cdot l_T}} \qquad k^0 = \frac{\hat{s}+\hat{t}+2k_T\cdot l_T}{2\sqrt{\hat{s}+\hat{t}+\hat{u}+2k_T\cdot l_T}} \\ p^0 &= \frac{-\hat{t}-\hat{u}}{2\sqrt{\hat{s}+\hat{t}+\hat{u}+2k_T\cdot l_T}} \qquad r^0 = \frac{1}{2}\sqrt{\hat{s}+\hat{t}+\hat{u}+2k_T\cdot l_T}\,. \end{aligned} \tag{4.9}$$

  Keep in mind that pseudorapidities and also the half-opening angle δ of the jet cone are different in the two frames. To make this distinction clear, the half-opening angle in the partonic frame is denoted as δ'

Back to the computation of the former quark fragmentation channel: the final-state gluon is inside the jet if the angle of its three-momentum $\boldsymbol{r}$ with the quark's three-momentum $\boldsymbol{p}$ is smaller than δ'. Thus one finds the approximation

$$p\cdot r = p^0 r^0(1-\cos\theta') \approx p^0 r^0 \frac{(\theta')^2}{2} + \cdots = \mathcal{O}\left((\delta')^2\right)\,. \tag{4.10}$$

As a consequence, this scalar product can be neglected everywhere in the numerator of any expression and one only has to keep $p \cdot r$ if it appears as a denominator. Indeed, one finds terms $\propto \frac{1}{p \cdot r}$ in the partonic cross sections before phase space integration, which are the only terms that will contribute to the considered order in R. For all other terms, one can generally approximate $r \approx \frac{r^0}{p^0} p$ which also simplifies other scalar products including r. The next step is to perform the phase space integration, which involves angular integrals over the azimuthal angle ϕ of the gluon as well as over the angle $\theta' < \delta'$ between quark and gluon, cf. Eq. (2.77). Thus one needs the following integral, expanded around $\delta' = 0$

$$\int_0^{\delta'} \mathrm{d}\theta' \frac{\sin^{1-2\varepsilon} \theta'}{1 - \cos\theta'} = -\frac{(\delta')^{-2\varepsilon}}{\varepsilon} \left(1 + \mathcal{O}\left((\delta')^2\right)\right) , \tag{4.11}$$

where technically $\varepsilon < 0$ was required for convergence. Now, to go back to the lepton-nucleon c.m.s. where the jet was defined in the first place, one needs to relate the original half-opening angle δ with the angle δ' in the partonic frame. In the SCA such a relation can be found without explicitly specifying the Lorentz transformation matrix Λ. For now, let unprimed symbols denote the quantities in the lepton-nucleon c.m.s. and primed symbols denote their counterparts in the partonic frame. Of course, the scalar product of the quark and gluon momenta is Lorentz invariant and being parallel to each other, p and r transform in the same way, giving

$$\begin{aligned} p \cdot r \approx p^0 r^0 \frac{\theta^2}{2} &= \left(p^0\right)' \left(r^0\right)' \frac{(\theta')^2}{2} \approx p' \cdot r' \\ \frac{r^0}{p^0} &= \frac{\left(r^0\right)'}{\left(p^0\right)'} , \end{aligned} \tag{4.12}$$

where the scalar products have been approximated for $\theta < \delta \ll 1$ and $\theta' < \delta' \ll 1$. The transformation of the angle θ between quark and gluon directly follows from the above equations and the half-opening angle of the jet cone obviously transforms in the same way, implying

$$\delta' = \frac{p^0}{\left(p^0\right)'} \delta + \mathcal{O}\left(\delta^3\right) .$$

In the present case of $p = P_j$ one can use Eqs. (4.7) and (4.9) as well as the relation between R and δ of Eq. (4.3) to directly relate δ' and R as follows

$$(\delta')^2 = \frac{4tu\left(\hat{s} + \hat{t} + \hat{u} + 2k_T \cdot l_T\right)}{s\left(\hat{t} + \hat{u}\right)^2} R^2 . \tag{4.13}$$

This is an essential point for the computation of the kinematical contributions. As elaborated on in Sec. 2.4.1, one needs to carry out the phase space integration keeping a non-zero k_T at all times and only afterwards expand in k_T. Through Eq. (4.13) an additional k_T-dependence enters the description. This generates an extra term in the first order k_T-expansion that could easily be missed. However, this term is crucial to cancel all $\frac{1}{\varepsilon}$ poles when combining kinematical and SGP contributions via Eq. (2.69). Also note that one encounters a term $\propto 1/(1-w)^{2+2\varepsilon}$ in the computation of the kinematical contribution to $\sigma_{q(g)}$, which needs to be handled by means of the procedure described in App. E.

Turning to the dynamical contribution to the partonic cross section $\sigma_{q(g)}$, one finds that only SGP terms $\propto F^q(x,x)$ enter, including a derivative term $\left(F^q\right)'(x,x)$. This is due to the simplified kinematics in the SCA. Also note that in both the kinematical and the dynamical contributions only the color factor C_F appears while N_c is absent. Again, the phase space integration can be carried out using Eqs. (4.11) and (4.13), but for $k_T = 0$. This completes the treatment of $\sigma_{q(g)}$, and the procedure for $\sigma_{g(q)}$ is analogous. Notably, no SGP derivative term is present in that case and at most terms $\propto 1/(1-w)^{1+2\varepsilon}$ appear, which are dealt with in the conventional way using Eq. (2.80).

4.2.2 Joint Jet Formation by Quark and Gluon

To complete the calculation of the jet-specific pieces one must compute the cross section σ_{qg} describing the case when quark and gluon of momenta q and r form the jet together, i.e. $P_j = p + r$. In the k_T algorithms, two particles are merged into a jet if and only if their distance to each other is smaller than both their beam distances. In the present case this translates to $d_{qg} < \min\left(d_{qB}, d_{gB}\right)$,

which implies $R_{qg} < R$, cf. Eq. (4.4). Interestingly, this is true regardless of the value for p, i.e. for all k_T-type jet algorithms. On the other hand, for a cone algorithm the quark and gluon would be merged into the same jet if and only if $R_{qj} < R$ and $R_{gj} < R$. The different conditions for being merged into the same jet lead to a dependence of σ_{qg} on the jet algorithm and for the present work, the k_T-type is chosen.

Because quark and gluon are combined into a single jet, one effectively has a two-particle final state consisting of the jet alongside the unobserved lepton. This leads to a different phase space integral compared to Eq. (4.11) for $\sigma_{q(g)}$ and $\sigma_{g(q)}$. Still, it is true that only terms $\propto \frac{1}{p\cdot r}$ contribute to the considered order in R in the SCA. For all other scalar products involving q or r it is useful to write them in terms of the jet momentum P_j. This is done by defining the fraction $0 < \tau < 1$ of the jet momentum carried by the gluon, i.e. $r = \tau P_j$ and $p = (1-\tau)P_j$. Thus, one has the following schematic form for the phase space integration (cf. Eq. (2.75))

$$\sigma \sim \frac{\mu^{2\varepsilon}}{(2\pi)^{d-1}} \int \mathrm{d}^d l' \delta^+ \left((l')^2\right) \int \mathrm{d}^d r \delta^+ \left(r^2\right) \delta^{(d)} \left(k + l - l' - P_j\right) \frac{E_j}{E_p} \frac{\hat{\sigma}(\tau)}{p \cdot r} \,, \tag{4.14}$$

where E_j and E_p are the energies of the jet and the quark respectively. The fraction of these two energies appears because the quark of momentum p no longer forms the jet alone, i.e. $E_p \neq E_j$.

Next, the l' integral is carried out using the d-dimensional δ-function, setting $l' = k + l - P_j$. Since $p \cdot r = E_p E_r (1 - \cos\theta_{qg})$, the angular dependence of the integrand is only through θ_{qg}. Thus it is convenient to use spherical coordinates for the momentum r and integrate out all angles beside θ_r. Here, it is important to distinguish between the polar angle of the gluon θ_r with respect to the jet axis and the angle between quark and gluon θ_{qg}, i.e. $\theta_r \neq \theta_{qg}$. Lastly, one introduces the substitution $E_r = \tau E_j$ for the gluon energy E_r, which also implies $E_p = (1-\tau)E_j$. This leads to the following expression

$$\sigma \sim \frac{S_\varepsilon}{2(2\pi)^2} \frac{\delta\left(x - x_0 - \left(\frac{-2k_T \cdot l_T}{s+t}\right)\right)}{s+t} \left(\frac{E_j^2}{\mu^2}\right)^{-\varepsilon} \int_0^1 \frac{\mathrm{d}\tau}{(1-\tau)^2} \tau^{-2\varepsilon} \hat{\sigma}(\tau) \int_0^{\theta_{\max}} \mathrm{d}\theta_r \frac{\sin^{1-2\varepsilon}\theta_r}{1-\cos\theta_{qg}} \,, \tag{4.15}$$

where $x_0 \equiv -\frac{u}{s+t}$ and $S_\varepsilon \equiv \frac{(4\pi)^\varepsilon}{\Gamma(1-\varepsilon)}$. The upper boundary $\theta_{\max}$ of the θ_r integral depends on the jet algorithm but is in any case of the order of the jet size R and thus assumed to be small in the SCA, i.e. $\theta_r < \theta_{\max} \ll 1$.

At this point, one can do the first order k_T-expansion for the kinematical part, i.e. for

$$\hat{\sigma}_{\mathrm{kin}}(k_T \cdot l_T, \tau) f_{1T}^{\perp(1),q}\left(x_0 - \tfrac{2k_T \cdot l_T}{s+t}\right) .$$

Taking the derivative with respect to the transverse momentum $k_{T\sigma}$ and subsequently setting $k_T = 0$ one finds explicitly

$$l_{T\sigma} \frac{\mathrm{d}\hat{\sigma}_{\mathrm{kin}}(k_T \cdot l_T, \tau)}{\mathrm{d}\left(k_T \cdot l_T\right)}\Big|_{k_T=0} f_{1T}^{\perp(1),q}(x_0) - \frac{2 l_{T\sigma}}{s+t} \hat{\sigma}_{\mathrm{kin}}(k_T \cdot l_T = 0, \tau) \left(f_{1T}^{\perp(1),q}\right)'(x_0) \,. \tag{4.16}$$

Because the δ-function in Eq. (4.15) sets x to a k_T-dependent quantity, a derivative term of the first moment of the Sivers function is generated via Eq. (4.16). In contrast, for the dynamical part one does not find a derivative term $F'(x,x)$ of the SGP function. Upon adding kinematical and dynamical contributions via Eq. (2.69) the partonic cross section multiplies the combination $\left(1 - x\frac{\mathrm{d}}{\mathrm{d}x}\right) F^q(x,x)$ of the SGP function and reads

$$\hat{\sigma}_{\mathrm{kin+dyn}}(\tau) \,=\, C_F \left[\frac{1+(1-\tau)^2}{\tau} - \varepsilon\tau\right] \frac{1 + v^2 - \varepsilon(1-v)^2}{(1-v)^3} \,=\, P_{gq}(\tau,\varepsilon)\tilde{\sigma}_{\mathrm{LO}}(v,\varepsilon) \,, \tag{4.17}$$

with the generalized quark-gluon splitting function $P_{gq}(\tau,\varepsilon)$ in $d = 4 - 2\varepsilon$ dimensions and a slight variation $\tilde{\sigma}_{\mathrm{LO}}(v,\varepsilon)$ of the LO cross section of Eq. (2.67). Also note that $v = v_1$, in accordance with Eq. (4.1).

To complete the calculation, one needs to perform the τ- and θ_r-integrals in Eq. (4.15). This will be done as in Ref. [129], where a substitution from θ_r to the invariant jet mass is employed,

$$m^2 = P_j^2 = 2p \cdot r = 2\tau(1-\tau)E_j^2(1-\cos\theta_{qg}) \,.$$

The relation between m^2 and the angles θ_r, θ_{qg} is given as

$$\cos\theta_{qg} \,=\, 1 - \frac{m^2}{2\tau(1-\tau)E_j^2} \qquad \cos\theta_r \,=\, \frac{2\tau E_j^2 - m^2}{2\tau E_j \sqrt{E_j^2 - m^2}} \,. \tag{4.18}$$

In the SCA, the small jet size R directly implies that $m^2 \ll 1$. Thus, approximating for a small invariant mass and using $x = \frac{x_0}{w}$ one finds

$$\sigma \sim \frac{S_\varepsilon}{2(-u)(2\pi)^2}\delta(1-w)\tilde{\sigma}_{\mathrm{LO}}(v,\varepsilon)\int_0^1 \mathrm{d}\tau\, \tau^{-\varepsilon}(1-\tau)^{-\varepsilon}P_{gq}(\tau,\varepsilon)\int_0^{m^2_{\max}}\frac{\mathrm{d}m^2}{m^2}\left(\frac{m^2}{\mu^2}\right)^{-\varepsilon}. \quad (4.19)$$

Now, one needs to find the upper bound $m^2_{\max}$ consistent with the constraint $R_{qg} < R$. To do so, parametrize the momenta p, r and P_j via their respective pseudorapidity η and azimuth ϕ, and using $|\boldsymbol{P}_j| = \sqrt{E_j^2 - m^2}$

$$\begin{aligned} P_j &= \left(E_j, |\boldsymbol{P}_j|\frac{\cos\phi_j}{\cosh\eta_j}, |\boldsymbol{P}_j|\frac{\sin\phi_j}{\cosh\eta_j}, |\boldsymbol{P}_j|\tanh\eta_j\right) \\ p &= E_p\left(1, \frac{\cos\phi_p}{\cosh\eta_p}, \frac{\sin\phi_p}{\cosh\eta_p}, \tanh\eta_p\right) \\ r &= E_r\left(1, \frac{\cos\phi_r}{\cosh\eta_r}, \frac{\sin\phi_r}{\cosh\eta_r}, \tanh\eta_r\right). \end{aligned} \quad (4.20)$$

Based on these parametrizations one can evaluate the invariant mass m^2 and then approximate the result for p, r and P_j all being collinear to each other, i.e. for $\eta_p \approx \eta_r \approx \eta_j$ as well as $\eta_p - \eta_r \ll 1$ and $\phi_p - \phi_r \ll 1$

$$\begin{aligned} m^2 &= \frac{2E_pE_r}{\cosh\eta_p\cosh\eta_r}\left(\cosh(\eta_p-\eta_r) - \cos(\phi_p-\phi_r)\right) \\ &\approx \frac{E_pE_r}{\cosh^2\eta_j}\left((\eta_p-\eta_r)^2 + (\phi_p-\phi_r)^2\right) = \frac{E_pE_r}{\cosh^2\eta_j}R_{qg}^2 < \frac{E_j^2R^2}{\cosh^2\eta_j}\tau(1-\tau). \end{aligned} \quad (4.21)$$

Plugging this result back into the m^2-integral in Eq. (4.19) and applying Eq. (4.7) leads to the following expression for the τ- and m^2-integrals (cf. Ref. [129])

$$-\frac{1}{\varepsilon}\left(\frac{tuR^2}{s\mu^2}\right)^{-\varepsilon}\int_0^1 \mathrm{d}\tau\,\tau^{-2\varepsilon}(1-\tau)^{-2\varepsilon}P_{gq}(\tau,\varepsilon) = -\frac{C_F}{\varepsilon}\left(\frac{tuR^2}{s\mu^2}\right)^{-\varepsilon}\left[-\frac{1}{\varepsilon} - \frac{3}{2} + \varepsilon\left(-\frac{13}{2} + \frac{2\pi^2}{3}\right)\right]. \quad (4.22)$$

As a final step, one collects all cross sections according to Eq. (4.5). The resulting expression will still contain collinear $\frac{1}{\varepsilon}$ poles, though. This is because a $\overline{\mathrm{MS}}$ subtraction was performed for the cross sections σ_q and σ_g, absorbing collinear singularities into the quark and gluon FFs D_1^q, D_1^g. This is, however, not appropriate for a jet cross section and one needs to add back the terms that were inappropriately $\overline{\mathrm{MS}}$-subtracted. This leads to the desired cancellation of the remaining $\frac{1}{\varepsilon}$ poles. Lastly, all regular, non-distributional terms accompanying $F'(x,x)$ were integrated by parts, as previously in the single-inclusive hadron calculation. The final jet results are presented in Sec. 6.2 with explicit partonic factors given in App. F.2.

Chapter 5

Single-Inclusive Photon Production $\ell N^\uparrow \to \gamma X$

This chapter will study the third and final single-inclusive process considered in this work: the photon production process $\ell(l)N^\uparrow(P) \to \gamma(P_\gamma)X$. Similarly to jet production highlighted in the previous chapter, twist-3 effects only enter on the distribution side, i.e. via correlations in the initial nucleon. Twist-3 fragmentation effects, on the other hand, are absent. The reason is that, unlike hadrons, photons are elementary particles without internal structure. Consequently, the following derivation yields the *complete* NLO result for this process.

The semi-inclusive analog of this process, dubbed γSIDIS, also constitutes an interesting observable for the study of twist-3 distribution functions. It will be considered for the numeric analysis in Ch. 7, and details on the corresponding calculation are given in Sec. 6.4. Related references include [39, 109].

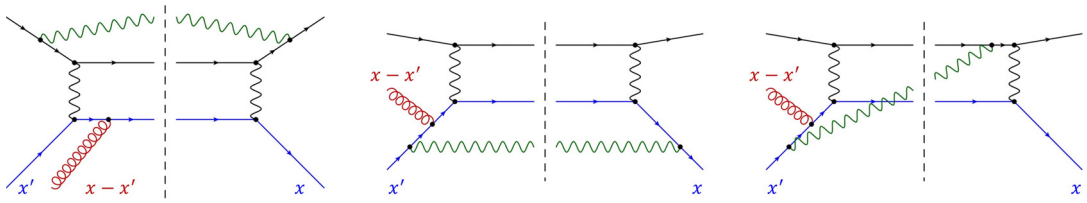

Figure 5.1: Overview of the production channels for single-inclusive photon production $\ell N^\uparrow \to \gamma X$. For each channel, one example diagram is shown, **Left:** Bethe Heitler, **Middle:** Compton, **Right:** Interference

Being the gauge boson of QED, the photon not only couples to quarks but also to leptons, opening up new production channels compared to hadron production. These channels can be classified by the power of the fractional quark charge e_q with which they enter:

- **Bethe Heitler, $\propto e_q^2$, Fig. 5.1 left:** For this channel, the observed final state photon is emitted from the lepton line and the fractional charge only enters via the vertex including the virtual photon and a quark. It turns out that the Bethe Heitler channel vanishes identically for the transversely polarized cross section. As described in Ref. [109] this is to be expected, since the photon emission happens exclusively on the lepton line. Then the same arguments as given in Ref. [134] apply. Essentially, time-reversal symmetry forbids a non-zero transverse SSA.

- **Compton, $\propto e_q^4$, Fig. 5.1 middle:** With the virtual photon coming from the lepton and the observed final state photon being emitted exclusively from the quark line, this channel is like quark-photon Compton scattering. It includes two production mechanisms for the photon: it can either be radiated directly in a point-like QED vertex from the quark, or it can be the result of fragmentation. The latter case is described by the quark-to-photon and gluon-to-photon fragmentation functions (FFs) $D_1^{\gamma/q}$ and $D_1^{\gamma/g}$. Both cases can be obtained from the results for hadron production derived in Ch. 3 as will be shown below.

- **Interference, $\propto e_q^3$, Fig. 5.1 right:** Finally, there is the interference of diagrams where the photon is emitted from the lepton line with diagrams where it is emitted from the quark line.

This channel has a unique, uncommon feature: it is not only sensitive to twist-3 quark-gluon-quark (qgq) functions F^q, G^q but also to their quark-photon-quark ($q\gamma q$) counterparts F^q_γ, G^q_γ (see App. C.7), and even gluon-photon-gluon ($g\gamma g$) functions O^1_γ, O^2_γ (see App. C.8). A rare example of another observable featuring $q\gamma q$ functions is the transverse SSA in two-photon exchange DIS, cf. Ref. [40]. Both qgq and $q\gamma q$ functions enter this channel in a valence-like combination, i.e. as the difference between quark and antiquark distributions.

Since the Bethe Heitler channel vanishes, one can write in general for the transversely polarized, differential cross section for single-inclusive photon production

$$E_\gamma \frac{\mathrm{d}\sigma}{\mathrm{d}^3\boldsymbol{P_\gamma}}(S) \;=\; E_\gamma \frac{\mathrm{d}\sigma^C}{\mathrm{d}^3\boldsymbol{P_\gamma}}(S) + E_\gamma \frac{\mathrm{d}\sigma^I}{\mathrm{d}^3\boldsymbol{P_\gamma}}(S)\,, \tag{5.1}$$

with σ^C and σ^I denoting the Compton and Interference contributions respectively. The unpolarized cross section constituting the denominator of the transverse SSA (2.61) was already calculated in Ref. [38]. In the following two sections the Compton and Interference channels will be analyzed in more detail for the case of transverse polarization, in particular the methods to perform the corresponding calculations will be highlighted.

5.1 Compton Channel

As elaborated on in the introduction to this chapter, the transversely polarized cross section for the Compton channel can be split in two parts corresponding to the production mechanism of the observed final state photon: first the production via fragmentation described by the FFs $D_1^{\gamma/q}$ and $D_1^{\gamma/g}$ and second the direct production in a point-like QED hard-scattering vertex

$$E_\gamma \frac{\mathrm{d}\sigma^C}{\mathrm{d}^3\boldsymbol{P_\gamma}}(S) \;=\; E_\gamma \frac{\mathrm{d}\sigma^{C,\mathrm{frag}}}{\mathrm{d}^3\boldsymbol{P_\gamma}}(S) + E_\gamma \frac{\mathrm{d}\sigma^{C,\mathrm{direct}}}{\mathrm{d}^3\boldsymbol{P_\gamma}}(S)\,. \tag{5.2}$$

The fragmentation contribution is generated by the same partonic hard scattering diagrams that were featured in the calculation of the single-inclusive hadron production process. The only difference is that the quark-to-hadron and gluon-to-hadron FFs need to be replaced by their photonic analogs

$$D_1^{h/q} \;\to\; D_1^{\gamma/q} \qquad D_1^{h/g} \;\to\; D_1^{\gamma/g}\,. \tag{5.3}$$

Here, it is important to remark a subtle detail regarding the counting of the perturbative order. One can show that the photonic fragmentation functions are of order $\mathcal{O}\left(\alpha_{em}/\alpha_s\right)$. Consequently, the lowest order for the photon production process is given for the convolution of the quark-to-photon FF $D_1^{\gamma/q}$ with the LO result given in Eq. (2.64), and it is of order $\mathcal{O}\left(\alpha_{em}^3/\alpha_s\right)$. On the other hand, convolution of the photonic FFs $D_1^{\gamma/q}, D_1^{\gamma/g}$ with the NLO results presented in Secs. 3.2-3.6 gives the NLO contribution of order $\mathcal{O}\left(\alpha_{em}^3\right)$. Both the LO and NLO results from hadron production are converted to the present case of photon production in the same way

$$E_\gamma \frac{\mathrm{d}\sigma^{C,\mathrm{frag}}}{\mathrm{d}^3\boldsymbol{P_\gamma}}\,(S) \;=\; E_h \frac{\mathrm{d}\sigma^{\mathrm{LO+NLO}}}{\mathrm{d}^3\boldsymbol{P_h}}\,(S)\,\bigg|_{D_1^{h/i}\to D_1^{\gamma/i}}\,. \tag{5.4}$$

Turning to the direct photon production part, one can make use of the results for the $qg \to g$ channel. Both gluon and photon are gauge bosons and share similarities regarding how they couple to quarks. If one makes a suitable replacement for the gluon-to-hadron FF, i.e. $D_1^{h/g}(z) \to \delta(1-z)$, one effectively gets a direct gluon production cross section. Then, one only needs to account for the different couplings in QCD and QED, i.e. replace $\alpha_s \to \alpha_{em}$, as well as for the abelian versus non-abelian nature of photons and gluons. This is achieved by replacing $N_c \to 0$, which gets rid of all the gluon self-interaction diagrams, and $C_F \to e_q^2$. The same separation as for the $qg \to g$ channel into the different pole contributions, namely integral (Int), soft-gluon pole (SGP) and soft-fermion pole (SFP), also applies to the direct Compton channel, leading to

$$\begin{aligned} E_\gamma \frac{\mathrm{d}\sigma^{C,\mathrm{direct}}}{\mathrm{d}^3\boldsymbol{P_\gamma}}\,(S) \;&=\; E_h \frac{\mathrm{d}\sigma^{\mathrm{NLO},qg\to g}}{\mathrm{d}^3\boldsymbol{P_h}}\,(S)\,\bigg|^{C_F\to e_q^2,\,N_c\to 0,\,\alpha_s\to\alpha_{em}}_{D_1^{h/g}(z)\to\delta(1-z)} \\ &=\; E_\gamma \frac{\mathrm{d}\sigma^{C,\mathrm{Int}}}{\mathrm{d}^3\boldsymbol{P_\gamma}}\,(S) \;+\; E_\gamma \frac{\mathrm{d}\sigma^{C,\mathrm{SGP}}}{\mathrm{d}^3\boldsymbol{P_\gamma}}\,(S) \;+\; E_\gamma \frac{\mathrm{d}\sigma^{C,\mathrm{SFP}}}{\mathrm{d}^3\boldsymbol{P_\gamma}}\,(S)\,. \end{aligned} \tag{5.5}$$

5.2 Interference Channel

The Interference channel features a wide variety of Feynman diagrams contributing to the end result, owing to the fact that also twist-3 quark-photon-quark ($q\gamma q$) functions F_γ^q, G_γ^q (see Sec. C.7) and even gluon-photon-gluon ($g\gamma g$) functions O_γ^1, O_γ^2 (see Sec. C.8) contribute. Contrary to the Compton channel, there are no fragmentation contributions, meaning that the observed final-state photon is always produced in a point-like QED hard scattering vertex. Consequently, no photon FFs will enter the formulas for the cross sections. Also note that the twist-3 qgq and $q\gamma q$ functions always enter as valence distributions, i.e. as the difference of quark and antiquark distribution. The general form of the transversely polarized, differential cross section for this channel is given by

$$E_\gamma \frac{\mathrm{d}\sigma^I}{\mathrm{d}^3\boldsymbol{P}_\gamma}(S) = E_\gamma \frac{\mathrm{d}\sigma^I_{\mathrm{LO}}}{\mathrm{d}^3\boldsymbol{P}_\gamma}(S) + E_\gamma \frac{\mathrm{d}\sigma^{I,\mathrm{virt}}_{\mathrm{NLO}}}{\mathrm{d}^3\boldsymbol{P}_\gamma}(S) + E_\gamma \frac{\mathrm{d}\sigma^{I,\mathrm{real}}_{\mathrm{NLO}}}{\mathrm{d}^3\boldsymbol{P}_\gamma}(S)\,. \tag{5.6}$$

5.2.1 NLO Real-Emission Contribution

The NLO real-emission contribution to the Interference channel has many similarities to the previously calculated channels in hadron production, such as the $qg \to g$ channel, see Sec. 3.5. It is thus convenient to start the calculation with these real-emission contributions, i.e. to compute the cross section $\sigma^{I,\mathrm{real}}_{\mathrm{NLO}}$. One can easily check that there are no intrinsic contributions – unsurprisingly, since this is also the case for all production channels in the single-inclusive hadron process.

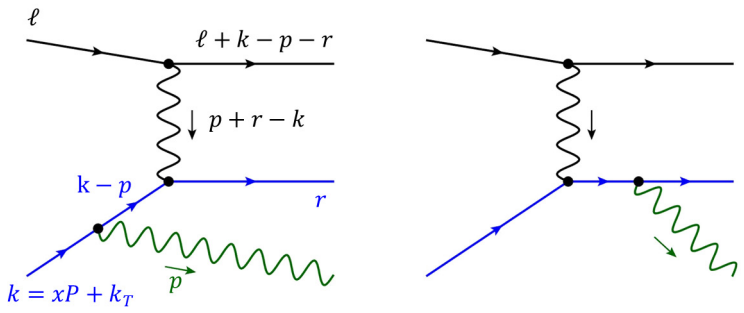

Figure 5.2: NLO real-photon-emission diagrams in the Interference channel, where the photon is emitted from the quark line. The interference of these diagrams with the ones from Fig. 5.3 generates the kinematical twist-3 effects.

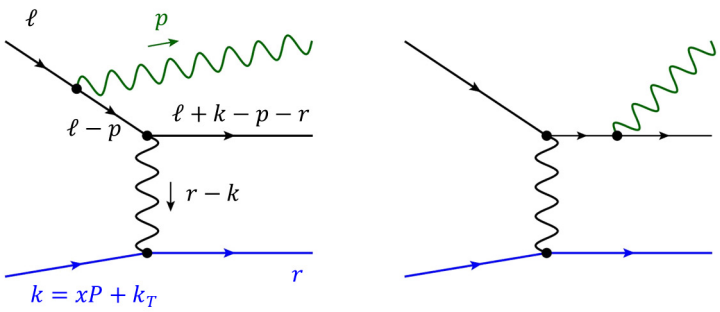

Figure 5.3: Same as Fig. 5.2, but for photon emission from the lepton line.

The first non-vanishing contributions are kinematical. They are given by the interference of the diagrams in Figs. 5.2 and 5.3. The calculational procedure is the same as before and revolves

around keeping a non-zero transverse quark momentum k_T. Only after all phase space integrations have been carried out, a first-order Taylor expansion around $k_T = 0$ is performed. The methods are described in more detail in Sec. 2.4.1. Note that there are only real but no virtual contributions to the kinematical part of the Interference channel.

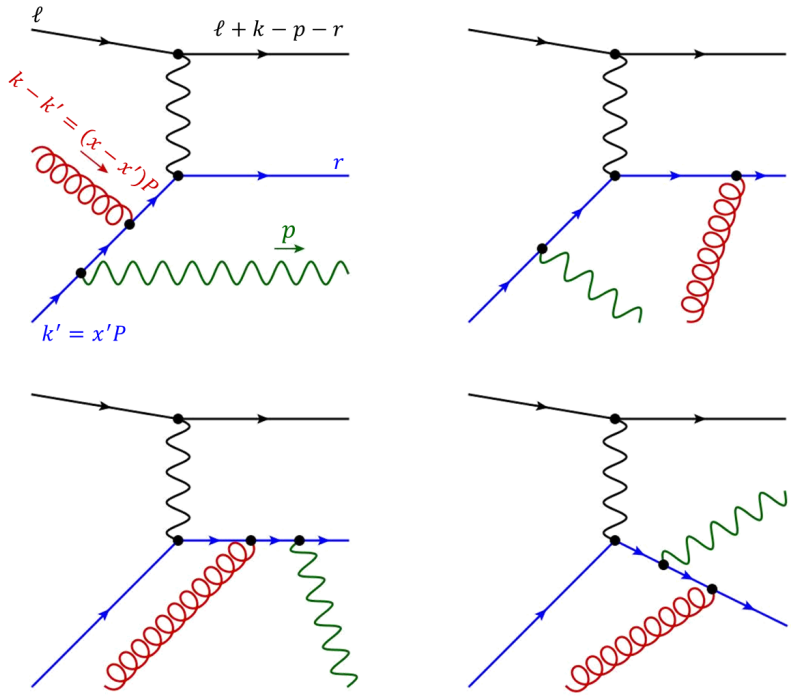

Figure 5.4: NLO real-photon-emission diagrams in the Interference channel, where the photon is emitted from the quark line. The interference of these diagrams with the ones from Fig. 5.3 (for $k_T = 0$) generates a dynamical twist-3 effect.

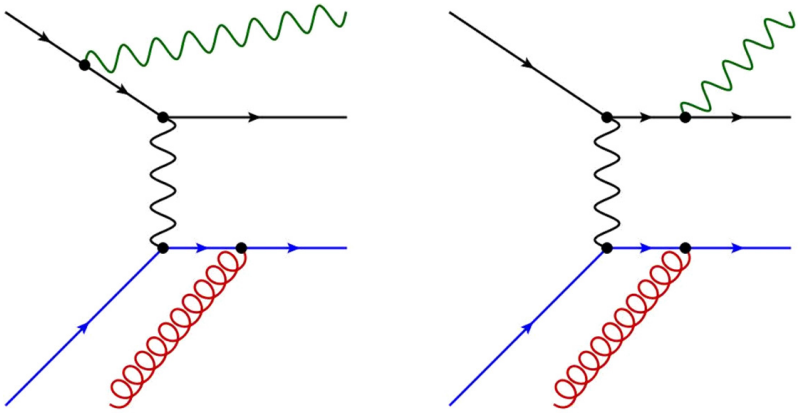

Figure 5.5: Same as Fig. 5.4, but for photon emission from the lepton line. The interference of these diagrams with the ones from Fig. 5.2, (for $k_T = 0$) generates a dynamical twist-3 effect.

Next, to compute the dynamical contributions one needs to consider the interference of the sum of the diagrams shown in Fig. 5.4 with the sum of the diagrams shown in Fig. 5.3 with $k_T = 0$. Another contribution is generated by the interference of the sum of diagrams in Fig. 5.5 with those in Fig. 5.2, for $k_T = 0$. As for the kinematical part, there are only real-photon-emission diagrams and no virtual corrections. Also for the dynamical part, the technicalities of the calculation are the same as for the hadron case, see for example Sec. 3.5. Note that there are again factors such as $1/(1-w)^{1+2\varepsilon}$, which diverge in the limit $w \to 1$. They are taken care of by the conventional expansion of Eq. (2.80). Using the relation of Eq. (2.69) to combine kinematical and dynamical parts, one finds that the kinematical contribution exactly cancels against the direct SGP contribution in this channel. This is a feature that was also observed in the $qg \to g$ channel

of Sec. 3.5 as well as for γSIDIS, see Ref. [109].

There are, however, also subtraction SGP terms originating from an integral contribution in the dynamical part. This contribution is computed in the same way as before, following the methods discussed below Eq. (2.82). Examining the pole structure of the resulting partonic cross sections, one finds singularities at the integration boundaries $\zeta = 0$ and $\zeta = 1$. The singular behavior comes from the denominator $\frac{1}{\zeta(1-\zeta)^2}$, the same as for the $qg \to g$ channel. This implies that one needs to introduce the same integrable combinations of qgq-functions F^q and G^q as given in Eqs. (3.21) and (3.22). Consequently, subtraction SGP contributions, including a derivative term, and subtraction SFP contributions are generated. As already mentioned, the direct SGP terms cancel against the kinematical contributions once Eq. (2.69) is applied and hence the subtraction SGP terms remain by themselves. On the other hand, there are also direct SFP terms which need to be combined with the subtraction SFP terms. To achieve a finite end result for both the SGP and SFP, one needs to perform renormalization.

Interestingly, there are no singularities connected with the vanishing lepton mass $m_\ell = 0$ and correspondingly no photon-in-lepton contributions are required. This is familiar from the Interference channel in the unpolarized case, see Ref. [38].

5.2.2 LO Contribution

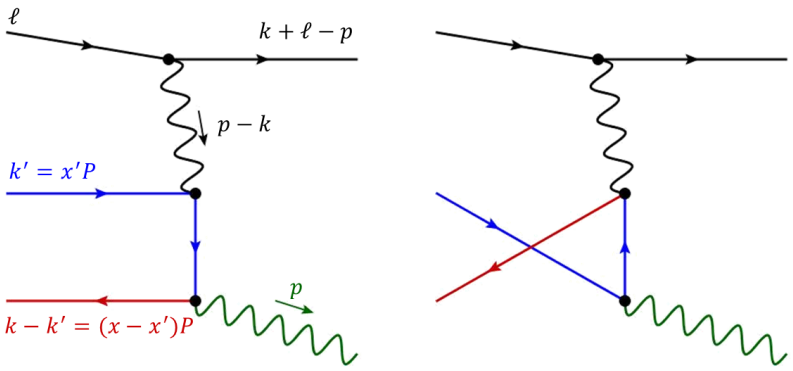

Figure 5.6: LO real-photon-emission diagrams in the Interference channel. The interference of these diagrams with the ones from Fig. 5.7 generates the LO dynamical twist-3 effects.

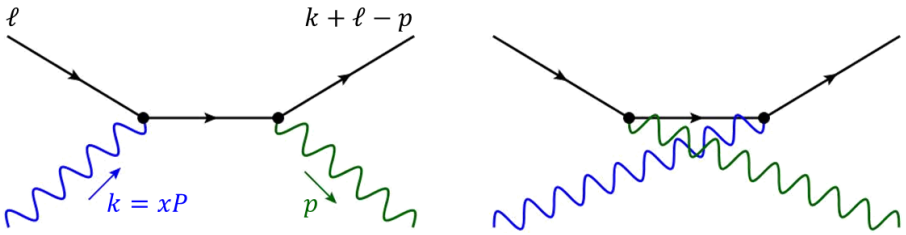

Figure 5.7: LO lepton-photon Compton scattering diagrams. The interference of these diagrams with the ones from Fig. 5.6 generates the LO dynamical twist-3 effects.

As mentioned in the previous subsection, there must be renormalization terms for the qgq-functions F^q, G^q coming from a LO contribution σ^I_{LO}. These terms are necessary for a finite result of the NLO real-emission contribution $\sigma^{I,\text{real}}_{\text{NLO}}$ in Eq. (5.6). However, this LO contribution does not involve F^q or G^q but instead their photonic analogs, the $q\gamma q$ functions F^q_γ, G^q_γ. The $q\gamma q$ functions are defined in complete analogy to the qgq functions, but with the gluon field strength tensor replaced by its electromagnetic counterpart, see Eq. (C.24). A direct implication of this fact is that the $q\gamma q$ functions share the same symmetry and support properties, see Eq. (C.25).

The required renormalization formulas have been derived and collected in Sec. 2.5.2. In this work it is conjectured that the $q\gamma q$-functions are of order $\mathcal{O}(\alpha_{em}/\alpha_s)$, in analogy to the (un-)polarized photon PDFs f_1^γ and g_1^γ, cf. Ref. [135], as well as the photon FFs D_1^γ. This implies that the LO contribution to the Interference channel has the perturbative order $\mathcal{O}\left(\alpha^3_{em}/\alpha_s\right)$, which is the same as the LO contribution of the Compton channel discussed above in Sec. 5.1. There is

no kinematical part to this LO contribution and the dynamical part is computed by taking the interference of the sum of diagrams in Fig. 5.6 with the sum of diagrams in 5.7.

Technically, the twist-3 functions entering the results via the diagrams in Figs. 5.6 and 5.7 correspond to a quark-antiquark-photon ($q\bar{q}\gamma$) configuration rather than a quark-photon-quark ($q\gamma q$) configuration. This is reflected by the fact that the functions enter the factorization formula evaluated at a certain combination of the longitudinal momentum fractions x, x', i.e. as $F_\gamma^q(x'-x,x')$ and $G_\gamma^q(x'-x,x')$. Also apparent from the Feynman diagrams is that one deals with a two-particle final-state. This leads to simpler kinematics and consequently a rather compact result for the spin-dependent cross section, given in Eq. (6.31).

Having computed the LO result, one can employ the renormalization formula in Eq. (2.108). This formula describes mixing of the $q\gamma q$ functions F_γ^q, G_γ^q with the qgq functions F^q, G^q. The aforementioned $\frac{1}{\varepsilon}$ poles in the SGP and SFP parts of the NLO real-photon-emission contributions indeed cancel upon inclusion of the renormalization terms, leading to the finite results presented in Eqs. (6.38) and (6.39).

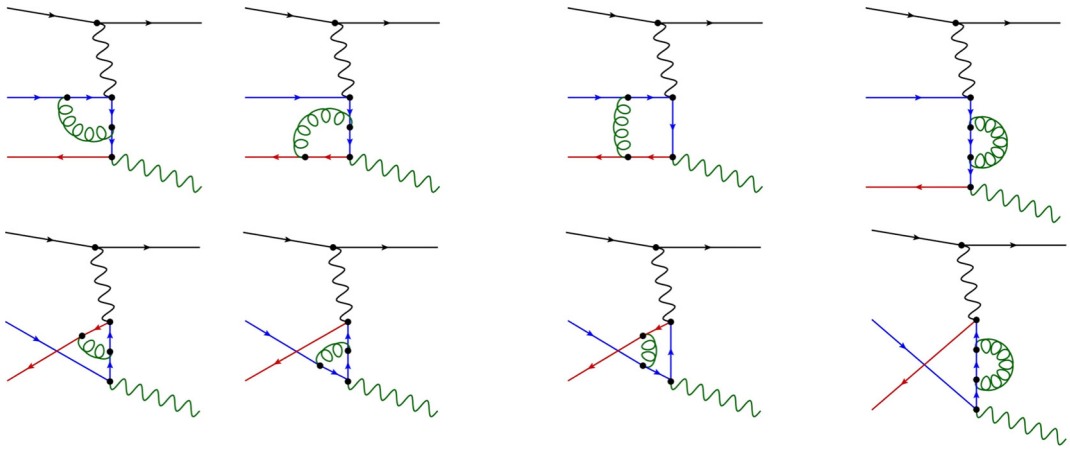

Figure 5.8: NLO virtual diagrams in the Interference channel. The interference of these diagrams with the ones from Fig. 5.7 generates a dynamical twist-3 contribution at NLO. The diagrams are **Left:** four vertex corrections, **Middle:** two box diagrams and **Right:** two self-energies.

5.2.3 NLO Virtual $q\gamma q$ Contribution

Considering the $q\gamma q$-functions as $\mathcal{O}(\alpha_{em}/\alpha_s)$ opens up further production channels at NLO: one needs to include diagrams that come with an extra factor of α_s compared to LO, giving a contribution of order $\mathcal{O}(\alpha_{em}^3)$. The possible diagrams all feature loops with a virtual gluon and contribute to $\sigma_{\text{NLO}}^{I,\text{virt}}$ in Eq. (5.6). They are shown in Fig. 5.8 and can be classified as four vertex correction diagrams (on the left), two box diagrams (in the middle) and two self-energy diagrams (on the right). One needs to compute the interference of their sum with the sum of the two diagrams shown in Fig. 5.7.

Note that this channel only has dynamical and no kinematical contributions. The evaluation of the loop integrals was performed using Feynman gauge, i.e. for $\kappa = 0$ in Eq. (2.70), such that denominators could be combined using the Feynman parameter method. Each of the eight diagrams in Fig. 5.8 leads to slightly different parameter integrals. Since an imaginary part must be generated for a non-zero dynamical contribution it is important to keep the causal $i\delta$ from the Feynman propagators, because it will determine the sign of said imaginary parts.

As before, there are two sources of imaginary parts:

- The decomposition of a propagator into principal value and δ-function, such as in Eq. (5.7)
- Imaginary parts can also emerge from the Feynman parameter integrals encountered in the loop integrations, in certain regions of x', such as in Eq. (5.8)

A sketch of these two sources is shown in Fig. 5.9. On the left, a solid bar indicates a propagator that goes on-shell corresponding to the following decomposition

$$\frac{1}{(k'-k+p)^2+i\delta} \propto \left(\mathcal{P}\frac{1}{x'-x} - i\pi\delta(x'-x)\right). \tag{5.7}$$

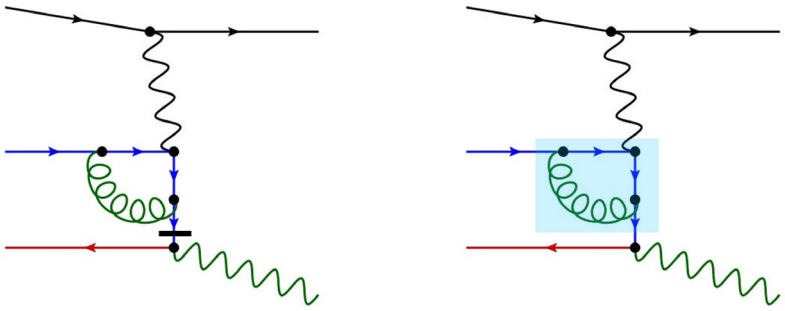

Figure 5.9: Sketch of possible sources for imaginary parts in the NLO virtual contribution to the Interference channel. **Left:** the propagator marked with the solid bar goes on-shell, **Right:** the Feynman parameter integral associated to the loop highlighted in light-blue develops an imaginary part.

The δ-function in the imaginary part sets the longitudinal momentum fractions equal to each other, i.e. $x' = x$, while due to the two-particle phase space one also has $x = x_0$. Using the *photonic* Mandelstam variables $s = (l+P)^2 \simeq 2l \cdot P$, $t = (P - P_\gamma)^2 \simeq -2P \cdot P_\gamma$ and $u = (l - P_\gamma)^2 \simeq -2l \cdot P_\gamma$ one has $x_0 = \frac{-u}{s+t}$. In terms of the dimensionless variable $w = \frac{x}{x_0}$ the condition $x = x_0$ is given as $w = 1$. Thus, contributions generated by the imaginary part of a propagator decomposition are $\propto \delta(1-w)$.

On the right of Fig. 5.9 a situation is sketched where a Feynman parameter integral develops an imaginary part. The integral could for example have the schematic form

$$\int_0^1 \mathrm{d}u_1 \int_0^{1-u_1} \mathrm{d}u_2 \left(-u_1 \hat{t} \left((1-u_1) \left(1 - \frac{x'}{x} \right) + u_2 \frac{x'}{x} \right) - i\delta \right)^{-\varepsilon} , \tag{5.8}$$

with the partonic analog $\hat{t} = (xP - P_\gamma)^2 = xt$ of the Mandelstam variable t. The term in brackets can become negative under the condition that $x < x' < 1$ and $u_2 < (1-u_1)\left(1 - \frac{x}{x'}\right)$, generating an imaginary part. One still has a two-particle phase space and consequently $x = x_0$, but x' is restrained to an interval rather than fixed to a specific value by a δ-function, unlike previously for the propagator decomposition. Using the substitution $x' = \frac{x_0}{w}$ one can write the contribution generated by the imaginary part of a loop integral via a w-integral over the interval $(x_0, 1)$, i.e. $\int_{x_0}^1 \frac{\mathrm{d}w}{w}$ *without* a δ-function $\delta(1-w)$. Another possible region in x' that can generate imaginary parts in the parameter integral is $-1 + x < x' < 0$, which can also be mapped onto the same w integral using the substitution $x' = -x_0 \frac{1-w}{w}$.

When extracting the imaginary parts from the loop integrals, one has to be careful with the overall sign. A typical "mass" M^2 introduced by the Feynman parameter method always contains a small negative imaginary part $-i\delta$. This means that whenever the real part becomes negative, i.e. $\mathrm{Re}\left\{M^2\right\} < 0$, one is *below* the branch cut of the logarithm on the negative real axis. The masses can enter integrals like in Eq. (5.8) with several different powers and the imaginary part can be extracted via

$$\mathrm{Im}\left\{ (a - i\delta)^{-n-\varepsilon} \right\} \overset{\delta \to 0}{\to} \theta(-a)(-a)^{-n-\varepsilon} \sin \pi(n+\varepsilon) , \tag{5.9}$$

where $a \in \mathbb{R}, n \in \mathbb{Z}$ and θ denotes the Heaviside step function. For the present purpose one only needs the cases $n \in \{0, 1, 2\}$, though.

One further technical detail is that in the calculation of the box integrals in the middle of Fig. 5.8 one encounters a Hypergeometric function ${}_2F_1(1, 2; 2-\varepsilon; 1) = -\frac{1-\varepsilon}{1+\varepsilon}$. This relation is derived for $\varepsilon < -1$, and by analytic continuation it will be also used for $\varepsilon > 0$.

Having extracted the imaginary parts from the loop integrals one finds factors of $1/(1-w)^{1+\varepsilon}$ that display a divergence in the limit $w \to 1$. This divergence is readily regularized using the expansion given in Eq. (2.80), which also introduces a part $\propto \delta(1-w)$. This part has to be combined with the contributions generated by a propagator decomposition such as in Eq. (5.7).

Still, the result one finds in this way is not yet free of $\frac{1}{\varepsilon}$ poles because one also has to consider the renormalization of the $q\gamma q$ functions. The relevant part of the renormalization formulas is the self-mixing of the $q\gamma q$ functions, see Eq. (2.126). These terms have to be plugged into the LO result given in Eq. (6.31), leading to the desired cancellation of the remaining collinear divergences. The final result for the NLO virtual $q\gamma q$ contribution is shown in Eq. (6.34) with partonic

factors collected in the appendix in Eq. (F.98). The $q\gamma q$ valence distributions enter in a hard pole configuration, i.e. as $F_\gamma^{q-\bar{q}}(x, x(1-w)), G_\gamma^{q-\bar{q}}(x, x(1-w))$.

5.2.4 NLO Virtual $g\gamma g$ Contribution

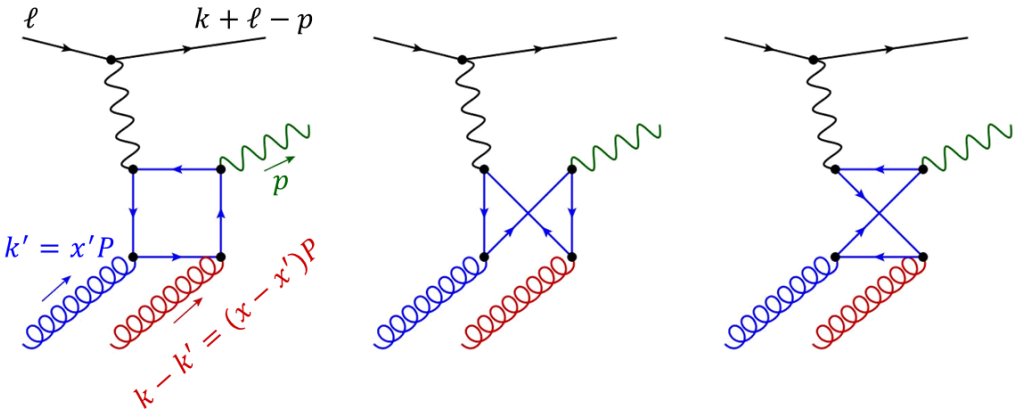

Figure 5.10: NLO virtual diagrams in the Interference channel. The interference of these diagrams with the ones from Fig. 5.7 generates a dynamical twist-3 effect.

Considering the $q\gamma q$ functions F_γ^q, G_γ^q to be of order $\mathcal{O}(\alpha_{\text{em}}/\alpha_s)$ relative to their QCD counterparts (the qgq functions F^q and G^q), one must also account for additional contributions at NLO. Specifically, a new set of multiparton twist-3 distribution functions appears. These are the previously unexplored $g\gamma g$ functions O_γ^1 and O_γ^2, defined similarly to the symmetric ggg function O (see App. C.8 and Eq. (C.26) for details). The $g\gamma g$ functions are also assumed to be of order $\mathcal{O}(\alpha_{\text{em}}/\alpha_s)$ and will make a $\mathcal{O}(\alpha_{\text{em}}^3)$ contribution to the cross section. To the author's knowledge, O_γ^1, O_γ^2 have not been addressed in the literature, making their appearance in this work especially significant. They generate the second part of the NLO virtual contribution $\sigma_{\text{NLO}}^{I,\text{virt}}$ in Eq. (5.6).

To perform the corresponding calculation one needs to compute the interference of the sum of the three box diagrams depicted in Fig. 5.10 with the sum of diagrams in Fig. 5.7. The general procedure is quite similar to the NLO virtual $q\gamma q$ contribution of the previous subsection. Like before, there are only dynamical contributions but no kinematical ones for this channel. Again, Feynman gauge and correspondingly $\kappa = 0$ is assumed such that loop integrals can be evaluated using the Feynman parameter method. Contrary to the $q\gamma q$ case, the imaginary parts for the dynamical $g\gamma g$ contribution are generated exclusively through the parameter integrals of the loops. There are no propagators that contribute an imaginary part.

The treatment of the parameter integrals follows the same principles as in the $q\gamma q$ case. Again, there are two regions in x' that can generate imaginary parts, $x < x' < 1$ and $-1 + x < x' < 0$, and they are extracted according to Eq. (5.9). However, the required parameter integrals are more involved and thus a more in-depth discussion is given. Due to the four propagators in the loop, one needs to solve the following type of four-fold integrals including a "mass" $M^2(x, x')$, which is introduced through the Feynman parameter method

$$\begin{aligned} I_{M,ijk}^n(x, x', \varepsilon) &= \int \mathcal{D}u\, u_1^i u_2^j u_3^k \left(M^2(x, x')\right)^{-n-\varepsilon} \\ \int \mathcal{D}u &\equiv \int_0^1 \mathrm{d}u_1 \mathrm{d}u_2 \mathrm{d}u_3 \mathrm{d}u_4 \delta(u_1 + u_2 + u_3 + u_4 - 1)\,. \end{aligned} \tag{5.10}$$

Here, the "masses" for the three diagrams in Fig. 5.10 are from left to right given as

$$\begin{aligned} M_1^2(x, x') &\equiv -u_2 \hat{t}\left(1 - u_2 - u_3 - \frac{x'}{x} u_4\right) - i\delta \\ M_2^2(x, x') &\equiv -\hat{t}\left(u_1 u_2 \frac{x'}{x} + u_2(1 - u_2)\left(1 - \frac{x'}{x}\right) + u_3\left(u_1 \frac{x'}{x} - u_2\left(1 - \frac{x'}{x}\right)\right)\right) - i\delta \\ M_3^2(x, x') &\equiv -u_2 \hat{t}\left(1 - u_2 - u_3 - u_4\left(1 - \frac{x'}{x}\right)\right) - i\delta\,. \end{aligned} \tag{5.11}$$

The relation $u_1+u_2+u_3+u_4=1$ helps in simplifying the expressions. A convenient substitution for this type of parameter integrals can be found in Refs. [117, 136] and introduces new parameters η_1,η_2 and ξ_1,ξ_2 in the following way

$$\begin{aligned} u_1 &= \eta_1\xi_1 \\ u_2 &= \eta_2(1-\xi_2) \\ u_3 &= \eta_2\xi_2 \\ u_4 &= \eta_1(1-\xi_1) \\ \mathrm{d}u_1\mathrm{d}u_2\mathrm{d}u_3\mathrm{d}u_4 &= \eta_1\eta_2\,\mathrm{d}\eta_1\mathrm{d}\eta_2\mathrm{d}\xi_1\mathrm{d}\xi_2\,. \end{aligned} \tag{5.12}$$

The advantage of the substitution is that the η integrals factorize from the ξ integrals. The diagrams on the left and right of Fig. 5.10 give a non-vanishing contribution for either $x<x'<1$ (left) or $-1+x<x'<0$ (right) respectively. Furthermore, also the ξ_1 and ξ_2 integrals factorize from each other and all remaining integrals are representations of the Euler Beta and Hypergeometric functions. For the middle diagram one gets contributions from *both* regions in x', i.e. $x<x'<1$ *and* $-1+x<x'<0$. In contrast to the other two diagrams, the ξ_1 and ξ_2 integrals do not factorize. Still, one can trace everything back to either Beta or Hypergeometric functions using suitable substitutions and the generalized binomial theorem. In the end, this leads to the following results, again corresponding to the diagrams from left to right in Fig. 5.10

$$\begin{aligned} \mathrm{Im}\left\{\int \mathcal{D}u\, u_2^i u_3^j u_4^k \left(M_1^2\right)^{-n-\varepsilon}\right\} &= \theta(x'-x)\sin\pi(n+\varepsilon)\left(-\hat{t}\left(\frac{x'}{x}-1\right)\right)^{-n-\varepsilon}\left(1-\frac{x}{x'}\right)\times \\ &\quad \frac{j!\Gamma(1+i-n-\varepsilon)\Gamma(2+k-n-\varepsilon)}{(1-n-\varepsilon)\Gamma(4+i+j+k-2n-2\varepsilon)}{}_2F_1\left(-k,1,2-n-\varepsilon,1-\frac{x}{x'}\right) \\ \mathrm{Im}\left\{\int \mathcal{D}u\, u_1^i u_2^j u_3^k \left(M_2^2\right)^{-n-\varepsilon}\right\} &= \sin\pi(n+\varepsilon)\frac{\Gamma(2+j+k-n-\varepsilon)\Gamma(1-n-\varepsilon)}{\Gamma(4+i+j+k-2n-2\varepsilon)}\times \\ &\quad \Bigg[\theta(-x')\left(\frac{-x'}{x-x'}\right)^{1+j}\left(-\hat{t}\left(\frac{-x'}{x}\right)\right)^{-n-\varepsilon}\times \\ &\qquad \sum_{n'=0}^{k}\binom{k}{n'}\frac{\left(\frac{-x'}{x-x'}\right)^{n'}(j+n')!(-1)^{n'}}{2+i+j+n'-n-\varepsilon}\frac{\Gamma(2+i-n-\varepsilon)}{\Gamma(2+j+n'-n-\varepsilon)} \\ &\qquad +\theta(x'-x)\left(1-\frac{x}{x'}\right)^{1+i}\left(-\hat{t}\left(\frac{x'}{x}-1\right)\right)^{-n-\varepsilon}\frac{i!k!\Gamma(2+i+j-n-\varepsilon)}{\Gamma(3+i+j+k-n-\varepsilon)}\Bigg] \\ \mathrm{Im}\left\{\int \mathcal{D}u\, u_2^i u_3^j u_4^k \left(M_3^2\right)^{-n-\varepsilon}\right\} &= \theta(-x')\sin\pi(n+\varepsilon)\left(-\hat{t}\left(-\frac{x'}{x}\right)\right)^{-n-\varepsilon}\frac{-x'}{x-x'}\times \\ &\quad \frac{j!\Gamma(1+i-n-\varepsilon)\Gamma(2+k-n-\varepsilon)}{(1-n-\varepsilon)\Gamma(4+i+j+k-2n-2\varepsilon)}{}_2F_1\left(-k,1,2-n-\varepsilon,\frac{-x'}{x-x'}\right)\,. \end{aligned} \tag{5.13}$$

The final steps resemble the $q\gamma q$ case discussed in the previous subsection. First, one needs to regularize divergences in the limit $w\to 1$ originating from factors $1/(1-w)^{1+\varepsilon}$, via the expansion (2.80). Then, one needs to add renormalization terms to cancel the remaining collinear divergences. This is achieved by plugging the results of Eq. (2.132) for the $q\gamma q\to g\gamma g$ mixing into the LO result given in Eq. (6.31). The end result is indeed free of $\frac{1}{\varepsilon}$ poles and thus finite. The result is shown in Eq. (6.35), with partonic factors given in App. F.3, and it features the $g\gamma g$ functions in a hard pole configuration, i.e. as $O^1_\gamma(x,x(1-w)), O^2_\gamma(x,x(1-w))$.

Chapter 6

Analytical Results

This chapter constitutes a complete overview off all analytical results derived in the previous chapters for the differential, transversely polarized cross sections of the considered processes. Each of the different processes, i.e. single-inclusive hadron production $\ell(l)N^\uparrow(P) \to h(P_h)X$, the related jet production $\ell(l)N^\uparrow(P) \to \text{jet}(P_j)X$ as well as single-inclusive photon production $\ell(l)N^\uparrow(P) \to \gamma(P_\gamma)X$ and the γSIDIS process $\ell(l)N^\uparrow(P) \to \ell'(l')\gamma(P_\gamma)X$, is presented separately in the following sections. The parentheses denote the external four-momenta for each reaction.

The corresponding partonic cross sections are too lengthy to show here and are instead given in Appendix F. The unpolarized counterparts required to calculate the spin asymmetries have already been computed previously, namely in [120] for hadrons and jets, in [38] for single-inclusive photons and both in [109] and [137] for γSIDIS.

The notation in the following will suppress several indices, sub-/superscripts and arguments of functions in order to achieve a better readability and less cluttered expressions. To be specific, the scale-dependence in all correlation and fragmentation functions will be omitted, the subscript "FT" for the qgq functions will be dropped as well as the "$\overline{\text{MS}}$" superscript for the modified minimal subtraction scheme. As an example, the notation will simply be $F^q(x,x')$ instead of $F_{FT}^{q,\overline{\text{MS}}}(x,x';\mu)$. In addition to that, possible scale dependence or dependence on the lepton mass m_ℓ will generally be suppressed for partonic cross sections.

The results are expressed in terms of the usual mandelstam variables and their partonic counterparts, the longitudinal momentum fractions x (distribution side) and z (fragmentation side), as well as further useful variables and a convenient, spin-dependent prefactor

$$\begin{aligned} s = (l+P)^2\,, \quad t = (P-P_h)^2\,, \quad u &= (l-P_h)^2\,; \quad \hat{s} = xs, \quad \hat{t} = \frac{xt}{z}, \quad \hat{u} = \frac{u}{z} \\ v_0 = \frac{u}{t+u}, \quad v_1 = 1+\frac{t}{s}, \quad x &= \frac{x_0}{w}, \quad x_0 = \frac{(1-v)}{v}\frac{u}{t}, \quad z = \frac{1-v_1}{1-v}; \\ \sigma_0(S) &= \frac{8\pi\alpha_{em}^2}{s^2}\frac{M\epsilon^{lPP_hS}}{u^2}\,. \end{aligned} \tag{6.1}$$

In the above equation, a shorthand notation for the contraction of the levi-civita tensor is used, $\epsilon^{lPP_hS} = l_\mu P_\nu (P_h)_\rho S_\lambda \epsilon^{\mu\nu\rho\lambda}$, with the sign convention $\epsilon^{0123} = +1$. Note that the mandelstam variables t, u and also the prefactor σ_0 are defined analogously via P_j for jet production and P_γ for photon production. The kinematics for the γSIDIS process are quite different from the single-inclusive processes and hence other variables will be employed for this case. They are given in the corresponding section below.

6.1 Hadron Production

Starting point of this chapter is the NLO pQCD formula for the transversely polarized cross section of single-inclusive hadron production $\ell(l)N^\uparrow(P) \to h(P_h)X$. The momenta of the external particles are indicated in brackets. According to the discussion in Ch. 3 and Refs. [36, 37], the differential cross section can be split up in the following manner

$$E_h\frac{\mathrm{d}\sigma_{\text{NLO}}^{\ell N^\uparrow \to hX}}{\mathrm{d}^3\boldsymbol{P_h}} = E_h\frac{\mathrm{d}\sigma_{\text{NLO}}^{qg\to q}}{\mathrm{d}^3\boldsymbol{P_h}} + E_h\frac{\mathrm{d}\sigma_{\text{NLO}}^{qq\to q}}{\mathrm{d}^3\boldsymbol{P_h}} + E_h\frac{\mathrm{d}\sigma_{\text{NLO}}^{qq\to q'}}{\mathrm{d}^3\boldsymbol{P_h}} + E_h\frac{\mathrm{d}\sigma_{\text{NLO}}^{gg\to g}}{\mathrm{d}^3\boldsymbol{P_h}} + E_h\frac{\mathrm{d}\sigma_{\text{NLO}}^{gg\to q}}{\mathrm{d}^3\boldsymbol{P_h}}\,. \tag{6.2}$$

Each of the five production channels in Eq. (6.2) is itself composed of several contributions which are characterized by the longitudinal momentum fractions that enter the twist-3 correlation functions.

All of the channels are discussed one by one in the following subsections.

6.1.1 Channel $qg \to q$:

Based on the derivation presented in Sec. 3.2 one finds a decomposition of this channel into integral (Int), soft-gluon pole (SGP), soft-fermion pole (SFP) and hard pole (HP) contributions

$$E_h \frac{\mathrm{d}\sigma_{\mathrm{NLO}}^{qg\to q}}{\mathrm{d}^3\boldsymbol{P_h}} = E_h \frac{\mathrm{d}\sigma_{\mathrm{Int}}^{qg\to q}}{\mathrm{d}^3\boldsymbol{P_h}} + E_h \frac{\mathrm{d}\sigma_{\mathrm{SGP}}^{qg\to q}}{\mathrm{d}^3\boldsymbol{P_h}} + E_h \frac{\mathrm{d}\sigma_{\mathrm{SFP}}^{qg\to q}}{\mathrm{d}^3\boldsymbol{P_h}} + E_h \frac{\mathrm{d}\sigma_{\mathrm{HP}}^{qg\to q}}{\mathrm{d}^3\boldsymbol{P_h}} \,. \tag{6.3}$$

The analytic expressions for the partonic cross sections encountered in the equations below are shown in Appendix F.1.1.

Integral Contribution

Beginning the collection of results with the integral contribution one has

$$\begin{aligned} E_h \frac{\mathrm{d}\sigma_{\mathrm{Int}}^{qg\to q}}{\mathrm{d}^3\boldsymbol{P_h}} &= \sigma_0(S)\,\frac{\alpha_s}{2\pi}\int_{v_0}^{v_1}\mathrm{d}v\int_{x_0}^{1}\frac{\mathrm{d}w}{w}\int_0^1\mathrm{d}\zeta\sum_{q,\bar q} e_q^2\,D_1^q(z)\,\times \\ &\quad\left[\hat\sigma_{\mathrm{Int}}^{qg\to q,1}(v,w,\zeta)\,F_{\mathrm{Int}}^{qg\to q}(x_0,w,\zeta)+\hat\sigma_{\mathrm{Int}}^{qg\to q,5}(v,w,\zeta)\,G_{\mathrm{Int}}^{qg\to q}(x_0,w,\zeta,)\right], \end{aligned} \tag{6.4}$$

where the flavor sum $\sum_{q,\bar q}$ in Eq. (6.4) runs over quarks q as well as antiquarks $\bar q$. As alluded to in previous chapters, the integral contributions feature certain linear combinations of twist-3 correlation functions evaluated at different momentum fractions. In case of the $qg \to q$ channel one has the following

$$\begin{aligned} F_{\mathrm{Int}}^{qg\to q}(x_0,w,\zeta) &\equiv \frac{1}{\zeta^2(1-\zeta)^2(w-\zeta)^2}\,[F^q(x,\zeta x) \\ &+\frac{\zeta^2(1-\zeta)^2}{(1-w)^3w^3}\left((5w^2+2\zeta-3w-4w\zeta)\,F^q(x,x_0)+(w-\zeta)(1-w)\,x_0(\partial_2F^q)(x,x_0)\right) \\ &-\frac{\zeta^2(w-\zeta)^2}{(1-w)^3}\left((5-4\zeta-3w+2w\zeta)\,F^q(x,x)-\frac{1}{2}(1-\zeta)(1-w)\,x(F^q)'(x,x)\right) \\ &-\frac{(w-\zeta)^2(1-\zeta)^2}{w^3}\left((2\zeta+w+2w\zeta)\;F^q(x,0)+\zeta\,x_0(\partial_2F^q)(x,0)\right)\Big] \\ G_{\mathrm{Int}}^{qg\to q}(x_0,w,\zeta) &\equiv \frac{1}{\zeta^2(1-\zeta)^2(w-\zeta)^2}\,[G^q(x,\zeta x) \\ &+\frac{\zeta^2(1-\zeta)^2}{(1-w)^3w^3}\left((5w^2+2\zeta-3w-4w\zeta)\,G^q(x,x_0)+(w-\zeta)(1-w)\,x_0(\partial_2G^q)(x,x_0)\right) \\ &+\frac{\zeta^2(w-\zeta)^2(1-\zeta)}{(1-w)^2}\,x(\partial_2G^q)(x,x) \\ &-\frac{(w-\zeta)^2(1-\zeta)^2}{w^3}\left((2\zeta+w+2w\zeta)\,G^q(x,0)+\zeta\,x_0(\partial_2G^q)(x,0)\right)\Big]\,. \end{aligned} \tag{6.5}$$

Soft-Gluon Pole Contribution

Moving on with the soft-gluon pole contribution, the analytic formula reads

$$\begin{aligned} E_h \frac{\mathrm{d}\sigma_{\mathrm{SGP}}^{qg\to q}}{\mathrm{d}^3\boldsymbol{P_h}} &= \sigma_0(S)\,\frac{\alpha_s}{2\pi}\int_{v_0}^{v_1}\mathrm{d}v\int_{x_0}^{1}\frac{\mathrm{d}w}{w}\sum_{q,\bar q} e_q^2\,D_1^q(z)\,\times \\ &\Big[\hat\sigma_{\mathrm{SGP},F}^{qg\to q,1}(v,w)\,F^q(x,x)+\hat\sigma_{\mathrm{SGP},F'}^{qg\to q,1}(v,w)\,(-x_0\,(F^q)'(x,x)) \\ &\quad+\hat\sigma_{\mathrm{SGP},F''}^{qg\to q,1}(v,w)\,(x_0^2\,(F^q)''(x,x))+\hat\sigma_{\mathrm{SGP},\partial_1^2F}^{qg\to q,1}(v,w)\,(x_0^2\,(\partial_1^2F^q)(x,x)) \\ &\quad+\hat\sigma_{\mathrm{SGP},\partial_1G}^{qg\to q,5}(v,w)\,(-x_0\,(\partial_1G^q)(x,x))+\hat\sigma_{\mathrm{SGP},\partial_1^2G}^{qg\to q,5}(v,w)\,(x_0^2\,(\partial_1^2G^q)(x,x))\Big], \end{aligned} \tag{6.6}$$

Soft-Fermion Pole Contribution

Next is the result for the soft-fermion pole contribution

$$E_h \frac{\mathrm{d}\sigma_{\mathrm{SFP}}^{qg\to q}}{\mathrm{d}^3\boldsymbol{P_h}} = \sigma_0(S)\,\frac{\alpha_s}{2\pi}\int_{v_0}^{v_1}\mathrm{d}v\int_{x_0}^{1}\frac{\mathrm{d}w}{w}\sum_{q,\bar{q}} e_q^2\,D_1^q\,(z)\,\times$$
$$\Big[\hat{\sigma}_{\mathrm{SFP},F}^{qg\to q,1}(v,w)\,F^q(x,0)+\hat{\sigma}_{\mathrm{SFP},\partial_2 F}^{qg\to q,1}(v,w)\,(-x_0\,(\partial_2 F^q)(x,0))$$
$$+\hat{\sigma}_{\mathrm{SFP},G}^{qg\to q,5}(v,w)\,G^q(x,0)+\hat{\sigma}_{\mathrm{SFP},\partial_2 G}^{qg\to q,5}(v,w)\,(-x_0\,(\partial_2 G^q)(x,0))\Big]\,. \tag{6.7}$$

Hard Pole Contribution

The $qg\to q$ channel results are concluded by the hard pole contribution

$$E_h \frac{dd\sigma_{\mathrm{HP}}^{qg\to q}}{\mathrm{d}^3\boldsymbol{P_h}} = \sigma_0(S)\frac{\alpha_s}{2\pi}\int_{v_0}^{v_1}\mathrm{d}v\int_{x_0}^{1}\frac{\mathrm{d}w}{w}\sum_{q,\bar{q}} e_q^2 D_1^q(z)\,\times$$
$$\Big[\hat{\sigma}_{\mathrm{HP},F}^{qg\to q,1}(v,w)\,F^q(x,x_0)-\hat{\sigma}_{\mathrm{HP},\partial_1 F}^{qg\to q,1}(v,w)\,x_0(\partial_1 F^q)(x,x_0)$$
$$-\hat{\sigma}_{\mathrm{HP},\partial_2 F}^{qg\to q,1}(v,w)\,x_0(\partial_2 F^q)(x,x_0)+\hat{\sigma}_{\mathrm{HP},\partial_1^2 F}^{qg\to q,1}(v,w)\,x_0^2(\partial_1^2 F^q)(x,x_0)$$
$$+\hat{\sigma}_{\mathrm{HP},\partial_1\partial_2 F}^{qg\to q,1}(v,w)\,x_0^2(\partial_1\partial_2 F^q)(x,x_0)+\hat{\sigma}_{\mathrm{HP},G}^{qg\to q,5}(v,w)\,G^q(x,x_0)$$
$$-\hat{\sigma}_{\mathrm{HP},\partial_1 G}^{qg\to q,5}(v,w)\,x_0(\partial_1 G^q)(x,x_0)-\hat{\sigma}_{\mathrm{HP},\partial_2 G}^{qg\to q,5}(v,w)\,x_0(\partial_2 G^q)(x,x_0)$$
$$+\hat{\sigma}_{\mathrm{HP},\partial_1^2 G}^{qg\to q,5}(v,w)\,x_0^2(\partial_1^2 G^q)(x,x_0)+\hat{\sigma}_{\mathrm{HP},\partial_1\partial_2 G}^{qg\to q,5}(v,w)\,x_0^2(\partial_1\partial_2 G^q)(x,x_0)\Big]\,. \tag{6.8}$$

6.1.2 Channel $qq\to q$:

Similar to the previous channel $qg\to q$, the result for the channel $qq\to q$ can be split up in terms of several contributions

$$E_h \frac{\mathrm{d}\sigma_{\mathrm{NLO}}^{qq\to q}}{\mathrm{d}^3\boldsymbol{P_h}} = E_h \frac{\mathrm{d}\sigma_{\mathrm{Int}}^{qq\to q}}{\mathrm{d}^3\boldsymbol{P_h}} + E_h \frac{\mathrm{d}\sigma_{\mathrm{SFP}}^{qq\to q}}{\mathrm{d}^3\boldsymbol{P_h}} + E_h \frac{\mathrm{d}\sigma_{\mathrm{HP}}^{qq\to q}}{\mathrm{d}^3\boldsymbol{P_h}}\,. \tag{6.9}$$

Note that in this case there is no soft-gluon pole contribution. Explicit analytical expressions for the various partonic cross sections are listed in Appendix F.1.2.

Integral Contribution

Starting again with the integral contribution

$$E_h \frac{\mathrm{d}\sigma_{\mathrm{Int}}^{qq\to q}}{\mathrm{d}^3\boldsymbol{P_h}} = \sigma_0(S)\,\frac{\alpha_s}{2\pi}\int_{v_0}^{v_1}\mathrm{d}v\int_{x_0}^{1}\frac{\mathrm{d}w}{w}\int_0^1\mathrm{d}\zeta\sum_{q,\bar{q}} e_q^2\,D_1^q\,(z)\,\times$$
$$\Big[\hat{\sigma}_{\mathrm{Int},1}^{qq\to q,1}(v,w,\zeta)\,F_{\mathrm{Int},1}^{qq\to q}(x_0,w,\zeta)+\hat{\sigma}_{\mathrm{Int},1}^{qq\to q,5}(v,w,\zeta)\,G_{\mathrm{Int},1}^{qq\to q}(x_0,w,\zeta)$$
$$+\hat{\sigma}_{\mathrm{Int},2}^{qq\to q,1}(v,w,\zeta)\,F_{\mathrm{Int},2}^{qq\to q}(x_0,w,\zeta)+\hat{\sigma}_{\mathrm{Int},2}^{qq\to q,5}(v,w,\zeta)\,G_{\mathrm{Int},2}^{qq\to q}(x_0,w,\zeta)\Big]\,, \tag{6.10}$$

one encounters two separate linear combinations, both for the vector-like function F^q as well as the axial-vector-like function G^q

$$\begin{aligned}
F_{\mathrm{Int},1}^{qq\to q}(x_0,w,\zeta) &\equiv \frac{1}{\zeta\,(w-\zeta)^2}\Big[F^q\,(-(1-\zeta)\,x,\zeta\,x)-\frac{\zeta\,(2w-\zeta)}{w^2}\,F^q\,(-(1-w)x,x_0)\\
&\quad -\frac{\zeta\,(\zeta-w)}{w^2}\,x_0\,[\partial_1 F^q+\partial_2 F^q]\,(-(1-w)x,x_0)-\frac{(w-\zeta)^2}{w^2}\,F^q\,(-x,0)\Big]\\
G_{\mathrm{Int},1}^{qq\to q}(x_0,w,\zeta) &\equiv \frac{1}{\zeta\,(w-\zeta)^2}\Big[G^q\,(-(1-\zeta)\,x,\zeta\,x)-\frac{\zeta\,(2w-\zeta)}{w^2}\,G^q\,(-(1-w)x,x_0)\\
&\quad -\frac{\zeta\,(\zeta-w)}{w^2}\,x_0\,[\partial_1 G^q+\partial_2 G^q]\,(-(1-w)x,x_0)-\frac{(w-\zeta)^2}{w^2}\,G^q\,(-x,0)\Big]\\
F_{\mathrm{Int},2}^{qq\to q}(x_0,w,\zeta) &\equiv \frac{1}{1-\zeta}\,[F^q\,(-(1-\zeta)\,x,\zeta\,x)-\,F^q\,(0,x)]\\
G_{\mathrm{Int},2}^{qq\to q}(x_0,w,\zeta) &\equiv \frac{1}{1-\zeta}\,[G^q\,(-(1-\zeta)\,x,\zeta\,x)-\,G^q\,(0,x)]\,.
\end{aligned} \tag{6.11}$$

Soft-Fermion Pole Contribution

The soft-fermion pole contribution has the analytic form

$$E_h \frac{\mathrm{d}\sigma_{\mathrm{SFP}}^{qq\to q}}{\mathrm{d}^3\boldsymbol{P_h}} = \sigma_0(S)\,\frac{\alpha_s}{2\pi}\int_{v_0}^{v_1}\mathrm{d}v\int_{x_0}^{1}\frac{\mathrm{d}w}{w}\sum_{q,\bar{q}} e_q^2\,D_1^q\,(z)\,\times \\ \left[\hat{\sigma}_{\mathrm{SFP},F}^{qq\to q,1}(v,w)\,F^q(-x,0)+\hat{\sigma}_{\mathrm{SFP},G}^{qq\to q,5}(v,w)\,G^q(-x,0)\right], \tag{6.12}$$

Hard Pole Contribution

The concluding contribution for this channel is due to hard poles and reads

$$E_h \frac{\mathrm{d}\sigma_{\mathrm{HP}}^{qq\to q}}{\mathrm{d}^3\boldsymbol{P_h}} = \sigma_0(S)\,\frac{\alpha_s}{2\pi}\int_{v_0}^{v_1}\mathrm{d}v\int_{x_0}^{1}\frac{\mathrm{d}w}{w}\sum_{q,\bar{q}} e_q^2\,D_1^q\,(z)\,\times \tag{6.13}$$

$$\Bigg[\hat{\sigma}_{\mathrm{HP},F}^{qq\to q,1}(v,w)\,F^q(-(1-w)x,x_0)-\hat{\sigma}_{\mathrm{HP},\partial F}^{qq\to q,1}(v,w)\,x_0\,(\partial_1 F^q+\partial_2 F^q)(-(1-w)x,x_0) \\ +\hat{\sigma}_{\mathrm{HP},G}^{qq\to q,5}(v,w)\,G^q(-(1-w)x,x_0)-\hat{\sigma}_{\mathrm{HP},\partial G}^{qq\to q,5}(v,w)\,x_0\,(\partial_1 G^q+\partial_2 G^q)(-(1-w)x,x_0)\Bigg].$$

6.1.3 Channel $qq \to q'$:

Next up, the channel $qq \to q'$ only receives integral and soft-fermion pole contributions

$$E_h \frac{\mathrm{d}\sigma_{\mathrm{NLO}}^{qq\to q'}}{\mathrm{d}^3\boldsymbol{P_h}} = E_h \frac{\mathrm{d}\sigma_{\mathrm{Int}}^{qq\to q'}}{\mathrm{d}^3\boldsymbol{P_h}} + E_h \frac{\mathrm{d}\sigma_{\mathrm{SFP}}^{qq\to q'}}{\mathrm{d}^3\boldsymbol{P_h}}\,. \tag{6.14}$$

The partonic cross sections for this channel are written out explicitly in Appendix F.1.3.

Integral Contribution

The integral contribution can be given in the following way

$$E_h \frac{\mathrm{d}\sigma_{\mathrm{Int}}^{qq\to q'}}{\mathrm{d}^3\boldsymbol{P_h}} = \sigma_0(S)\,\frac{\alpha_s}{2\pi}\int_{v_0}^{v_1}\mathrm{d}v\int_{x_0}^{1}\frac{\mathrm{d}w}{w}\int_0^1\mathrm{d}\zeta\sum_{q'}\left(D_1^{q'}-D_1^{\bar{q}'}\right)(z)\,\times \\ \sum_q e_q^2\left[\hat{\sigma}_{\mathrm{Int}}^{qq\to q',1}(v,w,\zeta)\,F_{\mathrm{Int}}^{qq\to q'}(x,\zeta)+\hat{\sigma}_{\mathrm{Int}}^{qq\to q',5}(v,w,\zeta)\,G_{\mathrm{Int}}^{qq\to q'}(x,\zeta)\right], \tag{6.15}$$

where the correlation functions F_{Int} and G_{Int} are defined as

$$F_{\mathrm{Int}}^{qq\to q'}(x,\zeta) \equiv \frac{F^q\,(-(1-\zeta)\,x,\zeta\,x)-\zeta\,F^q\,(0,x)-(1-\zeta)\,F^q\,(-x,0)}{\zeta(1-\zeta)} \\ G_{\mathrm{Int}}^{qq\to q'}(x,\zeta) \equiv \frac{G^q\,(-(1-\zeta)\,x,\zeta\,x)-\zeta\,G^q\,(0,x)-(1-\zeta)\,G^q\,(-x,0)}{\zeta(1-\zeta)}\,. \tag{6.16}$$

Contrary to the other channels, the flavor sums in the present case, $\sum_q$ and $\sum_{q'}$, only run over quarks $q(q')$ but not over antiquarks $\bar{q}(\bar{q}')$. The antiquark cases are already included in the partonic cross sections because of their (anti-)symmetry properties, see Eqs. (3.17) and (3.18).

Soft-Fermion Pole Contribution

This also applies to the soft-fermion pole contribution below which can be cast into the form

$$E_h \frac{\mathrm{d}\sigma_{\mathrm{SFP}}^{qq\to q'}}{\mathrm{d}^3\boldsymbol{P_h}} = \sigma_0(S)\,\frac{\alpha_s}{2\pi}\int_{v_0}^{v_1}\mathrm{d}v\int_{x_0}^{1}\frac{\mathrm{d}w}{w}\sum_{q'}\left(D_1^{q'}-D_1^{\bar{q}'}\right)(z)\,\times \\ \sum_q e_q^2\Bigg[\hat{\sigma}_{\mathrm{SFP},F}^{qq\to q',1}(v,w)\;(F^q(-x,0)-F^q(0,x)) \\ +\hat{\sigma}_{\mathrm{SFP},G}^{qq\to q',5}(v,w)\;(G^q(-x,0)+G^q(0,x))\Bigg]. \tag{6.17}$$

6.1.4 Channel $qg \to g$:

The results for the channel $qg \to g$ can be decomposed as follows

$$E_h \frac{\mathrm{d}\sigma_{\mathrm{NLO}}^{qg\to g}}{\mathrm{d}^3\boldsymbol{P_h}} = E_h \frac{\mathrm{d}\sigma_{\mathrm{Int}}^{qg\to g}}{\mathrm{d}^3\boldsymbol{P_h}} + E_h \frac{\mathrm{d}\sigma_{\mathrm{SGP}}^{qg\to g}}{\mathrm{d}^3\boldsymbol{P_h}} + E_h \frac{\mathrm{d}\sigma_{\mathrm{SFP}}^{qg\to g}}{\mathrm{d}^3\boldsymbol{P_h}} \,. \tag{6.18}$$

For explicitly written out expressions of all partonic cross sections featured in the following, refer to Appendix F.1.4.

Integral Contribution

First is once more the integral contribution given as

$$\begin{aligned} E_h \frac{\mathrm{d}\sigma_{\mathrm{Int}}^{qg\to g}}{\mathrm{d}^3\boldsymbol{P_h}} &= \sigma_0(S)\,\frac{\alpha_s}{2\pi}\int_{v_0}^{v_1}\mathrm{d}v\int_{x_0}^{1}\frac{\mathrm{d}w}{w}\int_0^1 \mathrm{d}\zeta\, D_1^g(z)\,\times \\ &\sum_{q,\bar{q}} e_q^2\left[\hat{\sigma}_{\mathrm{Int}}^{qg\to g,1}(v,w,\zeta)\,F_{\mathrm{Int}}^{qg\to g}(x_0,w,\zeta) + \hat{\sigma}_{\mathrm{Int}}^{qg\to g,5}(v,w,\zeta)\,G_{\mathrm{Int}}^{qg\to g}(x_0,w,\zeta)\right], \end{aligned} \tag{6.19}$$

The linear combinations of qgq functions in Eq. (6.19) read

$$\begin{aligned} F_{\mathrm{Int}}^{qg\to g}(x_0,w,\zeta) &\equiv \frac{1}{\zeta\,(1-\zeta)^2}\Bigg[F^q(x,\zeta\,x) - \zeta(2-\zeta)\,F^q(x,x) + \tfrac{\zeta\,(1-\zeta)}{2\,w}\,x_0\,(F^q)'(x,x) \\ &\qquad -(1-\zeta)^2\,F^q(x,0)\Bigg] \\ G_{\mathrm{Int}}^{qg\to g}(x_0,w,\zeta) &\equiv \frac{1}{\zeta\,(1-\zeta)^2}\left[G^q(x,\zeta\,x) + \tfrac{\zeta\,(1-\zeta)}{w}\,x_0\,(\partial_2 G^q)(x,x) - (1-\zeta)^2\,G^q(x,0)\right]. \end{aligned} \tag{6.20}$$

Soft-Gluon Pole Contribution

Next, the soft-gluon pole contribution can be written as

$$\begin{aligned} E_h \frac{\mathrm{d}\sigma_{\mathrm{SGP}}^{qg\to g}}{\mathrm{d}^3\boldsymbol{P_h}} &= \sigma_0(S)\,\frac{\alpha_s}{2\pi}\int_{v_0}^{v_1}\mathrm{d}v\int_{x_0}^{1}\frac{\mathrm{d}w}{w}\,D_1^g(z)\,\times \\ \sum_{q,\bar{q}} e_q^2&\left[\hat{\sigma}_{\mathrm{SGP},F}^{qg\to g,1}(v,w)\,F^q(x,x) - \hat{\sigma}_{\mathrm{SGP},\partial_2 G}^{qg\to g,5}(v,w)\,x_0\,(\partial_2 G^q)(x,x)\right], \end{aligned} \tag{6.21}$$

Soft-Fermion Pole Contribution

Finally, the soft-fermion pole contributions to this channel read

$$\begin{aligned} E_h \frac{\mathrm{d}\sigma_{\mathrm{SFP}}^{qg\to g}}{\mathrm{d}^3\boldsymbol{P_h}} &= \sigma_0(S)\,\frac{\alpha_s}{2\pi}\int_{v_0}^{v_1}\mathrm{d}v\int_{x_0}^{1}\frac{\mathrm{d}w}{w}\,D_1^g(z)\,\times \\ \sum_{q,\bar{q}} e_q^2&\left[\hat{\sigma}_{\mathrm{SFP},F}^{qg\to g,1}(v,w)\,F^q(x,0) + \hat{\sigma}_{\mathrm{SFP},G}^{qg\to g,5}(v,w)\,G^q(x,0)\right]. \end{aligned} \tag{6.22}$$

6.1.5 Channel $gg \to q$:

The last remaining partonic channel for single-inclusive hadron production, the channel $gg \to q$, is described by the following analytic formula

$$\begin{aligned} E_h \frac{\mathrm{d}\sigma_{\mathrm{NLO}}^{gg\to q}}{\mathrm{d}^3\boldsymbol{P_h}} &= \sigma_0(S)\,\frac{\alpha_s}{2\pi}\int_{v_0}^{v_1}\mathrm{d}v\int_{x_0}^{1}\frac{\mathrm{d}w}{w}\,\sum_{q,\bar{q}} e_q^2\,D_1^q(z)\,\times \\ &\left[-\hat{\sigma}_{xx}^{gg\to q}(v,w)\,\frac{N(x,x)+O(x,x)}{x} + \hat{\sigma}_{x0}^{gg\to q}(v,w)\,\frac{O(x,0)-N(x,0)}{x}\right], \end{aligned} \tag{6.23}$$

with the special feature that there are neither integral nor hard pole contributions to this channel. The corresponding partonic cross sections can be found in Appendix F.1.5.

6.2 Jet Production

This section presents the explicit analytical result for the second single-inclusive process considered in this work: jet production $\ell(l)N^\uparrow(P) \to \text{jet}(P_j)X$. As elaborated on in Ch. 4, the transversely polarized, differential jet production cross section at NLO is obtained within the small cone approximation, i.e. in the limit $\delta, R \ll 1$ for the jet half-opening angle δ and jet radius R. The result reads

$$\begin{aligned} E_j \frac{\mathrm{d}\sigma^{\ell N^\uparrow \to \text{jet}X}_{\text{NLO}}}{\mathrm{d}^3\boldsymbol{P_j}}(S,R) &= \left(E_h \frac{\mathrm{d}\sigma^{\ell N^\uparrow \to hX}_{\text{NLO}}}{\mathrm{d}^3\boldsymbol{P_h}}(S) \right) \Bigg|_{D_1^{h/(q,g)}(z) \to \delta(1-z)} \\ &\quad + E_j \frac{\mathrm{d}\sigma^{\ell N^\uparrow \to \text{jet}X}_{\text{NLO, jet def}}}{\mathrm{d}^3\boldsymbol{P_j}}(S,R)\,. \end{aligned} \tag{6.24}$$

In the above equation, the first term is obtained by simply replacing the quark and gluon fragmentation functions by a delta function, as indicated. The second piece is calculated in the SCA and can be written as

$$\begin{aligned} E_j \frac{\mathrm{d}\sigma^{\ell N^\uparrow \to \text{jet}X}_{\text{NLO, jet def}}}{\mathrm{d}^3\boldsymbol{P_j}}(S,R) &= \sigma_0(S)\,\frac{\alpha_s}{2\pi}\int_{x_0}^1 \frac{\mathrm{d}w}{w} \times \\ &\quad \sum_{q,\bar{q}} e_q^2 \left[\hat{\sigma}^{qg\to\text{jet}}_{\text{SGP,F}}(w,R) F^q(x,x) + \hat{\sigma}^{qg\to\text{jet}}_{\text{SGP},F'}(w,R) \left(-x \left(F^q\right)'(x,x) \right) \right]. \end{aligned} \tag{6.25}$$

The partonic cross sections in the above formula depend on the specific choice of the algorithm used to construct the jet. They are given in Appendix F.2 for a k_T-type algorithm [132], cf. the discussion in Sec. 4.2.2. Note that the only partonic channels contributing to Eq. (6.25) are the former $qg \to q$ and $qg \to g$ channels. The former $qq \to q$ and $gg \to q$ channels do not receive any R-dependent contribution, i.e. it is sufficient to simply replace the quark fragmentation function for these channels. The former $qq \to q'$ channel identically vanishes because it was proportional to the difference of quark and antiquark fragmentation functions, which both get replaced by the same δ-function and thus cancel.

6.3 Single-Inclusive Photon Production

Shifting to processes with measured photons in the final state, the next reaction to be presented is the single-inclusive case $\ell(l)N^\uparrow(P) \to \gamma(P_\gamma)X$. Chapter 5 discusses how one can separate contributions based on the power of the fractional charge e_q. The power depends on whether the photon is emitted from the lepton line (e_q^2, *Bethe Heitler*) or quark line (e_q^4, *Compton*), or one has an interference of both cases (e_q^3, *Interference*). For the transversely polarized, differential cross section, the Bethe Heitler contribution vanishes and one finds the following form in pQCD at NLO

$$E_\gamma \frac{\mathrm{d}\sigma}{\mathrm{d}^3\boldsymbol{P_\gamma}}(S) = E_\gamma \frac{\mathrm{d}\sigma^C}{\mathrm{d}^3\boldsymbol{P_\gamma}}(S) + E_\gamma \frac{\mathrm{d}\sigma^I}{\mathrm{d}^3\boldsymbol{P_\gamma}}(S)\,. \tag{6.26}$$

6.3.1 Compton Channel:

The Compton channel receives contributions from parton-to-photon fragmentation processes as well as direct, hard scattering photon production. Thus one writes

$$E_\gamma \frac{\mathrm{d}\sigma^C}{\mathrm{d}^3\boldsymbol{P_\gamma}}(S) = E_\gamma \frac{\mathrm{d}\sigma^{C,\text{frag}}}{\mathrm{d}^3\boldsymbol{P_\gamma}}(S) + E_\gamma \frac{\mathrm{d}\sigma^{C,\text{direct}}}{\mathrm{d}^3\boldsymbol{P_\gamma}}(S)\,. \tag{6.27}$$

Both contributions can be obtained with some suitable adaptations (see Sec. 5.1) from the hadron production process $\ell(l) + N^\uparrow(P) \to h(P_h) + X$, for which the results are shown in Sec. 6.1 and Refs. [36, 37].

Photon Fragmentation Contribution

For the photon fragmentation contribution one simply has to replace the parton-to-hadron fragmentation functions $D_1^{h/i}$ by parton-to-photon fragmentation functions $D_1^{\gamma/i}$, where i can stand

for both quarks or gluons

$$E_\gamma \frac{\mathrm{d}\sigma^{C,\mathrm{frag}}}{\mathrm{d}^3\boldsymbol{P_\gamma}}(S) = E_h \frac{\mathrm{d}\sigma^{\mathrm{LO+NLO}}}{\mathrm{d}^3\boldsymbol{P_h}}(S)\bigg|_{D_1^{h/i}\to D_1^{\gamma/i}} . \tag{6.28}$$

Direct Photon Contribution

The direct photon production part can also be deduced from hadron production simply by utilizing the analytical results for the gluon fragmentation channel, but reducing the gluon to a photon $\left(C_F \to e_q^2,\, N_c \to 0,\, \alpha_s \to \alpha_{em}\right)$ and replacing the gluon fragmentation function by a delta function $(D_1^{h/g}(z) \to \delta(1-z))$

$$\begin{aligned} E_\gamma \frac{\mathrm{d}\sigma^{C,\mathrm{direct}}}{\mathrm{d}^3\boldsymbol{P_\gamma}}(S) &= E_h \frac{\mathrm{d}\sigma^{\mathrm{NLO},qg\to g}}{\mathrm{d}^3\boldsymbol{P_h}}(S)\bigg|^{C_F\to e_q^2,\, N_c\to 0,\, \alpha_s\to\alpha_{em}}_{D_1^{h/g}(z)\to\delta(1-z)} \\ &= E_\gamma \frac{\mathrm{d}\sigma^{C,\mathrm{Int}}}{\mathrm{d}^3\boldsymbol{P_\gamma}}(S) + E_\gamma \frac{\mathrm{d}\sigma^{C,\mathrm{SGP}}}{\mathrm{d}^3\boldsymbol{P_\gamma}}(S) + E_\gamma \frac{\mathrm{d}\sigma^{C,\mathrm{SFP}}}{\mathrm{d}^3\boldsymbol{P_\gamma}}(S) . \end{aligned} \tag{6.29}$$

As in the previous sections the various contributions to the total Compton cross section are denoted as integral (Int), soft-gluon pole (SGP) and soft-fermion pole (SFP).

6.3.2 Interference Channel:

In contrast to the Compton channel treated in the preceding section, the Interference channel only receives a direct photon production contribution of the following form

$$E_\gamma \frac{\mathrm{d}\sigma^{I}}{\mathrm{d}^3\boldsymbol{P_\gamma}}(S) = E_\gamma \frac{\mathrm{d}\sigma^{I}_{\mathrm{LO}}}{\mathrm{d}^3\boldsymbol{P_\gamma}}(S) + E_\gamma \frac{\mathrm{d}\sigma^{I,\mathrm{virt}}_{\mathrm{NLO}}}{\mathrm{d}^3\boldsymbol{P_\gamma}}(S) + E_\gamma \frac{\mathrm{d}\sigma^{I,\mathrm{real}}_{\mathrm{NLO}}}{\mathrm{d}^3\boldsymbol{P_\gamma}}(S) . \tag{6.30}$$

All partonic hard functions featured by the following formulas are collected in App. F.3. It is important to note that since the photon is produced directly in a hard-scattering vertex, one has $z = 1$. Consequently, in the following it is $v = v_1 = 1 + \frac{t}{s}$ with the photonic Mandelstam variables $s = (l+P)^2$, $t = (P - P_\gamma)^2$ (and $u = (l - P_\gamma)^2$).

LO Contribution

The LO cross section can be written in the compact form

$$E_\gamma \frac{\mathrm{d}\sigma^{I}_{\mathrm{LO}}}{\mathrm{d}^3\boldsymbol{P_\gamma}} = \sigma_0(S)\left(-\frac{1+v^2}{(1-v)^2}\right)\sum_q e_q^2\left[F_\gamma^{q-\bar{q}}(x_0,0) + G_\gamma^{q-\bar{q}}(x_0,0)\right] , \tag{6.31}$$

with the $q\gamma q$ functions F_γ, G_γ. Note that here and in the following the sum $\sum_q$ generally only runs over quarks q but not antiquarks $\bar{q}$ unless explicitly stated. Furthermore, the correlation functions enter as difference between the quark and antiquark case. Moreover, one also has NLO virtual and real corrections. The virtual loop corrections can be split into a part that is again generated by quark-photon-quark $(q\gamma q)$ correlations inside the nucleon and a second part featuring gluon-photon-gluon $(g\gamma g)$ correlations

$$E_\gamma \frac{\mathrm{d}\sigma^{I,\mathrm{virt}}_{\mathrm{NLO}}}{\mathrm{d}^3\boldsymbol{P_\gamma}}(S) = E_\gamma \frac{\mathrm{d}\sigma^{I,\mathrm{virt},q\gamma q}_{\mathrm{NLO}}}{\mathrm{d}^3\boldsymbol{P_\gamma}}(S) + E_\gamma \frac{\mathrm{d}\sigma^{I,\mathrm{virt},g\gamma g}_{\mathrm{NLO}}}{\mathrm{d}^3\boldsymbol{P_\gamma}}(S) . \tag{6.32}$$

The real corrections distinguish between integral (Int), soft-gluon pole (SGP) and soft-fermion pole (SFP) contributions

$$E_\gamma \frac{\mathrm{d}\sigma^{I,\mathrm{real}}_{\mathrm{NLO}}}{\mathrm{d}^3\boldsymbol{P_\gamma}}(S) = E_\gamma \frac{\mathrm{d}\sigma^{I,\mathrm{Int}}_{\mathrm{NLO}}}{\mathrm{d}^3\boldsymbol{P_\gamma}}(S) + E_\gamma \frac{\mathrm{d}\sigma^{I,\mathrm{SGP}}_{\mathrm{NLO}}}{\mathrm{d}^3\boldsymbol{P_\gamma}}(S) + E_\gamma \frac{\mathrm{d}\sigma^{I,\mathrm{SFP}}_{\mathrm{NLO}}}{\mathrm{d}^3\boldsymbol{P_\gamma}}(S) . \tag{6.33}$$

NLO Virtual $q\gamma q$ Contribution

Starting with the $q\gamma q$ virtual contribution at NLO, the corresponding analytic formula for the transversely polarized, differential cross section can be written in a similar way as the leading

order contribution

$$E_\gamma \frac{\mathrm{d}\sigma^{I,\mathrm{virt},q\gamma q}_{\mathrm{NLO}}}{\mathrm{d}^3\boldsymbol{P_\gamma}} = \sigma_0(S)\frac{\alpha_s}{2\pi}\left(-\frac{1+v^2}{(1-v)^2}\right)\int_{x_0}^1 \frac{\mathrm{d}w}{w} \times \sum_q e_q^2 \left[\hat{\sigma}_1^{I,q\gamma q}(v,w)\, F_\gamma^{q-\bar{q}}(x, x(1-w)) + \hat{\sigma}_5^{I,q\gamma q}(v,w)\, G_\gamma^{q-\bar{q}}(x, x(1-w))\right], \quad (6.34)$$

NLO Virtual $g\gamma g$ Contribution

The second part of the NLO virtual correction features the $g\gamma g$-functions $O_\gamma^{1,2}$ and can be written as

$$E_\gamma \frac{\mathrm{d}\sigma^{I,\mathrm{virt},g\gamma g}_{\mathrm{NLO}}}{\mathrm{d}^3\boldsymbol{P_\gamma}} = \sigma_0(S)\frac{\alpha_s}{2\pi}\frac{1+v^2}{(1-v)^2}\left(\sum_{q,\bar{q}} e_q^2\right)\int_{x_0}^1 \frac{\mathrm{d}w}{wx}\left[\hat{\sigma}_1^{I,g\gamma g}(v,w)\, O_\gamma^1(x, x(1-w)) + \hat{\sigma}_2^{I,g\gamma g}(v,w)\, O_\gamma^2(x, x(1-w)) + \hat{\sigma}_3^{I,g\gamma g}(v,w)\, O_\gamma^2(x(1-w), x)\right], \quad (6.35)$$

where it is noteworthy that the sum in 6.35 runs over both quarks q and anti-quarks $\bar{q}$.

Integral Contribution

Now, turning to the real NLO corrections and beginning with the integral contribution in 6.33 one finds that the result can be expressed in a more compact form by introducing the linear combinations $F^q \pm G^q$ of the qgq functions. The cross section then takes on the following form

$$E_\gamma \frac{\sigma^{I,\mathrm{Int}}_{\mathrm{NLO}}}{\mathrm{d}^3\boldsymbol{P_\gamma}} = \sigma_0(S)\frac{\alpha_{em}}{2\pi}\int_{x_0}^1 \frac{\mathrm{d}w}{w}\int_0^1 \mathrm{d}\zeta \times \sum_q e_q^3 \left[\hat{\sigma}_+^{I,\mathrm{Int}}(v,w,\zeta) F_{I,\mathrm{Int},+}^{q-\bar{q}}(x,\zeta) + \hat{\sigma}_-^{I,\mathrm{Int}}(v,w,\zeta) F_{I,\mathrm{Int},-}^{q-\bar{q}}(x,\zeta)\right], \quad (6.36)$$

where the following integrable combinations of the correlation functions have been used

$$F_{I,\mathrm{Int},\pm}^{q-\bar{q}}(x,\zeta) = \frac{1}{\zeta(1-\zeta)^2}\left(F_\pm^{q-\bar{q}}(x, x\zeta) - \zeta(2-\zeta)F_\pm^{q-\bar{q}}(x,x) + \zeta(1-\zeta)x\left(\partial_2 F_\pm^{q-\bar{q}}\right)(x,x) - (1-\zeta)^2 F_\pm^{q-\bar{q}}(x,0)\right). \quad (6.37)$$

Soft-Gluon Pole Contribution

For the soft-gluon pole contribution in 6.33 there is no use in introducing $F_\pm^q$ as above, since $G^q(x,x) = 0$, and one writes the cross section as follows

$$E_\gamma \frac{\sigma^{I,\mathrm{SGP}}_{\mathrm{NLO}}}{\mathrm{d}^3\boldsymbol{P_\gamma}} = \sigma_0(S)\frac{\alpha_{em}}{2\pi}\int_{x_0}^1 \frac{\mathrm{d}w}{w} \times \sum_q e_q^3 \left[\hat{\sigma}_1^{I,\mathrm{SGP}}(v,w)\, F^{q-\bar{q}}(x,x) + \hat{\sigma}_5^{I,\mathrm{SGP}}(v,w)\left(-x_0(\partial_2 G^{q-\bar{q}})(x,x)\right)\right]. \quad (6.38)$$

Soft-Fermion Pole Contribution

Finally, in the formula for the soft-fermion pole contribution to Eq. 6.33 it is again beneficial to utilize the linear combinations $F_\pm^q = F^q \pm G^q$ to get more compact partonic cross sections $\hat{\sigma}_\pm^{I,\mathrm{SFP}}$. This yields

$$E_\gamma \frac{\sigma^{I,\mathrm{SFP}}_{\mathrm{NLO}}}{\mathrm{d}^3\boldsymbol{P_\gamma}} = \sigma_0(S)\frac{\alpha_{em}}{2\pi}\int_{x_0}^1 \frac{\mathrm{d}w}{w} \times \sum_q e_q^3 \left[\hat{\sigma}_+^{I,\mathrm{SFP}}(v,w)\, F_+^{q-\bar{q}}(x,0) + \hat{\sigma}_-^{I,\mathrm{SFP}}(v,w)\, F_-^{q-\bar{q}}(x,0)\right]. \quad (6.39)$$

6.4 γSIDIS

This chapter is concluded by a discussion of the γSIDIS process, $\ell(l)N^{\uparrow}(P) \to \ell'(l')\gamma(p_\gamma)X$. It is the semi-inclusive counterpart of the single-inclusive photon production process studied in the preceding section and thus has some common features. The first one is that the cross section is again split according to the power of the fractional charge e_q into Bethe Heitler (e_q^2), Compton (e_q^4) and Interference (e_q^3) contributions. Furthermore, the Bethe Heitler contribution also vanishes for this process.

The difference between the two processes is the observed final state lepton, which leads to different kinematics. In addition to the external momenta one also defines the combinations $q = l - l' - p_\gamma$ and $\tilde{q} = l - l'$. Moreover, one has the related kinematic variables $Q^2 = -q^2$, $\tilde{Q}^2 = -\tilde{q}^2$, $x_B = Q^2/(2P\cdot q)$ and $\tilde{x}_B = \tilde{Q}^2/(2P\cdot\tilde{q})$.

Due to the more exclusive nature of the process, the cross section is differential not only in the photon's transverse momentum p_T^γ, rapidity η^γ and azimuthal angle ϕ^γ but also the respective counterparts of the final state lepton, i.e. p_T', η' and ϕ'. For the final result of the transversely polarized cross section at leading order in pQCD one finds (see Ref. [39])

$$\frac{d\sigma_{\gamma\text{SIDIS}}}{dp_T' d\eta' d\phi' dp_T^\gamma d\eta^\gamma d\phi^\gamma} = \frac{\alpha_{em}^3 M}{4\pi s Q^8} p_T' p_T^\gamma \left[\epsilon^{Pll'S}\,\sigma_{\gamma\text{SIDIS}}^{\phi'} + \epsilon^{PlP_\gamma S}\,\sigma_{\gamma\text{SIDIS}}^{\phi^\gamma}\right]. \tag{6.40}$$

Compared to an earlier derivation in [109] there are two modifications employed in the above result. First, the set of four azimuthal spin correlations used in this reference, $\epsilon^{Pll'S}$, $\epsilon^{PlP_\gamma S}$, $l_T'\cdot S_T\,\epsilon^{Pll'P_\gamma}$ and $P_{\gamma T}\cdot S_T\,\epsilon^{Pll'P_\gamma}$, is over-complete in the sense that it can be reduced down to just two independent quantities, namely $\epsilon^{Pll'S}$ and $\epsilon^{PlP_\gamma S}$, by means of the identity

$$g^{\alpha\beta}\epsilon^{\mu\nu\rho\sigma} = g^{\mu\beta}\epsilon^{\alpha\nu\rho\sigma} + g^{\nu\beta}\epsilon^{\mu\alpha\rho\sigma} + g^{\rho\beta}\epsilon^{\mu\nu\alpha\sigma} + g^{\sigma\beta}\epsilon^{\mu\nu\rho\alpha}\,.$$

Second, the cross sections $\sigma_{\gamma\text{SIDIS}}^{\phi'}, \sigma_{\gamma\text{SIDIS}}^{\phi^\gamma}$ are given in terms of linear combinations of the qgq functions F and G

$$\begin{aligned} F_\pm^C(x,x') &= \sum_q e_q^4 \left(F^{q+\bar{q}}(x,x') \pm G^{q+\bar{q}}(x,x')\right) \\ F_\pm^I(x,x') &= \sum_q e_q^3 \left(F^{q-\bar{q}}(x,x') \pm G^{q-\bar{q}}(x,x')\right). \end{aligned} \tag{6.41}$$

The cross sections can be written in the following way, as a sum of hard pole and soft-fermion pole contributions

$$\begin{aligned} \sigma_{\gamma\text{SIDIS}}^{\phi'(\phi^\gamma)} = \sum_{n=\text{C,I}} \Big[&\hat{\sigma}_{\text{HP},+}^{n,\phi'(\phi^\gamma)}\, F_+^n(x_B,\tilde{x}_B,\mu_n) + \hat{\sigma}_{\text{HP},-}^{n,\phi'(\phi^\gamma)}\, F_-^n(x_B,\tilde{x}_B,\mu_n) \\ &+\hat{\sigma}_{\text{SFP},+}^{n,\phi'(\phi^\gamma)}\, F_+^n(x_B,0,\mu_n) + \hat{\sigma}_{\text{SFP},-}^{n,\phi'(\phi^\gamma)}\, F_-^n(x_B,0,\mu_n)\Big]. \end{aligned} \tag{6.42}$$

Unlike all other formulas presented so far, the scale dependence is explicitly shown in Eq. (6.42). This is because the scale is chosen differently for Compton and Interference contributions, as well as the Bethe Heitler contribution in the unpolarized case

$$\mu_{BH} = Q, \qquad \mu_C = \tilde{Q}, \qquad \mu_I = \sqrt{Q\tilde{Q}}\,. \tag{6.43}$$

Notably, there are no soft-gluon pole terms because of cancellations between kinematical and dynamical contributions. The partonic cross sections are collected in Appendix F.4 along with explicit expressions for the contracted levi-civita tensors $\epsilon^{Pll'S}$, $\epsilon^{PlP_\gamma S}$.

Chapter 7

Numerical Study

In this chapter, numerical analyses for the transverse SSA (2.61) are performed for each of the considered processes that were discussed in the previous chapters. The study is focused on the upcoming Electron-Ion Collider. Thus, a typical center-of-mass (c.m.) energy accessible at the EIC of $\sqrt{s} = 100\,\mathrm{GeV}$ is considered in the following. Additionally, a comparison of the asymmetry with HERMES data [25] is performed for $ep^\uparrow \to \pi^\pm X$, at a somewhat lower c.m. energy of $\sqrt{s} = 7.25$ GeV. In the case of γSIDIS, the influence of $\sqrt{s}$ is explored even further by computing the corresponding asymmetry $A_{UT}^{\gamma\mathrm{SIDIS}}$ for $\sqrt{s} = 29$ GeV as well as $\sqrt{s} = 63$ GeV (also accessible at the EIC). The phenomenological study is carried out in the lepton-nucleon c.m. frame rather than in the asymmetric laboratory frame. The single-inclusive differential cross sections and the corresponding SSAs are considered in terms of the hadron's, jet's and photon's pseudorapidity η_h, η_j, η_γ and transverse momentum $P_{h,T}$, $P_{j,T}$, $P_{\gamma,T}$ respectively. The γSIDIS process is also differential in the final state lepton degrees of freedom and consequently the numerical study is more involved. This will be addressed below in the corresponding section.

The frame chosen for the single-inclusive processes is explicitly specified for the case of hadrons in the following, but it is completely analogous for jets and photons. The direction of the lepton defines the positive z-axis, such that positive pseudorapidity indicates the forward lepton direction:

$$\begin{aligned} l^\mu &= \tfrac{1}{2}\sqrt{s}\,(1,\,0,\,0\,,+1)\,, \\ P^\mu &= \tfrac{1}{2}\sqrt{s}\,(1,\,0,\,0\,,-1)\,, \\ P_h^\mu &= P_{h,T}\,(\cosh\eta_h,\,\cos\phi_h,\,\sin\phi_h,\,\sinh\eta_h)\,, \end{aligned} \tag{7.1}$$

The hadronic Mandelstam variables are expressed in terms of η_h and $P_{h,T}$ as

$$\begin{aligned} t &= -P_{h,T}\,\sqrt{s}\,\mathrm{e}^{+\eta_h}\,, \\ u &= -P_{h,T}\,\sqrt{s}\,\mathrm{e}^{-\eta_h}\,, \end{aligned} \tag{7.2}$$

again likewise for jet and photon production. The unpolarized cross section depends only on pseudorapidity and transverse momentum, so the azimuthal angle ϕ_h of the observed final state particle can be integrated out:

$$\frac{\mathrm{d}\sigma}{\mathrm{d}\eta_h\,\mathrm{d}P_{h,T}} = 2\pi\,P_{h,T}\,\left(E_h\frac{\mathrm{d}\sigma}{\mathrm{d}^3\boldsymbol{P}_h}\right)\,. \tag{7.3}$$

In contrast, the spin-dependent cross section contains the prefactor $\sigma_0(S)$ defined in Eq. (2.65), which introduces a dependence on the azimuth ϕ_h. To work out this dependence explicitly, one must first parametrize the spin vector S. This vector is constrained by $P\cdot S = 0$ and is normalized to $S^2 = -1$. Thus, in the chosen reference frame of Eq. (7.1), one can parametrize S as follows:

$$S^\mu = \left(S^0,\,\cos\phi_s,\,\sin\phi_s,\,-S^0\right)\,. \tag{7.4}$$

The azimuthal angle ϕ_s of the transverse components determines the location of the spin vector in a plane transverse to the beam direction. For the present study, the *right-left* asymmetry A_{RL} is considered. It is defined in Eq. (2.62) for a generic cross section and in the specific case of single-inclusive hadron production it can be written as

$$A_{RL} = \frac{\int_{\phi_s+\pi}^{\phi_s+2\pi}\mathrm{d}\phi_h\,\frac{\mathrm{d}\sigma(S)}{\mathrm{d}\eta_h\,\mathrm{d}P_{h,T}\,\mathrm{d}\phi_h} - \int_{\phi_s}^{\phi_s+\pi}\mathrm{d}\phi_h\,\frac{\mathrm{d}\sigma(S)}{\mathrm{d}\eta_h\,\mathrm{d}P_{h,T}\,\mathrm{d}\phi_h}}{\int_0^{2\pi}\mathrm{d}\phi_h\,\frac{\mathrm{d}\sigma}{\mathrm{d}\eta_h\,\mathrm{d}P_{h,T}\,\mathrm{d}\phi_h}}\,. \tag{7.5}$$

The spin vector only appears through $\sigma_0(S)$ where it enters via a totally antisymmetric tensor as ϵ^{lPP_hS}. One can easily work out this term in the c.m. frame (7.1), along with (7.4). This leads to a typical $\sin(\phi_s - \phi_h)$ modulation, which is then integrated according to (7.5) with the result that one can effectively replace the Levi-Civita tensor as follows

$$\epsilon^{lPP_hS} = \tfrac{1}{2}\sqrt{stu}\,\sin(\phi_s - \phi_h) \to 2\sqrt{stu}\,. \tag{7.6}$$

To compute the various convolution integrals in the analytic results, one needs input distributions for the qgq functions F^q, G^q for all flavors q, as well as for the ggg correlation functions N, O. Since none of these functions are currently known to a satisfactory extent, a precise theoretical prediction is not feasible. Furthermore, as discussed below (2.64), one would also need to include multiparton correlations in the fragmentation process for single-inclusive hadron production. Again, the treatment of these twist-3 fragmentation effects is beyond the scope of this study.

However, one can study the generic effect of the NLO corrections compared to the LO approximation for A_{RL}. For this purpose, three scenarios are explored (labeled *Scenario 0,1,2*) for the qgq functions F^q and G^q for u and d-quarks, assuming all other multiparton correlation functions to vanish. An in-depth discussion of the model and in particular the three scenarios is given in App. G.

For the plots shown below, the focus is on the pseudorapidity dependence of this observable at fixed transverse momentum $P_{\pi,T}$, $P_{j,T}$ or $P_{\gamma,T}$, which is set to 5 GeV throughout this study. The default renormalization/factorization scale is chosen as the pion transverse momentum, that is, $\mu = P_{\pi,T}$ (analogously for jets and photons).

Estimated Scale Dependence Although the numerical implementation of QCD evolution is standard for the leading-twist PDFs and FFs (cf. [59, 60, 61]), it is more involved for the multiparton correlation functions: only few numerical codes have been released so far [121, 138], and valid only at LO. The main purpose of the present numerical analysis is to see how much the observable A_{RL} is affected by the NLO corrections to the partonic hard-scattering functions. The analysis does not aim to provide cutting-edge predictions for A_{RL}. For this reason, the numerical code used for the plots below does not implement the proper scale evolution of the multiparton correlation functions. Instead, an estimate is made. The twist-3 correlation functions F^q and G^q are formulated in terms of the unpolarized f_1^q quark PDFs (see Appendix G) as the only non-perturbative input. Hence, the evolution of f_1^q is used to get a first approximation for the scale dependence of the twist-3 functions and hence of the SSAs. In other words, it is assumed that the evolution of the twist-3 functions follows that of the twist-2 PDFs. In view of the similarity of the respective evolution kernels (see [121, 122]), this approximation is expected to be reasonable.

For f_1^q, the scale is varied between $\mu = P_{\pi,T}/2$ and $\mu = 2P_{\pi,T}$ for pion production and analogously for jets and photons. The theoretical uncertainty bands obtained by the approximated scale dependence are only shown for the asymmetries. Nonetheless, the proper implementation of the true scale dependence and the study of the dependence of the asymmetry on transverse momentum remain important tasks for the future, once NLO corrections to the evolution of the twist-3 matrix elements have also been derived.

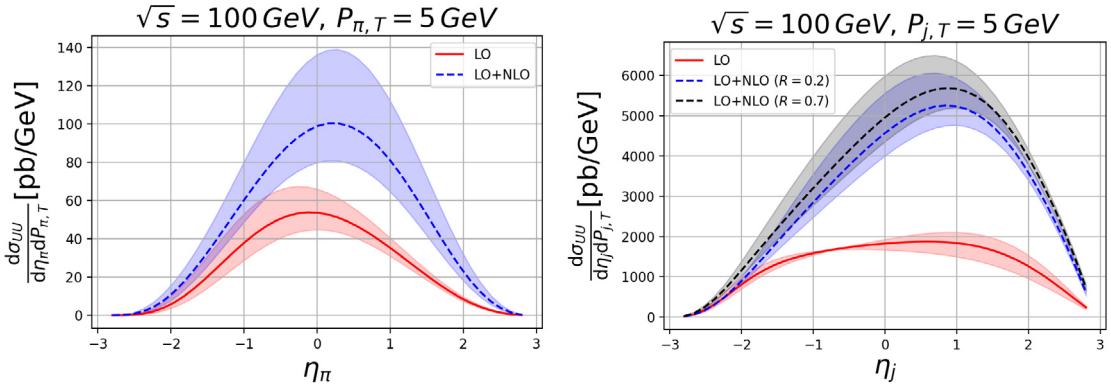

Figure 7.1: Unpolarized differential cross section (7.3) plotted vs. the pseudorapidity η of a π^+ **(left)** or a jet **(right)**. The transverse momentum is fixed to 5 GeV in both cases. The NLO jet cross section is plotted for two jet radii, $R_1 = 0.2$ and $R_2 = 0.7$.

Unpolarized Hadron and Jet Cross Sections Starting point of the numerical study is the denominator of the right-left asymmetry A_{RL} in (7.5), the unpolarized NLO cross section. Here, results are taken from Ref. [120] to calculate the cross sections for $ep \to \pi^+ X$ and $ep \to \text{jet}X$, given the kinematics of interest to the present study. For the proton's PDFs, the MSTW2008 parameterization of [59] is used, and the DSS parameterization [139] for the pion FFs. The results are presented in Fig. 7.1. Theoretical uncertainty bands are generated by varying the scale between $\mu = P_T/2$ and $\mu = 2P_T$.

The LO cross sections for both single-inclusive pions and jets receive sizable NLO corrections, of about a factor two to three. This is in line with observations made previously in Refs. [120, 140].

7.1 Single-Inclusive π^+-Production

7.1.1 Scenario 0

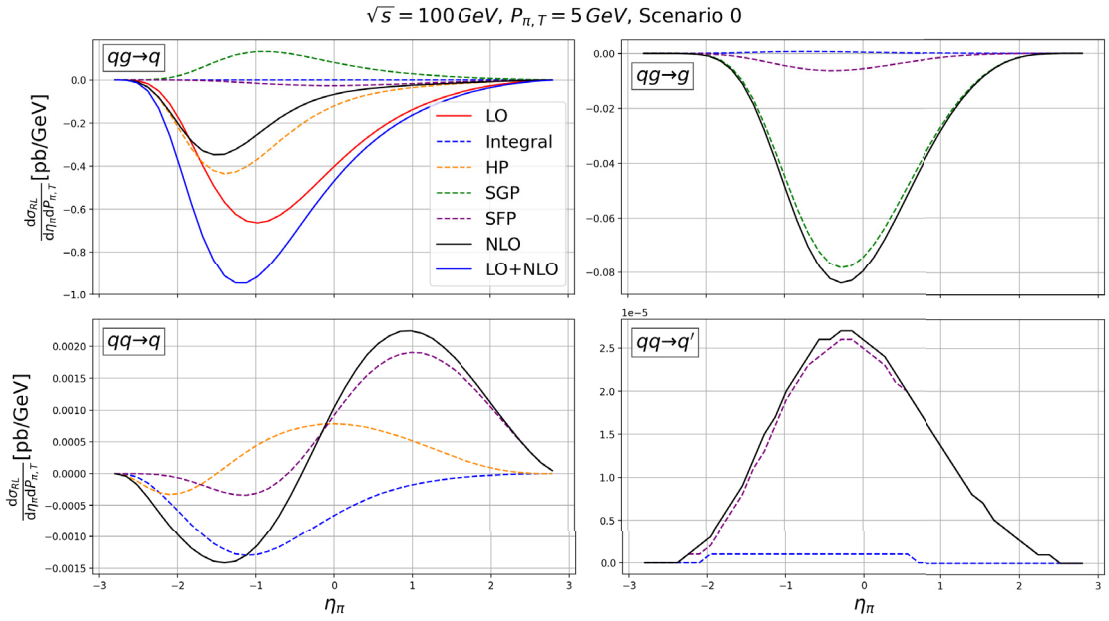

Figure 7.2: Cross sections for the various NLO channels of Eq. (6.2) plotted vs. the pion's pseudorapidity η_π at fixed transverse momentum $P_{\pi,T} = 5\,\text{GeV}$. The curves are produced for Scenario 0 (G.16).

Turning to the transversely polarized case, first consider the "minimalistic" Scenario 0 of App. G.1: most parameters in Eq. (G.16) are set to zero, such that the contour plot of F^q in Fig. G.1 only shows very moderate variation in x, x'. Additionally, it is assumed that $G^q = 0$.

Figure 7.2 shows the NLO right-left cross section for this scenario. The different panels show the individual partonic channels in Eq.(6.2). Each plot also shows separate curves for the different pole contributions. The $qg \to q$ gives the largest NLO correction. Notably, the hard-pole (HP) contribution is dominating in this channel. The soft-gluon pole (SGP) contributions are of opposite sign, but only partially cancel the HP contributions. The soft-fermion pole (SFP) and integral contributions are negligible in this scenario. The channel $qg \to g$ is the second largest and it is dominated by its SGP part. Again, SFP and integral contributions are negligible for this channel. The two remaining channels $qq \to q$ and $qq \to q'$ are generated by $q\bar{q}g$ correlations. While they do give a non-zero numerical results, they are irrelevant compared to $qg \to q$ and $qg \to g$ (note that the y-axis is scaled by a factor 10^{-5} for the $qq \to q'$ channel!).

7.1.2 Scenario 1

Moving on with Scenario 1, discussed in App. G.2, one now has moderately more "off-diagonal structure" for the qgq functions F^q, G^q (see Figs. G.2, G.3) compared to Scenario 0. In particular, one now has $G^q \neq 0$.

The NLO results for the spin-dependent cross section are shown for the various channels in Fig. 7.3. Compared to before, the hard-pole contribution for $qg \to q$ differs quite a lot. For

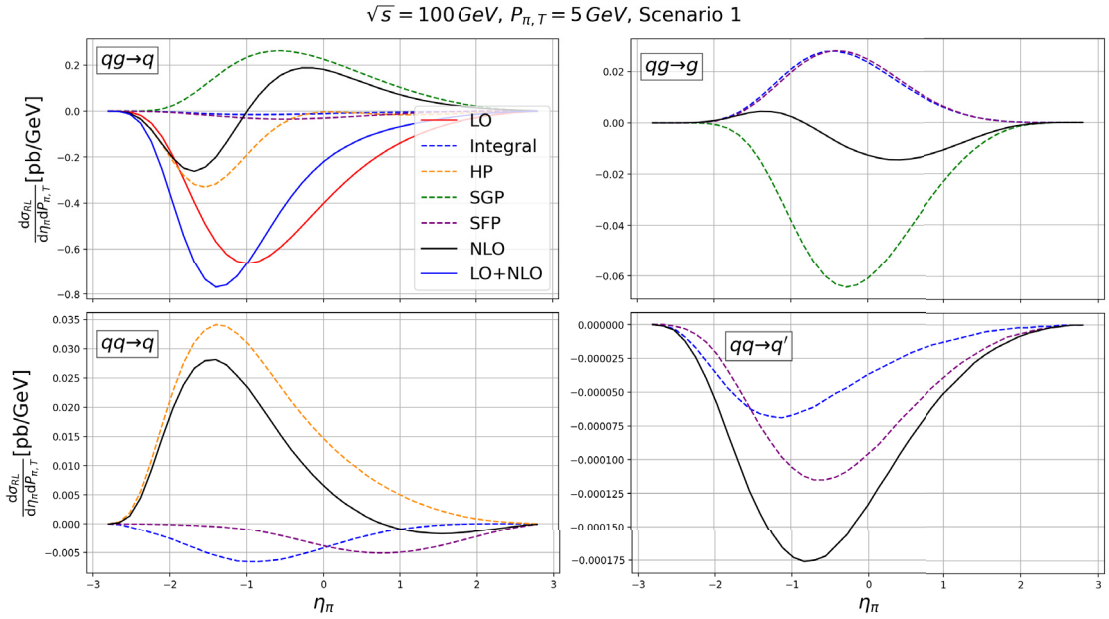

Figure 7.3: Same as Fig. 7.2, but for Scenario 1.

$qg \to g$, the SFP and integral contributions roughly cancel against the SGP contribution; this leads to a much smaller numerical contribution from this channel than in the previous Scenario 0. For both the $qq \to q$ and the $qq \to q'$ channel the NLO contributions increase in size for Scenario 1, but they remain negligible.

7.1.3 Scenario 2

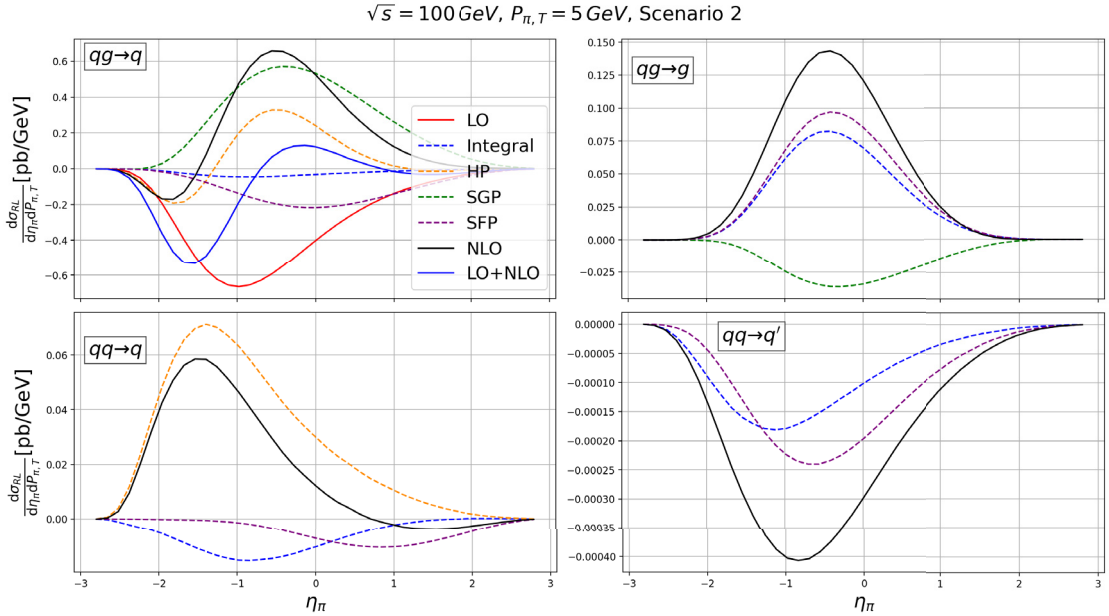

Figure 7.4: Same as Fig. 7.2, but for Scenario 2.

Scenario 2 is described in Appendix G.3, and the corresponding contour plots for the correlation functions F and G are shown in Figs. G.4, G.5. These plots show more variation away from the $x = x'$ diagonal, due to the Fourier coefficients in Eq. (G.18) being multiplied by a factor of three compared to Scenario 1 (G.17). Notably, a model calculation in Ref. [141] based on an overlap representation of the functions F^q and G^q in terms of light-cone wave functions supports such a behavior. In any case, all three scenarios agree with every known constraint.

Fig. 7.4 displays plots for the numerator of A_{RL} in Scenario 2 for all contributing partonic channels at NLO. As for the other scenarios, $qg \to q$ is the dominating channel. Unlike previous

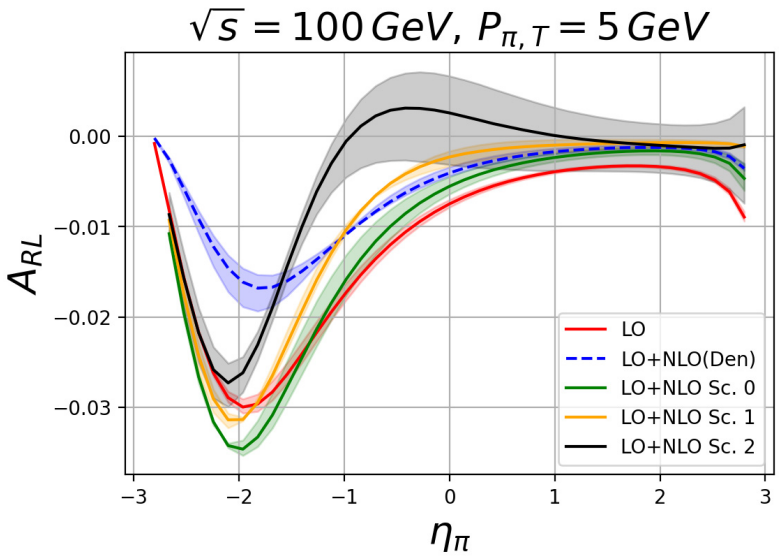

Figure 7.5: Right-left asymmetry A_{RL} of (7.5) plotted vs. the pion's pseudorapidity η_π at fixed transverse momentum $P_{\pi,T} = 5\,\text{GeV}$.

scenarios, NLO corrections have a drastic impact. In particular, the $qg \to q$ channel's HP contribution flips sign compared to Scenario 0. All other contributions, i.e., SGP, SFP and integral contributions, are larger as well. Note that for all plots in Figs. 7.2,7.3,7.4 the LO curve is always the same, since it is only sensitive to $x = x'$ and thus not affected by the choice of model parameters (cf. App. G). Comparing the second largest channel $qg \to g$ in Scenarios 0 and 2, one observes a sign change of the NLO corrections. This is caused by non-trivial cancellations of SGP, SFP and integral contributions. The other channels $qq \to q$ and $qq \to q'$ are still irrelevant.

7.1.4 Asymmetry

Next, all partonic channels are added to calculate the right-left asymmetry A_{RL} at NLO accuracy. Fig. 7.5 shows the corresponding pseudorapidity plots, again at fixed pion transverse momentum. All Scenarios are shown in a combined plot. The peak of the asymmetry is located in the far backward region around $\eta_\pi \approx -2$. Recall that this is the nucleon direction in the chosen frame (7.1). At the peak, a value of about $-3.5\,\%$ is predicted for the LO asymmetry. Moving to forward rapidities, it drops to about $-0.2\,\%$. Following Refs. [120] and Ref. [48], a separate curve is shown where NLO corrections are only included in the denominator of A_{RL}. This roughly cuts the asymmetry by half, in agreement with the two references.

The behavior of Scenarios 0 and 1 is generally similar to each other in Figure 7.5, when taking NLO corrections into account in *both* the numerator and the denominator. Near the peak, corrections to the numerator overcompensate those to the denominator, thus increasing the asymmetry. The opposite is true for the forward region, where the NLO corrections of the denominator dominate. The NLO contributions have the largest effect for Scenario 2, where A_{RL} flips its sign around the mid-rapidity region. One can expect that such a large deviation will be measurable at an upcoming EIC and that the experimental data will distinguish between Scenario 2 and Scenarios 0 and 1.

Taking into account the simple estimate for the scale dependence of the asymmetry, only moderate uncertainty bands for the NLO corrections are generated for Scenarios 0 and 1, and a larger uncertainty for Scenario 2, such that the sign change around mid-rapidity is no longer displayed as cleanly. Still, the uncertainty bands do not overlap in the backward rapidity region and especially around the peak of the asymmetry, indicating that precise experimental data will be able to constrain the model and provide new insights on the quark-gluon-quark correlations inside the nucleon.

7.1.5 Comparison with HERMES

To conclude the numerical study of pion production, a few exploratory results are given for a different facility than the EIC. To this end, kinematics relevant for comparison to HERMES data

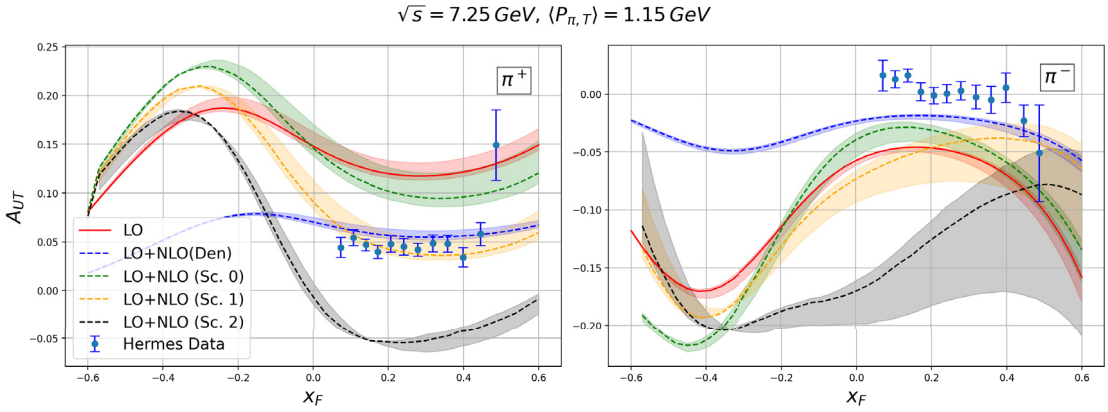

Figure 7.6: A_{UT} at LO and NLO for the three scenarios of qgq functions, compared to HERMES data [25] for $ep^\uparrow \to \pi^+ X$ **(left)** and $ep^\uparrow \to \pi^- X$ **(right)**.

[25] taken at c.m. energy $\sqrt{s} = 7.25$ GeV are chosen. The scale μ is set equal to the average pion transverse momentum $\langle P_{\pi,T}\rangle \simeq 1.15$ GeV accessed in the data set. Theoretical uncertainty bands are estimated in the same way as before, see Paragraph 7 above. The scale is varied between the lower and upper boundaries of the P_T-binning, $\mu = P_{\pi,T}^{min} \simeq 1$ GeV and $\mu = P_{\pi,T}^{max} \simeq 2.2$ GeV. For the pion FFs and the unpolarized proton PDFs the same data sets are chosen as before, i.e. the DSS parametrization [139] and the MSTW2008 parameterization [59] respectively. It should be stressed again that twist-3 fragmentation contributions are disregarded.

Figure 7.6 shows the asymmetries A_{UT} for π^+ (left) and π^- (right) production, as functions of the pion's Feynman variable x_F. Both LO as well as the NLO results for the three scenarios, cf. App. G, are presented. The main finding is that the NLO asymmetry is highly sensitive to the set of twist-3 matrix elements chosen. This can be attributed primarily to an intricate interplay among the various pole contributions. Furthermore, the preliminary uncertainty bands do not overlap over a wide range in x_F. This clean separation of the different Scenarios proves the potential of experimental data for constraining the model.

Note that, arguably accidentally, Scenario 1 (App. G.2) actually describes the HERMES π^+ data rather well, while none of the scenarios does a particularly good job for π^-. The NLO corrections are crucial in this context, and the complexity of the twist-3 framework at NLO becomes apparent. By construction, the LO result is the same for each of the three model sets of twist-3 matrix elements since it only probes the $x = x'$ diagonal. For further comparison, the asymmetry computed with NLO corrections only in the denominator (dashed lines) is shown as well. Thanks to sizable positive NLO corrections for the unpolarized cross section it is strongly reduced relative to LO, as was first observed in [48]. The presented results demonstrate that inclusion of NLO corrections also in the numerator of A_{UT} is essential for phenomenology.

7.2 Single-Inclusive Jet Production

To study the numerical NLO effects on the right-left asymmetry A_{RL} in jet production, the analytical result (6.24) for the NLO spin-dependent cross section is used, along with the NLO result for the unpolarized cross section taken from Refs. [120, 133]. The input for the qgq functions F^q, G^q are the same model Scenarios 0, 1, 2 as above. Exemplary numerical studies are carried out for two jet radii, $R_1 = 0.2$ and $R_2 = 0.7$. Note that the results in (6.24) are obtained within the small cone approximation (SCA), which was validated to be rather accurate even for the larger considered jet radius R_2 in Ref.[127]. The numerical results for A_{RL} as well as its numerator are shown in the following for the three Scenarios. As for single-inclusive pion production, the NLO contributions to the numerator in (7.5) are separated by the various partonic channels. Note that the $qq \to \text{jet}(q')$ channel vanishes for jets.

The jet asymmetry is the cleaner observable compared to the pion asymmetry. The main reason is that jet production is independent of fragmentation. As laid out before, this is pivotal for the polarized case: There are no twist-3 fragmentation effects for jets. In this sense, the plots presented below represent a complete NLO prediction for A_{RL}, based on the adopted model of App. G. Additionally, the asymmetry peaks in the backward rapidity region, which has a sizeable event rate for jets: there, the event rate is larger roughly by a factor of 100 compared to pion production.

7.2.1 Scenario 0

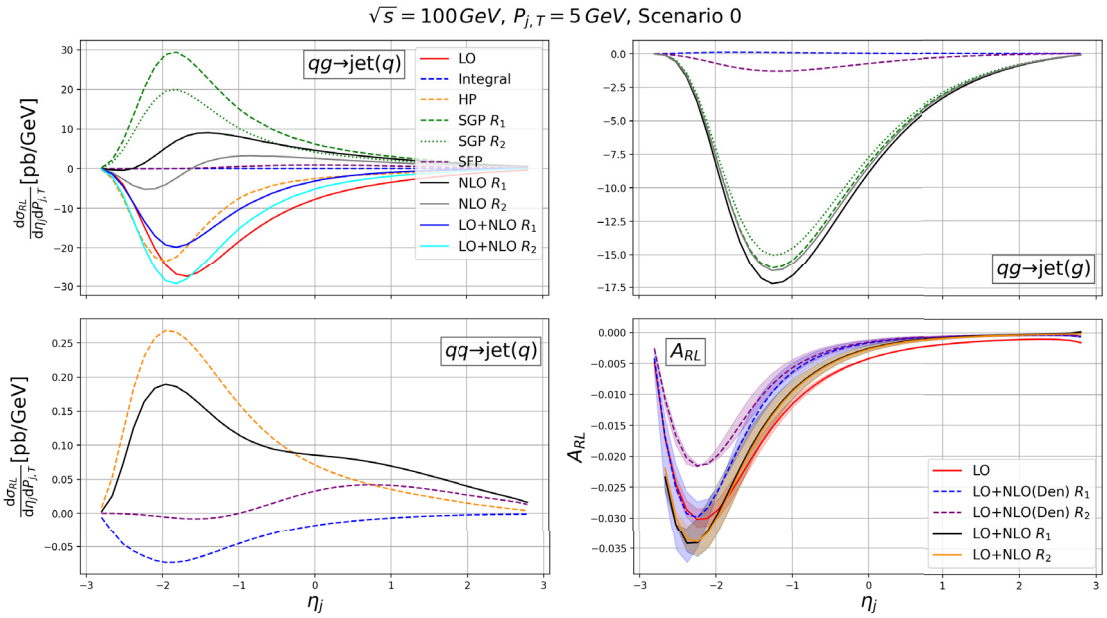

Figure 7.7: Contributions by the various NLO channels plotted versus the jet's pseudorapidity η_j at fixed transverse momentum $P_{j,T} = 5\,\text{GeV}$ and the full NLO asymmetry A_{RL} for two jet radii, $R_1 = 0.2$ and $R_2 = 0.7$ at the EIC. The curves are obtained for Scenario 0 (G.16).

Starting again with Scenario 0, the plots in Fig. 7.7 establish which channels give the most substantial contribution to the numerator of A_{RL}. These are the channels originating from qgq correlations ($x' \geq 0$), where either a radiated quark or gluon generates a jet. Unlike pion production, however, the largest channel is not $qg \to \text{jet}(q)$ but rather $qg \to \text{jet}(g)$. This is because SGP and HP contributions partially cancel for $qg \to \text{jet}(q)$, while SFP and integral contributions are negligible. The $qg \to \text{jet}(g)$ channel, on the other hand, is larger because it does not receive HP contributions and is generated solely by the SGP contribution. The $qq \to \text{jet}(q)$ channel remains irrelevant.

The right-left asymmetry A_{RL} for single-inclusive jet production is shown in the bottom-right plot of Fig. 7.7 as function of the jet's pseudorapidity. In Scenario 0, it displays a similar behavior for this process as for π^+-production: again, the numerator receives slightly larger corrections than the denominator of A_{RL}. In contrast to the numerator and denominator individually, the overall sensitivity of the asymmetry to NLO corrections is only moderate. The jet radius R also has quite small impact on the NLO results. Moreover, one observes a strong similarity between the jet results and their π^+ counterpart in Fig. 7.5.

7.2.2 Scenario 1

Next, Scenario 1 (see (G.17)) is considered. Numerical results for this Scenario are shown in Fig. 7.8. The general behavior is again similar to pion production in Fig. 7.3. Exceptions are the HP contribution of the $qg \to \text{jet}(q)$ channel and the SFP contribution in the $qg \to \text{jet}(g)$ channel, which noticeably differ from Scenario 0. As a result, the asymmetry displays a sign change that indicates a larger NLO effect in Scenario 1 for jets compared to pions.

7.2.3 Scenario 2

Fig. 7.9 shows how this effect is further amplified in Scenario 2. Again, the HP contribution of the $qg \to \text{jet}(q)$ channel as well as the SFP contribution in the $qg \to \text{jet}(g)$ channel have a significant impact on A_{RL}. The peak of the asymmetry is still in the backward pseudorapidity region between $-2 < \eta_j < -1$, but now with a positive value around $+4\,\%$. This means that NLO corrections to the jet asymmetry are highly sensitive to the precise choice of model parameters, and thus of the behavior of the qgq functions F^q and G^q away from the diagonal at $x = x'$. Again, this is a promising result for the potential of future EIC data: experimental results for A_{RL} or the related A_{UT} might constrain these functions enough to rule out some of the model scenarios. To illustrate

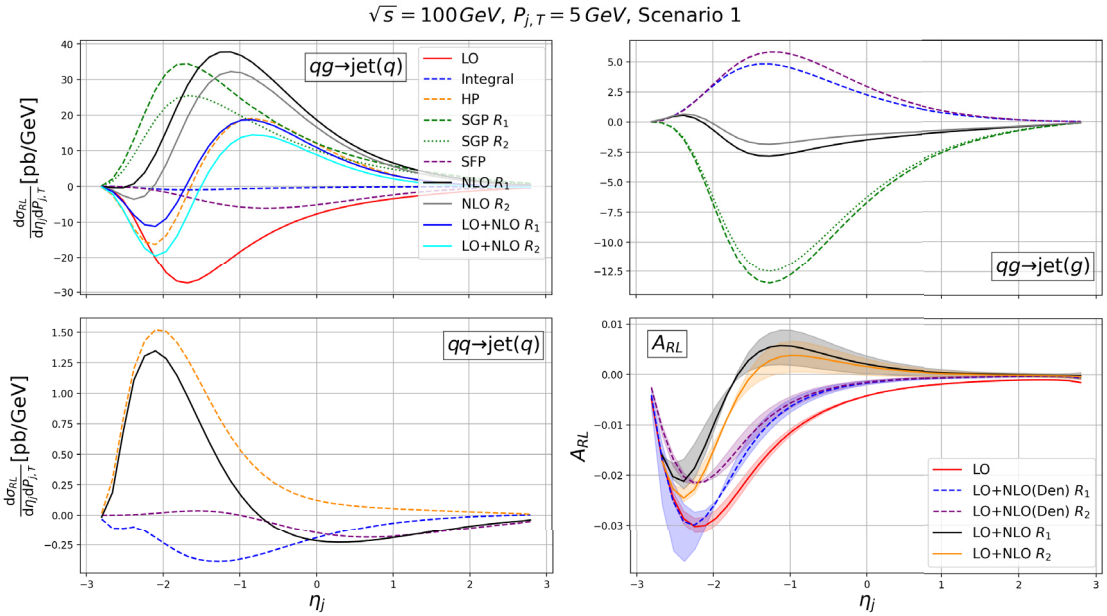

Figure 7.8: Same as Fig. 7.7, but for Scenario 1.

this key finding in an accessible way, all jet asymmetries at NLO within Scenarios 0,1 and 2 are plotted together in Fig. 7.10, again for both jet radii.

7.3 Single-Inclusive Photon Production

The exploratory numerical study of transverse SSAs continues with single-inclusive photon production $e(l)p^{\uparrow}(P) \to \gamma(P_\gamma)X$. The plots presented in the following are obtained using the analytical results for the transversely polarized cross section from Eq. (6.26) and the results for the unpolarized cross section provided by Ref. [38]. Compared to the previously considered cases of hadrons or jets in the final state, one needs additional non-perturbative input for the parton-to-photon FFs. Here, the GRV NLO set of Ref. [142] is chosen. As elaborated on in Sec. 5.2, not only the qgq functions F^q, G^q enter the description of the transversely polarized cross section. In fact, two further types of twist-3 multiparton distribution functions are introduced via the Interference channel. These are the $q\gamma q$ functions F^q_γ, G^q_γ as well as the $g\gamma g$ functions O^1_γ, O^2_γ. For the former, the same model as for the qgq case is adopted (see App. G) and simply scaled as follows

$$F^q_\gamma = \frac{\alpha_{em}}{\alpha_s} F^q \qquad G^q_\gamma = \frac{\alpha_{em}}{\alpha_s} G^q \,. \tag{7.7}$$

The latter are not included in the numerical study, i.e. they are set to zero $O^1_\gamma = O^2_\gamma = 0$, just like the triple-gluon functions N, O.

Starting point of this section is the unpolarized cross section, which is differential in the photon's pseudorapidity η_γ and its transverse momentum $P_{\gamma,T}$. The cross section is given as in Eq. (7.3), but with the subscripts h corresponding to the hadron replaced by γ for the photon. The corresponding plot is presented in Fig. 7.11 for a fixed transverse momentum $P_{\gamma,T} = 5$ GeV. The central curve is obtained for the choice $\mu = P_{\gamma,T}$ and theoretical uncertainties are estimated by varying the scale μ between $\mu = P_{\gamma,T}/2$ and $\mu = 2P_{\gamma,T}$.

The cross section is of substantial size in the forward region of positive η_γ but rapidly falls off to zero when going to mid or backwards pseudorapidities. As discussed in Sec. 5.1, the parton-to-photon FFs are of order $\mathcal{O}(\alpha_{em}/\alpha_s)$ and thus one has to also consider NLO α_s corrections to be consistent with the given perturbative order of $\mathcal{O}(\alpha^3_{em})$. The sum of LO and NLO is shown as the blue dashed curve in Fig. 7.11. The main takeaway is that the NLO contribution has a considerable effect on the size of the cross section, multiplying it by at least a factor of 2 over the whole range in η_γ. The increase is most notable in the mid and backward regions, which however remain small compared to the forward region.

One may regard the photon case as the middle ground between hadron and jet production in terms of how clean it is as an observable to probe twist-3 multiparton distribution functions. While photon production does feature its own FFs, they are at least not present in every production

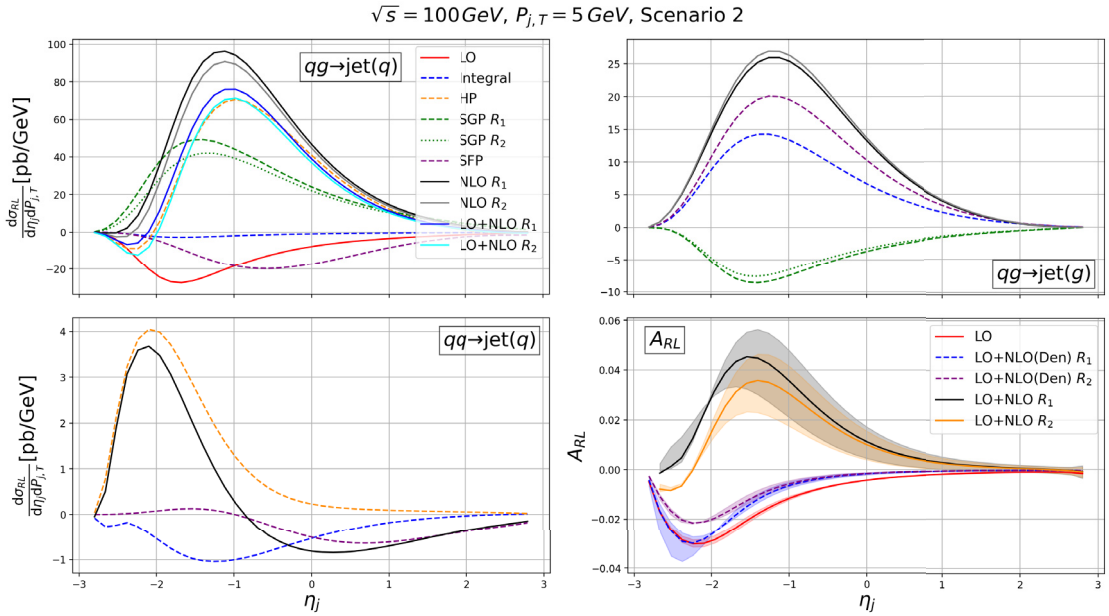

Figure 7.9: Same as Fig. 7.7, but for Scenario 2.

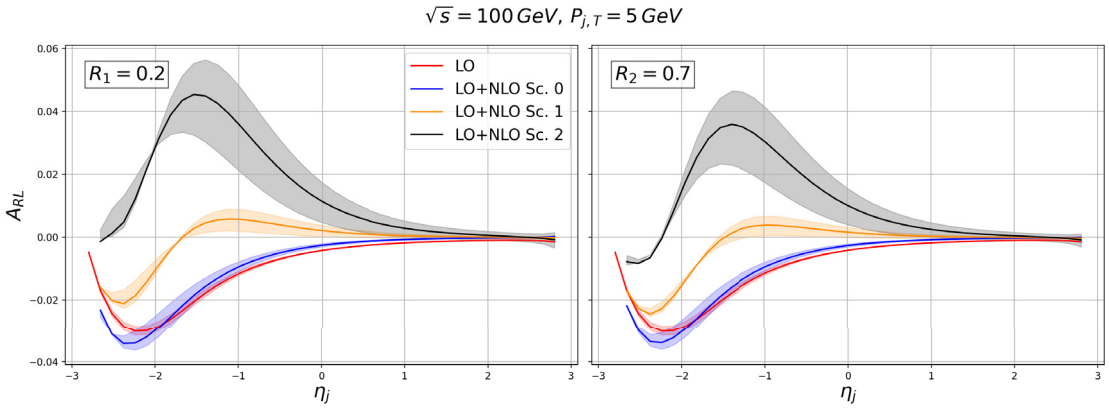

Figure 7.10: Comparison of the NLO asymmetries A_{RL} computed for Scenarios 0,1,2.

channel like for hadron production. Still, there are no FFs at all for jets and thus jet production would be the cleanest observable of the three. Another similarity between jets and photons is the absence of twist-3 fragmentation effects. Hence, the plots for both cases give the complete NLO prediction based on the model built in App. G. From Figs. 7.1 and 7.11, one can conclude that the unpolarized cross sections for hadron and photon production are roughly of comparable size, while jet production has an approximately 100 times larger event rate.

7.3.1 Scenario 0

Turning to the numerator of the right-left asymmetry (7.5), the numerical results for the "minimal" model Scenario 0 are shown in Fig. 7.12. They are separated into the Compton and Interference channels following Eq. (6.26). The Compton channel is further split up into its fragmentation and direct contributions, see Eq. (6.27). For a better comparison, each channel as well as the total cross section are shown together in the bottom right panel of Fig. 7.12.

Both parts of the Compton channel as well as the Interference channel are of comparable magnitude. However, due to the fragmentation channel giving a negative contribution to the total cross section, there is a partial cancellation between the channels at moderate backward pseudorapidities, which is also the region where the channels are individually the largest. In the forward region the Compton channel becomes negligible compared to the Interference channel. Looking at the two Compton channels separately, one finds that the fragmentation channel receives sizeable NLO corrections for backward pseudorapidities, while the direct channel is entirely dominated by its SGP contribution. On the other hand, NLO corrections to the Interference channel do not play

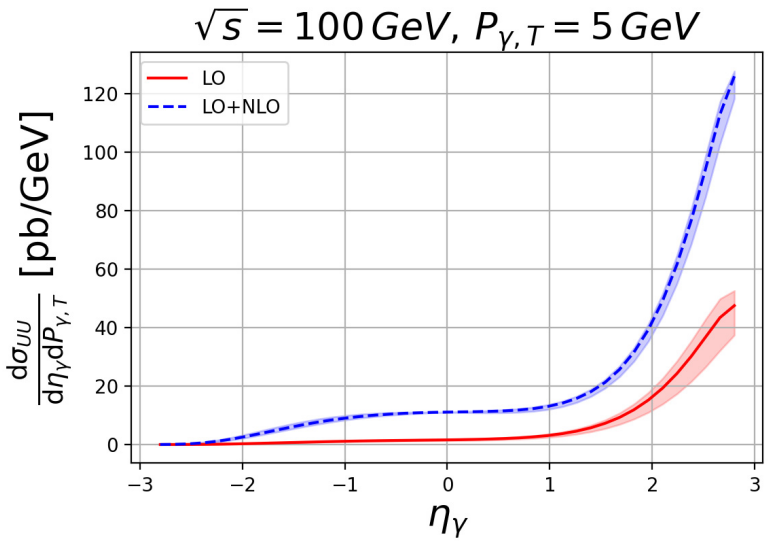

Figure 7.11: Unpolarized differential cross section for photon production plotted vs. the photon's pseudorapidity η_γ for fixed transverse momentum $P_{\gamma,T} = 5$ GeV.

a significant role for this Scenario, whereat the virtual corrections are slightly larger than the real corrections. Another interesting feature of this Scenario is that the Compton channel contributions generally peak for negative values of η_γ, i.e. in the backward region, while the Interference channel peaks in the forward region, at least for its dominant LO part.

7.3.2 Scenario 1

Next, the "realistic" Scenario 1 including the axial-vector type qgq function G^q and more "off-diagonal structure", see App. G.2, is discussed. Notably, the plots have several qualitative differences compared to the previous Scenario. Starting with the Fragmentation channel in the top left of Fig. 7.13, the NLO contribution changes sign slightly below $\eta_\gamma \approx -1$ and the total LO plus NLO contribution is in general smaller than before. A more drastic change can be observed for the direct Compton channel, where the SGP contribution no longer dominates and also flips its sign. Instead, the integral contribution is the largest and roughly twice as big as the SGP and SFP contributions. This is interesting since for hadron or jet production the integral contributions never dominate any production channel. The total contribution of the direct Compton channel is more sizeable and has the opposite sign as in Scenario 0.

Unlike the LO Fragmentation channel, the LO contribution to the Interference channel is not given by a SGP configuration but rather a SFP configuration of the involved distribution functions. As a consequence, the LO Interference contribution is sensitive to the off-diagonal support of the $q\gamma q$ functions. Hence, the specific choice for the model Scenario impacts the numerical results and for Scenario 1 there is a sign flip compared to Scenario 0.

Furthermore, the NLO corrections become more important, although they remain small except for the virtual corrections at far forward pseudorapidities $\eta_\gamma > 2$. Comparing the different channels in the bottom right of Fig. 7.13, one finds that they all contribute with the same sign and thus lead to a much larger magnitude, with the largest contribution being generated by the direct Compton channel.

7.3.3 Scenario 2

Finally, Scenario 2 is studied, which uses the largest Fourier coefficients in the model ansatz, see App. G.3. Qualitatively, the plots shown in Fig. 7.14 are similar to Scenario 1. Most notably, the NLO contribution to the Fragmentation channel becomes rather large and has the opposite sign as the LO contribution. This leads to a moderately sized result for the combination of LO plus NLO. Consequently, the contribution to the total cross section is quite negligible. This is in contrast to Scenario 0, where the Compton fragmentation channel was actually dominating. In the Interference channel, NLO contributions further increase in size. Interestingly, the peak of the total Interference cross section shifts from forward pseudorapidity for Scenario 0 to the central region around $\eta_\gamma \approx 0$ for Scenarios 1 and 2. Overall, the direct Compton channel dominates the

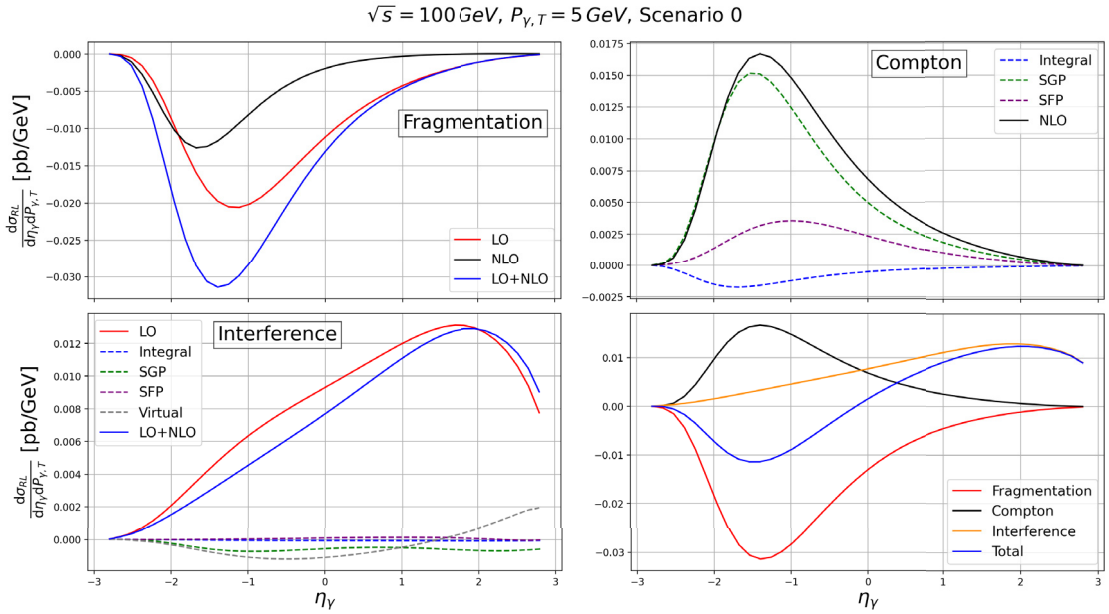

Figure 7.12: Cross sections for the Compton and Interference channels in Eq. (6.26) plotted vs. the photon's pseudorapidity η_γ at fixed transverse momentum $P_{\gamma,T} = 5$ GeV. The curves are produced for Scenario 0 (G.16).

total cross section, just like in Scenario 1, and it becomes even larger in magnitude. Excluding Scenario 0, one also generally observes that the Interference channel is negligible for the total cross section. This feature is familiar from the unpolarized and longitudinally polarized versions of the process studied in Ref. [38].

7.3.4 Asymmetry

Combining all previous results into the right-left asymmetry A_{RL}, one obtains the curves shown in Fig. 7.15 for the three different scenarios. The uncertainty bands shown in this plot correspond to the simple estimate for the scale dependence discussed in Par. 7 in the beginning of this chapter. The non-perturbative input $f_1^q(x,\mu)$ entering the model is simply evaluated at the scales $\mu = P_{\gamma,T}$ (central curve) as well as $\mu = P_{\gamma,T}/2$ and $\mu = 2P_{\gamma,T}$.

The qualitative picture is the same in any of the considered Scenarios. The asymmetry peaks at far backward pseudorapidity and monotonically decreases for increasing η_γ. The magnitude, however, significantly differs between the Scenarios, in particular in the mid and backward pseudorapidity regions. There one observes a clean separation of the three curves, even taking into account the estimated uncertainty bands. This boosts confidence in the ability of future collider facilities like the EIC to distinguish between different models and to constrain the twist-3 multiparton distribution functions. Still, it remains to be seen whether it is possible to disentangle the impact of the various types of distribution functions, for example the qgq and $q\gamma q$ functions. Moreover, the triple-gluon functions N, O along with the $g\gamma g$ functions O_γ^1, O_γ^2 have not yet been included in the numerical analysis. Consequently, it might prove to be rather challenging to extract information on the individual functions from the experiment. Nonetheless, the exploratory study performed in this chapter shows that there is a lot of potential and that one should be optimistic towards the long-term goal of a global analysis.

7.4 γSIDIS

The final section of this chapter presents numerical results for the γSIDIS process $e(l)p^\uparrow(P) \to e'(l')\gamma(p_\gamma)X$, i.e. the semi-inclusive production of an isolated real photon in electron-proton scattering. The numerical predictions presented in the following are explicitly for electrons e and (transversely polarized) protons $p^\uparrow$. This section recaps parts of Ref. [39], i.e. it is based on the work of a different collaboration than the rest of this chapter, and consequently uses different conventions. The kinematics change compared to the previously considered single-inclusive processes and one defines $q = l - l' - p_\gamma$ and $\tilde{q} = l - l'$. The reference frame chosen for the following analysis

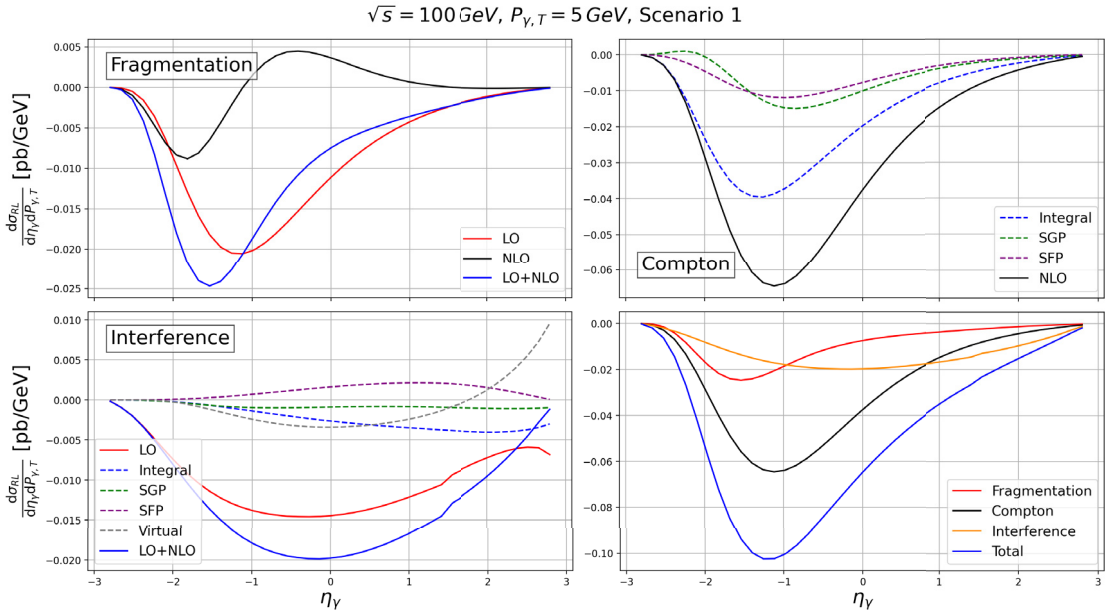

Figure 7.13: Same as Fig. 7.12, but for Scenario 1.

will be the electron-proton center-of-mass (CM) system with the proton moving along $+z$ and the electron moving along $-z$ (reversed compared to before, cf. Eq. (7.1)). The transverse proton spin $\boldsymbol{S_T}$ is assumed to point along the $+y$ axis. Some relevant kinematic variables are $s = (P + l)^2$, $Q^2 = -q^2$, $\tilde{Q}^2 = -\tilde{q}^2$, $x_B = Q^2/(2P\cdot q)$, and $\tilde{x}_B = \tilde{Q}^2/(2P\cdot\tilde{q})$. The rapidity and transverse momentum of the scattered electron (produced photon), respectively, are η' (η^γ) and $\boldsymbol{p}'_T$ ($\boldsymbol{p}^\gamma_T$), with ϕ' (ϕ^γ) being the azimuthal angle of the latter. Note that the notation for the photon's momentum, rapidity and azimuthal angle slightly deviates from the previous sections, to match Ref. [39]. Given these kinematical variables, the asymmetry $A_{UT}^{\gamma\text{SIDIS}}$ to be considered in the following analysis is defined as

$$A_{UT}^{\gamma\text{SIDIS}}(p'_T,\eta',\phi',p^\gamma_T,\eta^\gamma,\phi^\gamma) \equiv \frac{\frac{1}{2}\left(d\sigma_{UT}(\uparrow) - d\sigma_{UT}(\downarrow)\right)}{d\sigma_{UU}} = \frac{d\sigma_{UT}(\phi_s = \frac{\pi}{2})}{d\sigma_{UU}}\,. \tag{7.8}$$

Here, the unpolarized cross section in the denominator was calculated in Refs. [109, 137], and the transversely polarized counterpart in the numerator is given in Eq. (6.40). The proton spin along the $\pm y$ axis is denoted by $\uparrow$ ($\downarrow$). Eq. (7.8) explicitly shows the dependence of $A_{UT}^{\gamma\text{SIDIS}}$ on the six variables $(p'_T,\eta',\phi',p^\gamma_T,\eta^\gamma,\phi^\gamma)$ and Sec. 7.4.1 explores this phase space in an attempt to isolate in which regions the asymmetry could be measurable at the EIC. The advantage of $A_{UT}^{\gamma\text{SIDIS}}$ is the ability to probe the qgq functions F^q, G^q point-by-point in their full support on x, x'. This is an unprecedented feature of this observable. If the asymmetry is sizable enough to be measured at the EIC, then first-of-its-kind information could be obtained on multiparton distributions in the proton. In order to provide such estimates, the model built in App. G for F^q and G^q is used below.

To produce the plots, the choice for the non-perturbative input entering the observable must be specified. For γSIDIS, this input is chosen differently from the previous sections of this chapter. Now, the PDFs f_1^q used for the unpolarized cross section in the denominator of Eq. (7.8) will be the central curves from CT18NLO, cf. Ref. [143]. Furthermore, the first moment of the Sivers function $f_{1T}^{\perp(1),q}$, which enters the model for the qgq functions F^q, G^q in Eq. (G.8), is also taken from a different extraction. Here, the numerics are done using the central curves of the JAM3D-22 extraction of $f_{1T}^{\perp(1),q}(x)$, cf. Ref. [144], specifically the one where (up and down) antiquarks are included (see Sec. IV of Ref. [144]), i.e., $q = u, d, \bar{u}, \bar{d}$.

As before, the full twist-3 evolution of the qgq functions F^q, G^q will *not* be employed in the analysis. Although numerical code to perform the proper evolution has been published in Ref. [138], it would be beyond the scope of the present analysis to include it. Again, the goal is not to give high-precision predictions, but rather to get a first estimate for the asymmetry $A_{UT}^{\gamma\text{SIDIS}}$ and identify regions of the phase space where it could become particularly large. Hence, the evolution of F^q, G^q is simply "inherited" from the evolution of $f_{1T}^{\perp(1),q}(x)$ in Eq. (G.8), which is sufficient for this purpose. The JAM3D-22 Sivers function uses a DGLAP-type evolution, see Refs. [144, 145], with the inclusion of a double-logarithmic Q^2-dependent term to mimic the full twist-3 evolution. Any

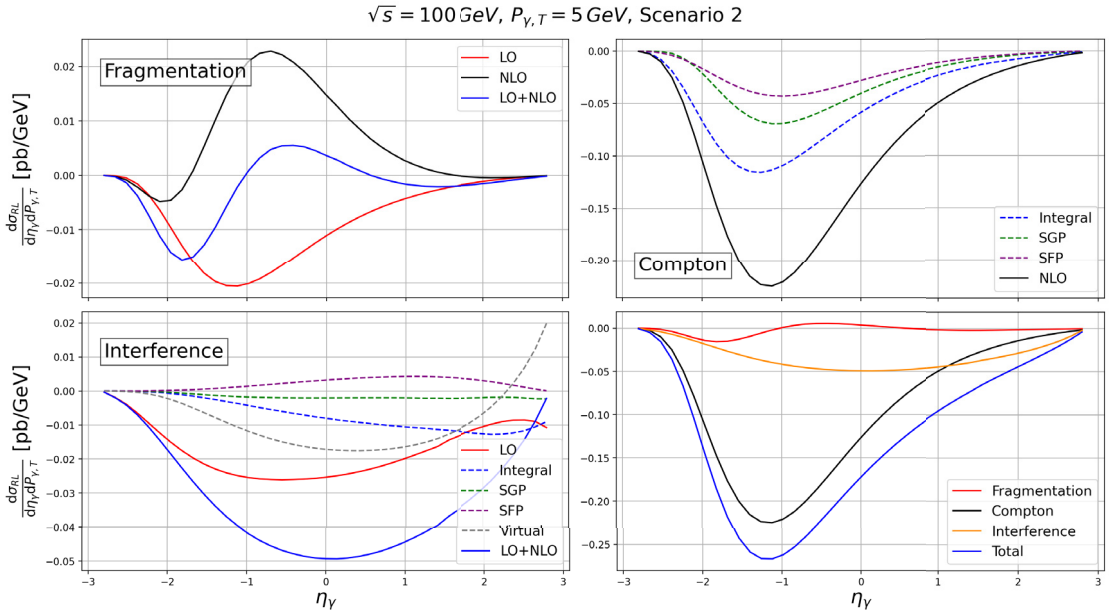

Figure 7.14: Same as Fig. 7.12, but for Scenario 2.

mixing with triple-gluon functions N, O or off-diagonal qgq functions $F^q(x,x'), G^q(x,x')$ for $x \neq x'$ is ignored in the evolution.

The contributions to the γSIDIS process can be distinguished by the respective power of the fractional charge e_q entering the analytic result. One has the Bethe Heitler (BH) contribution (e_q^2), Compton (C, e_q^4) and Interference (I, e_q^3). The scale μ is chosen differently for each of the three, see Refs. [39, 109]

$$\mu_{BH} = Q, \qquad \mu_C = \tilde{Q}, \qquad \mu_I = \sqrt{Q\tilde{Q}}\,. \tag{7.9}$$

Due to the differences explained above, for example in the choice for the non-perturbative input, the model Scenarios slightly change compared to the previously considered single-inclusive processes. In the following, the modified Scenarios S0 and S1 of App. G.4 will be considered.

7.4.1 Numerical Estimates for the Electron-Ion Collider

This section presents selected results for $A_{UT}^{\gamma\text{SIDIS}}$, see Eq. (7.8), for kinematics relevant to a future EIC. By sampling a wide kinematic range, the goal is to identify regions with large asymmetries. This will be valuable information to guide future experiments. Thus, multi-dimensional "heat map" plots of $\left|A_{UT}^{\gamma\text{SIDIS}}\right|$ are presented. The plots are organized in coarser bins of (η', p_T') and finer bins of $(\eta^\gamma, p_T^\gamma)$ with ϕ' and ϕ^γ fixed. With the user-friendly Google Colab notebook available in [146] the reader can explore other choices of model parameters for F^q, G^q as well as alternative experimental configurations.

Note that kinematic points for which either $Q^2 < 1\,\text{GeV}^2$, $\tilde{Q}^2 < 1\,\text{GeV}^2$, or $Q^2 - \tilde{Q}^2 < 1\,\text{GeV}^2$ are discarded as well as points that cause $\left|A_{UT}^{\gamma\text{SIDIS}}\right| > 1$, as can sometimes happen for $x, x' \to 1$. The color mapping in the plots indicates the different values for the asymmetries:

- purple: asymmetries close to zero
- light bluish/greenish: asymmetries of several percent
- red: asymmetries of *at least* 10%

As alluded to above, large asymmetries at the periphery of the subgraphs should be taken with caution. Instead, one should focus on the central regions away from the edges, which provide the most reliable estimates. Also note that the "γSIDIS" superscript on the $|A_{UT}|$ label has been dropped in all plots for brevity.

Fig. 7.16 shows the results for CM energy $\sqrt{s} = 29\,\text{GeV}$ with $\phi' = \phi^\gamma = 0$ for Scenario S0 of Eq. G.19. Recall that this is the "minimalistic" choice of parameters with most of them being set to zero and inparticular $G^q(x,x') = 0$. Away from the edges of the kinematics, $\left|A_{UT}^{\gamma\text{SIDIS}}\right|$ can be around 3–5% at mid to backward rapidity of the outgoing electron ($\eta' = 0$ or -1), mid to forward

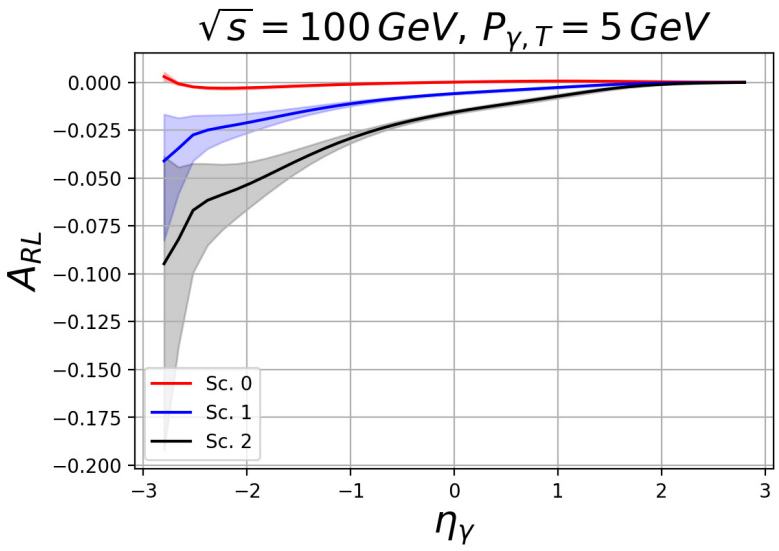

Figure 7.15: Right-left asymmetry A_{RL} of (7.5) plotted vs. the photon's pseudorapidity η_γ at fixed transverse momentum $P_{\gamma,T} = 5$ GeV for all Scenarios.

rapidity of the photon ($\eta^\gamma \gtrsim 0$), smaller outgoing electron transverse momenta ($p'_T \lesssim 3\,\text{GeV}$), and larger photon transverse momenta ($p^\gamma_T \gtrsim 3\,\text{GeV}$).

The same experimental configuration but now within Scenario S1 given by Eq. G.20 is displayed in Fig. 7.17. Now, all parameters for F^q, G^q are nonzero. Similar kinematic regions as previously give the largest $\left|A_{UT}^{\gamma\text{SIDIS}}\right|$, but it is now 10% or more. Now, asymmetries around $p^\gamma_T \sim 1\,\text{GeV}$ also become measurable, in particular at mid-rapidity of the outgoing electron.

There are also some general findings for both scenarios: it is preferable for both the outgoing electron and photon to be produced in the same direction (i.e., $\phi' = \phi^\gamma = 0$ or $\phi' = \phi^\gamma = \pi$) in order to obtain the largest asymmetries. If $\phi' = 0$ and $\phi^\gamma = \pi$ (or vice versa), then the asymmetry drops down to ∼1–3%. Furthermore, the regions of phase space where $\left|A_{UT}^{\gamma\text{SIDIS}}\right|$ is the largest do not qualitatively change if different values for the d_2-moments are used in the model of App. G. This was confirmed explicitly by picking $d_2^u = -0.00365$, $d_2^d = 0$ based on Ref. [147]. The same is true for using a different extraction of the Sivers function, like the one from Ref. [148], which has a larger magnitude and different x behavior than JAM3D-22.

In Fig. 7.18, the $x_B, \tilde{x}_B$ coverage is displayed for the experimental setup in Fig. 7.17. The left panel uses the same binning as in Fig. 7.17: 4 bins of η', 6 bins of p'_T, and 20 bins each of η^γ and p^γ_T. In the right panel a finer binning in η' and p'_T is used, where each now has 10 bins. The $x_B = \tilde{x}_B$ diagonal is indicated by the dashed black line. In an experiment, only points below this line are accessed. However, using the symmetry properties $F^q(x, x') = F^q(x', x)$ and $G^q(x, x') = -G^q(x', x)$, one can reflect the points across this line. This means that information on F^q, G^q at $(x_B, \tilde{x}_B)$ also gives information about the point $(\tilde{x}_B, x_B)$. The magnitude of $A_{UT}^{\gamma\text{SIDIS}}$ is again indicated using the same color scale as before. Thus, one can identify the regions of (x, x') for F^q, G^q to which the observable $A_{UT}^{\gamma\text{SIDIS}}$ will be most sensitive: $(x, x') \in ([0.2, 0.8], [0, 0.1])$ and $(x, x') \in ([0, 0.1], [0.2, 0.8])$.

There is, however, a caveat to the direct probe of F^q and G^q at off-diagonal momentum fractions: the transversely polarized cross section (Eqs. (6.40), (6.42)) depends not only on the HP structure $F^q(x_B, \tilde{x}_B) \pm G^q(x_B, \tilde{x}_B)$ but also the SFP structure $F^q(x_B, 0) \pm G^q(x_B, 0)$. In most of the phase space where $\left|A_{UT}^{\gamma\text{SIDIS}}\right|$ is sizable, the SFP contribution is comparable or larger than the HP, potentially "diluting" the signal from $F^q(x_B, \tilde{x}_B)$ and $G^q(x_B, \tilde{x}_B)$. On the other hand, the SFP functions $F^q(x, 0)$ and $G^q(x, 0)$ have never been extracted from experimental data either, so sensitivity to them from $A_{UT}^{\gamma\text{SIDIS}}$ is also valuable.

In Fig. 7.19, the effect of larger EIC CM energies on the asymmetries is demonstrated, in this case $\sqrt{s} = 63\,\text{GeV}$, using Scenario S1. There is a dramatic decrease in $\left|A_{UT}^{\gamma\text{SIDIS}}\right|$ to basically zero everywhere except at mid to forward rapidity of the outgoing electron ($\eta' = 0$ or 1), forward rapidity of the photon ($\eta^\gamma \gtrsim 1$), smaller outgoing electron transverse momenta ($p'_T \lesssim 2\,\text{GeV}$ at electron mid-rapidity and $p'_T \lesssim 4\,\text{GeV}$ at electron forward rapidity), and larger photon transverse momenta ($p^\gamma_T \gtrsim 5\,\text{GeV}$, although at electron forward rapidity, $p^\gamma_T \gtrsim 1\,\text{GeV}$ can still give sizable asymmetries). If the CM energy is further increased to $\sqrt{s} = 141\,\text{GeV}$, the asymmetry is zero

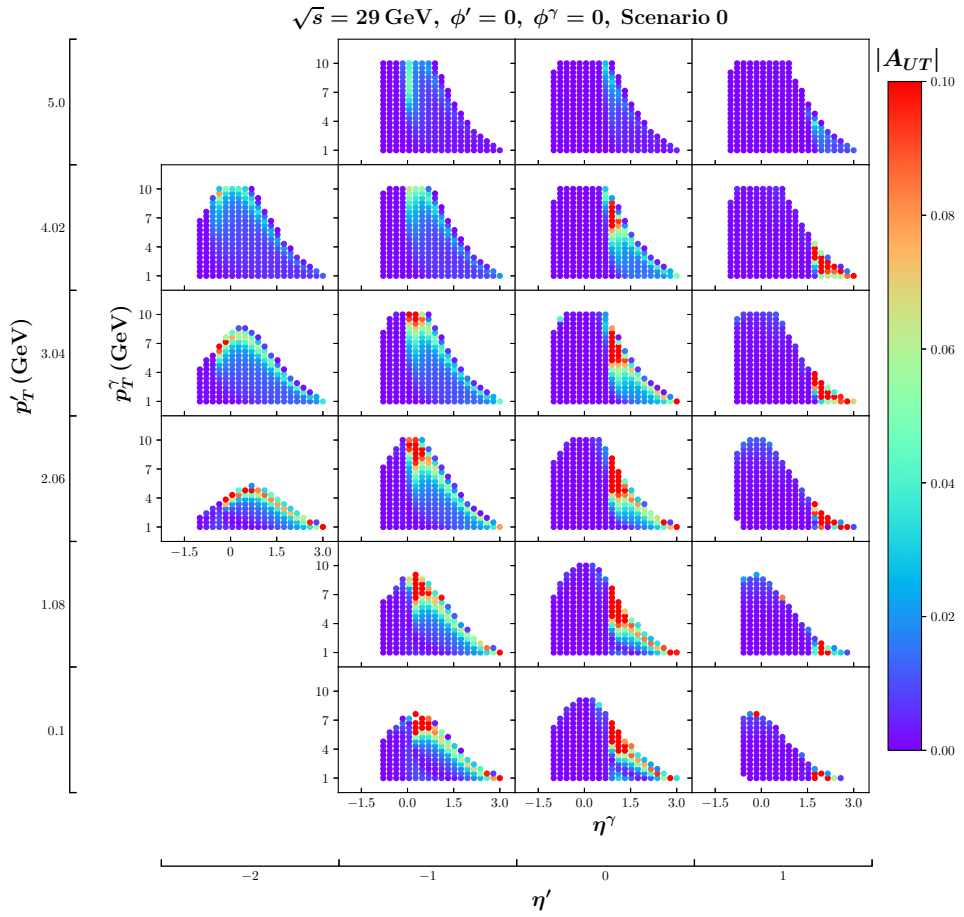

Figure 7.16: $\left|A_{UT}^{\gamma\mathrm{SIDIS}}\right|$ vs. $(\eta', p'_T, \eta^\gamma, p_T^\gamma)$ for $\sqrt{s} = 29\,\mathrm{GeV}$ with $\phi' = \phi^\gamma = 0$ for Scenario S0. The outer axes are bins of (η', p'_T) and the inner axes are bins of $(\eta^\gamma, p_T^\gamma)$.

everywhere except at the most forward kinematics of $\eta' = 1$ and $\eta^\gamma \gtrsim 2$.

Finally, there exists in principle the possibility to experimentally disentangle the Compton (C) and Interference (I) channels in Eq. (7.8). This could be done using an electron as well as a positron beam. Figs. 7.16, 7.17, 7.19 show that both channels make similar-sized contributions to $A_{UT}^{\gamma\mathrm{SIDIS}}$. Neither of them dominates the other over the full kinematic range. Specifically, a *beam charge asymmetry* will cleanly probe the Interference channel on its own. This would be important since the Interference channel is generated by *valence-type* $q - \bar{q}$ (instead of $q + \bar{q}$) combinations of multi-parton correlation functions (see Eq. (6.41)). Such information on $q - \bar{q}$ distributions would be most helpful for separating quark- and antiquark correlation functions. Note that there is the opportunity for a positron beam at Jefferson Lab [149, 150] as well as the EIC [151], and the beam charge asymmetry would definitely be an interesting measurement at those facilities.

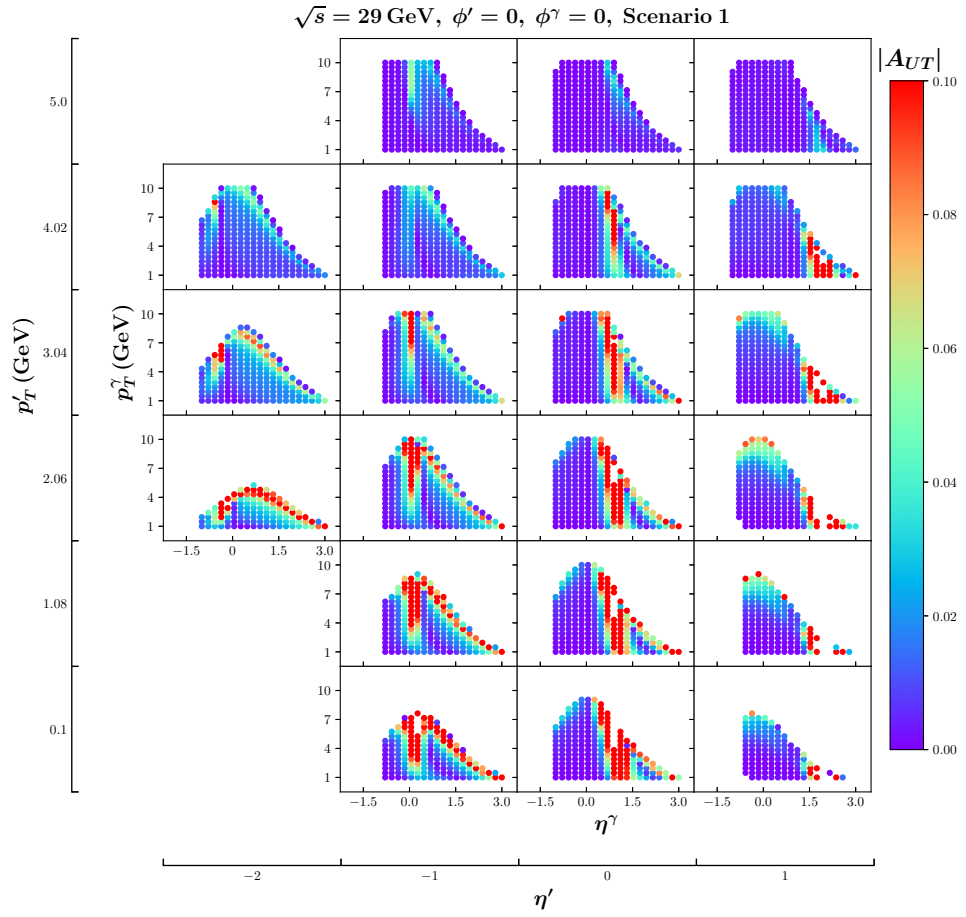

Figure 7.17: Same as Fig. 7.16 but for Scenario S1

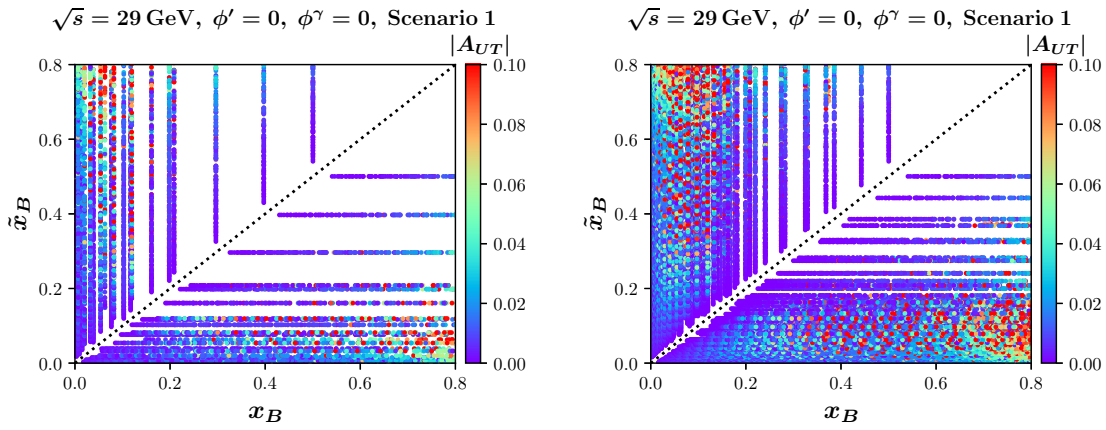

Figure 7.18: Kinematic points $\tilde{x}_B$ vs. x_B that enter the arguments of F^q, G^q in Fig. 7.17 ($\sqrt{s} = 29\,\mathrm{GeV}$ with $\phi' = \phi^\gamma = 0$ for Scenario S1). **Left:** binning as in Fig. 7.17, **Right:** finer binning in η' and p'_T

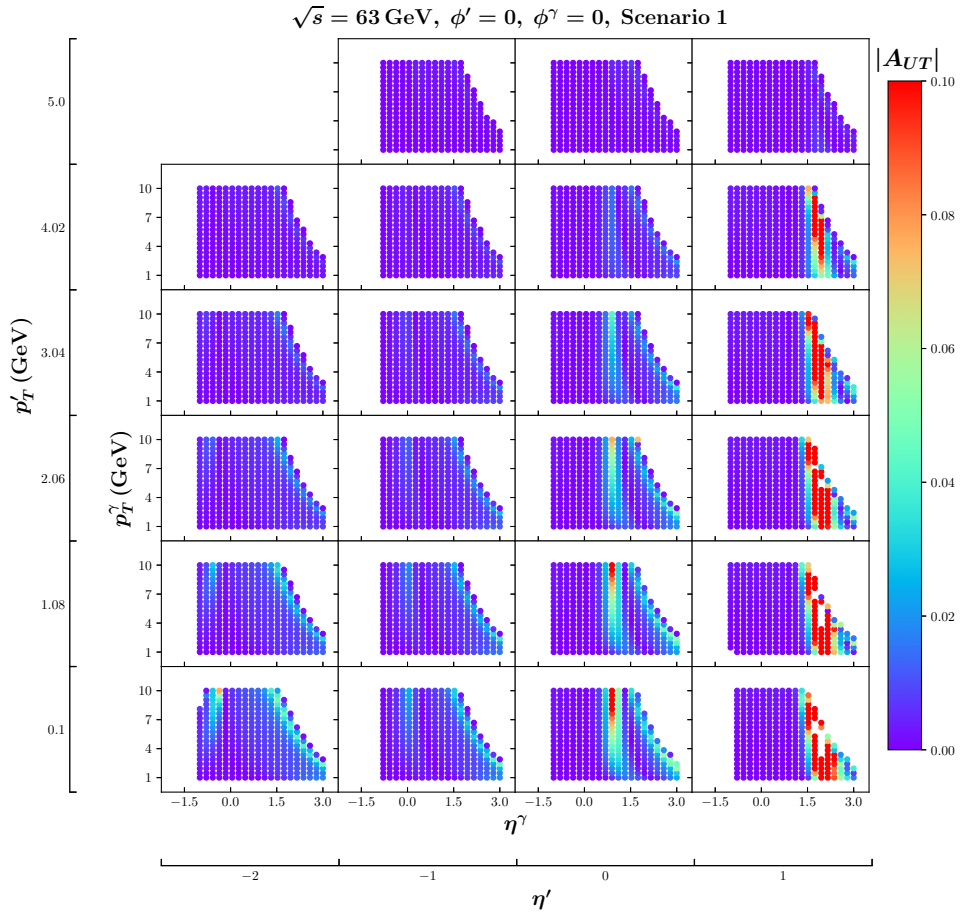

Figure 7.19: Same as Fig. 7.17 (Scenario S1) but for $\sqrt{s} = 63\,\mathrm{GeV}$

Chapter 8

Summary and Outlook

In this thesis, an explicit and fully analytic derivation of transverse spin-dependent cross sections within the formalism of collinear twist-3 factorization was performed. The results for several single-inclusive final states in lepton-nucleon scattering were computed at NLO accuracy in pQCD, demonstrating that the formalism holds at the one-loop level and thereby solidifying the theoretical confidence in its validity.

The specific processes considered were the production of hadrons, jets and photons, $\ell N^\uparrow \to (h \,\text{or jet or}\, \gamma)\, X$. The focus was on multiparton distribution functions of the initial state nucleon, while twist-3 fragmentation effects were disregarded. For jets and photons, where twist-3 effects are absent on the fragmentation side, the derivations provide the complete NLO result.

For single-inclusive photon production, the inclusion of $q\gamma q$ and $g\gamma g$ distribution functions of the nucleon was required. These functions are scarcely discussed in the literature and for the $q\gamma q$ functions a detailed derivation of the necessary and previously unknown renormalization formulas was given, while for the $g\gamma g$ case an explicit parametrization of the corresponding correlator was derived. Furthermore, the γSIDIS process $\ell N^\uparrow \to \ell' \gamma X$ was reviewed and a more compact form of the known analytical result was presented.

In addition, a model was built for the twist-3 qgq functions F^q, G^q entering the analytical formulas. The model is consistent with all known constraints on the functions and can be customized via the choice of parameters. Using this model along with results for the unpolarized cross sections in the literature, the transverse SSA was calculated numerically.

The numerical analysis was performed for the expected kinematical setup of a future Electron-Ion Collider (EIC) for each of the considered processes. For hadron production, a preliminary comparison to existing HERMES data on $ep^\uparrow \to \pi^\pm X$ was also performed. In general, NLO corrections can be sizeable and the predictions are highly sensitive to the precise choice of model parameters. Since the qgq functions are probed on their full support in longitudinal momentum fractions x, x', this implies that future precision data provided by the EIC can shed light on the entirely unexplored region $x \neq x'$.

A special role is played by the γSIDIS process, as it offers the possibility for a point-by-point scan of the x, x' support. Regions of phase space where the corresponding asymmetry $A_{UT}^{\gamma\text{SIDIS}}$ becomes largest were identified, and it was also shown that the x, x' coverage in γSIDIS is well suited to gain information about the off-diagonal support regions. Moreover, a google colab notebook is available [146], allowing users to test arbitrary experimental setups and model parameters to explore the numerical results even further.

The calculations for the *single-inclusive* processes highlighted in this work are the first of their kind at NLO within the collinear twist-3 formalism. Previous NLO calculations have been restricted to processes in which the photon virtuality q^2 is fully determined by external momenta, leading to simpler kinematics and, hence, less complex computations. This thesis thus represents a significant milestone in the development of the formalism and lays the groundwork for its extension to $pp^\uparrow$ collisions – a crucial step for comparison with the wealth of experimental data from RHIC.

A more direct extension would be to compute the twist-3 fragmentation effects in $\ell N^\uparrow \to hX$. This would complete the theoretical picture and improve the comparison with the HERMES data discussed earlier. However, it would also introduce further non-perturbative objects that need to be modeled as there are no data sets available yet. Additionally, one should also include the contributions by the triple-gluon functions N, O and, in the case of single-inclusive photon production, also the $g\gamma g$ functions O_γ^1, O_γ^2 for the numerical analyses. Again, this would require further modeling.

The implementation of the proper twist-3 evolution of the qgq functions would also constitute a

valuable improvement of this study. So far, only the twist-2 evolution of the PDF f_1^q was considered, as it is the only non-perturbative input entering the model of App. G. The Honeycomb/Snowflake code of Ref. [138] is publicly available and already implements LO twist-3 evolution. An NLO version, which is needed to match the perturbative order of the present work, is however not expected to become available in the near future. Access to proper twist-3 evolution would notably enhance the phenomenological analysis. Moreover, it would also allow to produce plots versus the transverse momentum p_T of the observed final state particles.

Finally, there are some remarks on the next perturbative order, i.e. next-to-next-to-leading order (NNLO). One could argue that the tools and methods developed in this work at NLO provide the foundation to tackle NNLO. The four-particle phase space as well as the two-loop integrals, which will both be necessary ingredients, could probably be computed using techniques from leading power NNLO calculations. However, several non-trivial challenges must be acknowledged. For the integral contributions, the extraction of imaginary parts will become more involved, as one expects to also encounter polylogarithms. For the double-virtual corrections, extracting the imaginary parts from the two-loop integrals will also become more difficult. This is in particular due to the necessity of all-order-in-ε results, or at least a general method to systematically retain the $1/(1-w)^{n+\varepsilon}$ terms. These terms already required special treatment at NLO and will probably be even more laborious to handle at NNLO. Lastly, the real-virtual corrections may reveal entirely new features that demand their own tools and methods. In summary, going to NNLO would represent a truly monumental task.

Appendix A

Wilson Lines

This appendix gives some further details on the definition and properties of Wilson lines. It focuses on the most important aspects, which are used in the discussion of operator definitions for PDFs in Sec. 2.1.4. It also gives some explicit derivations which are too lengthy for the main text.

A.1 Definition

First, a general definition for Wilson lines is given. Consider a path C parametrized by the trajectory $x^\mu(s)$ with $0 < s < 1$. The corresponding Wilson line is a path-ordered exponential (cf. Ref. [56])

$$\mathcal{W}[C] \,=\, \hat{P} \exp\left[-ig \int_0^1 \mathrm{d}s \frac{\mathrm{d}x^\mu}{\mathrm{d}s} G_\mu^\alpha\left(x(s)\right) t^\alpha\right] \,=\, \hat{P} \exp\left[-ig \int_C \mathrm{d}x^\mu G_\mu^\alpha\left(x\right) t^\alpha\right] , \tag{A.1}$$

where G_μ^α is the gluon field of Lorentz index μ and adjoint color index α and t^α are the usual SU(3) generators in the fundamental representation. For gluon correlators containing gluon field strength tensors in their matrix elements, one correspondingly needs slightly modified Wilson lines. They would include the generators of the adjoint representation in their definition.

The path-ordering symbol $\hat{P}$ introduced in Eq. (A.1) fixes the order of the terms when expanding the exponential. It moves terms evaluated at larger parameters s to the left and those at smaller s to the right. For example, let $1 > s_n > \cdots > s_1 > 0$, and P be some permutation of $\{1, \ldots, n\}$. Then, the action of $\hat{P}$ on operators $O(x(s))$ evaluated along the trajectory $x^\mu(s)$ is given as

$$\hat{P} O(x(s_{P(1)})) \ldots O(x(s_{P(n)})) \,=\, O(x(s_n)) \ldots O(x(s_1)) \,.$$

A.2 Gauge Transformation of Wilson Lines

An important fact is that the bilocal combination of fields $\bar{q}(w)\mathcal{W}[C]q(v)$ is color gauge invariant for a path C with endpoints $x(0) = v$ and $x(1) = w$. These combinations show up between the nucleon states in operator definitions of PDFs, such as Eq. (2.51). To show their invariance, one must know the transformation law of the Wilson lines.

One could, in principle, plug the transformed gluon field into the definition (A.1) and derive an expression for the transformed Wilson line by brute force. It is, however, very difficult to arrive at a concise and simplified result using this approach. A more elegant solution is presented, for example, in the book by Peskin and Schröder [66]. The basis of the derivation is that Wilson lines are the solution to the following first order differential equation[1]

$$\frac{\mathrm{d}}{\mathrm{d}t} \mathcal{W}\left[x(t)\right] \,=\, -ig \frac{\mathrm{d}x^\mu}{\mathrm{d}t} G_\mu^\alpha\left(x(t)\right) t^\alpha \mathcal{W}\left[x(t)\right] . \tag{A.2}$$

Here, $\mathcal{W}\left[x(t)\right]$ is the Wilson line for a path with trajectory $x^\mu(s)$, but the upper integration bound of 1 in Eq. (A.1) is replaced by $0 < t < 1$. The boundary condition is that $\mathcal{W}\left(x(0)\right) = 1$. The solution of a first order differential equation is unique for a given boundary condition. Hence, a solution $\mathcal{W}'$ for the gauge transformed differential equation with correct boundary condition must

[1] analogous to the time-evolution operator in quantum mechanics being the solution of the time-dependent Schrödinger equation

be the unique gauge transformation of the Wilson line. This solution, and consequently the gauge transformed Wilson line, can be written as

$$\mathcal{W}'\left[x(t)\right] = U\left(x(t)\right)\mathcal{W}\left[x(t)\right]U^{\dagger}\left(x(0)\right)\,, \tag{A.3}$$

where U is the unitary gauge transformation matrix introduced for the transformation of the quark field in Eq. (2.2).

One immediately recognizes that the boundary condition $\mathcal{W}'\left(x(0)\right) = 1$ is fulfilled exactly if $\mathcal{W}\left(x(0)\right) = 1$. Recall that the gluon field transforms as $G_\mu^\alpha(x)t^\alpha \to (-i/g)U(x)D_\mu U^\dagger(x)$ with the covariant derivative $D_\mu = \partial_\mu + igG_\mu^\alpha t^\alpha$. Then, one quickly verifies that $\mathcal{W}'$ indeed solves the transformed differential equation if and only if $\mathcal{W}$ solves the untransformed version:

$$\begin{aligned}
\frac{\mathrm{d}}{\mathrm{d}t}\mathcal{W}'\left[x(t)\right] &= -ig\frac{\mathrm{d}x^\mu}{\mathrm{d}t}\left(G'\right)_\mu^\alpha\left(x(t)\right)t^\alpha\mathcal{W}'\left[x(t)\right] \\
\frac{\mathrm{d}}{\mathrm{d}t}\left[U\left(x(t)\right)\mathcal{W}\,U^\dagger\left(x(0)\right)\right] &= -ig\frac{\mathrm{d}x^\mu}{\mathrm{d}t}\left[U(x(t))\left(G_\mu^\alpha + \partial_\mu\omega^\alpha\right)t^\alpha U^\dagger(x(t))\right] \\
&\qquad \times\left[U\left(x(t)\right)\mathcal{W}\,U^\dagger\left(x(0)\right)\right] \\
\left[-ig\partial_\mu\omega^\alpha\,\frac{\mathrm{d}x^\mu}{\mathrm{d}t}t^\alpha\mathcal{W} + \frac{\mathrm{d}\mathcal{W}}{\mathrm{d}t}\right] &= -ig\frac{\mathrm{d}x^\mu}{\mathrm{d}t}\left[G_\mu^\alpha t^\alpha + \partial_\mu\omega^\alpha\,t^\alpha\right]\mathcal{W} \\
\frac{\mathrm{d}}{\mathrm{d}t}\mathcal{W}\left[x(t)\right] &= -ig\frac{\mathrm{d}x^\mu}{\mathrm{d}t}G_\mu^\alpha\left(x(t)\right)t^\alpha\mathcal{W}\left[x(t)\right]\,.
\end{aligned} \tag{A.4}$$

Here, from the second to the third line the product rule is used for the t derivative and both sides are multiplied by $U^\dagger(x(t))$ from the left as well as $U(x(0))$ from the right. This proves the transformation law for the Wilson line. Consequently, one indeed finds that the bilocal field combination is gauge invariant

$$\begin{aligned}
\bar{q}(w)\mathcal{W}[C]q(v) &\to \bar{q}(w)U^\dagger(w)U\left(x(1)\right)\mathcal{W}[C]U^\dagger\left(x(0)\right)U(v)q(v) \\
&= \bar{q}(w)\left(U^\dagger(w)U(w)\right)\mathcal{W}[C]\left(U^\dagger(v)U(v)\right)q(v) = \bar{q}(w)\mathcal{W}[C]q(v)\,.
\end{aligned} \tag{A.5}$$

A.3 Reparametrization and Path Dependence

The path C of a Wilson line can always be reparametrized, $x^\mu \to (x')^\mu$. Such a reparametrization leaves the Wilson line unchanged, since it is merely a substitution for the integral inside the exponential. However, Wilson lines do in general depend on the exact path C, even if the endpoints remain fixed. A special case and an exception to this rule is the path along a straight line such as in Eq.(2.51), where only the endpoints matter. To see this, consider the product of two Wilson lines along the same straight path defined by a vector n^μ, i.e. $\mathcal{W}\left[\mu n;\lambda n\right]\mathcal{W}\left[\lambda n;\nu n\right]$. By a quick calculation one shows that the derivative with respect to the midpoint λ vanishes and thus $\mathcal{W}\left[\mu n;\lambda n\right]\mathcal{W}\left[\lambda n;\nu n\right] = \mathcal{W}\left[\mu n;\nu n\right]$. This property is sometimes used in parton densities to insert an intermediate step at light-cone infinity [56]

$$\mathcal{W}\left[\mu n;\nu n\right] = \mathcal{W}\left[\mu n;\infty n\right]\mathcal{W}\left[\infty n;\nu n\right] = \left(\mathcal{W}\left[\infty n;\mu n\right]\right)^\dagger\mathcal{W}\left[\infty n;\nu n\right]\,. \tag{A.6}$$

This is part of the justification for the rather complicated link structure in the kinematical quark-quark and gluon-gluon correlators (C.1), (C.3).

Appendix B

Discrete Transformation Laws

In this part of the appendix, a brief review on discrete symmetries of the fields is presented. The main purpose is to collect the relevant properties for the quark and gluon fields such that the behavior of the quark-quark correlator Φ^q in (2.53) under these transformations can be studied. From the transformation relations of Φ^q one can deduce a parametrization of this correlator in terms of parton distribution functions (PDFs). To keep this appendix self-contained, the definition of Φ^q is also given here:

$$\Phi^q\left(x;n,P,S\right) \;=\; \int_{-\infty}^{\infty}\frac{\mathrm{d}\lambda}{2\pi}e^{i\lambda x}\langle P,S|\bar{q}(0)\mathcal{W}\left[0;\lambda n\right]q(\lambda n)|P,S\rangle\,, \tag{B.1}$$

with an auxiliary light-cone vector n, the nucleon momentum P and its spin S. The vector n is unphysical since it only has to satisfy the constraints $n^2=0$, $P\cdot n=1$ and is otherwise arbitrary. The fields inside the matrix element are the quark spinors $q(\lambda n)$ and $\bar{q}(0)$. The straight-path Wilson line $\mathcal{W}\left[0;\lambda n\right]$ ensures color gauge invariance. The variable x denotes the longitudinal momentum fraction that the quark takes from the nucleon.

Another important ingredient is the translational property of the fields. While it is not a discrete symmetry, it nonetheless proves useful in the following. One can shift the spacetime argument of the fields by multiplying from the left and right with an exponential of the momentum operator $\hat{\Pi}$. This shift also translates to the straight-path Wilson line, and one finds the relations

$$\begin{aligned} q(x) &= e^{i\hat{\Pi}\cdot y}q(x-y)e^{-i\hat{\Pi}\cdot y}\\ G_\mu^\alpha(x) &= e^{i\hat{\Pi}\cdot y}G_\mu^\alpha(x-y)e^{-i\hat{\Pi}\cdot y}\\ \mathcal{W}\left[\mu n;\nu n\right] &= e^{i\hat{\Pi}\cdot\lambda n}\mathcal{W}\left[(\mu-\lambda)n;(\nu-\lambda)n\right]e^{-i\hat{\Pi}\cdot\lambda n}\,, \end{aligned} \tag{B.2}$$

In the following, hermitian conjugation, parity and time-reversal will be discussed one-by-one. For each transformation, the corresponding behavior of the correlator Φ^q will also be derived.

B.1 Hermitian Conjugation

Hermitian conjugation is applied to a general matrix element with color indices $a_1,\ldots,a_n$ as follows

$$\langle f|\left[\ldots\right]_{a_1,\ldots,a_n}|i\rangle^* \;=\; \langle i|\left[\ldots\right]^\dagger_{a_1,\ldots,a_n}|f\rangle\,, \tag{B.3}$$

and for the fields and consequently the straight-path Wilson line one has

$$\begin{aligned} q^\dagger(x) &= \bar{q}(x)\gamma^0\\ \left(G_\mu^\alpha(x)\right)^\dagger &= G_\mu^\alpha(x)\\ \mathcal{W}^\dagger\left[\mu n;\nu n\right] &= \mathcal{W}\left[\nu n;\mu n\right]\,. \end{aligned} \tag{B.4}$$

Having summarized the necessary prerequisites, one can also derive how the quark-quark correlator Φ^q defined in Eq. (B.1) behaves under hermitian conjugation

$$\begin{aligned}
\left[(\Phi^q)^\dagger\right]_{ij} = \left(\Phi^q_{ji}\right)^* &= \int_{-\infty}^{\infty}\frac{\mathrm{d}\lambda}{2\pi}e^{-i\lambda x}\langle P,S|\bar{q}_i(0)\mathcal{W}\left[0;\lambda n\right]q_j(\lambda n)|P,S\rangle^* \\
&= \int_{-\infty}^{\infty}\frac{\mathrm{d}\lambda}{2\pi}e^{-i\lambda x}\langle P,S|\bar{q}_l(\lambda n)\left(\gamma^0\right)_{lj}\mathcal{W}\left[\lambda n;0\right]\left(\gamma^0\right)_{ik}q_k(0)|P,S\rangle \\
&= \int_{-\infty}^{\infty}\frac{\mathrm{d}\lambda}{2\pi}e^{-i\lambda x}\langle P,S|\bar{q}_l(0)\left(\gamma^0\right)_{lj}\mathcal{W}\left[0;-\lambda n\right]\left(\gamma^0\right)_{ik}q_k(-\lambda n)|P,S\rangle \\
&= \int_{-\infty}^{\infty}\frac{\mathrm{d}\lambda}{2\pi}e^{+i\lambda x}\langle P,S|\bar{q}_l(0)\left(\gamma^0\right)_{lj}\mathcal{W}\left[0;\lambda n\right]\left(\gamma^0\right)_{ik}q_k(\lambda n)|P,S\rangle \\
&= \left(\gamma^0\right)_{ik}\Phi^q_{kl}\left(\gamma^0\right)_{lj}\,. \qquad \text{(B.5)}
\end{aligned}$$

From the first to the second line, the hermitian conjugate of the fields and the Wilson line (cf. (B.4)) is taken. This is followed by applying the translational properties given in Eq. (B.2) and finally a substitution $\lambda \to -\lambda$. Interestingly, the behavior of Φ^q is identical to the gamma matrices, i.e. $(\gamma^\mu)^\dagger = \gamma^0\gamma^\mu\gamma^0$.

B.2 Parity

Next is parity. The transformation is described by the unitary operator $\mathcal{P}$ with $\mathcal{P}\mathcal{P}^\dagger = \mathbb{1}$. Using the notation $\bar{x} = \left(x^0, -\mathbf{x}\right)$ for a general parity-reversed vector one has the following list of properties

$$\begin{aligned}
\mathcal{P}|P,S\rangle &= |\bar{P},-\bar{S}\rangle \\
\mathcal{P}q(x)\mathcal{P}^\dagger &= \gamma^0 q(\bar{x}) \\
\mathcal{P}\bar{q}(x)\mathcal{P}^\dagger &= \bar{q}(\bar{x})\gamma^0 \\
\mathcal{P}G^\alpha_\mu(x)\mathcal{P}^\dagger &= \bar{G}^\alpha_\mu(\bar{x}) \\
\mathcal{P}\mathcal{W}\left[\mu n;\nu n\right]\mathcal{P}^\dagger &= \mathcal{W}\left[\mu\bar{n};\nu\bar{n}\right]\,. \qquad \text{(B.6)}
\end{aligned}$$

Keep in mind that the bar over a quantity can either mean reversed parity, which is the case for vectors ($\bar{x}$, $\bar{P}$, $\bar{S}$, ...), or it can denote the adjoint of a Dirac spinor ($\bar{q}$). Using these properties one finds the following transformation law for the quark-quark correlator Φ^q under parity

$$\begin{aligned}
\Phi^q_{ij}(x;n,P,S) &= \int_{-\infty}^{\infty}\frac{\mathrm{d}\lambda}{2\pi}e^{i\lambda x}\langle P,S|\mathcal{P}^\dagger\mathcal{P}\bar{q}_j(0)\mathcal{P}^\dagger\mathcal{P}\mathcal{W}\left[0;\lambda n\right]\mathcal{P}^\dagger\mathcal{P}q_i(\lambda n)\mathcal{P}^\dagger\mathcal{P}|P,S\rangle \\
&= \int_{-\infty}^{\infty}\frac{\mathrm{d}\lambda}{2\pi}e^{i\lambda x}\langle \bar{P},-\bar{S}|\bar{q}_l(0)\left(\gamma^0\right)_{lj}\mathcal{W}\left[0;\lambda\bar{n}\right]\left(\gamma^0\right)_{ik}q_k(\lambda\bar{n})|\bar{P},-\bar{S}\rangle \\
&= \left(\gamma^0\right)_{ik}\Phi^q_{kl}\left(x;\bar{n},\bar{P},-\bar{S}\right)\left(\gamma^0\right)_{lj}\,. \qquad \text{(B.7)}
\end{aligned}$$

B.3 Time-Reversal

Lastly, time-reversal is introduced via the *anti*-unitary operator $\mathcal{T}$ with $\mathcal{T}^\dagger\mathcal{T} = \mathbb{1}$ and $\mathcal{T}c\mathcal{T}^\dagger = c^*$ for any complex number c. For a general matrix element with color indices $a_1,\ldots,a_n$ one has

$$\langle f|\left[\ldots\right]_{a_1\ldots a_n}|i\rangle^* = \langle f|\mathcal{T}^\dagger\mathcal{T}\left[\ldots\right]_{a_n\ldots a_1}\mathcal{T}^\dagger\mathcal{T}|i\rangle\,. \qquad \text{(B.8)}$$

Furthermore, one also has the following properties

$$\begin{aligned}
\mathcal{T}|P,S\rangle &= |\bar{P},\bar{S}\rangle \\
\mathcal{T}q(x)\mathcal{T}^\dagger &= -i\gamma_5 C q\left(-\bar{x}\right) \\
\mathcal{T}\bar{q}(x)\mathcal{T}^\dagger &= \bar{q}\left(-\bar{x}\right)\left(-i\gamma_5 C\right) \\
\mathcal{T}G^\alpha_\mu(x)\mathcal{T}^\dagger &= \bar{G}^\alpha_\mu\left(-\bar{x}\right) \\
\mathcal{T}\mathcal{W}\left[\mu n;\nu n\right]\mathcal{T}^\dagger &= \mathcal{W}\left[-\mu\bar{n};-\nu\bar{n}\right]\,, \qquad \text{(B.9)}
\end{aligned}$$

where $C = i\gamma^2\gamma^0$ is the charge conjugation matrix. Consequently, one finds for the quark-quark correlator

$$\begin{aligned}
\left(\Phi^q_{ij}\right)^* (x; n, P, S) &= \int_{-\infty}^{\infty} \frac{\mathrm{d}\lambda}{2\pi} e^{-i\lambda x} \langle P, S | \mathcal{T}^\dagger \mathcal{T} \bar{q}_j(0) \mathcal{T}^\dagger \mathcal{T} \mathcal{W}\left[0; \lambda n\right] \mathcal{T}^\dagger \mathcal{T} q_i(\lambda n) \mathcal{T}^\dagger \mathcal{T} | P, S \rangle \\
&= \int_{-\infty}^{\infty} \frac{\mathrm{d}\lambda}{2\pi} e^{-i\lambda x} \langle \bar{P}, \bar{S} | \bar{q}_l(0) \left(-i\gamma_5 C\right)_{lj} \mathcal{W}\left[0; -\lambda \bar{n}\right] \left(-i\gamma_5 C\right)_{ik} q_k(-\lambda \bar{n}) | \bar{P}, \bar{S} \rangle \\
&= \int_{-\infty}^{\infty} \frac{\mathrm{d}\lambda}{2\pi} e^{+i\lambda x} \langle \bar{P}, \bar{S} | \bar{q}_l(0) \left(-i\gamma_5 C\right)_{lj} \mathcal{W}\left[0; \lambda \bar{n}\right] \left(-i\gamma_5 C\right)_{ik} q_k(\lambda \bar{n}) | \bar{P}, \bar{S} \rangle \\
&= \left(-i\gamma_5 C\right)_{ik} \Phi^q_{kl}\left(x; \bar{n}, \bar{P}, \bar{S}\right) \left(-i\gamma_5 C\right)_{lj} . \qquad \text{(B.10)}
\end{aligned}$$

Again the substitution $\lambda \to -\lambda$ is employed going from the second to the third line. This concludes the collection of all necessary consistency conditions for Φ^q required to parametrize this correlator in terms of PDFs.

Appendix C

(Multiparton) Distribution and Fragmentation Functions

This appendix collects the definitions for all (multiparton) correlation and fragmentation functions relevant to the calculations presented in the main text. Most of the correlators shown in the following have been studied thoroughly in the literature and Refs. [101, 110, 111] are only a handful of the numerous works on this subject, serving as resources for further details. Additionally, two rather exotic multiparton correlators are discussed, the quark-photon-quark and gluon-photon-gluon correlators. The former is also featured in the transversely polarized cross section for the two-photon exchange DIS process studied in Ref [40], while the latter has so far not been considered in the literature (to the best of the author's knowledge). Finally, a discussion on the various conventions and notations found throughout the literature is given.

C.1 Quark-Quark Correlator

Starting point of the discussion is the bare, unrenormalized quark-quark correlator

$$\begin{aligned}\Phi^{q,\rho}_{\partial}(x) &= \int_{-\infty}^{\infty}\frac{\mathrm{d}\lambda}{2\pi}\,\mathrm{e}^{i\lambda x}\langle P,S|\,\bar{q}(0)\,\mathcal{W}[0,\infty n]\,\times \\ &\qquad\qquad \lim_{z_T\to 0} i\partial^{\rho}_{z_T}\left(\mathcal{W}[\infty n+z_T,\lambda n+z_T]\,q(\lambda n+z_T)\right)\,|P,S\rangle \\ &= \frac{1}{2}\,M\,\epsilon^{Pn\rho S}\,\not{P}\,f_{1T}^{\perp(1),q}(x)+\ldots\,. \end{aligned} \tag{C.1}$$

This definition contains a diagonal matrix element of two quark fields between nucleon states of given momentum P and spin S. Gauge independence requires Wilson lines $\mathcal{W}[\lambda n,\xi n]$ from light-cone position ξ to λ along an additional light-like vector n^μ (see Ref. [101]). Apart from the two constraints $n^2=0$ and $P\cdot n=1$, this vector is completely arbitrary. Nonetheless, n^μ defines the transverse direction via the projector

$$g_T^{\mu\nu}\equiv g^{\mu\nu}-P^\mu n^\nu-P^\nu n^\mu\,,\ \text{with}\quad a_T^\mu\equiv g_T^{\mu\nu}a_\nu\,, \tag{C.2}$$

that separates out the transverse components a_T^μ of an arbitrary vector a^μ. Given this definition, transverse polarization translates to the constraint $S^\mu=S_T^\mu$, or $n\cdot S=0$.

The parameterization (C.1) features the collinear function $f_{1T}^{\perp(1),q}(x)$ which is commonly referred to as the *first (transverse) moment of the Sivers function* (see Refs. [152, 153]). It is accompanied by the nucleon mass M and a factor $\epsilon^{\mu\nu\rho\sigma}P_\mu n_\nu S_\sigma\equiv\epsilon^{Pn\rho S}$, where ϵ is the totally antisymmetric tensor with $\epsilon^{0123}=+1$. The ellipsis ... in (C.1) indicates that there are several more terms in the parameterization which, however, do not enter the calculations in this work.

In the collinear twist-3 formalism the contribution to a transverse nucleon spin-dependent observable generated via Φ_∂ is accompanied by partonic cross sections $\hat{\sigma}_\partial$. These are calculated in a kinematical approximation to the momentum k^μ of the initial state quarks (cf. Eq. (2.71))

$$k^\mu\simeq x\,P^\mu-\tfrac{k_T^2}{2x}n^\mu+k_T^\mu\,,$$

with a subsequent expansion in the quark's transverse momentum k_T. It is the first-order coefficient $\mathcal{O}(k_T^1)$ in this expansion that then constitutes the result for this contribution. Since they are an indirect result of a non-zero transverse parton momentum, the contributions generated by Φ_∂ received the name *kinematical* twist-3 contributions in Ref. [101].

C.2 Gluon-Gluon Correlator

Similarly to the quark-quark correlator one can define the following analog for gluons (see Ref. [110], note that this reference uses a different sign convention for the ϵ-tesnor):

$$\begin{aligned}\Phi_{\partial}^{g,\mu\nu\rho}(x) &= \int_{-\infty}^{\infty}\frac{\mathrm{d}\lambda}{2\pi}e^{i\lambda x}\langle P,S|F^{n\mu}(0)\,\mathcal{W}[0,\infty n]\,\times \\ &\qquad \lim_{z_T\to 0} i\partial_{z_T}^{\rho}\left(\mathcal{W}[\infty n+z_T,\lambda n+z_T]\,F^{n\nu}(\lambda n+z_T)\right)|P,S\rangle \\ &= -\frac{M}{2}g_T^{\mu\nu}\epsilon^{PnS\rho}G_T^{(1)}(x)-\frac{M}{8}\left(\epsilon^{PnS\{\mu}g_T^{\nu\}\rho}+\epsilon^{Pn\rho\{\mu}S_T^{\nu\}}\right)\Delta H_T^{(1)}(x)+\dots\,, \end{aligned} \tag{C.3}$$

where $F^{n\mu}\equiv n_\alpha F^{\alpha\mu}$ and $F^{n\nu}$ are gluonic field strength tensors and an implicit sum over their color indices (adjoint representation) is understood. Again, the ellipsis ... in (C.3) indicates terms in the parameterization that do not enter the calculation. Like the collinear function $f_{1T}^{\perp(1),q}(x)$ from (C.1), the kinematical distributions $G_T^{(1)}(x)$ and $\Delta H_T^{(1)}(x)$ in (C.3) are the first moments of the corresponding transverse momentum dependent distributions (TMDs). For the same reason as for the quark-quark correlator, the contribution to an observable generated by the gluon-gluon correlator is counted as a *kinematical* twist-3 contribution.

C.3 Quark-Gluon-Quark Correlator

Highly relevant for this work is the quark-gluon-quark correlator

$$\begin{aligned}\Phi_F^{q,\rho}(x,x') &= \int_{-\infty}^{\infty}\frac{\mathrm{d}\lambda}{2\pi}\int_{-\infty}^{\infty}\frac{\mathrm{d}\mu}{2\pi}\,\mathrm{e}^{i\lambda x'}\mathrm{e}^{i\mu(x-x')}\,\times \\ &\qquad \langle P,S|\,\bar{q}(0)\,\mathcal{W}[0,\mu n]\,ig\,F^{n\rho}(\mu n)\,\mathcal{W}[\mu n,\lambda n]\,q(\lambda n)\,|P,S\rangle \\ &= \frac{1}{2}M\,i\epsilon^{Pn\rho S}\,\not{P}\,F_{FT}^q(x,x')-\frac{1}{2}M\,S_T^{\rho}\,\not{P}\gamma_5\,G_{FT}^q(x,x')+\dots\,. \end{aligned} \tag{C.4}$$

The above matrix element contains, in addition to two quark fields $\bar{q}$ and q, the gluonic field strength tensor $F^{n\rho}\equiv n_\mu F^{\mu\rho}$. Because of the appearance of this third dynamical quantum field, contributions to spin observables generated by Φ_F are called *dynamical* twist-3 contributions (see Ref. [101]). The *quark-gluon-quark* correlation functions F_{FT}^q and G_{FT}^q, as introduced, for example, in Ref. [101], are key to this work whereas other structures in the second line of Eq. (C.4), denoted by ..., do not enter the calculation. The subscript FT indicates that the functions are defined via a field strength tensor (F) rather than a covariant derivative and that they are only relevant for transverse (T) spin polarization, see [102]. In order to ease the notation, this subscript FT is dropped everywhere throughout this work for all qgq functions.

The functions F and G depend on two light-cone momentum fractions x and x'. Their support is constrained by the conditions $-1\le x,x'\le 1$ and $|x-x'|\le 1$. Most importantly, the vector-type function F is symmetric under exchange $x\leftrightarrow x'$, while the axial vector-type function G is antisymmetric:

$$\begin{aligned}F(x,x') &= +F(x',x)\,, \\ G(x,x') &= -G(x',x)\,. \end{aligned} \tag{C.5}$$

Consequently, $G(x,x)=0$. The functions F^q, G^q also contain information on their corresponding antiquark content in the region of negative x and x', that is, $F^{\bar{q}}(x,x')=F^q(-x,-x')$ and $G^{\bar{q}}(x,x')=G^q(-x,-x')$ [101].

Not only the qgq functions but also their derivatives are important for the computation of transverse-spin observables. To illustrate the properties of these derivatives and introduce some convenient notation, consider two generic functions $F(x_1,x_2)$ and $G(x_1,x_2)$. Partial derivatives are performed with respect to x_1 or x_2, followed by the replacement $(x_1,x_2)\to(x,x')$. In this way, one can easily examine how the (anti)symmetry properties of F and G in (C.5) extend to their derivatives. As a short-hand notation, one may introduce (n_1, n_2 integers)

$$\begin{aligned}(\partial_1^{n_1}\partial_2^{n_2}F)(x,x') &\equiv \left(\frac{\partial^{n_1+n_2}F}{\partial x_1^{n_1}\,\partial x_2^{n_2}}\right)(x_1=x,x_2=x')\,, \\ (\partial_1^{n_1}\partial_2^{n_2}G)(x,x') &\equiv \left(\frac{\partial^{n_1+n_2}G}{\partial x_1^{n_1}\,\partial x_2^{n_2}}\right)(x_1=x,x_2=x')\,. \end{aligned} \tag{C.6}$$

If the qgq functions are assumed to be smooth, then the order of the partial derivatives is arbitrary.

In this notation it is easy to see that the (anti-)symmetry properties of the functions F, G are inherited by their partial derivatives,

$$\begin{aligned}(\partial_1^{n_1}\partial_2^{n_2}F)(x,x') &= (\partial_1^{n_2}\partial_2^{n_1}F)(x',x)\,,\\ (\partial_1^{n_1}\partial_2^{n_2}G)(x,x') &= -(\partial_1^{n_2}\partial_2^{n_1}G)(x',x)\,.\end{aligned} \tag{C.7}$$

Of particular interest is the so-called *soft-gluon pole*, where $x' = x$. From (C.7) follows:

$$\begin{aligned}&(\partial_1 F)(x,x) = (\partial_2 F)(x,x), \quad (\partial_1^2 F)(x,x) = (\partial_2^2 F)(x,x), \quad (\partial_1\partial_2 F)(x,x) = (\partial_2\partial_1 F)(x,x),\\ &(\partial_1 G)(x,x) = -(\partial_2 G)(x,x), \quad (\partial_1^2 G)(x,x) = -(\partial_2^2 G)(x,x), \quad (\partial_1\partial_2 G)(x,x) = 0\,.\end{aligned} \tag{C.8}$$

An even shorter notation for derivative terms along the *diagonal* support can be used

$$\begin{aligned}F'(x,x) &\equiv \tfrac{\mathrm{d}}{\mathrm{d}x}F(x,x) = (\partial_1 F + \partial_2 F)(x,x) = 2(\partial_1 F)(x,x) = 2(\partial_2 F)(x,x),\\ F''(x,x) &\equiv \tfrac{\mathrm{d}^2}{\mathrm{d}x^2}F(x,x) = (\partial_1^2 F + \partial_2^2 F + \partial_1\partial_2 F + \partial_2\partial_1 F)(x,x).\end{aligned} \tag{C.9}$$

Lastly, the derivatives of antiquark correlation functions $F^{\bar q}$, $G^{\bar q}$ are considered. Their first partial derivatives differ by a sign, while the second derivatives keep their sign, $(i,j = 1,2)$

$$\begin{aligned}(\partial_i F^{\bar q})(x,x') &= -(\partial_i F^q)(-x,-x'), \qquad (\partial_i G^{\bar q})(x,x') = -(\partial_i G^q)(-x,-x')\,,\\ (\partial_i\partial_j F^{\bar q})(x,x') &= +(\partial_i\partial_j F^q)(-x,-x'), \qquad (\partial_i\partial_j G^{\bar q})(x,x') = +(\partial_i\partial_j G^q)(-x,-x')\,.\end{aligned} \tag{C.10}$$

C.4 Triple-Gluon Correlator

The next type of nucleon correlator needed in this work's calculations is the triple-gluon correlator. It appears in the following two varieties (cf. Refs. [110, 111]; note that these references use a different sign convention for the ϵ-tensor):

$$\begin{aligned}N_F^{\mu\nu\rho}(x,x') &= \int_{-\infty}^{\infty}\frac{\mathrm{d}\lambda}{2\pi}\int_{-\infty}^{\infty}\frac{\mathrm{d}\kappa}{2\pi}e^{i\lambda x}e^{i\kappa(x'-x)}\ \times \\ &\qquad \langle P,S|i\,f^{\alpha\beta\gamma}\,(F^{n\mu}(0)\,\mathcal{W}[0,\kappa\,n])^{\alpha}\ ig\,F^{n\rho,\beta}(\kappa n)\ (\mathcal{W}[\kappa\,n,\lambda\,n]\,F^{n\nu}(\lambda n))^{\gamma}\,|P,S\rangle \\ &= 2iM\left[g_T^{\mu\nu}\epsilon^{\rho PnS}N(x,x') - g_T^{\nu\rho}\epsilon^{\mu PnS}N(x,x-x') - g_T^{\rho\mu}\epsilon^{\nu PnS}N(x',x'-x)\right],\end{aligned} \tag{C.11}$$

$$\begin{aligned}O_F^{\mu\nu\rho}(x,x') &= \int_{-\infty}^{\infty}\frac{\mathrm{d}\lambda}{2\pi}\int_{-\infty}^{\infty}\frac{\mathrm{d}\kappa}{2\pi}e^{i\lambda x}e^{i\kappa(x'-x)}\ \times \\ &\qquad \langle P,S|\,d^{\alpha\beta\gamma}\,(F^{n\mu}(0)\,\mathcal{W}[0,\kappa\,n])^{\alpha}\ ig\,F^{n\rho,\beta}(\kappa n)\ (\mathcal{W}[\kappa\,n,\lambda\,n]\,F^{n\nu}(\lambda n))^{\gamma}\,|P,S\rangle \\ &= 2iM\left[g_T^{\mu\nu}\epsilon^{\rho PnS}O(x,x') + g_T^{\nu\rho}\epsilon^{\mu PnS}O(x,x-x') + g_T^{\rho\mu}\epsilon^{\nu PnS}O(x',x'-x)\right].\end{aligned} \tag{C.12}$$

Here, $d^{\alpha\gamma\beta}$ and $f^{\alpha\gamma\beta}$ are the totally symmetric/antisymmetric SU(3) structure constants. One encounters the real-valued functions $N(x,x')$ and $O(x,x')$ with the same support properties as $F^q(x,x')$ and $G^q(x,x')$, as well as certain symmetries:

$$\begin{aligned}\text{support}: &\qquad |x|,|x'|,|x-x'| \le 1\\ \text{symmetry at diagonal}: &\qquad (N,O)(x,x') = (N,O)(x',x)\\ \text{symmetry at origin}: &\qquad N(x,x') = -N(-x,-x')\\ &\qquad O(x,x') = O(-x,-x')\,.\end{aligned} \tag{C.13}$$

Naturally, the contributions to a spin observable generated by the triple-gluon correlators N_F and O_F are counted as *dynamical* twist-3 contributions.

C.5 Fragmentation Functions

Turning to twist-2, this section introduces the more familiar parton-to-hadron fragmentation functions (FFs). They describe the hadronization of a quark or a gluon into a specific hadron. Both

FFs may be provided by the following well-known collinear fragmentation correlators (cf. the review article [154] on FFs):

$$\begin{aligned}\Delta^{h/q}(z) &= \frac{1}{N_c}\sum\!\!\!\!\!\!\int_X \int_{-\infty}^{\infty}\frac{\mathrm{d}\lambda}{2\pi}\,\mathrm{e}^{-i\lambda/z}\,\langle\Omega|\,\mathcal{W}[\infty\,m,0]\,q(0)\,|P_h;X\rangle\langle P_h;X|\,\bar{q}(\lambda m)\,\mathcal{W}[\lambda\,m,\infty\,m]\,|\Omega\rangle \\ &= z^{-1+2\varepsilon}\,\not{P}_h\,D_1^{h/q}(z)+\ldots\,, \qquad \text{(C.14)} \\ \Delta^{h/g}_{\mu\nu}(z) &= \frac{1}{N_c^2-1}\sum\!\!\!\!\!\!\int_X \int_{-\infty}^{\infty}\frac{\mathrm{d}\lambda}{2\pi}\,\mathrm{e}^{-i\lambda/z}\,\langle\Omega|\,F^m{}_\mu(0)\,\mathcal{W}[0,\infty m]\,|P_h;X\rangle\,\times \\ &\qquad\qquad \langle P_h;X|\,\mathcal{W}[\infty m,\lambda m]\,F^m{}_\nu(\lambda m)\,|\Omega\rangle \\ &= -z^{-2+2\varepsilon}\,g_{\perp\mu\nu}\,D_1^{h/g}(z)+\ldots\,. \qquad \text{(C.15)}\end{aligned}$$

These definitions introduce another light-cone vector m^μ with $m^2=0$ and $m\cdot P_h=1$. This vector m^μ may differ from n^μ in the definitions of nucleon correlators from before. Together, P_h^μ and m^μ provide a different transverse projector

$$g_\perp^{\mu\nu}\equiv g^{\mu\nu}-P_h^\mu m^\nu-P_h^\nu m^\mu\,. \qquad \text{(C.16)}$$

Note that that the hadron is observed with a fixed momentum P_h^μ, and thus the summation over intermediate states $|P_h;X\rangle$ is incomplete, which is always the case for a fragmentation process. Furthermore, $|\Omega\rangle$ represents the full QCD vacuum state. The definitions (C.14),(C.15) are given in $d=4-2\varepsilon$ dimensions. The ellipsis in (C.14),(C.15) indicates other fragmentation functions that do not enter the observables studied in this work.

As explained in Sec. 2.5, an $\overline{\text{MS}}$-subtraction of UV-divergences emerging in the perturbative calculation is required. Following the discussion in, e.g., Refs. [38, 120]) one needs to replace $D_{1,\text{bare}}^{h/q}$ by the subtracted, $\overline{\text{MS}}$-renormalized fragmentation function in the following way

$$\begin{aligned}D_{1,\text{bare}}^{h/q}(z,\mu) &= D_1^{h/q,\overline{\text{MS}}}(z,\mu)+\frac{\alpha_s(\mu)}{2\pi}\frac{S_\varepsilon}{\varepsilon}(P_{qq}\otimes D_1^{h/q,\overline{\text{MS}}})(z,\mu) \\ &\quad+\frac{\alpha_s(\mu)}{2\pi}\frac{S_\varepsilon}{\varepsilon}(P_{gq}\otimes D_1^{h/g,\overline{\text{MS}}})(z,\mu)+\mathcal{O}(\alpha_s^2)\,, \qquad \text{(C.17)}\end{aligned}$$

where μ denotes the renormalization/factorization scale, $S_\varepsilon=(4\pi)^\varepsilon/\Gamma(1-\varepsilon)$ is a convenient prefactor consistent with the $\overline{\text{MS}}$-scheme at NLO, and P_{qq}, P_{gq} are the well-known LO splitting functions

$$\begin{aligned}P_{qq}(w) &= C_F\left[\frac{1+w^2}{(1-w)_+}+\frac{3}{2}\delta(1-w)\right], \\ P_{gq}(w) &= C_F\left[\frac{1+(1-w)^2}{w}\right]. \qquad \text{(C.18)}\end{aligned}$$

The convolution integral in Eq. (C.17) is defined as usual as

$$(P\otimes D)(z,\mu)=\int_z^1\frac{\mathrm{d}w}{w}\,P(w)\,D\left(\tfrac{z}{w},\mu\right). \qquad \text{(C.19)}$$

C.6 Photon-in-Lepton Distribution

The photon-in-lepton distribution is defined in terms of the following matrix element (cf. Refs. [38, 120, 133]):

$$\begin{aligned}\Phi^{\gamma/\ell,\mu\nu}(x) &= \int_{-\infty}^{\infty}\frac{\mathrm{d}\lambda}{2\pi}\,\mathrm{e}^{i\lambda x}\,\langle\ell(l)|\,F_\gamma^{o\nu}(0)\,F_\gamma^{o\mu}(\lambda\,o)|\ell(l)\rangle \\ &= -\frac{x}{2}\frac{\tilde{g}_T^{\mu\nu}}{1-\varepsilon}\,f^{\gamma/\ell}(x)+\ldots\,. \qquad \text{(C.20)}\end{aligned}$$

The two photon field-strength tensors $F_\gamma^{o\sigma}(x)=o_\rho F_\gamma^{\rho\sigma}(x)=o_\rho(\partial^\rho A^\sigma(x)-\partial^\sigma A^\rho(x))$, A being the photon field, are to be evaluated between lepton states of momentum l^μ. The definition (C.20) utilizes yet another light-cone vector o^μ with $o^2=0$ and $o\cdot l=1$; the corresponding transverse projector $\tilde{g}_T$ reads

$$\tilde{g}_T^{\mu\nu}\equiv g^{\mu\nu}-l^\mu o^\nu-l^\nu o^\mu\,. \qquad \text{(C.21)}$$

The photon-in-lepton distribution $f_1^{\gamma/\ell}(x)$ generates so-called *Weizsäcker-Williams* (WW) contributions that are required to cancel singularities that arise in the calculation for massless leptons.

Also the bare photon-in-lepton distribution $f_{1,\mathrm{bare}}^{\gamma/\ell}(x)$ has to be renormalized. The distribution includes a UV-divergence that needs to be $\overline{\mathrm{MS}}$-subtracted. Following Ref. [120] the $\overline{\mathrm{MS}}$-subtraction term reads

$$f_{1,\mathrm{bare}}^{\gamma/\ell}(x,\mu) \;=\; f_1^{\gamma/\ell,\overline{\mathrm{MS}}}(x,\mu) + \frac{\alpha_{\mathrm{em}}}{2\pi}\frac{S_\varepsilon}{\varepsilon}\,(P_{\gamma\ell}\otimes f_1^{\ell/\ell,\overline{\mathrm{MS}}})(x,\mu) + \mathcal{O}(\alpha_{\mathrm{em}}^2)\,, \tag{C.22}$$

where $P_{\gamma\ell}(w) = P_{gq}(w)/C_F$ is the lepton-to-photon QED splitting function and $f^{\ell/\ell}(x)$ the lepton-in-lepton distribution which, at LO in QED, reduces to $\delta(1-x)$. In contrast to the QCD parton distributions, the renormalized photon-in-lepton distribution $f_1^{\gamma/\ell,\overline{\mathrm{MS}}}(x,\mu)$ can be calculated in QED perturbation theory, and one obtains [120],

$$f_1^{\gamma/\ell,\overline{\mathrm{MS}}}(x,\mu) = \frac{\alpha_{\mathrm{em}}}{2\pi}\,P_{\gamma\ell}(x)\,\left[\log\left(\frac{\mu^2}{x^2\,m_\ell^2}\right) - 1\right] + \mathcal{O}(\alpha_{\mathrm{em}}^2)\,. \tag{C.23}$$

It depends explicitly on the lepton mass m_ℓ in the logarithm in (C.23). Since the renormalization/factorization scale μ is typically of the order of the hard scale of the underlying process, that is, of the order of several GeV at least, the logarithm $\log\left(\mu^2/(x^2\,m_\ell^2)\right)$ can potentially become large and its resummation to all orders may be necessary. This is, however, beyond the scope of this study.

More discussion on the treatment of the lepton mass m_ℓ in (C.23) is included in Sec. 2.4.3.

C.7 Quark-Photon-Quark Correlator

In the computation of the Interference channel for single-inclusive photon production one encounters the following photonic analog of the quark-gluon-quark (qgq) correlator of Eq.(C.4). Following Ref. [40] one introduces the quark-photon-quark ($q\gamma q$) correlator in a very similar way

$$\begin{aligned}(\Phi_\gamma)_F^{q,\rho}\,(x,x') \;&=\; \int_{-\infty}^{\infty}\frac{\mathrm{d}\lambda}{2\pi}\int_{-\infty}^{\infty}\frac{\mathrm{d}\mu}{2\pi}\,\mathrm{e}^{i\lambda x'}\mathrm{e}^{i\mu(x-x')}\;\times \\ &\qquad\qquad \langle P,S|\,\bar q(0)\,\mathcal{W}[0,\lambda n]\,ie\,F_\gamma^{n\rho}(\mu n)\,q(\lambda n)\,|P,S\rangle \\ &=\; \frac{1}{2}M\,i\epsilon^{Pn\rho S}\,\not{P}\,F_\gamma^q(x,x') - \frac{1}{2}M\,S_T^\rho\,\not{P}\gamma_5\,G_\gamma^q(x,x') + \ldots\,.\end{aligned} \tag{C.24}$$

Instead of the gluonic field strength tensor this definition includes the electromagnetic one, $F_\gamma^{n\rho} = n_\mu F_\gamma^{\mu\rho}$. Since this tensor is gauge independent in the abelian case, one only needs a single Wilson line for the two quark fields q. Like previously, because of the three dynamical fields in the $q\gamma q$ correlator it generates *dynamical contributions*. The functions F_γ and G_γ are analogous to the vector-like function F and the axial vector-like function G from Eq. (C.4). They have the same properties in terms of support, symmetry and charge conjugation. It is well-known that the (un)polarized twist-2 photonic parton distribution functions (PDFs) of the nucleon start at the order $\mathcal{O}\left(\alpha_{em}/\alpha_s\right)$ in the $\overline{\mathrm{MS}}$-scheme ([38, 135]). Thus, it is reasonable to conjecture that the same applies for F_γ and G_γ. Consequently, one has to include α_s corrections to the leading order $q\gamma q$ contribution. Then one is at order $\mathcal{O}\left((\alpha_{em}/\alpha_s)\times\alpha_{em}^2\alpha_s\right)$, which is consistent with the order $\mathcal{O}\left(\alpha_{em}^3\right)$ for the contributions generated by qgq correlations. To conclude this section, a brief summary of the properties of F_γ^q, G_γ^q is given

$$\begin{aligned}\text{support}: &\qquad |x|,|x'|,|x-x'| \;\le\; 1 \\ \text{symmetry at diagonal}: &\qquad F_\gamma^q(x,x') \;=\; F_\gamma^q(x',x) \\ &\qquad G_\gamma^q(x,x') \;=\; -G_\gamma^q(x',x) \\ \text{charge conjugation}: &\qquad \left(F_\gamma^{\bar q},G_\gamma^{\bar q}\right)(x,x') = \left(F_\gamma^q,G_\gamma^q\right)(-x,-x') \\ \text{perturbative order}: &\qquad \mathcal{O}\left(\tfrac{\alpha_{em}}{\alpha_s}\right)\,.\end{aligned} \tag{C.25}$$

C.8 Gluon-Photon-Gluon Correlator

Lastly, the gluon-photon-gluon ($g\gamma g$) correlator is introduced as follows

$$\begin{aligned}(O_\gamma)_F^{\mu\nu\rho}(x,x') &= \int_{-\infty}^{\infty}\frac{\mathrm{d}\lambda}{2\pi}\int_{-\infty}^{\infty}\frac{\mathrm{d}\kappa}{2\pi}e^{i\lambda x}e^{i\kappa(x'-x)}\ \times \\ &\qquad \langle P,S|\ (F^{n\mu}(0)\,\mathcal{W}[0,\lambda n])^{\alpha}\ ie\,F_\gamma^{n\rho}(\kappa n)\,F^{n\nu,\alpha}(\lambda n)|P,S\rangle \\ &= 2iM\left[g_T^{\mu\nu}\epsilon^{\rho PnS}O_\gamma^1(x,x')+g_T^{\nu\rho}\epsilon^{\mu PnS}O_\gamma^2(x,x')+g_T^{\rho\mu}\epsilon^{\nu PnS}O_\gamma^2(x',x)\right],\end{aligned} \tag{C.26}$$

where two gluonic ($F^{n\mu}, F^{n\nu}$) and one electromagnetic ($F_\gamma^{n\rho}$) field strength tensor appear in a diagonal matrix element between nucleon states of momentum P and spin S. As before, shorthand notations for the contraction with the totally antisymmetric tensor are used, e.g. $\epsilon^{\rho PnS} = P_\mu n_\nu S_\sigma \epsilon^{\rho\mu\nu\sigma}$, with the sign convention $\epsilon^{0123} = +1$.

To the best of the author's knowledge this definition is new and has so far not been considered in the literature. To parametrize this correlator the close resemblance to the triple-gluon case with symmetric structure constant given in Eq. (C.12) is employed. To find possible terms for the parametrization one needs to study the behavior of the correlator under hermitian conjugation, parity and time-reversal. Due to the similarity of the triple-gluon and the $g\gamma g$ correlators, they share the same transformation properties for all of these operations. Thus, one includes the same Lorentz structures in the ansatz for the $g\gamma g$ correlator, i.e. $g_T^{\mu\nu}\epsilon^{\rho PnS}$, $g_T^{\nu\rho}\epsilon^{\mu PnS}$ and $g_T^{\rho\mu}\epsilon^{\nu PnS}$, but *a priori* each accompanied by its own, separate function

$$(O_\gamma)_F^{\mu\nu\rho}(x,x') \propto g_T^{\mu\nu}\epsilon^{\rho PnS}O_\gamma^1(x,x')+g_T^{\nu\rho}\epsilon^{\mu PnS}O_\gamma^2(x,x')+g_T^{\rho\mu}\epsilon^{\nu PnS}O_\gamma^3(x,x')\,. \tag{C.27}$$

For the triple-gluon correlator there are symmetry relations between any permutation of the three gluonic field strengths inside the matrix element. These relations, combined with the relation derived from hermitian conjugation, can be used to eliminate all but one of the coefficient functions of the Lorentz structures in the ansatz for its parametrization. Hence, there is only one twist-3 correlation function $O(x,x')$ in Eq. (C.12).

The $g\gamma g$ correlator in (C.26) has the property $\left(O_\gamma^*\right)_F^{\mu\nu\rho}(x,x') = -\,(O_\gamma)_F^{\nu\mu\rho}(x',x)$ for hermitian conjugation, leading to $O_\gamma^1(x,x') = O_\gamma^1(x',x)$ and $O_\gamma^2(x,x') = O_\gamma^3(x',x)$. Thus, the number of independent coefficient functions in the ansatz (C.27) is reduced by one. Furthermore, there is also a symmetry relation for an interchange of the two gluonic field strengths inside the matrix element in Eq. (C.26) (Wilson lines are not shown for simplicity):

$$\begin{aligned}(O_\gamma)_F^{\mu\nu\rho}(x,x') &= \int_{-\infty}^{\infty}\frac{\mathrm{d}\lambda}{2\pi}\int_{-\infty}^{\infty}\frac{\mathrm{d}\kappa}{2\pi}e^{i\lambda x}e^{i\kappa(x'-x)}\ \times \\ &\qquad \underbrace{\langle P,S|\,F^{n\nu,\alpha}(\lambda n)\,ie\,F^{n\rho}(\kappa n)\,F^{n\mu,\alpha}(0)|P,S\rangle}_{\langle P,S|\,F^{n\nu,\alpha}(0)\,ie\,F^{n\rho}((\kappa-\lambda)n)\,F^{n\mu,\alpha}(-\lambda n)|P,S\rangle} \\ &= \int_{-\infty}^{\infty}\frac{\mathrm{d}\lambda'}{2\pi}\int_{-\infty}^{\infty}\frac{\mathrm{d}\kappa'}{2\pi}e^{i\lambda'(-x)}e^{i\kappa'(-x'-(-x))}\ \times \\ &\qquad \langle P,S|\,F^{n\nu,\alpha}(0)\,ie\,F^{n\rho}(\kappa' n)\,F^{n\mu,\alpha}(\lambda' n)|P,S\rangle \\ &= (O_\gamma)_F^{\nu\mu\rho}(-x',-x)\,,\end{aligned} \tag{C.28}$$

where a substitution $\lambda = -\lambda'$, $\kappa = \kappa' - \lambda'$ is used. Plugging the ansatz in Eq. (C.27) into this relation one finds $O_\gamma^1(x,x') = O_\gamma^1(-x',-x)$ and $O_\gamma^2(x,x') = O_\gamma^3(-x',-x)$. This, however, does not further reduce the number of independent functions and one is left with the two $g\gamma g$ functions O_γ^1 and O_γ^2. Their properties can be summarized as follows

$$\begin{aligned}\text{support}: &\qquad |x|,|x'|,|x-x'| \le 1 \\ \text{symmetry at diagonal}: &\qquad O_\gamma^1(x,x') = O_\gamma^1(x',x) \\ \text{symmetry at origin}: &\qquad O_\gamma^{(1,2)}(x,x') = O_\gamma^{(1,2)}(-x,-x') \\ \text{perturbative order}: &\qquad \mathcal{O}\left(\tfrac{\alpha_{em}}{\alpha_s}\right).\end{aligned} \tag{C.29}$$

C.9 Different Conventions and Notation

This section concludes the appendix with a "dictionary" for the conversion between different conventions for the twist-3 multiparton distribution functions discussed so far. When considering

their evolution equations it is often beneficial to employ a formulation in terms of functions of three arguments x_1, x_2, x_3, which are then constrained by $x_1 + x_2 + x_3 = 0$. This approach was adopted for example in Refs. [121, 138]. Directly from the definitions given therein one can work out the relations to the qgq functions defined in Eq. (C.4) as well as the triple-gluon functions in Eqs. (C.11) and (C.12). In the qgq case one finds a one-to-one correspondence

$$\begin{aligned} F^q\left(x,x'\right) &= \frac{1}{(-M)} T_{\bar{q}Fq}\left(-x', x'-x, x\right) \\ G^q\left(x,x'\right) &= -\frac{1}{(M)} \Delta T_{\bar{q}Fq}\left(-x', x'-x, x\right) , \end{aligned} \tag{C.30}$$

where the terms in brackets, i.e. the nucleon mass M and in case of the vector-type function an additional minus sign, are only present for [121]. The additional sign is due to a different convention $\epsilon_{0123} = +1$ for the antisymmetric tensor in Ref. [121], while both this work and Ref. [138] use $\epsilon^{0123} = +1$ instead. The case is more subtle for the triple-gluon functions. There one can only express a given convention in terms of a linear combination of the other, for example

$$\begin{aligned} T_{3F}^{+}\left(-x', x'-x, x\right) &= 2(-M)\left[-2N\left(x,x'\right) + N\left(x, x-x'\right) + N\left(x', x'-x\right)\right] \\ T_{3F}^{-}\left(-x', x'-x, x\right) &= -2(-M)\left[2O\left(x,x'\right) + O\left(x, x-x'\right) + O\left(x', x'-x\right)\right] \\ \Delta T_{3F}^{+}\left(-x', x'-x, x\right) &= 2(-M)\left[N\left(x, x-x'\right) - N\left(x', x'-x\right)\right] \\ \Delta T_{3F}^{-}\left(-x', x'-x, x\right) &= 2(-M)\left[O\left(x', x'-x\right) - O\left(x, x-x'\right)\right] , \end{aligned} \tag{C.31}$$

where, again, the brackets are only needed for conversion to Ref. [121]. Going one step further, both references introduce definite-C-parity functions via $\mathfrak{F}^{\pm}\left(x_1,x_2,x_3\right) = T_{3F}^{\pm}\left(x_1,x_2,x_3\right) - \Delta T_{3F}^{\pm}\left(x_1,x_2,x_3\right)$. For these one finds the conversions

$$\begin{aligned} \mathfrak{F}^{+}\left(-x', x'-x, x\right) &= 4(-M)\left[N\left(x', x'-x\right) - N\left(x,x'\right)\right] \\ \mathfrak{F}^{-}\left(-x', x'-x, x\right) &= -4(-M)\left[O\left(x', x'-x\right) + O\left(x,x'\right)\right] , \end{aligned} \tag{C.32}$$

with the same caveat about the factor $-M$ in brackets. For the calculations in this work only two configurations are relevant, namely $x' = x$ and $x' = 0$. In both cases the conversion simplifies and can be inverted to yield

$$\begin{aligned} N(x,x) &= -\frac{1}{4(-M)}\mathfrak{F}^{+}(-x,0,x) - \frac{1}{8(-M)}\mathfrak{F}^{+}(0,-x,x) \\ N(x,0) &= -\frac{1}{8(-M)}\mathfrak{F}^{+}(0,-x,x) \\ O(x,x) &= -\frac{1}{4(-M)}\mathfrak{F}^{-}(-x,0,x) + \frac{1}{8(-M)}\mathfrak{F}^{-}(0,-x,x) \\ O(x,0) &= -\frac{1}{8(-M)}\mathfrak{F}^{-}(0,-x,x) . \end{aligned} \tag{C.33}$$

Appendix D

Choice of Gauge and Light-Cone Vectors

This appendix discusses the gauge conditions imposed throughout this work. In addition, the special role of the light-cone vector n^μ is addressed, which is featured in several of the definitions in the previous Appendix C for the (multiparton) correlation functions.

D.1 Light-Cone Gauge

First, note that this work makes use of a specific light-cone gauge for the gluon field $G^{\mu,\alpha}(x)$, with antisymmetric boundary conditions

$$n_\mu G^{\mu,\alpha}(x) = 0 \quad \text{and} \quad G_T^\alpha(P\cdot x = +\infty) + G_T^\alpha(P\cdot x = -\infty) = 0\,, \tag{D.1}$$

where α is a color index in the adjoint representation. This gauge is familiar from other NLO calculations, e.g. for the production of polarized Λ particles in electron-positron collisions [46]. It leads to simplifications since the gluonic field-strength tensors $F^{n\rho}$ in the definitions (C.3),(C.4),(C.11), and (C.12) reduce to $(n\cdot\partial)G_T^\rho$, which can be easily inverted. In addition, the Wilson lines in these definitions reduce to unity. All of this simplifies the handling of the qgq and triple-gluon correlations.

In addition, the matrix element (C.1) simplifies in the light-cone gauge (D.1). However, one must be careful when applying this gauge to the Sivers function $f_{1T}^\perp$. As described in Ref. [114], in light-cone gauge the Sivers function is generated by *transverse* Wilson lines at light-cone infinity and the boundary conditions are important. According to Ref. [155], the anti-symmetric boundary condition in (D.1) guarantees a non-zero Sivers function for both a DIS-like process (such as the single-inclusive hadron production $\ell N \to hX$) and a Drell-Yan(DY)-like process. However, the Sivers functions in DIS and DY differ by a sign [156]. This is important for the following identity derived for a DIS-type process in Ref. [114]

$$f_{1T}^{\perp(1),q}(x) \;=\; +\pi F^q(x,x)\,, \tag{D.2}$$

which requires a sign change for a DY-type process.

On the other hand, the light-cone gauge (D.1) leads to slight complications for the calculation of partonic hard factors at NLO: gluonic polarization sums as well as the numerator of gluonic Feynman propagators are more complicated compared to covariant Feynman gauge. It is well known that both must be modified in light-cone gauge (D.1) according to

$$-g^{\mu\nu} \to -d^{\mu\nu}(k,n) \equiv -\left(g^{\mu\nu} - \kappa\,\mathcal{P}\frac{k^\mu n^\nu + k^\nu n^\mu}{k\cdot n + i\delta}\right)\,, \tag{D.3}$$

where $\mathcal{P}$ denotes the Cauchy principal value prescription and a small imaginary part $i\delta$ is included, which can become relevant for the computation of loop integrals, cf. the discussion below Eq. (2.113). The parameter κ switches between Feynman gauge ($\kappa = 0$) and light-cone gauge ($\kappa = 1$). In the end, all terms proportional to κ in the final result for the partonic hard factors cancel upon application of Eq. (D.2). This means that the partonic hard factors coincide in Feynman gauge and in light-cone gauge, indicating color gauge invariance. Hence, one can use the gauge-invariant extensions of the twist-3 matrix elements (C.1),(C.4).

Nonetheless, it should be emphasized that the choice of a light-cone gauge (D.1) is certainly not a necessity for an NLO calculation; one may also choose Feynman gauge instead.

D.2 Choice of the Light-Cone Vector

Secondly, as discussed in Sec. 2.3, there is an additional potential dependence on the light-cone vector n^μ of physical observables through the parameterizations (C.1),(C.3),(C.4),(C.11) and (C.12). In Ref. [101] it was shown for the LO contribution to the SSA (2.61) that an arbitrary light-cone vector n^μ can be adopted, parameterized by the three external physical vectors of the process. Applying the identity Eq. (D.2), one finds that all dependence on n^μ cancels in the final LO result, Eq. (2.64). However, at NLO, working with an arbitrary light-cone vector n^μ would require the computation of redundant terms that eventually cancel. To avoid this, the LO finding of Ref. [101] is taken for granted also at NLO, and a specific light-cone vector is chosen right away

$$n^\mu = -\tfrac{2}{t} P_h^\mu \,. \tag{D.4}$$

This corresponds to a natural choice in the frame where the nucleon momentum P^μ and the momentum P_h^μ of the produced hadron are collinear along one axis, e.g. the z-axis. In this work it is assumed that any arbitrariness of the choice (D.4) drops out at NLO once the constraint (D.2) is applied.

The only exception where an arbitrary light-cone vector n^μ is kept in the same way as in Ref. [101] is the $gg \to q$ channel. There, one has the kinematical gluon distributions $G_T^{(1)}$, $\Delta H_T^{(1)}$ and the dynamical triple-gluon function N which need to be related to each other in a similar way as the Sivers function $f_{1T}^{\perp,q}$ and the SGP qgq function F^q in Eq. (D.2). Such relations are derived in the literature in $d = 4$ dimensions, see [110], but for the present work one needs the $\mathcal{O}(\varepsilon)$ extension for $d = 4 - 2\varepsilon$. By keeping a general n^μ and demanding that all arbitrariness cancels in the end, one arrives at the following two relations

$$\begin{aligned} G_T^{(1)} &= 4\pi \left(N(x,x) - (1+\varepsilon) N(x,0) \right) \\ \Delta H_T^{(1)} &= -8\pi (1-\varepsilon) N(x,0) \end{aligned} \tag{D.5}$$

Upon application of Eq. (D.5) one indeed finds that all arbitrary constants in the parametrization of n^μ cancel. Thus, the result is manifestly independent of the choice of n^μ.

Appendix E

Analytic Continuation and Integration by Parts

At several points throughout the various calculations of the main text, one finds terms of the form $1/(1-w)^{n+\varepsilon}$ with $n \in \mathbb{N}$, $n > 1$ that require careful treatment with respect to the soft limit $w \to 1$. *A priori* such terms are only integrable on an interval $(x_0, 1)$ under the condition that $\varepsilon < -(n-1)$. However, integration by parts can be applied to find an analytic continuation of such terms that extends also to the region $-(n-1) < \varepsilon < 0$.

Although only the specific cases $n = 2$ and $n = 3$ are needed in the calculation, a closed form can also be found for a general integer n. Let f be a sufficiently differentiable function satisfying the boundary conditions $f(1) = f'(1) = \cdots = f^{(n-2)}(1) = 0$ (where $f^{(n)}$ denotes the n-th derivative) and let x_0 be a real constant with $0 < x_0 < 1$. Then the following identity holds

$$\int_{x_0}^1 \mathrm{d}w \frac{f\left(\frac{x_0}{w}\right)}{(1-w)^{n+\varepsilon}} = \int_{x_0}^1 \mathrm{d}w \frac{(-1)^{n-1}}{(1-w)^{1+\varepsilon}} \frac{\Gamma(1+\varepsilon)}{\Gamma(n+\varepsilon)} \frac{\mathrm{d}^{n-1}}{\mathrm{d}w^{n-1}} f\left(\tfrac{x_0}{w}\right) . \tag{E.1}$$

This can be shown in a straightforward way by induction. The induction step from n to $n+1$ looks like this:

$$\begin{aligned}
\int_{x_0}^1 \mathrm{d}w \frac{f\left(\frac{x_0}{w}\right)}{(1-w)^{n+1+\varepsilon}} &= -\frac{(1-w)^{-n-\varepsilon}}{-n-\varepsilon} f\left(\tfrac{x_0}{w}\right)\Big|_{x_0}^1 + \int_{x_0}^1 \mathrm{d}w \frac{(1-w)^{-n-\varepsilon}}{-n-\varepsilon} \frac{\mathrm{d}}{\mathrm{d}w} f\left(\tfrac{x_0}{w}\right) \\
&= \int_{x_0}^1 \mathrm{d}w \frac{-1}{n+\varepsilon} \frac{(-1)^{n-1}}{(1-w)^{1+\varepsilon}} \frac{\Gamma(1+\varepsilon)}{\Gamma(n+\varepsilon)} \frac{\mathrm{d}^{n-1}}{\mathrm{d}w^{n-1}} \left(\frac{\mathrm{d}}{\mathrm{d}w} f\left(\tfrac{x_0}{w}\right)\right) \\
&= \int_{x_0}^1 \mathrm{d}w \frac{(-1)^n}{(1-w)^{1+\varepsilon}} \frac{\Gamma(1+\varepsilon)}{\Gamma(n+1+\varepsilon)} \frac{\mathrm{d}^n}{\mathrm{d}w^n} f\left(\tfrac{x_0}{w}\right) ,
\end{aligned} \tag{E.2}$$

where the boundary term at $w = 1$ vanishes because $\varepsilon < -n$ and the boundary term at $w = x_0$ because $f(1) = 0$. It must be emphasized that one needs to apply the analytic continuation (E.1) as the first step following the extraction of factors $1/(1-w)^{n+\varepsilon}$. Only afterwards one can proceed with the small-ε expansion and make use of the identity Eq. (2.80).

For completeness, this appendix also gives the explicit formulas for the specific cases $n = 2$ and $n = 3$ that are encountered in the calculations, and with the generic function f replaced by the functions that are relevant there.

E.1 Kinematical Contributions

For the analytic continuation of the term $1/(1-w)^{2+2\varepsilon}$ appearing in the computation of kinematical contributions, such as in the $qg \to q$ channel, it is convenient to use the following identity:

$$\begin{aligned}
\int_{x_0}^1 \frac{\mathrm{d}w}{w} \frac{\sigma_1(v,w,\varepsilon)\, f_{1T}^{\perp(1)}\left(\frac{x_0}{w}\right)}{(1-w)^{2+2\varepsilon}} &= -\frac{1}{1+2\varepsilon} \int_{x_0}^1 \frac{\mathrm{d}w}{w} \frac{\left[(\partial_w \sigma_1) - \frac{1}{w}\sigma_1\right](v,w,\varepsilon)\, f_{1T}^{\perp(1)}\left(\frac{x_0}{w}\right)}{(1-w)^{1+2\varepsilon}} \\
&\quad + \frac{1}{1+2\varepsilon} \int_{x_0}^1 \frac{\mathrm{d}w}{w} \frac{\frac{1}{w}\sigma_1(v,w,\varepsilon)\, \frac{x_0}{w} \left(f_{1T}^{\perp(1)}\right)'\left(\frac{x_0}{w}\right)}{(1-w)^{1+2\varepsilon}} .
\end{aligned} \tag{E.3}$$

E.2 Hard Poles

For the calculation of the hard-pole contributions in the $qg \to q$-channel, that is, the partonic factors accompanying the functions $F\left(\frac{x_0}{w}, x_0\right)$ and $G\left(\frac{x_0}{w}, x_0\right)$, one can apply the following identities:

$$\begin{aligned}
\int_{x_0}^1 \mathrm{d}w\, \frac{\sigma_3(v,\varepsilon)}{(1-w)^{3+\varepsilon}} F\left(\tfrac{x_0}{w}, x_0\right) &= \frac{\sigma_3(v,\varepsilon)}{(1+\varepsilon)(2+\varepsilon)} \times \\
&\quad \int_{x_0}^1 \frac{\mathrm{d}w}{w}\, \frac{\frac{1}{w^3}\left(x_0^2\, \partial_1^2 F\right)\left(\frac{x_0}{w}, x_0\right) - \frac{2}{w^2}\left(-x_0\, \partial_1 F\right)\left(\frac{x_0}{w}, x_0\right)}{(1-w)^{1+\varepsilon}}\,, \qquad \text{(E.4)} \\
\int_{x_0}^1 \mathrm{d}w\, \frac{\sigma_2(v,\varepsilon)}{(1-w)^{2+\varepsilon}} F\left(\tfrac{x_0}{w}, x_0\right) &= -\frac{\sigma_2(v,\varepsilon)}{1+\varepsilon} \int_{x_0}^1 \frac{\mathrm{d}w}{w}\, \frac{\frac{1}{w}\left(-x_0\, \partial_1 F\right)\left(\frac{x_0}{w}, x_0\right)}{(1-w)^{1+\varepsilon}}\,. \qquad \text{(E.5)}
\end{aligned}$$

The right-hand-sides of Eqs. (E.4),(E.5) can then be expanded in ε using (2.80). Note that the above procedure works for both correlation functions F and G. The hard-pole subtraction terms in (2.90),(2.91) also contain contributions of other derivative terms $-x_0\,(\partial_2 F)(\frac{x_0}{w}, x_0)$ and $-x_0\,(\partial_2 G)(\frac{x_0}{w}, x_0)$. These terms need to be dealt with in the same way as described in Eq. (E.5), followed by application of (2.80), and (only afterwards) expansion in ε.

Eventually, all results are organized in such a way that derivative terms are integrated by parts as much as possible. This applies to all regular, non-distributional terms of the corresponding partonic cross sections. Consequently, only delta- and plus distributions remain for the partonic factors that accompany derivatives of the qgq functions. This procedure is performed using the following list of useful formulas:

$$\begin{aligned}
\int_{x_0}^1 \frac{\mathrm{d}w}{w}\, \sigma(w)\, x_0^2\, \left(\partial_1^2 F\right)\left(\tfrac{x_0}{w}, x_0\right) &= -\left(\sigma(1) + \sigma'(1)\right) F(x_0, x_0) - \frac{\sigma(1)}{2}\, x_0\, F'(x_0, x_0) \\
&\quad + \int_{x_0}^1 \frac{\mathrm{d}w}{w}\, \left[2w^2\, \sigma(w) + 4w^3\, \sigma'(w) + w^4\, \sigma''(w)\right] F\left(\tfrac{x_0}{w}, x_0\right)\,, \\
\int_{x_0}^1 \frac{\mathrm{d}w}{w}\, \sigma(w)\, (-x_0)\, \left(\partial_1 F\right)\left(\tfrac{x_0}{w}, x_0\right) &= \sigma(1)\, F(x_0, x_0) - \int_{x_0}^1 \frac{\mathrm{d}w}{w} w\, (w\sigma(w))'\, F\left(\tfrac{x_0}{w}, x_0\right)\,, \\
\int_{x_0}^1 \frac{\mathrm{d}w}{w}\, \frac{\log(1-w)}{w}\, (-x_0)\, \left(\partial_1 F\right)\left(\tfrac{x_0}{w}, x_0\right) &= \int_{x_0}^1 \frac{\mathrm{d}w}{w}\, \frac{F\left(\frac{x_0}{w}, x_0\right)}{(1-w)_+} - \int_{x_0}^1 \frac{\mathrm{d}w}{w}\, F\left(\tfrac{x_0}{w}, x_0\right)\,. \qquad \text{(E.6)}
\end{aligned}$$

E.3 Soft-Gluon Poles

The NLO computation of the SGP contributions (in the $qg \to q$ channel) gets even more technical. Consider the SGP subtraction terms in the third lines of Eqs. (2.90),(2.91). As for the hard poles, the all-order-in-ε results for the partonic cross sections involve terms $1/(1-w)^{3+\varepsilon}$, $1/(1-w)^{2+\varepsilon}$ that are dealt with via Eq. (E.1), leading to the following two identities:

$$\begin{aligned}
\int_{x_0}^1 \mathrm{d}w\, \frac{F\left(\frac{x_0}{w}, \frac{x_0}{w}\right)}{(1-w)^{3+\varepsilon}} &= \frac{1}{(2+\varepsilon)(1+\varepsilon)} \int_{x_0}^1 \mathrm{d}w\, \frac{\frac{1}{w^4}\left(x_0^2\, F''\left(\frac{x_0}{w}, \frac{x_0}{w}\right)\right) - \frac{2}{w^3}\left(-x_0\, F'\left(\frac{x_0}{w}, \frac{x_0}{w}\right)\right)}{(1-w)^{1+\varepsilon}}\,, \\
\int_{x_0}^1 \mathrm{d}w\, \frac{F\left(\frac{x_0}{w}, \frac{x_0}{w}\right)}{(1-w)^{2+\varepsilon}} &= -\frac{1}{1+\varepsilon} \int_{x_0}^1 \mathrm{d}w\, \frac{\frac{1}{w^2}\left(-x_0\, F'\left(\frac{x_0}{w}, \frac{x_0}{w}\right)\right)}{(1-w)^{1+\varepsilon}}\,. \qquad \text{(E.7)}
\end{aligned}$$

Moreover, the all-ε-order results for the partonic cross sections also contain terms that are proportional to a hypergeometric function along with a term $1/(1-w)^{2+2\varepsilon}$,

$$\frac{{}_2F_1\left(-\varepsilon, -\varepsilon; 1-\varepsilon; \frac{w}{1-v+v\,w}\right)}{(1-w)^{2+2\varepsilon}}.$$

This term needs extra care. One can again perform an integration by parts, which in turn requires a derivative of the hypergeometric function, given by the following identity:

$$\frac{\mathrm{d}}{\mathrm{d}w}\, {}_2F_1\left(-\varepsilon, -\varepsilon; 1-\varepsilon; \tfrac{w}{1-v+v\,w}\right) = \varepsilon\, \frac{(1-v)\, {}_2F_1\left(-\varepsilon, -\varepsilon; 1-\varepsilon; \frac{w}{1-v+v\,w}\right)}{w(1-v+v\,w)} - \varepsilon\, \frac{(1-v)^{1+\varepsilon}(1-w)^{\varepsilon}}{w\,(1-v+v\,w)^{1+\varepsilon}}.$$

By means of this identity one derives the following integral:

$$\int_{x_0}^1 \mathrm{d}w \, \frac{{}_2F_1\left(-\varepsilon,-\varepsilon;1-\varepsilon;\frac{w}{1-v+vw}\right) F\left(\frac{x_0}{w},\frac{x_0}{w}\right)}{(1-w)^{2+2\varepsilon}} = -\frac{1}{1+2\varepsilon}\int_{x_0}^1 \mathrm{d}w \times$$
$$\left[\frac{\frac{1}{w^2}\,{}_2F_1\left(-\varepsilon,-\varepsilon;1-\varepsilon;\frac{w}{1-v+vw}\right)\left(-x_0\,F'\left(\frac{x_0}{w},\frac{x_0}{w}\right)\right)}{(1-w)^{1+2\varepsilon}} - \frac{\varepsilon\,(1-v)^{1+\varepsilon}\,F\left(\frac{x_0}{w},\frac{x_0}{w}\right)}{(1-w)^{1+\varepsilon}\,w\,(1-v+vw)^{1+\varepsilon}}\right.$$
$$\left. + \frac{\frac{1-v}{w\,(1-v+vw)}\,\varepsilon\,{}_2F_1\left(-\varepsilon,-\varepsilon;1-\varepsilon;\frac{w}{1-v+vw}\right) F\left(\frac{x_0}{w},\frac{x_0}{w}\right)}{(1-w)^{1+2\varepsilon}}\right]. \qquad \text{(E.8)}$$

These expressions can now safely be expanded in ε by virtue of Eq. (2.80) (with a replacement $\varepsilon \to 2\varepsilon$ where needed), and an expansion of the hypergeometric function

$${}_2F_1\left(-\varepsilon,-\varepsilon;1-\varepsilon;\frac{w}{1-v+vw}\right) = 1+\varepsilon^2\,\mathrm{Li}_2\left(\frac{w}{1-v+vw}\right)+\mathcal{O}\left(\varepsilon^3\right).$$

The partonic cross sections for the derivative parts $F'\left(\frac{x_0}{w},\frac{x_0}{w}\right)$, $(\partial_2 G)\left(\frac{x_0}{w},\frac{x_0}{w}\right)$ of the SGP subtraction terms in Eq. (2.90),(2.91) are accompanied only by a factor $1/(1-w)^{2+\varepsilon}$ and can be handled using (E.7),(E.8) in a similar way.

As for the HP contributions, a list of useful formulas is given that facilitates the integration by parts of all regular, non-distributional terms in the partonic factors accompanying the derivatives of qgq functions:

$$\int_{x_0}^1 \frac{\mathrm{d}w}{w}\,\sigma(w)\,\left(-x_0\,F'\left(\frac{x_0}{w},\frac{x_0}{w}\right)\right) = \sigma(1)\,F(x_0,x_0) - \int_{x_0}^1 \frac{\mathrm{d}w}{w}\,w\,(w\,\sigma(w))'\,F\left(\frac{x_0}{w},\frac{x_0}{w}\right),$$

$$\int_{x_0}^1 \frac{\mathrm{d}w}{w}\,\sigma(w)\,\log(1-w)\,\left(-x_0\,F'\left(\frac{x_0}{w},\frac{x_0}{w}\right)\right) = \int_{x_0}^1 \frac{\mathrm{d}w}{w}\,\frac{w^2\,\sigma(w)}{(1-w)_+}\,F\left(\frac{x_0}{w},\frac{x_0}{w}\right)$$
$$- \int_{x_0}^1 \frac{\mathrm{d}w}{w}\,w\,(w\,\sigma(w))'\,\log(1-w)\,F\left(\frac{x_0}{w},\frac{x_0}{w}\right),$$

$$\int_{x_0}^1 \frac{\mathrm{d}w}{w}\,\sigma(w)\,\left(x_0^2\,F''\left(\frac{x_0}{w},\frac{x_0}{w}\right)\right) = \sigma(1)\,\left(-x_0\,F'(x_0,x_0)\right) - (w\,\sigma(w))'\Big|_{w=1} F(x_0,x_0)$$
$$+ \int_{x_0}^1 \frac{\mathrm{d}w}{w}\,w\,\left[w^2\,(w\,\sigma(w))'\right]'\,F\left(\frac{x_0}{w},\frac{x_0}{w}\right),$$

$$\int_{x_0}^1 \frac{\mathrm{d}w}{w}\,\sigma(w)\,\left(x_0^2\,\left(\partial_1^2 G\right)\left(\frac{x_0}{w},\frac{x_0}{w}\right)\right) = \sigma(1)\,\left(-x_0\,\left(\partial_1 G\right)(x_0,x_0)\right)$$
$$- \int_{x_0}^1 \frac{\mathrm{d}w}{w}\,w\,(w\,\sigma(w))'\,\left(-x_0\,\left(\partial_1 G\right)\left(\frac{x_0}{w},\frac{x_0}{w}\right)\right). \qquad \text{(E.9)}$$

Appendix F

Analytical Results for the Partonic Cross Sections

F.1 Hadron Production

This appendix is a collection of all results for partonic cross sections that have been featured in the several analytic NLO pQCD formulas of Sec. 6.1. The following subsections each present the results for the different partonic channels one by one. The shorthand notations $\chi_\mu = \frac{su}{t\mu^2}$ and $\chi_m = \frac{su}{tm_\ell^2}$ respectively indicate a frequently encountered scale and lepton mass dependence.

F.1.1 Channel $qg \to q$:

Integral Contribution

The partonic cross section that accompanies $F_{\text{Int}}^{qg\to q}$ in the result for the $qg \to q$ channel integral contribution in Eq. (6.4) reads explicitly

$$\begin{aligned}
\hat{\sigma}_{\text{Int}}^{qg\to q,1}(v,w,\zeta) \;=\; & \frac{w}{4(1-v)^4}\Bigg(\frac{(N_c-2\,C_F)\,\zeta\,(1-v)^2 v(w-\zeta)^2(1+v(w-\zeta))}{\sqrt{1-2\zeta v+2(2\zeta-1)vw+v^2(w-\zeta)^2}} \\
& -2C_F\,v(w-\zeta)^2\Big(\zeta^2+2(\zeta-1)\zeta^2v^3w\left(6w^2-8w+3\right) \\
& +2\zeta v\left(-\zeta+\left(\zeta^2+3\zeta-3\right)w+1\right) \\
& +v^2\left(\zeta^2+\left(8\zeta^3-4\zeta^2-2\right)w^2+2\zeta\left(-4\zeta^2+2\zeta+1\right)w\right) \\
& +\mathrm{sgn}(w-\zeta)\left(\zeta(\zeta+1)+v^2\left(\zeta^2+\zeta+2w^2-2\zeta w\right)+2\zeta v(w-\zeta)\right)\Big) \\
& -N_c\Big(v(w-\zeta)^2\left(\zeta(\zeta+2)+v^2\left(\zeta^2+\left(4\zeta^2-2\right)w^2+2(1-2\zeta)\zeta w\right)\right. \\
& +v\left(\left(4\zeta^2-2\right)w-2\zeta^2\right)\Big) \\
& +\mathrm{sgn}(w-\zeta)\left(v^3(w-\zeta)^2\left((\zeta-1)\zeta+2w^2-2\zeta w\right)\right. \\
& +2v^2\left(-(\zeta-1)\zeta^3+w^3-\zeta(\zeta+1)w^2+\zeta\left(3\zeta^2-\zeta-1\right)w\right) \\
& \left.+\zeta(\zeta+1)v(w-\zeta)^2+2\zeta\left(\zeta^2-1\right)w\right)\Big)\Bigg), \qquad \text{(F.1)}
\end{aligned}$$

with the sign function $\mathrm{sgn}(x)$. Analogously, for the function $G_{\mathrm{Int}}^{qg\to q}$ in Eq. 6.4 it is

$$\begin{aligned}
\hat{\sigma}_{\mathrm{Int}}^{qg\to q,5}(v,w,\zeta) &= \frac{w}{4(1-v)^4}\Bigg(\frac{(N_c-2\,C_F)\,\zeta(1-v)^2v(w-\zeta)^2(1+v(w-\zeta))}{\sqrt{1-2\zeta v+2(2\zeta-1)vw+v^2(w-\zeta)^2}}\\
&+2C_F\,v(w-\zeta)^2\Big(\zeta^2+2(\zeta-1)\zeta^2v^3w\left(6w^2-8w+3\right)\\
&+2\zeta v\left(-\zeta+\left(\zeta^2-\zeta+1\right)w-1\right)\\
&+v^2\left(\zeta^2+\left(8\zeta^3-4\zeta^2-2\right)w^2+2\zeta\left(-4\zeta^2+2\zeta+1\right)w\right)\\
&+\mathrm{sgn}(w-\zeta)\left((\zeta-1)\zeta+v^2\left((\zeta-1)\zeta+2w^2-2\zeta w\right)+2\zeta v(w-\zeta)\right)\Big)\\
&+N_c\Big(v(w-\zeta)^2\left((\zeta-2)\zeta+v^2\left(\zeta^2+\left(4\zeta^2-2\right)w^2+2(1-2\zeta)\zeta w\right)\right.\\
&+v\left(\left(4\zeta^2-2\right)w-2\zeta^2\right)\Big)\\
&+\mathrm{sgn}(w-\zeta)\left(v^3(w-\zeta)^2\left(\zeta^2+\zeta+2w^2-2\zeta w\right)\right.\\
&+2v^2\left(-\zeta^3(\zeta+1)+w^3-\zeta(\zeta+3)w^2+\zeta\left(3\zeta^2+\zeta+1\right)w\right)\\
&\left.+(\zeta-1)\zeta v(w-\zeta)^2+2(\zeta-1)^2\zeta w\right)\Big)\Bigg). \qquad \text{(F.2)}
\end{aligned}$$

Soft-Gluon Pole Contribution

Next, the partonic cross sections of Eq. (6.6) are listed, which constitutes the $qg\to q$ channel soft-gluon pole contribution

$$\begin{aligned}
\hat{\sigma}_{\mathrm{SGP},F}^{qg\to q,1}(v,w,\chi_\mu,\chi_m) &= N_c\,\hat{\sigma}_{\mathrm{SGP},F,N_c}^{qg\to q,1}(v,w,\chi_\mu,\chi_m)\\
&+C_F\,\hat{\sigma}_{\mathrm{SGP},F,C_F}^{qg\to q,1}(v,w,\chi_\mu,\chi_m)\,, \qquad \text{(F.3)}
\end{aligned}$$

where the partonic cross section is separated by color factors. The N_c part reads,

$$\begin{aligned}
\hat{\sigma}_{\mathrm{SGP},F,N_c}^{qg\to q,1}(v,w,\chi_\mu,\chi_m) &= A_{1,\mathrm{SGP},F,N_c}^{qg\to q,1}(v,\chi_\mu,\chi_m)\,\delta(1-w)\\
&+A_{2,\mathrm{SGP},F,N_c}^{qg\to q,1}(v)\left(\frac{\log(1-w)}{1-w}\right)_+ + A_{3,\mathrm{SGP},F,N_c}^{qg\to q,1}(v,\chi_\mu)\,\frac{1}{(1-w)_+}\\
&+A_{4,\mathrm{SGP},F,N_c}^{qg\to q,1}(v,w)\,\log(\chi_m) + A_{5,\mathrm{SGP},F,N_c}^{qg\to q,1}(v,w)\,\log(1-w)\\
&+A_{6,\mathrm{SGP},F,N_c}^{qg\to q,1}(v)\,\log(\chi_\mu) + A_{7,\mathrm{SGP},F,N_c}^{qg\to q,1}(v,w)\,\log(1-v\,w)\\
&+A_{8,\mathrm{SGP},F,N_c}^{qg\to q,1}(v,w)\,\log(1-v) + A_{9,\mathrm{SGP},F,N_c}^{qg\to q,1}(v,w)\,\log(1-v+v\,w)\\
&+A_{10,\mathrm{SGP},F,N_c}^{qg\to q,1}(v,w)\,. \qquad \text{(F.4)}
\end{aligned}$$

with the following ten coefficients,

$$\begin{aligned}
A_{1,\mathrm{SGP},F,N_c}^{qg\to q,1}(v,\chi_\mu,\chi_m) &= \frac{v^5-4v^4-12v^3+38v^2-49v+18}{4\,v^2\,(1-v)^4}\log(1-v)\\
&-\frac{1+v^2}{2\,(1-v)^4}\log(\chi_\mu)-\frac{1+v^2}{2\,(1-v)^3}\log(\chi_m)-\frac{(1+v)v}{(1-v)^4}\log(v)\\
&-\frac{9v^4-58v^3-150v^2+150v-108}{24\,v\,(1-v)^4}\,,\\
A_{2,\mathrm{SGP},F,N_c}^{qg\to q,1}(v) &= -\frac{1+v^2}{(1-v)^4}\,,\\
A_{3,\mathrm{SGP},F,N_c}^{qg\to q,1}(v,\chi_\mu) &= -\frac{1+v^2}{(1-v)^4}\,\log(\chi_\mu)-\frac{3v^4+16v^3-43v^2+50v-18}{2\,v^2\,(1-v)^4}\log(1-v)\\
&-\frac{10v^4-61v^3-176v^2+151v-108}{12\,v\,(1-v)^4},\\
A_{4,\mathrm{SGP},F,N_c}^{qg\to q,1}(v,w) &= \frac{2v^5(1-2w)w^4+v^4w^2\left(8w^2-4w+1\right)}{2\,(1-v)^4\,(1-vw)^2}\\
&-\frac{2v^3w\left(2w^2+w-1\right)+v^2\left(1-w^2\right)-2vw+1}{2\,(1-v)^4\,(1-vw)^2},
\end{aligned}$$

$$
\begin{aligned}
A^{qg\to q,1}_{5,\mathrm{SGP},F,N_c}(v,w) &= -\frac{v^2 w\left(v^3 w^2\left(3w^2-2w+1\right)+2v^2 w\left(-2w^2+w-2\right)\right)}{2\,(1-v)^4\,(1-vw)^2} \\
&\quad -\frac{v^2 w\left(v\left(-w^2+6w+1\right)-2\right)}{2\,(1-v)^4\,(1-vw)^2}\,, \\
A^{qg\to q,1}_{6,\mathrm{SGP},F,N_c}(v) &= \frac{1+v^2}{2\,(1-v)^4}\,, \\
A^{qg\to q,1}_{7,\mathrm{SGP},F,N_c}(v,w) &= \frac{2v^2w^2}{(1-v)^2\,(1-vw)^2}\,,
\end{aligned}
$$

$$
\begin{aligned}
A^{qg\to q,1}_{8,\mathrm{SGP},F,N_c}(v,w) &= -\frac{v^4-20v^3+47v^2-50v+18}{2\,v^2\,(1-v)^4}-\frac{\left(v^3-9v+16\right)w}{4\,v^2\,(1-v)^2} \\
&\quad -\frac{(3v-5)w^2}{v^2\,(1-v)^2}+\frac{1-2vw}{(1-v)^2\,(1-v\,w)^2}\,, \\
A^{qg\to q,1}_{9,\mathrm{SGP},F,N_c}(v,w) &= \frac{vw}{4\,(1-v)^2}\,,
\end{aligned}
$$

$$
\begin{aligned}
A^{qg\to q,1}_{10,\mathrm{SGP},F,N_c}(v,w) &= \frac{w^2\,\log(w)}{(1-w)^2}\times \\
&\left(\frac{v^3(w-1)^2(2w-1)+2v^2(w-2)w+2v-2}{(1-v)^4}+\frac{1-v(2w-1)}{(1-v)\,(1-v\,w)^2}\right) \\
&-\frac{1+v^2}{(1-v)^4(1-w)}+\frac{13v^4-76v^3-95v^2+130v-108}{12\,v\,(1-v)^4} \\
&+\frac{\left(37v^4-122v^3-313v^2+228v-192\right)w}{48\,v\,(1-v)^4}+\frac{\left(5v^4+38v^2-63v+30\right)w^2}{6\,v\,(1-v)^4} \\
&+\frac{\left(17v^3+6v^2+v+8\right)w^3}{48\,(1-v)^4}+\frac{4v^2w-v(5w+2)+3}{(1-v)^3(1-v\,w)^2}+\frac{1}{4(1-v+v\,w)}\,. \qquad \text{(F.5)}
\end{aligned}
$$

Notice that the last one, $A^{qg\to q,1}_{10,\mathrm{SGP},F,N_c}(v,w)$, is regular as $w\to 1$, despite the factors $\log(w)/(1-w)^2$ and $1/(1-w)$. Its limit for $w\to 1$ is

$$
\lim_{w\to 1} A^{qg\to q,1}_{10,\mathrm{SGP},F,N_c}(v,w)=\frac{6v^5+49v^4-210v^3-314v^2+168v-192}{24\,v\,(1-v)^4}\,.
$$

The C_F part in (F.3) takes a similar form as the N_c part,

$$
\begin{aligned}
\hat{\sigma}^{qg\to q,1}_{\mathrm{SGP},F,C_F}(v,w,\chi_\mu,\chi_m) &= A^{qg\to q,1}_{1,\mathrm{SGP},F,C_F}(v,\chi_\mu,\chi_m)\,\delta(1-w) \\
&\quad +A^{qg\to q,1}_{2,\mathrm{SGP},F,C_F}(v)\left(\frac{\log(1-w)}{1-w}\right)_+ + A^{qg\to q,1}_{3,\mathrm{SGP},F,C_F}(v,\chi_\mu)\,\frac{1}{(1-w)_+} \\
&\quad +A^{qg\to q,1}_{4,\mathrm{SGP},F,C_F}(v,w)\,\log(\chi_m)+A^{qg\to q,1}_{5,\mathrm{SGP},F,C_F}(v,w)\,\log(1-w) \\
&\quad +A^{qg\to q,1}_{6,\mathrm{SGP},F,C_F}(v,w)\,\log(\chi_\mu)+A^{qg\to q,1}_{7,\mathrm{SGP},F,C_F}(v,w)\,\log(1-v\,w) \\
&\quad +A^{qg\to q,1}_{8,\mathrm{SGP},F,C_F}(v,w)\,\log(1-v)+A^{qg\to q,1}_{9,\mathrm{SGP},F,C_F}(v,w)\log(1-v+v\,w) \\
&\quad +A^{qg\to q,1}_{10,\mathrm{SGP},F,C_F}(v,w)\,. \qquad \text{(F.6)}
\end{aligned}
$$

with the following ten coefficients,

$$
\begin{aligned}
A^{qg\to q,1}_{1,\mathrm{SGP},F,C_F}(v,\chi_\mu,\chi_m) &= \frac{1+v^2}{(1-v)^4}\log(v)\,(4\log(1-v)+2\log(\chi_\mu)-\log(v)) \\
&-\frac{9v^5+4v^4+12v^3+30v^2-49v+18}{2(v-1)^4v^2}\log(1-v)-\frac{2v^3+v^2+6v-3}{(1-v)^4}\log(\chi_\mu) \\
&+\frac{1+v^2}{(1-v)^3}\log(\chi_m)-5\frac{1+v^2}{(1-v)^4}\log(v)+\frac{45v^5-21v^4-365v^3-840v^2+780v-540}{60\,v\,(1-v)^4},
\end{aligned}
$$

$$
\begin{aligned}
A^{qg\to q,1}_{2,\mathrm{SGP},F,C_F}(v) &= 8\frac{1+v^2}{(1-v)^4}\,,\\
A^{qg\to q,1}_{3,\mathrm{SGP},F,C_F}(v,\chi_\mu) &= 4\frac{1+v^2}{(1-v)^4}\log(\chi_\mu)+\frac{7v^4+16v^3-39v^2+50v-18}{v^2\,(1-v)^4}\log(1-v)\\
&\quad+\frac{75v^5-340v^4-509v^3-2440v^2+2280v-1080}{60\,v\,(1-v)^4}\,,\\
A^{qg\to q,1}_{4,\mathrm{SGP},F,C_F}(v,w) &= \frac{2v^5w^4(2w-1)-v^4w^2\left(8w^2-4w+1\right)}{(1-v)^4\,(1-v\,w)^2}\\
&\quad+\frac{2v^3w\left(2w^2+w-1\right)-v^2\left(w^2-1\right)-2vw+1}{(1-v)^4\,(1-v\,w)^2}\,,\\
A^{qg\to q,1}_{5,\mathrm{SGP},F,C_F}(v,w) &= \frac{6v^4w^4}{(1-v)^4}-\frac{v^3(8v-17)w^3}{(1-v)^4}+\frac{v^2\left(3v^2-10v+13\right)w^2}{(1-v)^4}+\frac{v^2w}{(1-v)^4}\\
&\quad-\frac{4\left(2v^2-v+2\right)}{(1-v)^4}+\frac{2-4vw}{(1-v)^2(1-v\,w)^2}\,,\\
A^{qg\to q,1}_{6,\mathrm{SGP},F,C_F}(v,w) &= \frac{v^4w^2\left(6w^2-8w+3\right)+4v^3w^2(3w-2)+v^2\left(9w^2-3\right)-3}{(1-v)^4}\,,\\
A^{qg\to q,1}_{7,\mathrm{SGP},F,C_F}(v,w) &= -\frac{4v^2w^2}{(1-v)^2\,(1-v\,w)^2}\,,\\
A^{qg\to q,1}_{8,\mathrm{SGP},F,C_F}(v,w) &= \frac{-3v^4-20v^3+43v^2-50v+18}{v^2\,(1-v)^4}+\frac{\left(v^3-9v+16\right)w}{2\,v^2\,(1-v)^2}\\
&\quad+\frac{2\left(3v^6-8v^5+9v^4+3v^3-11v^2+13v-5\right)w^2}{v^2\,(1-v)^4}\\
&\quad-\frac{8v^3(2v-3)w^3}{(1-v)^4}+\frac{12v^4w^4}{(1-v)^4}+\frac{4vw-2}{(1-v)^2\,(1-v\,w)^2}\,,\\
A^{qg\to q,1}_{9,\mathrm{SGP},F,C_F}(v,w) &= -\frac{vw}{2(1-v)^2}\,,
\end{aligned}
$$

$$
\begin{aligned}
A^{qg\to q,1}_{10,\mathrm{SGP},F,C_F}(v,w) &= \log(w)\left(-\frac{6v^4w^4}{(1-v)^4}+\frac{8(v-2)v^3w^3}{(1-v)^4}-\frac{v^2\left(3v^2-10v+13\right)w^2}{(1-v)^4}\right.\\
&\quad\left.+\frac{2\left(3v^2-2v+3\right)}{(1-v)^4}+\frac{4\left(1+v^2\right)(2w-1)}{(1-v)^4\,(1-w)^2}+\frac{4vw-2}{(1-v)^2\,(1-v\,w)^2}\right)\\
&\quad-\frac{3v^4w^4}{(1-v)^4}+\frac{v\left(76v^3-15v^2+6v+1\right)w^3}{24(1-v)^4}\\
&\quad-\frac{\left(64v^5-210v^4-195v^3+360v^2-630v+300\right)w^2}{30\,v\,(1-v)^4}\\
&\quad-\frac{\left(114v^5-569v^4-1120v^3-2735v^2+1860v-960\right)w}{120\,v\,(1-v)^4}\\
&\quad-\frac{75v^5-310v^4-539v^3-1630v^2+2190v-1080}{60\,v\,(1-v)^4}\\
&\quad+\frac{4\left(1+v^2\right)}{(1-v)^4(1-w)}-\frac{8v^2w-2v(5w+2)+6}{(1-v)^3\,(1-v\,w)^2}-\frac{1}{2(1-v+v\,w)}\,. \qquad \text{(F.7)}
\end{aligned}
$$

As for the N_c part, the last coefficient appears to diverge for $w\to 1$, but actually has the finite limit

$$
\lim_{w\to 1} A^{qg\to q,1}_{10,\mathrm{SGP},F,C_F}(v,w)=\frac{-280v^5+1097v^4+1684v^3+2880v^2-1890v+960}{60\,v\,(1-v)^4}\,.
$$

The partonic cross section for the first derivative term can be decomposed as well. After integration by parts only distributions appear in the analytic forms,

$$
\hat\sigma^{qg\to q,1}_{\mathrm{SGP},F'}(v,w,\chi_\mu) = N_c\,\hat\sigma^{qg\to q,1}_{\mathrm{SGP},F',N_c}(v,w,\chi_\mu)+C_F\,\hat\sigma^{qg\to q,1}_{\mathrm{SGP},F',C_F}(v,w,\chi_\mu)\,, \qquad \text{(F.8)}
$$

where the N_c part reads

$$\begin{aligned}\hat{\sigma}^{qg\to q,1}_{\mathrm{SGP},F',N_c}(v,w,\chi_\mu) &= A^{qg\to q,1}_{1,\mathrm{SGP},F',N_c}(v,\chi_\mu)\,\delta(1-w) + A^{qg\to q,1}_{2,\mathrm{SGP},F',N_c}(v)\left(\frac{\log(1-w)}{1-w}\right)_+ \\ &\quad + A^{qg\to q,1}_{3,\mathrm{SGP},F',N_c}(v,\chi_\mu)\,\frac{1}{(1-w)_+}\,, \end{aligned} \tag{F.9}$$

with coefficients

$$\begin{aligned}A^{qg\to q,1}_{1,\mathrm{SGP},F',N_c}(v,\chi_\mu) &= -\frac{1+v^2}{(1-v)^4}\log(\chi_\mu) - \frac{7v^4+15v^3-33v^2+41v-14}{4\,v^2\,(1-v)^4}\log(1-v) \\ &\quad -\frac{6v^4-51v^3-142v^2+115v-84}{24\,v\,(1-v)^4}\,, \\ A^{qg\to q,1}_{2,\mathrm{SGP},F',N_c}(v) &= -\frac{1+v^2}{(1-v)^4}\,, \\ \\ A^{qg\to q,1}_{3,\mathrm{SGP},F',N_c}(v,\chi_\mu) &= -\frac{1+v^2}{(1-v)^4}\log(\chi_\mu) - \frac{6v^4+23v^3-52v^2+59v-20}{4\,v^2\,(1-v)^4}\log(1-v) \\ &\quad -\frac{15v^4-98v^3-427v^2+376v-240}{48\,v\,(1-v)^4}\,. \end{aligned} \tag{F.10}$$

Furthermore, the C_F part reads

$$\begin{aligned}\hat{\sigma}^{qg\to q,1}_{\mathrm{SGP},F',C_F}(v,w,\chi_\mu) &= A^{qg\to q,1}_{1,\mathrm{SGP},F',C_F}(v,\chi_\mu)\,\delta(1-w) + A^{qg\to q,1}_{2,\mathrm{SGP},F',C_F}(v)\left(\frac{\log(1-w)}{1-w}\right)_+ \\ &\quad + A^{qg\to q,1}_{3,\mathrm{SGP},F',C_F}(v,\chi_\mu)\,\frac{1}{(1-w)_+}\,, \end{aligned} \tag{F.11}$$

with the coefficients

$$\begin{aligned}A^{qg\to q,1}_{1,\mathrm{SGP},F',C_F}(v,\chi_\mu) &= \frac{1+v^2}{(1-v)^4}\log(v)\,\left(4\log(1-v)+2\log(\chi_\mu)-\log(v)\right) \\ &\quad + \frac{11v^4+15v^3-29v^2+41v-14}{2\,v^2\,(1-v)^4}\log(1-v) + 3\frac{1+v^2}{(1-v)^4}\,\log\left(\frac{\chi_\mu}{v}\right) \\ &\quad + \frac{27v^5-44v^4-669v^3-1600v^2+1080v-840}{120\,v\,(1-v)^4}\,, \\ A^{qg\to q,1}_{2,\mathrm{SGP},F',C_F}(v) &= 8\frac{1+v^2}{(1-v)^4}\,, \\ A^{qg\to q,1}_{3,\mathrm{SGP},F',C_F}(v,\chi_\mu) &= 4\frac{1+v^2}{(1-v)^4}\log(\chi_\mu) + \frac{14v^4+23v^3-44v^2+59v-20}{2\,v^2\,(1-v)^4}\log(1-v) \\ &\quad + \frac{12v^5-17v^4+154v^3-775v^2+980v-400}{40\,v\,(1-v)^4}\,. \end{aligned} \tag{F.12}$$

The partonic cross sections accompanying the second derivative F'' can similarly be written in the following form, where again parts with different color factors have been separated

$$\hat{\sigma}^{qg\to q,1}_{\mathrm{SGP},F''}(v,w) = N_c\,\hat{\sigma}^{qg\to q,1}_{\mathrm{SGP},F'',N_c}(v,w) + C_F\,\hat{\sigma}^{qg\to q,1}_{\mathrm{SGP},F'',C_F}(v,w)\,, \tag{F.13}$$

with the N_c part

$$\hat{\sigma}^{qg\to q,1}_{\mathrm{SGP},F'',N_c}(v,w) = A^{qg\to q,1}_{1,\mathrm{SGP},F'',N_c}(v)\left(\delta(1-w)+\frac{1}{(1-w)_+}\right), \tag{F.14}$$

and the coefficient

$$A^{qg\to q,1}_{1,\mathrm{SGP},F'',N_c}(v) = \frac{1}{4\,v^2\,(1-v)}\log(1-v) - \frac{v^4-4v^3-19v^2+20v-12}{48\,v\,(1-v)^4}\,. \tag{F.15}$$

The C_F part reads

$$\hat{\sigma}^{qg\to q,1}_{\mathrm{SGP},F'',C_F}(v,w) = A^{qg\to q,1}_{1,\mathrm{SGP},F'',C_F}(v)\left(\delta(1-w)+\frac{1}{(1-w)_+}\right), \tag{F.16}$$

with the coefficient

$$A^{qg\to q,1}_{1,\mathrm{SGP},F'',C_F}(v) = -\frac{\log(1-v)}{2\,v^2\,(1-v)} + \frac{2v^5-5v^4+22v^3-125v^2+150v-60}{120\,v\,(1-v)^4}\,. \quad \text{(F.17)}$$

The other type of second derivative term in Eq. (6.6) has the partonic cross section $\hat{\sigma}^{qg\to q,1}_{\mathrm{SGP},\partial_1^2 F}(v,w)$, which can be cast into the very compact form

$$\begin{aligned}\hat{\sigma}^{qg\to q,1}_{\mathrm{SGP},\partial_1^2 F}(v,w) &= \delta(1-w)\left[N_c\left(-\frac{\log(1-v)}{4\,v^2\,(1-v)} + \frac{v^4-4v^3-19v^2+20v-12}{48\,v\,(1-v)^4}\right)\right.\\ &\left. +C_F\left(\frac{\log(1-v)}{2\,v^2\,(1-v)} - \frac{2v^5-5v^4+22v^3-125v^2+150v-60}{120\,v\,(1-v)^4}\right)\right]. \quad \text{(F.18)}\end{aligned}$$

Next are the terms in Eq. (6.6) that appear in conjunction with the axial-vector type function G. Since $G(x,x)=0$ only derivatives can contribute to the SGP

$$\hat{\sigma}^{qg\to q,5}_{\mathrm{SGP},\partial_1 G}(v,w) = N_c\,\hat{\sigma}^{qg\to q,5}_{\mathrm{SGP},\partial_1 G,N_c}(v,w) + C_F\,\hat{\sigma}^{qg\to q,5}_{\mathrm{SGP},\partial_1 G,C_F}(v,w)\,, \quad \text{(F.19)}$$

where the partonic cross section is once more divided by color factors and the N_c part reads

$$\begin{aligned}\hat{\sigma}^{qg\to q,5}_{\mathrm{SGP},\partial_1 G,N_c}(v,w) &= A^{qg\to q,5}_{1,\mathrm{SGP},\partial_1 G,N_c}(v)\,\delta(1-w) + A^{qg\to q,5}_{2,\mathrm{SGP},\partial_1 G,N_c}(v)\,\frac{1}{(1-w)_+}\\ &+A^{qg\to q,5}_{3,\mathrm{SGP},\partial_1 G,N_c}(v,w)\,\log(1-w) + A^{qg\to q,5}_{4,\mathrm{SGP},\partial_1 G,N_c}(v)\,\log(1-v+v\,w)\\ &+A^{qg\to q,5}_{5,\mathrm{SGP},\partial_1 G,N_c}(v,w)\,\log(1-v) + A^{qg\to q,5}_{6,\mathrm{SGP},\partial_1 G,N_c}(v,w)\,, \quad \text{(F.20)}\end{aligned}$$

with the following six coefficients

$$\begin{aligned}A^{qg\to q,5}_{1,\mathrm{SGP},\partial_1 G,N_c}(v) &= -\frac{v^2-13v+14}{2\,v^2\,(1-v)^2}\log(1-v) - \frac{6v^4-39v^3+150v^2-209v+84}{12\,v\,(1-v)^4}\,,\\ A^{qg\to q,5}_{2,\mathrm{SGP},\partial_1 G,N_c}(v) &= \frac{8-7v}{2\,v^2\,(1-v)^2}\log(1-v) + \frac{9v^4-34v^3+155v^2-228v+96}{24\,v\,(1-v)^4}\,,\\ A^{qg\to q,5}_{3,\mathrm{SGP},\partial_1 G,N_c}(v,w) &= \frac{v^2\left(v\left(w^2-w+1\right)+w-2\right)}{(1-v)^4}\,,\\ A^{qg\to q,5}_{4,\mathrm{SGP},\partial_1 G,N_c}(v) &= -\frac{v}{2(1-v)^2}\,,\\ A^{qg\to q,5}_{5,\mathrm{SGP},\partial_1 G,N_c}(v,w) &= \frac{v^3+6vw+7v-10w-8}{2\,v^2\,(1-v)^2}\,,\\ A^{qg\to q,5}_{6,\mathrm{SGP},\partial_1 G,N_c}(v,w) &= -\frac{9v^4-34v^3+155v^2-228v+96}{24\,v\,(1-v)^4} - \frac{w\,(v^4-2v^3+73v^2-128v+60)}{12\,v\,(1-v)^4}\\ &-\frac{w^2\,(7v^3-6v^2-v-8)}{24\,(1-v)^4}\,. \quad \text{(F.21)}\end{aligned}$$

The C_F part is given by

$$\begin{aligned}\hat{\sigma}^{qg\to q,5}_{\mathrm{SGP},\partial_1 G,C_F}(v,w) &= A^{qg\to q,5}_{1,\mathrm{SGP},\partial_1 G,C_F}(v)\,\delta(1-w) + A^{qg\to q,5}_{2,\mathrm{SGP},\partial_1 G,C_F}(v)\,\frac{1}{(1-w)_+}\\ &+A^{qg\to q,5}_{3,\mathrm{SGP},\partial_1 G,C_F}(v,w)\,\log(1-w) + A^{qg\to q,5}_{4,\mathrm{SGP},\partial_1 G,C_F}(v)\,\log(1-v+v\,w)\\ &+A^{qg\to q,5}_{5,\mathrm{SGP},\partial_1 G,C_F}(v,w)\,\log(1-v) + A^{qg\to q,5}_{6,\mathrm{SGP},\partial_1 G,C_F}(v,w)\,, \quad \text{(F.22)}\end{aligned}$$

also with six coefficients

$$\begin{aligned}A^{qg\to q,5}_{1,\mathrm{SGP},\partial_1 G,C_F}(v) &= \frac{v^2-13v+14}{v^2\,(1-v)^2}\log(1-v)\\ &+\frac{27v^5-44v^4-309v^3+1520v^2-2040v+840}{60\,v\,(1-v)^4}\,,\\ A^{qg\to q,5}_{2,\mathrm{SGP},\partial_1 G,C_F}(v) &= -\frac{8-7v}{v^2\,(1-v)^2}\log(1-v)\\ &-\frac{18v^5-37v^4-120v^3+805v^2-1140v+480}{60\,v\,(1-v)^4}\,,\end{aligned}$$

$$
\begin{aligned}
A^{qg\to q,5}_{3,\mathrm{SGP},\partial_1 G,C_F}(v,w) &= -\frac{2v^2(1-w)(1+vw)}{(1-v)^4}\,,\\
A^{qg\to q,5}_{4,\mathrm{SGP},\partial_1 G,C_F}(v) &= \frac{v}{(1-v)^2}\,,\\
A^{qg\to q,5}_{5,\mathrm{SGP},\partial_1 G,C_F}(v,w) &= -\frac{v^3+6vw+7v-10w-8}{v^2\,(1-v)^2}\,,\\
A^{qg\to q,5}_{6,\mathrm{SGP},\partial_1 G,C_F}(v,w) &= \frac{18v^5-37v^4-120v^3+805v^2-1140v+480}{60\,v\,(1-v)^4}\\
&\quad+\frac{w\,(26v^5-25v^4-120v^3+375v^2-630v+300)}{30\,v\,(1-v)^4}\\
&\quad-\frac{w^2\,(20v^4-9v^3-6v^2-v)}{12\,(1-v)^4}+\frac{2\,w^3\,v^4}{(1-v)^4}\,.
\end{aligned}
\tag{F.23}
$$

Finally, there is a contribution from the second derivative of G given as

$$
\begin{aligned}
\hat{\sigma}^{qg\to q,5}_{\mathrm{SGP},\partial_1^2 G}(v,w) &= \left(\delta(1-w)-\frac{2}{(1-w)_+}\right)\times\\
&\quad\left[N_c\left(-\frac{\log(1-v)}{4\,v^2\,(1-v)}-\frac{v^4-4v^3+21v^2-28v+12}{48\,v\,(1-v)^4}\right)\right.\\
&\quad\left.+C_F\left(\frac{\log(1-v)}{2\,v^2\,(1-v)}+\frac{2v^5-5v^4-18v^3+115v^2-150v+60}{120\,v\,(1-v)^4}\right)\right].
\end{aligned}
\tag{F.24}
$$

Soft-Fermion Pole Contribution

The $qg\to q$ channel soft-fermion pole contribution is found in Eq. (6.7) and the corresponding partonic cross sections are presented below. As before, a separation by color factors is made

$$
\hat{\sigma}^{qg\to q,1}_{\mathrm{SFP},F}(v,w,\chi_m) = N_c\,\hat{\sigma}^{qg\to q,1}_{\mathrm{SFP},F,N_c}(v,w,\chi_m)+C_F\,\hat{\sigma}^{qg\to q,1}_{\mathrm{SFP},F,C_F}(v,w,\chi_m)\,,
\tag{F.25}
$$

where the N_c part reads

$$
\begin{aligned}
\hat{\sigma}^{qg\to q,1}_{\mathrm{SFP},F,N_c}(v,w,\chi_m) &= A^{qg\to q,1}_{1,\mathrm{SFP},F,N_c}(v,w)\,\log(\chi_m)+A^{qg\to q,1}_{2,\mathrm{SFP},F,N_c}(v,w)\,\log(1-w)\\
&\quad+A^{qg\to q,1}_{3,\mathrm{SFP},F,N_c}(v,w)\,\log(1-v\,w)+A^{qg\to q,1}_{4,\mathrm{SFP},F,N_c}(v,w)\,\log(1-v)\\
&\quad+A^{qg\to q,1}_{5,\mathrm{SFP},F,N_c}(v,w)\,\log(1-v+v\,w)+A^{qg\to q,1}_{6,\mathrm{SFP},F,N_c}(v,w)\,\log(w)\\
&\quad+A^{qg\to q,1}_{7,\mathrm{SFP},F,N_c}(v,w)\,,
\end{aligned}
\tag{F.26}
$$

with seven coefficients

$$
\begin{aligned}
A^{qg\to q,1}_{1,\mathrm{SFP},F,N_c}(v,w) &= -\frac{v^3w^3}{(1-v)^4}-\frac{v^2w^2}{(1-v)^3}-\frac{v\left(v^2-4v+5\right)w}{2(1-v)^4}\\
&\quad-\frac{v^2-4v+2}{(1-v)^4}+\frac{3-2v}{(1-v)^3(1-v\,w)}-\frac{1}{2(1-v)^2(1-v\,w)^2}\,,\\
A^{qg\to q,1}_{2,\mathrm{SFP},F,N_c}(v,w) &= -\frac{2v^3w^3}{(1-v)^4}+\frac{v^2(3v-1)w^2}{(1-v)^4}-\frac{v\left(3v^2-4v+5\right)w}{2\,(1-v)^4}\\
&\quad-\frac{v^2-4v+2}{(1-v)^4}+\frac{3-2v}{(1-v)^3(1-v\,w)}-\frac{1}{2(1-v)^2(1-v\,w)^2},\\
A^{qg\to q,1}_{3,\mathrm{SFP},F,N_c}(v,w) &= -\frac{vw\left(v^3(w-1)w^2+v^2(w-1)w+v-1\right)}{(1-v)^3\,(1-v\,w)^2},\\
A^{qg\to q,1}_{4,\mathrm{SFP},F,N_c}(v,w) &= \frac{2v-3}{(1-v)^2\,v^2\,w}-\frac{2v^3-10v^2+16v-9}{(1-v)^3\,v^2}-\frac{w\,(v^4-5v^3-v^2+5v-4)}{2\,(1-v)^3\,v^2}\\
&\quad+\frac{2(3v-5)w^2}{(1-v)^2\,v^2}-\frac{4v^2w-3v(2w+1)+5}{2\,(1-v)^3\,(1-v\,w)^2}\,,\\
A^{qg\to q,1}_{5,\mathrm{SFP},F,N_c}(v,w) &= \frac{vw(2vw-v-1)}{2\,(1-v)^3}\,,
\end{aligned}
$$

$$
\begin{aligned}
A^{qg\to q,1}_{6,\mathrm{SFP},F,N_c}(v,w) &= \frac{2v^2-4v+3}{(1-v)^4}+\frac{(2-v)vw}{(1-v)^3}-\frac{v^2(2v+1)w^2}{(1-v)^4}-\frac{4v^2w-3v(2w+1)+5}{2\,(1-v)^3\,(1-v\,w)^2},\\
A^{qg\to q,1}_{7,\mathrm{SFP},F,N_c}(v,w) &= -\frac{v^4-2v^3+24v^2-35v+18}{6\,(1-v)^4\,v\,w}+\frac{10v^4-23v^3+126v^2-203v+108}{12\,(1-v)^4\,v}\\
&\quad -\frac{\left(5v^4-5v^3-29v^2+9v-12\right)w}{6\,(1-v)^4\,v}\\
&\quad -\frac{\left(33v^4-16v^3+155v^2-238v+120\right)w^2}{12\,(1-v)^4\,v}+\frac{\left(31v^3-6v^2-v-8\right)w^3}{12\,(1-v)^4}\\
&\quad -\frac{4v^2w-v(7w+2)+5}{2\,(1-v)^3\,(1-v\,w)^2}+\frac{1}{2\,(1-v)\,(1-v+v\,w)}\,. \qquad \text{(F.27)}
\end{aligned}
$$

Similarly, the C_F part has the form

$$
\begin{aligned}
\hat{\sigma}^{qg\to q,1}_{\mathrm{SFP},F,C_F}(v,w,\chi_m) &= A^{qg\to q,1}_{1,\mathrm{SFP},F,C_F}(v,w)\,\log(\chi_m)+A^{qg\to q,1}_{2,\mathrm{SFP},F,C_F}(v,w)\,\log(1-w)\\
&\quad +A^{qg\to q,1}_{3,\mathrm{SFP},F,C_F}(v,w)\,\log(1-v\,w)+A^{qg\to q,1}_{4,\mathrm{SFP},F,C_F}(v,w)\,\log(1-v)\\
&\quad +A^{qg\to q,1}_{5,\mathrm{SFP},F,C_F}(v,w)\,\log(1-v+v\,w)+A^{qg\to q,1}_{6,\mathrm{SFP},F,C_F}(v,w)\,\log(w)\\
&\quad +A^{qg\to q,1}_{7,\mathrm{SFP},F,C_F}(v,w)\,, \qquad \text{(F.28)}
\end{aligned}
$$

also with seven coefficients

$$
\begin{aligned}
A^{qg\to q,1}_{1,\mathrm{SFP},F,C_F}(v,w) &= \frac{5-3v}{(1-v)^3}+\frac{w\,v\,\left(v^2-6v+3\right)}{(1-v)^4}+\frac{2\,w^2\,v^2\,(2-v)}{(1-v)^4}\\
&\quad +\frac{2\,w^3\,v^3}{(1-v)^4}-\frac{4v^2w-3v(2w+1)+5}{(1-v)^3\,(1-v\,w)^2}\,,\\
A^{qg\to q,1}_{2,\mathrm{SFP},F,C_F}(v,w) &= \frac{5-3v}{(1-v)^3}+\frac{3\,w\,v}{(1-v)^2}+\frac{2\,w^2\,v^2\,(2-3v)}{(1-v)^4}+\frac{4\,w^3\,v^3}{(1-v)^4}\\
&\quad -\frac{4v^2w-3v(2w+1)+5}{(1-v)^3\,(1-v\,w)^2}\,,\\
A^{qg\to q,1}_{3,\mathrm{SFP},F,C_F}(v,w) &= \frac{2vw\left(v^3(w-1)w^2+v^2(w-1)w+v-1\right)}{(1-v)^3\,(1-v\,w)^2},\\
A^{qg\to q,1}_{4,\mathrm{SFP},F,C_F}(v,w) &= \frac{6-4v}{(1-v)^2v^2w}+\frac{4v^3-20v^2+32v-18}{v^2\,(1-v)^3}\\
&\quad +\frac{w\,\left(v^4-5v^3-v^2+5v-4\right)}{v^2\,(1-v)^3}-\frac{4\,w^2\,(3v-5)}{v^2\,(1-v)^2}+\frac{4v^2w-v(6w+3)+5}{(1-v)^3\,(1-v\,w)^2},\\
A^{qg\to q,1}_{5,\mathrm{SFP},F,C_F}(v,w) &= \frac{v\,w\,(v(1-2w)+1)}{(1-v)^3},\\
A^{qg\to q,1}_{6,\mathrm{SFP},F,C_F}(v,w) &= -\frac{5-3v}{(1-v)^3}-\frac{2\,w\,(2-v)v}{(1-v)^3}+\frac{2\,w^2\,v^2(4v-3)}{(1-v)^4}-\frac{8\,w^3\,v^3}{(1-v)^4}\\
&\quad +\frac{4v^2w-v(6w+3)+5}{(1-v)^3\,(1-v\,w)^2}\,,\\
A^{qg\to q,1}_{7,\mathrm{SFP},F,C_F}(v,w) &= \frac{9v^5-22v^4-7v^3+240v^2-390v+180}{30\,v\,(1-v)^4\,w}\\
&\quad -\frac{75v^5-160v^4-151v^3+1380v^2-2220v+1080}{60\,v\,(1-v)^4}\\
&\quad +\frac{w\,\left(12v^5-14v^4+55v^3-90v^2+105v-60\right)}{15\,v\,(1-v)^4}\\
&\quad +\frac{w^2\,\left(128v^5-65v^4-115v^3+705v^2-1260v+600\right)}{30\,v\,(1-v)^4}\\
&\quad -\frac{w^3\,v\left(52v^3-3v^2+6v+1\right)}{6\,(1-v)^4}+\frac{5\,w^4\,v^4}{(1-v)^4}\\
&\quad +\frac{4v^2w-v(7w+2)+5}{(1-v)^3\,(1-v\,w)^2}-\frac{1}{(1-v)\,(1-v+v\,w)}\,. \qquad \text{(F.29)}
\end{aligned}
$$

Furthermore, the SFP contribution also has derivative terms which read

$$
\hat{\sigma}^{qg\to q,1}_{\mathrm{SFP},\partial_2 F}(v,w,\chi_m) = N_c\,\hat{\sigma}^{qg\to q,1}_{\mathrm{SFP},\partial_2 F,N_c}(v,w,\chi_m)+C_F\,\hat{\sigma}^{qg\to q,1}_{\mathrm{SFP},\partial_2 F,C_F}(v,w,\chi_m)\,, \qquad \text{(F.30)}
$$

where the N_c part has the form

$$\begin{aligned}\hat{\sigma}^{qg\to q,1}_{\mathrm{SFP},\partial_2 F,N_c}(v,w) &= A^{qg\to q,1}_{1,\mathrm{SFP},\partial_2 F,N_c}(v,w)\,\log(1-v) + A^{qg\to q,1}_{2,\mathrm{SFP},\partial_2 F,N_c}(v,w)\,\log(w)\\ &\quad + A^{qg\to q,1}_{3,\mathrm{SFP},\partial_2 F,N_c}(v,w)\,, \end{aligned} \tag{F.31}$$

with three coefficients

$$\begin{aligned}A^{qg\to q,1}_{1,\mathrm{SFP},\partial_2 F,N_c}(v,w) &= \frac{v\left(-6w^2+8w-2\right)+10w^2-12w+3}{2\,w\,v^2\,(1-v)^2}\,,\\ A^{qg\to q,1}_{2,\mathrm{SFP},\partial_2 F,N_c}(v,w) &= \frac{w\,v^2\,(1+v\,w)}{(1-v)^4}\,,\\ A^{qg\to q,1}_{3,\mathrm{SFP},\partial_2 F,N_c}(v,w) &= \frac{v^4-2v^3+24v^2-35v+18}{12\,w\,v\,(1-v)^4} - \frac{7v^4-16v^3+96v^2-144v+72}{12\,v\,(1-v)^4}\\ &\quad + \frac{\left(11v^4-9v^3+38v^2-63v+30\right)w}{6\,v\,(1-v)^4} - \frac{\left(31v^3-6v^2-v-8\right)w^2}{24\,(1-v)^4}. \end{aligned} \tag{F.32}$$

The C_F part reads

$$\begin{aligned}\hat{\sigma}^{qg\to q,1}_{\mathrm{SFP},\partial_2 F,C_F}(v,w) &= A^{qg\to q,1}_{1,\mathrm{SFP},\partial_2 F,C_F}(v,w)\,\log(1-v) + A^{qg\to q,1}_{2,\mathrm{SFP},\partial_2 F,C_F}(v,w)\,\log(w)\\ &\quad + A^{qg\to q,1}_{3,\mathrm{SFP},\partial_2 F,NC_F}(v,w)\,, \end{aligned} \tag{F.33}$$

with three coefficients

$$\begin{aligned}A^{qg\to q,1}_{1,\mathrm{SFP},\partial_2 F,C_F}(v,w) &= \frac{v\left(6w^2-8w+2\right)-10w^2+12w-3}{w\,v^2\,(1-v)^2}\,,\\ A^{qg\to q,1}_{2,\mathrm{SFP},\partial_2 F,C_F}(v,w) &= \frac{2v^3w^2}{(1-v)^4}\,,\\ A^{qg\to q,1}_{3,\mathrm{SFP},\partial_2 F,C_F}(v,w) &= \frac{-9v^5+22v^4+7v^3-240v^2+390v-180}{60\,w\,v\,(1-v)^4}\\ &\quad + \frac{27v^5-61v^4-15v^3+480v^2-780v+360}{30\,v\,(1-v)^4}\\ &\quad - \frac{w\,\left(64v^5-150v^4+15v^3+360v^2-630v+300\right)}{30\,v\,(1-v)^4}\\ &\quad + \frac{w^2\,v\,\left(28v^3-39v^2+6v+1\right)}{12\,(1-v)^4} - \frac{v^4w^3}{(1-v)^4}. \end{aligned} \tag{F.34}$$

Turning to SFP contributions by the function G, the corresponding partonic cross section is given as

$$\hat{\sigma}^{qg\to q,5}_{\mathrm{SFP},G}(v,w,\chi_m) = N_c\,\hat{\sigma}^{qg\to q,5}_{\mathrm{SFP},G,N_c}(v,w,\chi_m) + C_F\,\hat{\sigma}^{qg\to q,5}_{\mathrm{SFP},G,C_F}(v,w,\chi_m)\,, \tag{F.35}$$

where the N_c part reads

$$\begin{aligned}\hat{\sigma}^{qg\to q,5}_{\mathrm{SFP},G,N_c}(v,w,\chi_m) &= A^{qg\to q,5}_{1,\mathrm{SFP},G,N_c}(v,w)\,\log(\chi_m) + A^{qg\to q,5}_{2,\mathrm{SFP},G,N_c}(v,w)\,\log(1-w)\\ &\quad + A^{qg\to q,5}_{3,\mathrm{SFP},G,N_c}(v,w)\,\log(1-v\,w) + A^{qg\to q,5}_{4,\mathrm{SFP},G,N_c}(v,w)\,\log(1-v)\\ &\quad + A^{qg\to q,5}_{5,\mathrm{SFP},G,N_c}(v,w)\,\log(1-v+v\,w) + A^{qg\to q,5}_{6,\mathrm{SFP},G,N_c}(v,w)\,\log(w)\\ &\quad + A^{qg\to q,5}_{7,\mathrm{SFP},G,N_c}(v,w)\,, \end{aligned} \tag{F.36}$$

with seven coefficients

$$\begin{aligned}A^{qg\to q,5}_{1,\mathrm{SFP},G,N_c}(v,w) &= -\frac{v^3w^3}{(1-v)^4} - \frac{v^2w^2}{(1-v)^3} - \frac{v\left(v^2-4v+5\right)w}{2(1-v)^4} - \frac{v^2-4v+2}{(1-v)^4}\\ &\quad + \frac{4v^2w-v(6w+3)+5}{2\,(1-v)^3\,(1-v\,w)^2}\,,\\ A^{qg\to q,5}_{2,\mathrm{SFP},G,N_c}(v,w) &= -\frac{v^2(1+v)w^2}{(1-v)^4} - \frac{v^2-4v+2}{(1-v)^4} - \frac{v(5+v)w}{2\,(1-v)^3}\\ &\quad + \frac{4v^2w-v(6w+3)+5}{2\,(1-v)^3\,(1-v\,w)^2}\,, \end{aligned}$$

$$
\begin{aligned}
A^{qg\to q,5}_{3,\mathrm{SFP},G,N_c}(v,w) &= \frac{v^2w^2}{(1-v)^3} - \frac{(3-v)\,v\,w}{(1-v)^3} + \frac{3v-5}{(1-v)^3} + \frac{4v^2w - v(6w+3)+5}{(1-v)^3\,(1-v\,w)^2}\,,\\
A^{qg\to q,5}_{4,\mathrm{SFP},G,N_c}(v,w) &= \frac{2v-3}{v^2\,(1-v)^2\,w} - \frac{2v^3-10v^2+16v-9}{v^2\,(1-v)^3} + \frac{\left(3v^3-v+4\right)w}{2\,v^2\,(1-v)^2}\\
&\quad + \frac{2(3v-5)w^2}{v^2\,(1-v)^2} - \frac{4v^2w-3v(2w+1)+5}{2\,(1-v)^3\,(1-v\,w)^2}\,,\\
A^{qg\to q,5}_{5,\mathrm{SFP},G,N_c}(v,w) &= -\frac{v^2w^2}{(1-v)^3} + \frac{v(1+v)\,w}{2\,(1-v)^3}\,,\\
A^{qg\to q,5}_{6,\mathrm{SFP},G,N_c}(v,w) &= \frac{2v^3w^3}{(1-v)^4} + \frac{3v^2w^2}{(1-v)^4} + \frac{(2-v)v\,w}{(1-v)^3} + \frac{2v^2-4v+3}{(1-v)^4}\\
&\quad - \frac{4v^2w-3v(2w+1)+5}{2\,(1-v)^3\,(1-v\,w)^2}\,,\\
A^{qg\to q,5}_{7,\mathrm{SFP},G,N_c}(v,w) &= \frac{v^4-2v^3-24v^2+37v-18}{6\,(1-v)^4\,v\,w} - \frac{10v^4-35v^3-102v^2+181v-108}{12(1-v)^4v}\\
&\quad + \frac{\left(5v^4-17v^3+23v^2-33v+12\right)w}{6(1-v)^4v} + \frac{\left(9v^4+8v^3-149v^2+242v-120\right)w^2}{12(1-v)^4v}\\
&\quad - \frac{\left(7v^3-6v^2-v-8\right)w^3}{12(1-v)^4} - \frac{4v^2w-v(7w+2)+5}{2\,(1-v)^3\,(1-v\,w)^2} - \frac{1}{2\,(1-v)\,(1-v+v\,w)}\,. \qquad \text{(F.37)}
\end{aligned}
$$

Likewise, the C_F part has the form

$$
\begin{aligned}
\hat{\sigma}^{qg\to q,5}_{\mathrm{SFP},G,C_F}(v,w,\chi_m) &= A^{qg\to q,5}_{1,\mathrm{SFP},G,C_F}(v,w)\,\log(\chi_m) + A^{qg\to q,5}_{2,\mathrm{SFP},G,C_F}(v,w)\,\log(1-w)\\
&\quad + A^{qg\to q,5}_{3,\mathrm{SFP},G,C_F}(v,w)\,\log(1-v\,w) + A^{qg\to q,5}_{4,\mathrm{SFP},G,C_F}(v,w)\,\log(1-v)\\
&\quad + A^{qg\to q,5}_{5,\mathrm{SFP},G,C_F}(v,w)\,\log(1-v+v\,w) + A^{qg\to q,5}_{6,\mathrm{SFP},G,C_F}(v,w)\,\log(w)\\
&\quad + A^{qg\to q,5}_{7,\mathrm{SFP},G,C_F}(v,w)\,, \qquad \text{(F.38)}
\end{aligned}
$$

with seven coefficients

$$
\begin{aligned}
A^{qg\to q,5}_{1,\mathrm{SFP},G,C_F}(v,w) &= \frac{2v^3w^3}{(1-v)^4} - \frac{2(v-2)v^2w^2}{(1-v)^4} + \frac{v\left(v^2-6v+3\right)w}{(1-v)^4} + \frac{5-3v}{(1-v)^3}\\
&\quad - \frac{4v^2w-3v(2w+1)+5}{(1-v)^3\,(1-v\,w)^2}\,,\\
A^{qg\to q,5}_{2,\mathrm{SFP},G,C_F}(v,w) &= \frac{2v^2(v+2)w^2}{(1-v)^4} - \frac{v\left(v^2+6v-3\right)w}{(1-v)^4} + \frac{5-3v}{(1-v)^3} - \frac{4v^2w-3v(2w+1)+5}{(1-v)^3\,(1-v\,w)^2}\,,\\
A^{qg\to q,5}_{3,\mathrm{SFP},G,C_F}(v,w) &= -\frac{2v^2w^2}{(1-v)^3} + \frac{2(3-v)v\,w}{(1-v)^3} + \frac{2(5-3v)}{(1-v)^3} - \frac{2\left(4v^2w-3v(2w+1)+5\right)}{(1-v)^3\,(1-v\,w)^2}\,,\\
A^{qg\to q,5}_{4,\mathrm{SFP},G,C_F}(v,w) &= \frac{6-4v}{(1-v)^2v^2\,w} + \frac{4v^3-20v^2+32v-18}{(1-v)^3v^2} - \frac{\left(3v^3-v+4\right)\,w}{(1-v)^2v^2}\\
&\quad + \frac{4(5-3v)\,w^2}{(1-v)^2v^2} + \frac{4v^2w-v(6w+3)+5}{(1-v)^3\,(1-v\,w)^2}\,,\\
A^{qg\to q,5}_{5,\mathrm{SFP},G,C_F}(v,w) &= -\frac{v(1+v)w}{(1-v)^3} + \frac{2v^2w^2}{(1-v)^3}\,,\\
A^{qg\to q,5}_{6,\mathrm{SFP},G,C_F}(v,w) &= \frac{4v^3w^3}{(1-v)^4} - \frac{2v^2(2v+1)w^2}{(1-v)^4} + \frac{2(v-2)vw}{(1-v)^3} + \frac{3v-5}{(1-v)^3}\\
&\quad + \frac{4v^2w-v(6w+3)+5}{(1-v)^3\,(1-v\,w)^2}\,,
\end{aligned}
$$

$$
\begin{aligned}
A^{qg\to q,5}_{7,\mathrm{SFP},G,C_F}(v,w) &= \frac{-9v^5+22v^4-33v^3+240v^2-390v+180}{30(1-v)^4vw} \\
&+\frac{75v^5-160v^4+129v^3-1140v^2+2100v-1080}{60\,v\,(1-v)^4} \\
&-\frac{\left(12v^5-14v^4-75v^3+60v^2-105v+60\right)w}{15\,v\,(1-v)^4} \\
&-\frac{\left(128v^5-185v^4+325v^3-735v^2+1260v-600\right)w^2}{30\,v\,(1-v)^4} \\
&+\frac{v\left(52v^3-27v^2+6v+1\right)w^3}{6(1-v)^4}-\frac{5v^4w^4}{(1-v)^4} \\
&+\frac{4v^2w-v(7w+2)+5}{(1-v)^3\,(1-v\,w)^2}+\frac{1}{(1-v)\,(1-v+v\,w)}\,. \qquad \text{(F.39)}
\end{aligned}
$$

There is also a SFP derivative term for G with the partonic cross section

$$
\hat{\sigma}^{qg\to q,5}_{\mathrm{SFP},\partial_2 G}(v,w,\chi_m) = N_c\,\hat{\sigma}^{qg\to q,5}_{\mathrm{SFP},\partial_2 G,N_c}(v,w,\chi_m)+C_F\,\hat{\sigma}^{qg\to q,5}_{\mathrm{SFP},\partial_2 G,C_F}(v,w,\chi_m)\,, \qquad \text{(F.40)}
$$

where the N_c part reads

$$
\begin{aligned}
\hat{\sigma}^{qg\to q,5}_{\mathrm{SFP},\partial_2 G,N_c}(v,w) &= A^{qg\to q,5}_{1,\mathrm{SFP},\partial_2 G,N_c}(v,w)\,\log(1-v)+A^{qg\to q,5}_{2,\mathrm{SFP},\partial_2 G,N_c}(v,w)\,\log(w) \\
&+A^{qg\to q,5}_{3,\mathrm{SFP},\partial_2 G,N_c}(v,w)\,, \qquad \text{(F.41)}
\end{aligned}
$$

with three coefficients

$$
\begin{aligned}
A^{qg\to q,5}_{1,\mathrm{SFP},\partial_2 G,N_c}(v,w) &= \frac{3-2v}{2\,v^2\,(1-v)^2\,w}+\frac{2(2v-3)}{v^2\,(1-v)^2}+\frac{(5-3v)w}{v^2\,(1-v)^2}\,, \\
A^{qg\to q,5}_{2,\mathrm{SFP},\partial_2 G,N_c}(v,w) &= -\frac{v^2w\,(1+v\,w)}{(1-v)^4}\,, \\
A^{qg\to q,5}_{3,\mathrm{SFP},\partial_2 G,N_c}(v,w) &= \frac{-v^4+2v^3+24v^2-37v+18}{12\,v\,(1-v)^4\,w}+\frac{7v^4-16v^3-96v^2+144v-72}{12\,v\,(1-v)^4} \\
&-\frac{\left(11v^4-9v^3-38v^2+57v-30\right)w}{6\,v\,(1-v)^4}+\frac{\left(31v^3-6v^2-v-8\right)w^2}{24\,(1-v)^4}. \qquad \text{(F.42)}
\end{aligned}
$$

The C_F part has the analogous form

$$
\begin{aligned}
\hat{\sigma}^{qg\to q,5}_{\mathrm{SFP},\partial_2 G,C_F}(v,w) &= A^{qg\to q,5}_{1,\mathrm{SFP},\partial_2 G,C_F}(v,w)\,\log(1-v)+A^{qg\to q,5}_{2,\mathrm{SFP},\partial_2 G,C_F}(v,w)\,\log(w) \\
&+A^{qg\to q,5}_{3,\mathrm{SFP},\partial_2 G,NC_F}(v,w)\,, \qquad \text{(F.43)}
\end{aligned}
$$

with three coefficients

$$
\begin{aligned}
A^{qg\to q,5}_{1,\mathrm{SFP},\partial_2 G,C_F}(v,w) &= \frac{2v-3}{v^2\,(1-v)^2\,w}-\frac{4(2v-3)}{v^2\,(v-1)^2}+\frac{2(3v-5)w}{v^2\,(1-v)^2}\,, \\
A^{qg\to q,5}_{2,\mathrm{SFP},\partial_2 G,C_F}(v,w) &= -\frac{2v^3w^2}{(1-v)^4}\,, \\
A^{qg\to q,5}_{3,\mathrm{SFP},\partial_2 G,C_F}(v,w) &= \frac{9v^5-22v^4+33v^3-240v^2+390v-180}{60\,v\,(1-v)^4\,w} \\
&-\frac{27v^5-61v^4+65v^3-480v^2+780v-360}{30\,v\,(1-v)^4} \\
&+\frac{\left(64v^5-150v^4+55v^3-360v^2+630v-300\right)w}{30\,v\,(1-v)^4} \\
&-\frac{v\left(28v^3-39v^2+6v+1\right)w^2}{12\,(1-v)^4}+\frac{v^4w^3}{(1-v)^4}\,. \qquad \text{(F.44)}
\end{aligned}
$$

Hard-Pole Contribution

In this paragraph the analytic results of all partonic cross sections encountered in Eq. (6.8) are listed, which gives the $qg \to q$ channel hard-pole contribution

$$\begin{aligned}
\hat{\sigma}^{qg\to q,1}_{\text{HP},F}(v,w,\chi_\mu) &= C_F\Bigg[\frac{\left(v^2-14v+18\right)\log(1-v)}{v^2\,(1-v)^2\,(1-w)_+} \\
&\quad -\frac{75v^5-100v^4+151v^3-1720v^2+2460v-1080}{60\,v\,(1-v)^4\,(1-w)_+}+\frac{2(2v-3)\,\log(1-v)}{v^2\,w\,(1-v)^2} \\
&\quad +\frac{v^5(75w-9)+v^4(22-130w)+v^3(7-30w)-20v^2(w+12)+390v-180}{30\,v\,w\,(1-v)^4}\Bigg] \\
&\quad +N_c\Bigg[\frac{1+v^2}{(1-v)^4}\left(\frac{\log(1-w)}{1-w}\right)_+ +\frac{\left(3v^4+16v^3-43v^2+50v-18\right)\log(1-v)}{2v^2(1-v)^4\,(1-w)_+} \\
&\quad +\frac{(1+v^2)\log(\chi_\mu)}{(1-v)^4\,(1-w)_+}+\frac{16v^4-85v^3-176v^2+133v-108}{12v(1-v)^4\,(1-w)_+} \\
&\quad -\frac{\left(v^4w+2v^3+v^2(w-7)+8v-3\right)\log(1-v)}{v^2\,(1-v)^4w}-\frac{\left(1+v^2\right)\left(\log(1-w)+\log(\chi_\mu)\right)}{2\,(1-v)^4} \\
&\quad +\frac{18+4v^2(6+w)-v^4(13w-1)}{6v\,(1-v)^4w}+\frac{3\left(1+v^2\right)w\left(w^2+2w-1\right)\log(w)}{6\,(1-v)^4w\,(1-w)^2} \\
&\quad -\frac{\left(35w^2-76w+35+v^2\left(45w^2-53w+2\right)\right)}{6\,(1-v)^4w\,(1-w)}\Bigg]. \qquad \text{(F.45)}
\end{aligned}$$

The last two terms are individually divergent for $w \to 1$ but combined they have a well-defined limit.

$$\begin{aligned}
\hat{\sigma}^{qg\to q,1}_{\text{HP},\partial_1 F}(v,w,\chi_\mu) &= C_F\Bigg[-\frac{27v^5-44v^4+291v^3-1600v^2+2040v-840}{60\,v\,(1-v)^4\,(1-w)_+} \\
&\quad +\frac{\left(v^2-13v+14\right)\log(1-v)}{v^2\,(1-v)^2\,(1-w)_+}\Bigg] \\
&\quad +N_c\Bigg[\frac{1+v^2}{(1-v)^4}\left(\frac{\log(1-w)}{1-w}\right)_+ +\frac{\left(3v^4+15v^3-37v^2+41v-14\right)\log(1-v)}{2\,v^2\,(1-v)^4\,(1-w)_+} \\
&\quad +\frac{\left(1+v^2\right)\log(\chi_\mu)}{(1-v)^4\,(1-w)_+}+\frac{6v^4-51v^3-142v^2+115v-84}{12\,v\,(1-v)^4\,(1-w)_+}\Bigg]. \qquad \text{(F.46)}
\end{aligned}$$

$$\begin{aligned}
\hat{\sigma}^{qg\to q,1}_{\text{HP},\partial_1^2 F}(v,w) &= \hat{\sigma}^{qg\to q,1}_{\text{HP},\partial_1\partial_2 F}(v,w) \\
&= C_F\left[\frac{\log(1-v)}{v^2\,(1-v)\,(1-w)_+}-\frac{2v^5-5v^4+22v^3-125v^2+150v-60}{60\,v\,(1-v)^4\,(1-w)_+}\right] \\
&\quad +N_c\left[-\frac{\log(1-v)}{2\,v^2\,(1-v)\,(1-w)_+}+\frac{v^4-4v^3-19v^2+20v-12}{24\,v\,(1-v)^4\,(1-w)_+}\right]. \qquad \text{(F.47)}
\end{aligned}$$

$$
\begin{aligned}
\hat{\sigma}^{qg\to q,1}_{\mathrm{HP},\partial_2 F}(v,w,\chi_\mu) &= C_F\left[\frac{\left(v^2-6v+6\right)\log(1-v)}{v^2\,(1-v)^2\,(1-w)_+}\right.\\
&\quad -\frac{9v^5-7v^4+171v^3-725v^2+900v-360}{60\,v\,(1-v)^4\,(1-w)_+}+\frac{(2v-3)\log(1-v)}{w\,v^2\,(1-v)^2}\\
&\quad \left.+\frac{v^5(30w-9)+v^4(22-45w)+v^3(7-10w)-5v^2(w+48)+390v-180}{60\,w\,v\,(1-v)^4}\right]\\
&\quad +N_c\left[\frac{1+v^2}{(1-v)^4}\left(\frac{\log(1-w)}{1-w}\right)_+ +\frac{\left(3v^4+8v^3-15v^2+18v-6\right)\log(1-v)}{2\,v^2\,(1-v)^4\,(1-w)_+}\right.\\
&\quad +\frac{v\left(24\,v\,\left(1+v^2\right)\log\left(\chi_\mu\right)+3v^4-68v^3-143v^2+74v-72\right)}{24\,v^2\,(1-v)^4\,(1-w)_+}\\
&\quad -\frac{\left(2v^4w+2v^3+v^2(2w-7)+8v-3\right)\log(1-v)}{2\,v^2\,(1-v)^4\,w}-\frac{\left(1+v^2\right)\log(1-w)}{2(1-v)^4}\\
&\quad -\frac{\left(1+v^2\right)\,\log(\chi_\mu)}{2\,(1-v)^4}-\frac{\left(1+v^2\right)\,(1+w)\,\log(w)}{2\,(1-v)^4\,(1-w)}\\
&\quad \left.+\frac{v^4(2-9w)+v^3(70w-4)-v^2(w-48)+v(68w-70)+36}{24\,v\,w\,(1-v)^4}\right]. \qquad \text{(F.48)}
\end{aligned}
$$

$$
\begin{aligned}
\hat{\sigma}^{qg\to q,1}_{\mathrm{HP},G}(v,w,\chi_\mu) &= C_F\left[\frac{\left(v^2-14v+18\right)\log(1-v)}{v^2\,(1-v)^2\,(1-w)_+}+\frac{2(2v-3)\log(1-v)}{v^2\,w\,(1-v)^2}\right.\\
&\quad +\frac{75v^5-100v^4-369v^3+1640v^2-2460v+1080}{60\,v\,(1-v)^4\,(1-w)_+}\\
&\quad \left.+\frac{v^5(9-75w)+2v^4(65w-11)+v^3(30w+33)+20v^2(w-12)+390v-180}{30\,v\,w\,(1-v)^4}\right]\\
&\quad +N_c\left[-\frac{\left(v^2-14v+18\right)\,\log(1-v)}{2\,v^2\,(1-v)^2\,(1-w)_+}-\frac{16v^4-73v^3+160v^2-287v+108}{12\,v\,(1-v)^4\,(1-w)_+}\right.\\
&\quad +\frac{\left(v^4w-2v^3+v^2(w+7)-8v+3\right)\log(1-v)}{v^2\,w\,(1-v)^4}+\frac{1+v^2}{2(1-v)^4}\log\left(\tfrac{1-w}{w}\chi_\mu\right)\\
&\quad \left.+\frac{v^4(13w-1)+v^3(2-51w)-4v^2(w-6)-v(41w+37)+18}{6\,v\,w\,(1-v)^4}\right]. \qquad \text{(F.49)}
\end{aligned}
$$

Because of anti-symmetry $G^q(x_0,x_0)=0$. As a consequence the plus-distribution $1/(1-w)_+$ could be replaced by just $1/(1-w)$ in (F.49).

$$
\begin{aligned}
\hat{\sigma}^{qg\to q,1}_{\mathrm{HP},\partial_1 G}(v,w) &= C_F\left[\frac{27v^5-44v^4-309v^3+1520v^2-2040v+840}{60\,v\,(1-v)^4(1-w)_+}\right.\\
&\quad \left.+\frac{\left(v^2-13v+14\right)\log(1-v)}{v^2\,(1-v)^2\,(1-w)_+}\right]\\
&\quad +N_c\left[-\frac{\left(v^2-13v+14\right)\,\log(1-v)}{2\,v^2\,(1-v)^2\,(1-w)_+}-\frac{6v^4-39v^3+150v^2-209v+84}{12\,v\,(1-v)^4\,(1-w)_+}\right]. \qquad \text{(F.50)}
\end{aligned}
$$

$$
\begin{aligned}
\hat{\sigma}^{qg\to q,1}_{\mathrm{HP},\partial_1^2 G}(v,w) &= \hat{\sigma}^{qg\to q,1}_{\mathrm{HP},\partial_1\partial_2 G}(v,w)\\
&= C_F\left[\frac{\log(1-v)}{v^2\,(1-v)\,(1-w)_+}+\frac{2v^5-5v^4-18v^3+115v^2-150v+60}{60\,v\,(1-v)^4\,(1-w)_+}\right]\\
&\quad +N_c\left[-\frac{\log(1-v)}{2\,v^2\,(1-v)\,(1-w)_+}-\frac{v^4-4v^3+21v^2-28v+12}{24\,v\,(1-v)^4\,(1-w)_+}\right]. \qquad \text{(F.51)}
\end{aligned}
$$

$$\begin{aligned}\hat{\sigma}^{qg\to q,1}_{\text{HP},\partial_2 G}(v,w,\chi_\mu) &= C_F\left[\frac{\left(v^2-6v+6\right)\,\log(1-v)}{v^2\,(1-v)^2\,(1-w)_+}\right.\\ &+\frac{9v^5-7v^4-189v^3+715v^2-900v+360}{60\,v\,(1-v)^4\,(1-w)_+}+\frac{(2v-3)\,\log(1-v)}{v^2\,w\,(1-v)^2}\\ &\left.+\frac{v^5(9-30w)+v^4(45w-22)+v^3(10w+33)+5v^2(w-48)+390v-180}{60\,v\,w\,(1-v)^4}\right]\\ &+N_c\left[-\frac{\left(v^2-6v+6\right)\,\log(1-v)}{2\,v^2\,(1-v)^2\,(1-w)_+}-\frac{3v^4-44v^3+145v^2-190v+72}{24\,v\,(1-v)^4\,(1-w)_+}\right.\\ &+\frac{\left(2v^4w-2v^3+v^2(2w+7)-8v+3\right)\log(1-v)}{2\,v^2\,w\,(1-v)^4}+\frac{1+v^2}{2(1-v)^4}\log\left(\tfrac{1-w}{w}\chi_\mu\right)\\ &\left.+\frac{v^4(9w-2)+v^3(4-70w)+v^2(w+48)-2v(34w+37)+36}{24\,v\,w\,(1-v)^4}\right]. \end{aligned}\tag{F.52}$$

F.1.2 Channel $qq\to q$:

Integral Contribution

The $qq\to q$ channel integral contribution in Eq. 6.10 features partonic cross sections that have the following explicit form

$$\begin{aligned}\hat{\sigma}^{qq\to q,1}_{\text{Int},1}(v,w,\zeta) &= \frac{1}{N_c}\frac{w}{4(1-\zeta)\zeta(1-v)^4}\left[v(w-\zeta)^2\left(\zeta(2\zeta-1)\right.\right.\\ &+v^2\left(\zeta(2\zeta-1)+\left(8\zeta^2-4\zeta-2\right)w^2+2(3-4\zeta)\zeta w\right)-2v\left(\zeta^2-3\zeta w+w\right)\big)\\ &+\text{sgn}(w-\zeta)\left(v^3(w-\zeta)^2\left(\zeta(2\zeta-1)+2w^2-2\zeta w\right)\right.\\ &+\zeta v\left(\zeta^2(2\zeta-1)+(6\zeta-5)w^2+2(3-4\zeta)\zeta w\right)+2\zeta\left(2\zeta^2-3\zeta+1\right)w\\ &\left.\left.+2v^2\left(-\zeta^4+(\zeta+1)w^3-(\zeta+4)\zeta w^2+\left(3\zeta^3+\zeta\right)w\right)\right)\right], \end{aligned}\tag{F.53}$$

$$\begin{aligned}\hat{\sigma}^{qq\to q,5}_{\text{Int},1}(v,w,\zeta) &= -\frac{1}{N_c}\frac{w}{4(1-\zeta)\zeta(1-v)^4}\left[v(w-\zeta)^2\left(\zeta+v^2\left(\zeta+(4\zeta-2)w^2-2\zeta w\right)\right.\right.\\ &+v\left(\left(8\zeta^2-6\zeta-2\right)w-2\zeta^2\right)\big)+\text{sgn}(w-\zeta)\left(v^3(w-\zeta)^2\left(\zeta+2w^2-2\zeta w\right)\right.\\ &-2v^2\left(\zeta^4+(\zeta-1)w^3+\zeta^2w^2+\left(\zeta-3\zeta^3\right)w\right)\\ &\left.\left.+\zeta v\left(\zeta^2+(5-4\zeta)w^2+2\zeta(2\zeta-3)w\right)+2(\zeta-1)\zeta w\right)\right], \end{aligned}\tag{F.54}$$

$$\begin{aligned}\hat{\sigma}^{qq\to q,1}_{\text{Int},2}(v,w,\zeta) &= \frac{1}{N_c}\frac{v\,w}{4\,\zeta\,(1-v)^4}\left(\frac{2\zeta^2-3\zeta-2v^2(1-w-\zeta)^2\text{sgn}(1-w-\zeta)}{1-\zeta}\right.\\ &+\frac{v^2\left(2\zeta^2-3\zeta+2\left(4\zeta^2-6\zeta+1\right)w^2-2\left(4\zeta^2-5\zeta+1\right)w+1\right)+2(\zeta-1)v(w-\zeta)+1}{1-\zeta}\\ &+\frac{1-v}{\left[1-2v(1-w-\zeta+2\zeta w)+v^2(1-w-\zeta)^2\right]^{\frac{3}{2}}}\Big(2\zeta+v^4(1-2w)(1-w-\zeta)^3\\ &+v^3\left((1-\zeta)^2\left(2\zeta^2-3\zeta-2\right)+(5-6\zeta)w^3+\left(-6\zeta^2+17\zeta-12\right)w^2\right.\\ &+\left(2\zeta^3+\zeta^2-12\zeta+9\right)w\big)+v^2\left(3\zeta\left(2\zeta^2-5\zeta+3\right)+\left(3-4\zeta^2\right)w^2\right.\\ &\left.\left.-\left(4\zeta^3-22\zeta^2+12\zeta+3\right)w\right)-v\left(-6\zeta^2+9\zeta+12\zeta^2w-12\zeta w+w-2\right)-1\Big)\right), \end{aligned}\tag{F.55}$$

$$\hat{\sigma}^{qq\to q,5}_{\mathrm{Int},2}(v,w,\zeta) = \frac{1}{N_c}\frac{v\,w}{4\,\zeta\,(1-v)^4}\left(\frac{-\zeta-2v^2(1-\zeta-w)^2\,\mathrm{sgn}(1-w-\zeta)}{1-\zeta}\right.$$
$$+\frac{v^2\left(-\zeta+(2-4\zeta)w^2-2(1-\zeta)w+1\right)+2(1-\zeta)v((4\zeta-1)w-\zeta)+1}{1-\zeta}$$
$$+\frac{1-v}{[1-2v(1-w-\zeta+2\zeta w)+v^2(1-w-\zeta)^2]^{\frac{3}{2}}}\left(v^4(1-w-\zeta)^3(1-2w-2\zeta)\right.$$
$$+v^3\left[(1-\zeta)^2(5\zeta-2)+(5-16\zeta)w^3+\left(-32\zeta^2+45\zeta-12\right)w^2\right.$$
$$\left.\left.+\left(-16\zeta^3+45\zeta^2-38\zeta+9\right)w\right]+v^2\left[-3(1-\zeta)\zeta+\left(32\zeta^2-22\zeta+3\right)w^2\right.\right.$$
$$\left.\left.+\left(-22\zeta^2+22\zeta-3\right)w\right]-v(\zeta+2\zeta w+w-2)-1)\right)\,. \tag{F.56}$$

Soft-Fermion Pole Contribution

Next, in Eq. (6.12) for the soft-fermion pole contribution to the $qq\to q$ channel one has the partonic cross sections

$$\hat{\sigma}^{qq\to q,1}_{\mathrm{SFP},F}(v,w,\chi_m) = \frac{-1}{2N_c}\left[\frac{2v^3w\left(2w^2-2w+1\right)+v^2\left(-6w^2+2w-1\right)+4vw-1}{(1-v)^4}\log\chi_m\right.$$
$$+\frac{vw(1+v(1-4w))}{(1-v)^3}\log(1-v)+\frac{2v^2w^2}{(1-v)^3}\log(1-v\,w)-\frac{vw(1+v-2vw)}{(1-v)^3}\log(1-v+v\,w)$$
$$+\left(\frac{v}{(1-v)^2\,w}-\frac{1+4v}{(1-v)^2}+\frac{v\left(7v^2-8v+5\right)w}{(1-v)^4}-\frac{2v^2(3v+1)w^2}{(1-v)^4}+\frac{4v^3w^3}{(1-v)^4}\right)\log(1-w)$$
$$+\frac{2v^3(5-2w)w^2+v^2\left(-2w^2+6w-1\right)+2vw-1}{(1-v)^4}\log w-\frac{8v^3w^3}{(1-v)^4}+\frac{\left(7v^3-8v+4\right)w}{(1-v)^4}$$
$$\left.-\frac{v^3+v^2-7v+3}{(1-v)^4}+\frac{2v(3v-1)w^2}{(1-v)^4}+\frac{1}{(1-v)\,(1-v+v\,w)}\right], \tag{F.57}$$

$$\hat{\sigma}^{qq\to q,5}_{\mathrm{SFP},G}(v,w,\chi_m) = \frac{-1}{2N_c}\left[\frac{2v^3w\left(2w^2-2w+1\right)+v^2\left(-6w^2+2w-1\right)+4vw-1}{(1-v)^4}\log\chi_m\right.$$
$$+\frac{v\,(1+v)\,w}{(1-v)^3}\log(1-v)-\frac{2v^2w^2}{(1-v)^3}\log(1-v\,w)-\frac{vw(1+v-2vw)}{(1-v)^3}\log(1-v+v\,w)$$
$$+\left(-\frac{v}{(1-v)^2\,w}-\frac{4v^2-v+1}{(1-v)^3}+\frac{v(7v+3)w}{(1-v)^3}-\frac{6v^2w^2}{(1-v)^3}\right)\log(1-w)$$
$$+\frac{-6v^3w^2+v^2\left(6w^2-2w-1\right)+2vw-1}{(1-v)^4}\log w+\frac{8v^2w^2}{(1-v)^4}-\frac{v^3+v^2-5v+1}{(1-v)^4}$$
$$\left.-\frac{v(6v+5)w}{(1-v)^4}+\frac{1}{(1-v)\,(1-v+v\,w)}\right]. \tag{F.58}$$

Hard-Pole Contribution

The $qq\to q$ channel is concluded by the hard pole contribution in Eq. (6.13), where one has the following partonic cross sections

$$\hat{\sigma}^{qq\to q,1}_{\mathrm{HP},F}(v,w,\chi_\mu) = -\frac{1}{2N_c}\left[\delta(1-w)\,\frac{1+v^2}{(1-v)^4}\left(\log\chi_\mu+2\log(1-v)\right)\right.$$
$$+\frac{2(1+v^2)}{(1-v)^4\,(1-w)_+}+\frac{v^3\left(8w^2-7w+1\right)-9v^2w+v(7w-3)-8w+2}{(1-v)^4}$$
$$-\frac{1+v^2}{(1-v)^4}\left(\log\chi_\mu+2\,\log(1-v)\right)+\frac{2\,v\,(1+v)\,w}{(1-v)^4}\log v+\frac{1-4v^3w^2+v^2(1-4w)}{(1-v)^4}\log w$$
$$\left.+\frac{v^3\left(4w^3-6w^2+4w-1\right)+v^2\left(8w^2-9w+2\right)+v(2w-1)-w}{(1-v)^4\,w}\log(1-w)\right], \tag{F.59}$$

$$\hat{\sigma}^{qq\to q,1}_{\rm HP,\partial F}(v,w,\chi_\mu) = \frac{1}{2N_c}\Bigg[\frac{(1+v^2)\,(1-2w)}{(1-v)^4}\,(\log\chi_\mu+2\,\log(1-v))$$
$$+\frac{v^3\left(-4w^2+5w-1\right)+v^2(7w-2)+v(3-5w)+8w-4}{(1-v)^4}$$
$$+\frac{v^3\left(-2w^3+4w^2-3w+1\right)+v^2\left(-6w^2+7w-2\right)-vw+v-2w^2+w}{(1-v)^4\,w}\,\log(1-w)$$
$$+\frac{2v^3w^2+v^2(4w-1)+2w-1}{(1-v)^4}\,\log w\Bigg], \tag{F.60}$$

$$\hat{\sigma}^{qq\to q,5}_{\rm HP,G}(v,w,\chi_\mu) = -\frac{1}{2N_c}\Bigg[-\delta(1-w)\,\frac{1+v^2}{(1-v)^4}\,(\log\chi_\mu+2\log(1-v))$$
$$-\frac{2(1+v^2)}{(1-v)^4\,(1-w)_+}+\frac{v^3+v^2(w+4)+v(8w-1)+4}{(1-v)^4}$$
$$-\frac{1+v^2}{(1-v)^4}\,(\log\chi_\mu+2\,\log(1-v))+\frac{2\,v\,(1+v)\,w}{(1-v)^4}\log v+\frac{1+4v^3w^2+v^2(1+4w)}{(1-v)^4}\,\log w$$
$$+\frac{v^3\left(-4w^3+6w^2-4w+1\right)+v^2(3w-2)-2vw+v-w}{(1-v)^4\,w}\,\log(1-w)\Bigg], \tag{F.61}$$

$$\hat{\sigma}^{qq\to q,5}_{\rm HP,\partial G}(v,w,\chi_\mu) = \frac{1}{2N_c}\Bigg[\frac{1+v^2}{(1-v)^4}\,(\log\chi_\mu+2\,\log(1-v))$$
$$+\frac{-v^3+v^2(w-2)-4vw+v-2}{(1-v)^4}-\frac{2v^3w^2+v^2(2w+1)+1}{(1-v)^4}\,\log w$$
$$+\frac{v^3\left(2w^3-4w^2+3w-1\right)-v^2(w-2)+v(w-1)+w}{(1-v)^4\,w}\,\log(1-w)\Bigg], \tag{F.62}$$

F.1.3 Channel $qq\to q'$:

Integral Contribution

For the $qq\to q'$ channel integral contribution in Eq. (6.15) one has the following partonic cross sections

$$\hat{\sigma}^{qq\to q',1}_{\rm Int,1}(v,w,\zeta) = \frac{v\,w}{4\,(1-v)^4}\Bigg(\frac{(2\zeta-1)(1-v)^2(1+v(w-\zeta))}{\sqrt{1-2\zeta v+2(2\zeta-1)vw+v^2(w-\zeta)^2}}$$
$$+\frac{1}{\zeta}\mathrm{sgn}(w-\zeta)\left(\zeta(2\zeta-1)+v^2\left(\zeta(4\zeta-1)+4w^2-6\zeta w\right)+2\zeta v(w-\zeta)\right)$$
$$+\frac{2v}{\zeta}\Big(2(\zeta-1)\zeta v^2w\left(6\zeta+2(6\zeta-1)w^2+(2-16\zeta)w-1\right)$$
$$+v\left(\zeta^2+\left(8\zeta^2-4\zeta-2\right)w^2+\zeta\left(-4\zeta^2-2\zeta+3\right)w\right)$$
$$+\zeta\left(\zeta+\left(4\zeta^2-6\zeta+3\right)w-1\right)\Big)\Bigg),$$
$$\hat{\sigma}^{qq\to q',1}_{\rm Int,2}(v,w,\zeta) = -\hat{\sigma}^{qq\to q',1}_{\rm Int,1}(v,w,1-\zeta)\,,$$
$$\hat{\sigma}^{qq\to q',1}_{\rm Int}(v,w,\zeta) \equiv \hat{\sigma}^{qq\to q',1}_{\rm Int,1}(v,w,\zeta)+\hat{\sigma}^{qq\to q',1}_{\rm Int,2}(v,w,\zeta)\,. \tag{F.63}$$

$$
\begin{aligned}
\hat{\sigma}^{qq\to q',5}_{\text{Int},1}(v,w,\zeta) &= \frac{v\,w}{4\,(1-v)^4}\Bigg(- \frac{(1-v)^2(1+v(w-\zeta))}{\sqrt{1-2\zeta v+2(2\zeta-1)vw+v^2(w-\zeta)^2}} \\
&\quad -\frac{1}{\zeta}\text{sgn}(w-\zeta)\left(\zeta+v^2\left(2\zeta^2+\zeta+4w^2-6\zeta w\right)+2\zeta v(w-\zeta)\right) \\
&\quad -\frac{2v}{\zeta}\Big(-2(1-\zeta)\zeta v^2 w\left(2w^2-2w+1\right)+v\left(\zeta^2+(4\zeta-2)w^2+3(1-2\zeta)\zeta w\right) \\
&\quad +\zeta(-\zeta+(6\zeta-5)w+1)\Big)\Bigg)\,, \\
\hat{\sigma}^{qq\to q',5}_{\text{Int},2}(v,w,\zeta) &= +\hat{\sigma}^{qq\to q',5}_{\text{Int},1}(v,w,1-\zeta)\,, \\
\hat{\sigma}^{qq\to q',5}_{\text{Int}}(v,w,\zeta) &\equiv \hat{\sigma}^{qq\to q',5}_{\text{Int},1}(v,w,\zeta)+\hat{\sigma}^{qq\to q',5}_{\text{Int},2}(v,w,\zeta)\,.
\end{aligned}
\tag{F.64}
$$

Soft-Fermion Pole Contribution

The formula for the $qq\to q'$ channel soft-fermion pole contribution of Eq. 6.17 features the following partonic cross sections

$$
\begin{aligned}
\hat{\sigma}^{qq\to q',1}_{\text{SFP},F}(v,w,\chi_m) &= \frac{1}{2}\Bigg[\Bigg(\frac{4v^4w^4}{(1-v)^4}-\frac{4v^3(v+1)w^3}{(1-v)^4}+\frac{2v^2\left(v^2+2\right)w^2}{(1-v)^4} \\
&\quad -\frac{2v^2w}{(1-v)^4}+\frac{1}{(1-v)^2}-\frac{1}{(1-v)^2(1-v\,w)}\Bigg)\log\chi_m+\frac{w\left(4vw^2+v-4w\right)}{(1-v)^2\,(1-v\,w)}\log(1-v) \\
&\quad -\frac{vw(1+v\,w)}{(1-v)^2\,(1-v\,w)}\log(1-v\,w)-\frac{v\,w}{(1-v)^2}\log(1-v+v\,w) \\
&\quad +\Big(\frac{4v^4w^4}{(1-v)^4}-\frac{4v^4w^3}{(1-v)^4}+\frac{2\left(v^2-3v+3\right)v^2w^2}{(1-v)^4}+\frac{(1-3v)vw}{(1-v)^3}+\frac{1}{(1-v)^2} \\
&\quad -\frac{1}{(1-v)^2\,(1-v\,w)}\Big)\log(1-w)+\Bigg(-\frac{4v^4w^4}{(1-v)^4}+\frac{4v^4w^3}{(1-v)^4}-\frac{2\left(v^2+3v+1\right)v^2w^2}{(1-v)^4} \\
&\quad -\frac{vw}{(1-v)^2}-\frac{1}{(1-v)^2}+\frac{1}{(1-v)^2(1-v\,w)}\Bigg)\log w-\frac{12v^4w^4}{(1-v)^4}+\frac{12v^3(v+2)w^3}{(1-v)^4} \\
&\quad -\frac{2v^2\left(2v^2+8v+1\right)w^2}{(1-v)^4}+\frac{2v^2w}{(1-v)^4}\Bigg]\,,
\end{aligned}
\tag{F.65}
$$

$$
\begin{aligned}
\hat{\sigma}^{qq\to q',5}_{\text{SFP},G}(v,w,\chi_m) &= \frac{1}{2}\Bigg[\Bigg(\frac{4v^4w^4}{(1-v)^4}-\frac{4v^3(v+1)w^3}{(1-v)^4}+\frac{2v^2\left(v^2+2\right)w^2}{(1-v)^4} \\
&\quad -\frac{2v^2w}{(1-v)^4}+\frac{1}{(1-v)^2}-\frac{1}{(1-v)^2(1-v\,w)}\Bigg)\log\chi_m+\frac{v\,w}{(1-v)^2\,(1-v\,w)}\log(1-v) \\
&\quad -\frac{vw(1+v\,w)}{(1-v)^2\,(1-v\,w)}\log(1-v\,w)-\frac{v\,w}{(1-v)^2}\log(1-v+v\,w) \\
&\quad +\Bigg(\frac{4v^4w^4}{(1-v)^4}-\frac{4v^4w^3}{(1-v)^4}+\frac{2\left(v^2-3v+3\right)v^2w^2}{(1-v)^4}+\frac{(1-3v)vw}{(1-v)^3}+\frac{1}{(1-v)^2} \\
&\quad -\frac{1}{(1-v)^2\,(1-v\,w)}\Bigg)\log(1-w)+\Bigg(-\frac{4v^4w^4}{(1-v)^4}+\frac{4v^4w^3}{(1-v)^4}-\frac{2\left(v^2-3v+3\right)v^2w^2}{(1-v)^4} \\
&\quad -\frac{vw}{(1-v)^2}-\frac{1}{(1-v)^2}+\frac{1}{(1-v)^2(1-v\,w)}\Bigg)\log w-\frac{4v^4w^4}{(1-v)^4}+\frac{4v^4w^3}{(1-v)^4} \\
&\quad -\frac{2v^2w^2}{(1-v)^4}+\frac{2v^2w}{(1-v)^4}\Bigg]\,.
\end{aligned}
\tag{F.66}
$$

F.1.4 Channel $qg\to g$:

Integral Contribution

For the $qg\to g$ channel the collection of partonic cross sections is again started with the integral contribution, cf. Eq. (6.19). Once more the splitting by color factors C_F and N_c is performed,

familiar from the $qg \to q$ channel

$$\hat{\sigma}^{qg\to g,1}_{\rm Int}(v,w,\zeta) \;=\; C_F\,\hat{\sigma}^{qg\to g,1}_{{\rm Int},C_F}(v,w,\zeta) + N_c\,\hat{\sigma}^{qg\to g,1}_{{\rm Int},N_c}(v,w,\zeta)\,, \tag{F.67}$$

with

$$\begin{aligned}\hat{\sigma}^{qg\to g,1}_{{\rm Int},C_F}(v,w,\zeta) \;=\;& \frac{v\,w}{2\,(1-v)^4}\left(-\zeta(1-2v-v^2) - 2(1-\zeta)\zeta v^3 w\left(6w^2-8w+3\right)\right.\\ & -2\left(4\zeta^2-6\zeta+\tfrac{1}{\zeta}\right)v^2\,w^2 + 4\left(\zeta^2-3\zeta+1\right)v^2\,w + 2\left(\zeta^2+\zeta-2\right)v\,w + 2v\\ & + \frac{(1+\zeta)(1-v)^2(1+v(w-\zeta))}{\sqrt{1-2\zeta v+2(2\zeta-1)vw+v^2(w-\zeta)^2}}\\ & \left.+{\rm sgn}(w-\zeta)\left(1+v^2\left(1+\frac{2(w-\zeta)^2}{\zeta}\right)\right)\right)\,,\end{aligned} \tag{F.68}$$

$$\begin{aligned}\hat{\sigma}^{qg\to g,1}_{{\rm Int},N_c}(v,w,\zeta) \;=\;& \frac{vw}{4\,(1-v)^4}\left(-(2+\zeta) - v^2\left(\zeta+\left(4\zeta-\tfrac{2}{\zeta}\right)w^2 + 2(1-2\zeta)w\right)\right.\\ & -2(1-2\zeta)vw - {\rm sgn}(w-\zeta)\,\left(1+v^2+v^2\left(2\,\zeta+2\tfrac{w^2}{\zeta}-4\,w\right)\right)\\ & -\frac{(1-v)}{\left[1-2\zeta v+2(2\zeta-1)vw+v^2(w-\zeta)^2\right]^{\frac{3}{2}}}\left[-1-\zeta+v^4(w-\zeta)^3(-\zeta+2w-1)\right.\\ & +v^3\left(\zeta^2\left(\zeta^2-2\zeta-3\right)+(11\zeta-7)w^3+\left(-19\zeta^2+4\zeta+3\right)w^2+\zeta^2(7\zeta+5)w\right)\\ & +(\zeta-1)v^2\left(-3\zeta(\zeta+1)+(14\zeta-5)w^2+\left(2\zeta^2-2\zeta+1\right)w\right)\\ & \left.\left.+v\left(3\zeta^2+2\zeta+\left(-6\zeta^2+\zeta+1\right)w-1\right)\right]\right)\,,\end{aligned} \tag{F.69}$$

and

$$\hat{\sigma}^{qg\to g,5}_{\rm Int}(v,w,\zeta) \;=\; C_F\,\hat{\sigma}^{qg\to g,5}_{{\rm Int},C_F}(v,w,\zeta) + N_c\,\hat{\sigma}^{qg\to g,5}_{{\rm Int},N_c}(v,w,\zeta)\,, \tag{F.70}$$

with

$$\begin{aligned}\hat{\sigma}^{qg\to g,5}_{{\rm Int},C_F}(v,w,\zeta) \;=\;& \frac{v\,w}{2\,(1-v)^4}\left(\zeta(1-2v-v^2) + 2(1-\zeta)\zeta v^3 w\left(6w^2-8w+3\right)\right.\\ & +2\left(4\zeta^2-6\zeta+\tfrac{1}{\zeta}\right)v^2\,w^2 - 4\left(\zeta^2-3\zeta+1\right)v^2\,w - 2(1-\zeta)(2-\zeta)v\,w + 2v\\ & + \frac{(1-\zeta)(1-v)^2(1+v(w-\zeta))}{\sqrt{1-2\zeta v+2(2\zeta-1)vw+v^2(w-\zeta)^2}}\\ & \left.+{\rm sgn}(w-\zeta)\left(1+v^2-v^2\left(2\zeta+\tfrac{2w^2}{\zeta}-4w\right)\right)\right)\,,\end{aligned} \tag{F.71}$$

$$\begin{aligned}\hat{\sigma}^{qg\to g,5}_{{\rm Int},N_c}(v,w,\zeta) \;=\;& \frac{v\,w}{4\,(1-v)^4}\left(-(2-\zeta) + v^2\left(\zeta+\left(4\zeta-\tfrac{2}{\zeta}\right)w^2 + 2(1-2\zeta)w\right)\right.\\ & +2(1-2\zeta)vw - {\rm sgn}(w-\zeta)\left(1+v^2-v^2\,\left(2\,\zeta+\tfrac{2\,w^2}{\zeta}-4\,w\right)\right)\\ & +\frac{(1-v)}{\left[1-2\zeta v+2(2\zeta-1)vw+v^2(w-\zeta)^2\right]^{\frac{3}{2}}}\left[1-\zeta+v^4(w-\zeta)^3(-\zeta+2w+1)\right.\\ & +v^3\left(\zeta^2\left(\zeta^2-4\zeta+3\right)+(11\zeta-5)w^3+\left(-19\zeta^2+10\zeta-3\right)w^2+\zeta^2(7\zeta-1)w\right)\\ & +v^2\left(-3(\zeta-1)^2\zeta+\left(14\zeta^2-15\zeta+7\right)w^2+\left(2\zeta^3-8\zeta^2-\zeta+1\right)w\right)\\ & \left.\left.+v\left(3\zeta^2-4\zeta+\left(-6\zeta^2+13\zeta-5\right)w+1\right)\right]\right)\,.\end{aligned} \tag{F.72}$$

Soft-Gluon Pole Contribution

Next are the partonic cross sections for the $qg \to g$ channel soft-gluon pole appearing in Eq. (6.21). Again, separation by color factors is applied

$$\hat{\sigma}^{qg\to g,1}_{{\rm SGP},F}(v,w,\chi_\mu,\chi_m) = C_F\,\hat{\sigma}^{qg\to g,1}_{{\rm SGP},F,C_F}(v,w,\chi_\mu) + N_c\,\hat{\sigma}^{qg\to g,1}_{{\rm SGP},F,N_c}(v,w,\chi_m)\,, \tag{F.73}$$

with

$$\begin{aligned}\hat{\sigma}^{qg\to g,1}_{\mathrm{SGP},F,C_F}(v,w,\chi_\mu) &= A^{qg\to g,1}_{1,\mathrm{SGP},F,C_F}(v,\chi_\mu)\,\delta(1-w)\\ &\quad + A^{qg\to g,1}_{2,\mathrm{SGP},F,C_F}(v)\frac{1}{(1-w)_+} + A^{qg\to g,1}_{3,\mathrm{SGP},F,C_F}(v,w)\,\log(\chi_\mu)\\ &\quad + A^{qg\to g,1}_{4,\mathrm{SGP},F,C_F}(v,w)\,\log(1-w) + A^{qg\to g,1}_{5,\mathrm{SGP},F,C_F}(v,w)\,\log(1-v)\\ &\quad + A^{qg\to g,1}_{6,\mathrm{SGP},F,C_F}(v,w)\,\log(1-v+v\,w) + A^{qg\to g,1}_{7,\mathrm{SGP},F,C_F}(v,w)\,\log(w)\\ &\quad + A^{qg\to g,1}_{8,\mathrm{SGP},F,C_F}(v,w)\,. \end{aligned} \tag{F.74}$$

The eight coefficients are

$$\begin{aligned}A^{qg\to g,1}_{1,\mathrm{SGP},F,C_F}(v,\chi_\mu) &= \frac{v\left(1+v^2\right)}{(1-v)^4}\log\chi_\mu + \frac{2v^3+5v^2+1}{2\,(1-v)^4}\log(1-v) - \frac{v^4-8v^3+9v^2-6v}{4\,(1-v)^4}\,,\\ A^{qg\to g,1}_{2,\mathrm{SGP},F,C_F}(v) &= \frac{3\,v\,\left(1+v^2\right)}{2\,(1-v)^4}\,,\\ A^{qg\to g,1}_{3,\mathrm{SGP},F,C_F}(v,w) &= -\frac{6v^4w^4}{(1-v)^4} + \frac{8v^4w^3}{(1-v)^4} - \frac{\left(3v^2-2v+3\right)v^2w^2}{(1-v)^4} + \frac{2}{(1-v)^2}\\ &\quad + \frac{v(2-4w)-2}{(1-v)\,(1-v+v\,w)^2}\,,\\ A^{qg\to g,1}_{4,\mathrm{SGP},F,C_F}(v,w) &= -\frac{6v^4w^4}{(1-v)^4} + \frac{v^3(8v-1)w^3}{(1-v)^4} - \frac{v^2\left(3v^2-2v+3\right)w^2}{(1-v)^4} - \frac{v(v+1)w}{2(1-v)^3}\\ &\quad + \frac{2}{(1-v)^2} + \frac{v(2-4w)-2}{(1-v)\,(1-v+v\,w)^2}\,,\\ A^{qg\to g,1}_{5,\mathrm{SGP},F,C_F}(v,w) &= -\frac{12v^4w^4}{(1-v)^4} + \frac{16v^4w^3}{(1-v)^4} - \frac{2\left(3v^2-2v+3\right)v^2w^2}{(1-v)^4} + \frac{2}{(1-v)^2}\\ &\quad + \frac{v(2-4w)-2}{(1-v)\,(1-v+v\,w)^2}\,,\\ A^{qg\to g,1}_{6,\mathrm{SGP},F,C_F}(v,w) &= \frac{4v^2w^2}{(1-v)^2\,(1-v+v\,w)^2}\,,\\ A^{qg\to g,1}_{7,\mathrm{SGP},F,C_F}(v,w) &= \frac{6v^4w^4}{(1-v)^4} - \frac{v^3(8v-1)w^3}{(1-v)^4} + \frac{v^2\left(3v^2-2v+3\right)w^2}{(1-v)^4} - \frac{2}{(1-v)^2}\\ &\quad + \frac{v(4w-2)+2}{(1-v)\,(1-v+v\,w)^2}\,,\\ A^{qg\to g,1}_{8,\mathrm{SGP},F,C_F}(v,w) &= \frac{3v^4w^4}{(1-v)^4} - \frac{2v^3(8+v)w^3}{(1-v)^4} + \frac{v^2\,(11v-2)\,w^2}{(1-v)^4} + \frac{3v\left(v^2-4v+1\right)w}{2(1-v)^4}\\ &\quad + \frac{3v^3-26v^2+31v-14}{2(1-v)^4} + \frac{11-3v}{(1-v)(1-v+v\,w)} - \frac{4}{(1-v+v\,w)^2}\,. \end{aligned} \tag{F.75}$$

The N_c-part reads

$$\begin{aligned}\hat{\sigma}^{qg\to g,1}_{\mathrm{SGP},F,N_c}(v,w,\chi_m) &= A^{qg\to g,1}_{1,\mathrm{SGP},F,N_c}(v,\chi_m)\,\delta(1-w)\\ &\quad + A^{qg\to g,1}_{2,\mathrm{SGP},F,N_c}(v)\frac{1}{(1-w)_+} + A^{qg\to g,1}_{3,\mathrm{SGP},F,N_c}(v,w)\,\log(\chi_m)\\ &\quad + A^{qg\to g,1}_{4,\mathrm{SGP},F,N_c}(v,w)\,\log(1-w) + A^{qg\to g,1}_{5,\mathrm{SGP},F,N_c}(v,w)\,\log(1-v)\\ &\quad + A^{qg\to g,1}_{6,\mathrm{SGP},F,N_c}(v,w)\,\log(1-v\,w) + A^{qg\to g,1}_{7,\mathrm{SGP},F,N_c}(v,w)\,\log(w)\\ &\quad + A^{qg\to g,1}_{8,\mathrm{SGP},F,N_c}(v,w)\,, \end{aligned} \tag{F.76}$$

with the eight coefficients

$$
\begin{aligned}
A^{qg\to g,1}_{1,\mathrm{SGP},F,N_c}(v,\chi_m) &= \frac{v^3-2v^2+2v}{2\,(1-v)^4}\log(\chi_m)+\frac{1-2v}{2\,(1-v)^4}\log(1-v)-\frac{(1+v)v^2}{4\,(1-v)^4}\,,\\
A^{qg\to g,1}_{2,\mathrm{SGP},F,N_c}(v) &= \frac{v\,(3-v)}{4\,(1-v)^3}\,,\\
A^{qg\to g,1}_{3,\mathrm{SGP},F,N_c}(v,w) &= -\frac{2v^3w^3}{(1-v)^4}+\frac{v^2(v+1)w^2}{(1-v)^4}+\frac{1}{(1-v)^3}-\frac{3-v}{(1-v)^3\,(1-v\,w)}\\
&\quad+\frac{3-2v}{(1-v)^3(1-v\,w)^2}-\frac{1}{(1-v)^2\,(1-v\,w)^3}\,,
\end{aligned}
$$

$$
\begin{aligned}
A^{qg\to g,1}_{4,\mathrm{SGP},F,N_c}(v,w) &= -\frac{3v^3w^3}{2\,(1-v)^4}+\frac{v^2(v+1)w^2}{(1-v)^4}+\frac{v(1+v)w}{4\,(1-v)^3}-\frac{3-v}{(1-v)^3\,(1-v\,w)}\\
&\quad+\frac{3-2v}{(1-v)^3\,(1-v\,w)^2}-\frac{1}{(1-v)^2\,(1-v\,w)^3}+\frac{1}{(1-v)^3}\,,\\
A^{qg\to g,1}_{5,\mathrm{SGP},F,N_c}(v,w) &= -\frac{v^3(1-w)w^2}{(1-v)^3\,(1-v\,w)^3}\,,\\
A^{qg\to g,1}_{6,\mathrm{SGP},F,N_c}(v,w) &= \frac{2v^3(1-w)w^2}{(1-v)^3\,(1-v\,w)^3}\,,\\
A^{qg\to g,1}_{7,\mathrm{SGP},F,N_c}(v,w) &= \frac{3v^3w^3}{2\,(1-v)^4}-\frac{v^2(1+v)w^2}{(1-v)^4}+\frac{3-v}{(1-v)^3\,(1-v\,w)}\\
&\quad-\frac{3-2v}{(1-v)^3(1-v\,w)^2}+\frac{1}{(1-v)^2(1-v\,w)^3}-\frac{1}{(1-v)^3}\,,\\
A^{qg\to g,1}_{8,\mathrm{SGP},F,N_c}(v,w) &= \frac{3v^3w^3}{2\,(1-v)^4}-\frac{v^2(1+2v)w^2}{2\,(1-v)^4}-\frac{v\left(1+v^2\right)w}{4(1-v)^4}+\frac{8v^2-32v+25}{2\,(1-v)^4\,(1-v\,w)}\\
&\quad-\frac{v^3+4v^2-29v+26}{4(1-v)^4}+\frac{2}{(1-v)\,(1-v+v\,w)}\\
&\quad-\frac{21-13v}{2\,(1-v)^3\,(1-v\,w)^2}-\frac{1}{2\,(1-v+v\,w)^2}+\frac{3}{(1-v)^2\,(1-v\,w)^3}\,. \qquad \text{(F.77)}
\end{aligned}
$$

The SGP contribution associated to the axial-vector qgq function G has the rather simple form

$$
\begin{aligned}
\hat{\sigma}^{qg\to g,5}_{\mathrm{SGP},\partial_2 G}(v,w) &= \frac{v(2C_F-N_c)\left(v^2\left(2w^2-4w+1\right)-1\right)}{2\,(1-v)^4}\log(1-w)\\
&\quad-\frac{w\left(C_F(1-v)+N_c\left(1-v+v^2\right)\right)}{(1-v)^3}\log(1-v)-\frac{v^3w^2(2C_F-N_c)}{(1-v)^4}\log(w)\\
&\quad+\frac{N_cv^2w}{(1-v)^3}\log(1-v+v\,w)+C_F\,\frac{v\,w\left(v^3\left(6w^2-8w+3\right)-4v^2+v-2\right)}{2(1-v)^4}\\
&\quad+N_c\,\frac{v\,w\,\left(v^2(1-2w)+3v-2\right)}{2\,(1-v)^4}\,. \qquad \text{(F.78)}
\end{aligned}
$$

Soft-Fermion Pole Contribution

Separated by color factors, the partonic cross sections of the $qg\to g$ channel soft-fermion pole contribution in Eq. (6.22) reads explicitly

$$
\hat{\sigma}^{qg\to g,1}_{\mathrm{SFP},F}(v,w,\chi_m)=C_F\,\hat{\sigma}^{qg\to g,1}_{\mathrm{SFP},F,C_F}(v,w,\chi_m)+N_c\,\hat{\sigma}^{qg\to g,1}_{\mathrm{SFP},F,N_c}(v,w,\chi_m)\,, \qquad \text{(F.79)}
$$

with

$$
\begin{aligned}
\hat{\sigma}^{qg\to g,1}_{\mathrm{SFP},F,C_F}(v,w,\chi_m) &= A^{qg\to g,1}_{1,\mathrm{SFP},F,C_F}(v,w)\,\log(\chi_m)\\
&\quad+A^{qg\to g,1}_{2,\mathrm{SFP},F,C_F}(v,w)\,\log(1-w)+A^{qg\to g,1}_{3,\mathrm{SFP},F,C_F}(v,w)\,\log(1-v)\\
&\quad+A^{qg\to g,1}_{4,\mathrm{SFP},F,C_F}(v,w)\,\log(1-v+v\,w)+A^{qg\to g,1}_{5,\mathrm{SFP},F,C_F}(v,w)\,\log(1-v\,w)\\
&\quad+A^{qg\to g,1}_{6,\mathrm{SFP},F,C_F}(v,w)\,\log(w)+A^{qg\to g,1}_{7,\mathrm{SFP},F,C_F}(v,w)\,, \qquad \text{(F.80)}
\end{aligned}
$$

and the seven coefficients

$$
\begin{aligned}
A^{qg\to g,1}_{1,\mathrm{SFP},F,C_F}(v,w) &= \frac{v^2w^2\left(v^2\left(2w^2-2w+1\right)-2vw+1\right)}{(1-v)^4\,(1-v\,w)}\,,\\
A^{qg\to g,1}_{2,\mathrm{SFP},F,C_F}(v,w) &= \frac{v^2w\left(v^2w(2w-1)+v(2-4w)+w\right)}{(1-v)^4\,(1-v\,w)}\,,\\
A^{qg\to g,1}_{3,\mathrm{SFP},F,C_F}(v,w) &= -\frac{w\left(2v^3w(2w-1)+v^2\left(w^2-4w+1\right)-v\left(w^2+w-1\right)+w\right)}{(1-v)^3\,(1-v\,w)}\,,\\
A^{qg\to g,1}_{4,\mathrm{SFP},F,C_F}(v,w) &= \frac{v\,w\,(1+v(1-2w))}{(1-v)^3}\,,\\
A^{qg\to g,1}_{5,\mathrm{SFP},F,C_F}(v,w) &= \frac{v\,w\,\left(v^2w(2w-1)-v(w+1)+1\right)}{(1-v)^3\,(1-v\,w)}\,,\\
A^{qg\to g,1}_{6,\mathrm{SFP},F,C_F}(v,w) &= \frac{v^2\,w^2\,\left(v^2(6w-1)-4v(w+1)+3\right)}{(1-v)^4\,(1-v\,w)}\,,\\
A^{qg\to g,1}_{7,\mathrm{SFP},F,C_F}(v,w) &= -\frac{3v^4w^4}{(1-v)^4}+\frac{2v^3(2v+5)w^3}{(1-v)^4}-\frac{v\left(3v^3+20v^2-3v-2\right)w^2}{2(1-v)^4}\\
&\quad -\frac{vw}{(1-v)^3}-\frac{1}{(1-v)(1-v+v\,w)}+\frac{1}{(1-v)^2}\,.
\end{aligned}
\tag{F.81}
$$

The N_c part reads

$$
\begin{aligned}
\hat{\sigma}^{qg\to g,1}_{\mathrm{SFP},F,N_c}(v,w,\chi_m) &= A^{qg\to g,1}_{1,\mathrm{SFP},F,N_c}(v,w)\,\log(\chi_m)\\
&\quad +A^{qg\to g,1}_{2,\mathrm{SFP},F,N_c}(v,w)\,\log(1-w)+A^{qg\to g,1}_{3,\mathrm{SFP},F,N_c}(v,w)\,\log(1-v)\\
&\quad +A^{qg\to g,1}_{4,\mathrm{SFP},F,N_c}(v,w)\,\log(1-v+v\,w)+A^{qg\to g,1}_{5,\mathrm{SFP},F,N_c}(v,w)\,\log(1-v\,w)\\
&\quad +A^{qg\to g,1}_{6,\mathrm{SFP},F,N_c}(v,w)\,\log(w)+A^{qg\to g,1}_{7,\mathrm{SFP},F,N_c}(v,w)\,,
\end{aligned}
\tag{F.82}
$$

also with seven coefficients

$$
\begin{aligned}
A^{qg\to g,1}_{1,\mathrm{SFP},F,N_c}(v,w) &= \frac{v^2w^2\left(v^3w\left(2w^2-2w+1\right)+v^2\left(-6w^2+4w-2\right)+5vw-2\right)}{2\,(1-v)^4\,(1-v\,w)^2}\,,\\
A^{qg\to g,1}_{2,\mathrm{SFP},F,N_c}(v,w) &= \frac{v^2w\left(v^3w^2(2w-1)-2v^2w\left(w^2+2w-1\right)+v\left(3w^2+4w-2\right)-2w\right)}{2\,(1-v)^4\,(1-v\,w)^2}\,,\\
A^{qg\to g,1}_{3,\mathrm{SFP},F,N_c}(v,w) &= -\frac{\left(3v^2-v+1\right)w^2}{(1-v)^3}+\frac{v(1+v)w}{(1-v)^3}-\frac{3-v}{2\,(1-v)^3\,(1-v\,w)}\\
&\quad +\frac{1}{2\,(1-v)^2\,(1-v\,w)^2}+\frac{1}{(1-v)^3}\,,\\
A^{qg\to g,1}_{4,\mathrm{SFP},F,N_c}(v,w) &= -\frac{v\,w\,(1+v(1-2w))}{2\,(1-v)^3}\,,\\
A^{qg\to g,1}_{5,\mathrm{SFP},F,N_c}(v,w) &= \frac{v\,w\,\left(v^3w^2(4w-1)+v^2(2-9w)w+2vw+v+1\right)}{2\,(1-v)^3\,(1-v\,w)^2}\,,\\
A^{qg\to g,1}_{6,\mathrm{SFP},F,N_c}(v,w) &= \frac{v^2w^2\left(v^3w(6w-1)-2v^2\left(w^2+6w-1\right)+v(5w+4)-2\right)}{2\,(1-v)^4\,(1-v\,w)^2}\,,\\
A^{qg\to g,1}_{7,\mathrm{SFP},F,N_c}(v,w) &= -\frac{4v^3w^3}{(1-v)^4}+\frac{v\left(7v^2+7v-4\right)w^2}{2\,(1-v)^4}+\frac{2vw}{(1-v)^3}+\frac{4-v}{2\,(1-v)^3}\\
&\quad -\frac{7-4v}{2\,(1-v)^3\,(1-v\,w)}+\frac{1}{2\,(1-v)\,(1-v+v\,w)}+\frac{1}{(1-v)^2\,(1-v\,w)^2}\,.
\end{aligned}
\tag{F.83}
$$

Analogously, the partonic cross sections for the axial-vector part accompanying the function G can be written as

$$
\hat{\sigma}^{qg\to g,5}_{\mathrm{SFP},G}(v,w,\chi_m)=C_F\,\hat{\sigma}^{qg\to g,5}_{\mathrm{SFP},G,C_F}(v,w,\chi_m)+N_c\,\hat{\sigma}^{qg\to g,5}_{\mathrm{SFP},G,N_c}(v,w,\chi_m)\,.
\tag{F.84}
$$

Here, the axial-vector part $\hat{\sigma}^{qg\to g,5}_{\rm SFP,G}$ is quite similar to the vector part $\hat{\sigma}^{qg\to g,1}_{\rm SFP,F}$

$$\begin{aligned}\hat{\sigma}^{qg\to g,5}_{\rm SFP,G,C_F}(v,w,\chi_m) &= \hat{\sigma}^{qg\to g,1}_{\rm SFP,F,C_F}(v,w,\chi_m)+\frac{2\left(1-v-2v^2\right)w^2}{(1-v)^3}\log(1-v)\\ &+\frac{4v^2\,w^2}{(1-v)^3}\,\log(1-v\,w)-\frac{4v^2(1-3v)w^2}{(1-v)^4}\,\log(w)\\ &+\frac{v^2\,w^2\,\left(v^2\left(6w^2-8w+3\right)-16v(w-1)-1\right)}{(1-v)^4}\,,\end{aligned}\tag{F.85}$$

and

$$\begin{aligned}\hat{\sigma}^{qg\to g,5}_{\rm SFP,G,N_c}(v,w,\chi_m) &= \hat{\sigma}^{qg\to g,1}_{\rm SFP,F,N_c}(v,w,\chi_m)+\frac{2\left(1-v+2v^2\right)w^2}{(1-v)^3}\log(1-v)\\ &-\frac{4v^2w^2}{(1-v)^3}\,\log(1-v\,w)+\frac{2(1-3v)v^2w^2}{(1-v)^4}\,\log(w)+\frac{vw^2\left(v^2(6w-5)-4v+3\right)}{(1-v)^4}\,.\end{aligned}\tag{F.86}$$

F.1.5 Channel $gg\to q$:

Lastly, the explicit results for hadron production are concluded with the two partonic cross sections of Eq. (6.23), which constitutes the result for the $gg\to q$ channel

$$\begin{aligned}\hat{\sigma}^{gg\to q}_{xx}(v,w,\chi_m,\chi_\mu) &= A^{gg\to q}_{1,xx}(v,\chi_m,\chi_\mu)\delta(1-w)+A^{gg\to q}_{2,xx}(v)\frac{1}{(1-w)_+}\\ &+A^{gg\to q}_{3,xx}(v,w)\log(\chi_m)+A^{gg\to q}_{4,xx}(v,w)\log(1-w)\\ &+A^{gg\to q}_{5,xx}(v,w)\log(\chi_\mu)+A^{gg\to q}_{6,xx}(v,w)\log(1-v\,w)\\ &+A^{gg\to q}_{7,xx}(v,w)\log(1-v)+A^{gg\to q}_{8,xx}(v,w)\log(w)+A^{gg\to q}_{9,xx}(v,w)\,,\end{aligned}\tag{F.87}$$

where one has the following nine coefficients

$$\begin{aligned}A^{gg\to q}_{1,xx}(v,\chi_m,\chi_\mu) &= \frac{2(v-1)v+1}{(1-v)^4}\log(\chi_m)+\frac{1+v^2}{(1-v)^4}\log(\chi_\mu)+\frac{v^2-(1-v)^2}{(1-v)^4}\\ &+\frac{(3v-2)v+2}{(1-v)^4}\log(1-v)\,,\\ A^{gg\to q}_{2,xx}(v) &= \frac{2-2v+3v^2}{(1-v)^4}\,,\\ A^{gg\to q}_{3,xx}(v,w) &= \frac{2v\left(-2vw^2+v-2\right)+4}{(1-v)^4}-\frac{4(2-v)v^2w^2+(3-v)(1-3vw)}{(1-v)^3(1-v\,w)^3}\,,\\ A^{gg\to q}_{4,xx}(v,w) &= \frac{-2\left(3v^2+1\right)w^2+3v^2-4v+5}{(1-v)^4}-\frac{4(2-v)v^2w^2+(3-v)(1-3vw)}{(1-v)^3(1-v\,w)^3}\,,\\ A^{gg\to q}_{5,xx}(v,w) &= \frac{\left(1+v^2\right)\left(1-2w^2\right)}{(1-v)^4}\,,\\ A^{gg\to q}_{6,xx}(v,w) &= \frac{2v^2w^2((v-3)vw+v+1)}{(1-v)^3(1-v\,w)^3}\,,\\ A^{gg\to q}_{7,xx}(v,w) &= \frac{v\left(-6vw^2+v+4\right)-1-2w^2}{(1-v)^4}+\frac{4(2-v)v^2w^2+(3-v)(1-3vw)}{(1-v)^3(1-v\,w)^3}\,,\\ A^{gg\to q}_{8,xx}(v,w) &= \frac{2(v+1)w^2+v-3}{(1-v)^3}+\frac{4(2-v)v^2w^2+(3-v)(1-3vw)}{(1-v)^3(1-v\,w)^3}\,,\\ A^{gg\to q}_{9,xx}(v,w) &= \frac{8v^2w-2(v+1)(4v-1)w^2+(19-7v)v-20}{(1-v)^4}\\ &+\frac{12v^2-45v+34}{(1-v)^4(1-v\,w)}+\frac{15v-23}{(1-v)^3(1-v\,w)^2}+\frac{6}{(1-v)^2(1-v\,w)^3}\,,\end{aligned}\tag{F.88}$$

and

$$\begin{aligned}\hat{\sigma}^{gg\to q}_{x0}(v,w,\chi_m,\chi_\mu) &= A^{gg\to q}_{1,x0}(v,\chi_m,\chi_\mu)\delta(1-w)+A^{gg\to q}_{2,x0}(v)\frac{1}{(1-w)_+}\\ &+A^{gg\to q}_{3,x0}(v,w)\log(\chi_m)+A^{gg\to q}_{4,x0}(v,w)\log(1-w)\\ &+A^{gg\to q}_{5,x0}(v,w)\log(\chi_\mu)+A^{gg\to q}_{6,x0}(v,w)\log(1-v\,w)\\ &+A^{gg\to q}_{7,x0}(v,w)\log(1-v)+A^{gg\to q}_{8,x0}(v,w)\log(w)+A^{gg\to q}_{9,x0}(v,w)\end{aligned}\tag{F.89}$$

again with nine coefficients

$$
\begin{aligned}
A^{gg\to q}_{1,x0}(v,\chi_m,\chi_\mu) &= -\frac{2(v-1)v+1}{(1-v)^4}\log(\chi_m) - \frac{1+v^2}{(1-v)^4}\log(\chi_\mu) + \frac{(2-v)^2}{(1-v)^4} \\
&\quad + \frac{(2-3v)v-2}{(1-v)^4}\log(1-v)\,, \\
A^{gg\to q}_{2,x0}(v) &= \frac{-2+2v-3v^2}{(1-v)^4}\,, \\
A^{gg\to q}_{3,x0}(v,w) &= \frac{v^2\left(4w^2-2\right)+4v-4}{(1-v)^4} + \frac{4(2-v)v^2w^2+(3-v)(1-3vw)}{(1-v)^3(1-v\,w)^3}\,, \\
A^{gg\to q}_{4}(v,w) &= \frac{v\left(v\left(6w^2-3\right)+4\right)+2w^2-5}{(1-v)^4} + \frac{4(2-v)v^2w^2+(3-v)(1-3vw)}{(1-v)^3(1-v\,w)^3}\,, \\
A^{gg\to q}_{5,x0}(v,w) &= -\frac{\left(1+v^2\right)\left(1-2w^2\right)}{(1-v)^4}\,, \\
A^{gg\to q}_{6}(v,w) &= -\frac{2v^2w^2(-4v^2w^2(3-vw)+v(v+9)w+v-3)}{(1-v)^3(1-v\,w)^3}\,, \\
A^{gg\to q}_{7,x0}(v,w) &= \frac{\left((8v-2)v^2+2\right)w^2-v^2-4v+1}{(1-v)^4} - \frac{4(2-v)v^2w^2+(3-v)(1-3vw)}{(1-v)^3(1-v\,w)^3}\,, \\
A^{gg\to q}_{8,x0}(v,w) &= -\frac{2\left(4v^2+v+1\right)w^2+v-3}{(1-v)^3} - \frac{4(2-v)v^2w^2+(3-v)(1-3vw)}{(1-v)^3(1-v\,w)^3}\,, \\
A^{gg\to q}_{9,x0}(v,w) &= \frac{2\left(7v^2+v-4\right)w^2+8v^2+8(1-2v)vw-23v+25}{(1-v)^4} \\
&\quad - \frac{12v^2-49v+38}{(1-v)^4(1-v\,w)} - \frac{15v-23}{(1-v)^3(1-v\,w)^2} - \frac{6}{(1-v)^2(1-v\,w)^3}\,.
\end{aligned}
\tag{F.90}
$$

F.2 Jet Production

In this part of the appendix the partonic cross sections for the jet-specific contribution of Eq. (6.25) are collected. Their explicit forms depend on the choice of jet algorithm, see Ref. [129], and here they are given for the k_T-type algorithms. Because of the delta function $\delta(1-z)$ one has a fixed value for the kinematical variable v, namely $v = v_1 = 1 + \frac{t}{s}$. As before, the color factors are factored out explicitly (in this case there is only a C_F-contribution)

$$
\hat{\sigma}^{qg\to\mathrm{jet}(q+g)}_{\mathrm{SGP,\,jet},F}(w,R,\mu) = C_F\,\hat{\sigma}^{qg\to\mathrm{jet}(q)}_{\mathrm{SGP,\,jet},F}(w,R,\mu) + C_F\,\hat{\sigma}^{qg\to\mathrm{jet}(g)}_{\mathrm{SGP,\,jet},F}(w,R,\mu)\,,
\tag{F.91}
$$

where the first part corresponds to former quark fragmentation and reads

$$
\begin{aligned}
\hat{\sigma}^{qg\to\mathrm{jet}(q)}_{\mathrm{SGP,\,jet},F}(w,R,\mu) &= A^{qg\to\mathrm{jet}(q)}_{0,\mathrm{SGP,\,jet},F}(R,\mu)\,\delta(1-w) + A^{qg\to\mathrm{jet}(q)}_{1,\mathrm{SGP,\,jet},F}\left(\frac{\log(1-w)}{1-w}\right)_+ \\
&\quad + A^{qg\to\mathrm{jet}(q)}_{2,\mathrm{SGP,\,jet},F}(R,\mu)\,\frac{1}{(1-w)_+} \\
&\quad + A^{qg\to\mathrm{jet}(q)}_{3,\mathrm{SGP,\,jet},F}\,\log\left(R^2v^2(1-w)^2\,\frac{t\,u}{s\,\mu^2}\right) + A^{qg\to\mathrm{jet}(q)}_{4,\mathrm{SGP,\,jet},F},
\end{aligned}
\tag{F.92}
$$

with

$$
\begin{aligned}
A^{qg\to\mathrm{jet}(q)}_{0,\mathrm{SGP,\,jet},F}(R,\mu) &= \frac{4v^3+9v^2+12v+1-4(1+v^2)\,\log(v)}{2(1-v)^3}\log\left(R^2\,\frac{t\,u}{s\,\mu^2}\right) \\
&\quad -2\frac{1+v^2}{(1-v)^3}\log^2(v) + 4\frac{(1+v)^3}{(1-v)^3}\log(v) + \frac{1+v^2}{(1-v)^3}\left(\tfrac{13}{2}-\tfrac{2}{3}\pi^2\right)\,, \\
A^{qg\to\mathrm{jet}(q)}_{1,\mathrm{SGP,\,jet},F} &= -4\frac{1+v^2}{(1-v)^3}\,,
\end{aligned}
$$

$$
\begin{aligned}
A^{qg\to\mathrm{jet}(q)}_{2,\mathrm{SGP},\,\mathrm{jet},F}(R,\mu) &= 4\frac{(1+v)^3-(1+v^2)\log(v)}{(1-v)^3}-2\frac{1+v^2}{(1-v)^3}\,\log\left(R^2\,\tfrac{t\,u}{s\,\mu^2}\right)\,,\\
A^{qg\to\mathrm{jet}(q)}_{3,\mathrm{SGP},\,\mathrm{jet},F} &= -\frac{6v^4w^4}{(1-v)^3}+\frac{4v^3(2v-3)w^3}{(1-v)^3}-\frac{v^2\left(3v^2-8v+9\right)w^2}{(1-v)^3}+2\frac{1+v^2}{(1-v)^3}\,,\\
A^{qg\to\mathrm{jet}(q)}_{4,\mathrm{SGP},\,\mathrm{jet},F} &= -\frac{10v^4w^4}{(1-v)^3}+4\frac{v^3(3v-4)w^3}{(1-v)^3}-\frac{v^2\left(5v^2-8v+19\right)w^2}{(1-v)^3}\\
&\quad -\frac{4v\left(v^2+2v+3\right)w}{(1-v)^3}-4\frac{(1+v)^3}{(1-v)^3}\,.
\end{aligned}
\tag{F.93}
$$

The analogous result for former gluon fragmentation is given as

$$
\begin{aligned}
\hat{\sigma}^{qg\to\mathrm{jet}(g)}_{\mathrm{SGP},\,\mathrm{jet},F}(w,R,\mu) &= A^{qg\to\mathrm{jet}(g)}_{0,\mathrm{SGP},\,\mathrm{jet},F}(R,\mu)\,\delta(1-w)+A^{qg\to\mathrm{jet}(g)}_{1,\mathrm{SGP},\,\mathrm{jet},F}\,\frac{1}{(1-w)_+}\\
&\quad +A^{qg\to\mathrm{jet}(g)}_{2,\mathrm{SGP},\,\mathrm{jet},F}\,\log\left(R^2\,v^2(1-w)^2\,\tfrac{t\,u}{s\,\mu^2}\right)+A^{qg\to\mathrm{jet}(g)}_{3,\mathrm{SGP},\,\mathrm{jet},F},
\end{aligned}
\tag{F.94}
$$

with

$$
\begin{aligned}
A^{qg\to\mathrm{jet}(g)}_{0,\mathrm{SGP},\,\mathrm{jet},F}(R,\mu) &= -\frac{v\left(1+v^2\right)}{(1-v)^3}\left(\log\left(R^2\tfrac{t\,u}{s\,\mu^2}\right)+2\log(v)+1\right)\,,\\
A^{qg\to\mathrm{jet}(g)}_{1,\mathrm{SGP},\,\mathrm{jet},F} &= -\frac{2v\left(1+v^2\right)}{(1-v)^3}\,,\\
A^{qg\to\mathrm{jet}(g)}_{2,\mathrm{SGP},\,\mathrm{jet},F} &= \frac{6v^4w^4}{(1-v)^3}-\frac{8v^4w^3}{(1-v)^3}+\frac{\left(3v^2-2v+3\right)v^2w^2}{(1-v)^3}+\frac{4}{1-v+v\,w}\\
&\quad -\frac{2(1-v)}{(1-v+v\,w)^2}-\frac{2}{1-v}\,,\\
A^{qg\to\mathrm{jet}(g)}_{3,\mathrm{SGP},\,\mathrm{jet},F} &= \frac{10v^4w^4}{(1-v)^3}-\frac{4v^3(3v-2)w^3}{(1-v)^3}+\frac{v^2\left(5v^2-10v+9\right)w^2}{(1-v)^3}-\frac{2v\left(v^2-4v+1\right)w}{(1-v)^3}\\
&\quad -\frac{2\left(v^3-6v^2+5v-2\right)}{(1-v)^3}-\frac{4(1-v)}{1-v+v\,w}\,.
\end{aligned}
\tag{F.95}
$$

There is also a derivative term

$$
\begin{aligned}
\hat{\sigma}^{qg\to\mathrm{jet}(q)}_{\mathrm{SGP},\,\mathrm{jet},F'}(w,R,\mu) &= C_F\left(A^{qg\to\mathrm{jet}(q)}_{0,\mathrm{SGP},\,\mathrm{jet},F'}(R,\mu)\delta(1-w)+A^{qg\to\mathrm{jet}(q)}_{1,\mathrm{SGP},\,\mathrm{jet},F'}\left(\frac{\log(1-w)}{1-w}\right)_+\right.\\
&\quad \left.+A^{qg\to\mathrm{jet}(q)}_{2,\mathrm{SGP},\,\mathrm{jet},F'}\frac{1}{(1-w)_+}\right)\,,
\end{aligned}
\tag{F.96}
$$

with

$$
\begin{aligned}
A^{qg\to\mathrm{jet}(q)}_{0,\mathrm{SGP},\,\mathrm{jet},F'}(R,\mu) &= -\frac{1+v^2}{(1-v)^3}\left[2\log^2(v)+(\tfrac{3}{2}+2\,\log(v))\log\left(R^2\,\tfrac{t\,u}{s\,\mu^2}\right)-\tfrac{13}{2}+\tfrac{2}{3}\pi^2\right]\,,\\
A^{qg\to\mathrm{jet}(q)}_{1,\mathrm{SGP},\,\mathrm{jet},F'} &= -\frac{4\left(1+v^2\right)}{(1-v)^3}\,,\\
A^{qg\to\mathrm{jet}(q)}_{2,\mathrm{SGP},\,\mathrm{jet},F'} &= -\frac{2\left(1+v^2\right)}{(1-v)^3}\log\left(R^2\,\tfrac{t\,u}{s\,\mu^2}\right)-\frac{4\left(1+v^2\right)}{(1-v)^3}\log(v)\,.
\end{aligned}
\tag{F.97}
$$

F.3 Single-Inclusive Photon Production

In this appendix the explicit analytical expressions for the partonic cross sections featured in the results for single-inclusive photon production are listed. Note that only the formulas for the Interference channel are shown, since the Compton channel can be obtained from hadron production, as elaborated on in the main text. In this channel one only has direct photon production and as a consequence $v = v_1 = 1 + \frac{t}{s}$ throughout this section.

NLO Virtual $q\gamma q$ Contribution

Starting with the loop corrections, one finds the following results for the contribution by quark-photon-quark correlations in 6.34

$$\begin{aligned}
\hat{\sigma}_1^{I,q\gamma q}\left(v,w,-\tfrac{u}{\mu^2}\right) &= \left[\frac{3}{2}\log\left(-\frac{u(1-v)}{\mu^2 v}\right)-\frac{3\left(v^2+v+1\right)}{v^2+1}-\frac{\pi^2}{6}\right]\delta(1-w)\\
&+\left[\log\left(-\frac{u(1-v)}{\mu^2 v}\right)+\frac{(1-v)^2}{v^2+1}\right]\frac{1}{(1-w)_+}+\left(\frac{\log(1-w)}{1-w}\right)_+ +\frac{3}{2}-\frac{\log(w)}{1-w}\\
\hat{\sigma}_5^{I,q\gamma q}\left(v,w,-\tfrac{u}{\mu^2}\right) &= \left[\frac{3}{2}\log\left(-\frac{u(1-v)}{\mu^2 v}\right)-\frac{\pi^2}{6}-\frac{9}{2}\right]\delta(1-w)\\
&+\log\left(-\frac{u(1-v)}{\mu^2 v}\right)\frac{1}{(1-w)_+}+\left(\frac{\log(1-w)}{1-w}\right)_+ -\frac{7}{2}-\frac{\log(w)}{1-w}\,.
\end{aligned} \tag{F.98}$$

NLO Virtual $g\gamma g$ Contribution

The other NLO virtual correction, generated by gluon-photon-gluon correlations in 6.35, reads

$$\begin{aligned}
\hat{\sigma}_1^{I,g\gamma g}\left(v,w,-\tfrac{u}{\mu^2}\right) &= \left[4\log\left(-\frac{u(1-v)}{\mu^2 v}\right)-\frac{8v}{v^2+1}\right]\delta(1-w)+\frac{4}{(1-w)_+}\\
&\quad +4\log\left(-\frac{u(1-v)(1-w)}{\mu^2 vw}\right)-\frac{8v}{v^2+1}\\
\hat{\sigma}_2^{I,g\gamma g}\left(v,w,-\tfrac{u}{\mu^2}\right) &= \left[4\log\left(-\frac{u(1-v)}{\mu^2 v}\right)-\frac{2(v+1)^2}{v^2+1}\right]\delta(1-w)+\frac{4}{(1-w)_+}-\frac{2(v+1)^2}{v^2+1}\\
\hat{\sigma}_3^{I,g\gamma g}\left(v,w,-\tfrac{u}{\mu^2}\right) &= -\frac{2(v+1)^2}{v^2+1}\left(1+\delta(1-w)\right)+4\log\left(-\frac{u(1-v)(1-w)}{\mu^2 vw}\right).
\end{aligned} \tag{F.99}$$

Integral Contribution

Moving on with NLO real corrections and starting with the integral contribution given by Eq. 6.36 one finds

$$\begin{aligned}
\hat{\sigma}_+^{I,\mathrm{Int}}(v,w,\zeta) &= \frac{\mathrm{sgn}\left(\zeta-\frac{v^2(1-w)w}{(1-w)(1-v)^2+w}\right)(\zeta-1)v^2w^2}{2(v-1)(v(w-1)+1)^2(\zeta+v(w-\zeta))^2}\left(2\zeta^2-2\zeta+v^2(w-1)^2\right.\\
&\left.+2\zeta v(w-1)+1\right)+\frac{\mathrm{sgn}(w-\zeta)\zeta}{2(v-1)^2(\zeta+v(w-\zeta))^2}\left(\zeta+v^4(w-\zeta)^2-v^3\left(3\zeta^2+\zeta+2w^2-4\zeta w-2w\right)\right.\\
&\left.+v^2\left(\zeta^2+\zeta-w^2\right)-(\zeta-1)v(2w-\zeta)\right)+\frac{\zeta v^2(w-\zeta)+v(2\zeta-2\zeta w+w)-1}{2(v-1)\sqrt{v^2(w-\zeta)^2-2\zeta v+(4\zeta-2)vw+1}}\\
&-\frac{v(-\zeta+v(w-1)(\zeta(w-1)-1)+w-1)}{(v-1)^2(v(w-1)+1)^2}\\
\hat{\sigma}_-^{I,\mathrm{Int}}(v,w,\zeta) &= -\frac{\mathrm{sgn}(w-\zeta)v^2(w-\zeta)}{(v-1)^2(\zeta+v(w-\zeta))^2}\left(v^2w(w-\zeta)^2-\zeta v\left(\zeta^2+\zeta+w^2-2\zeta w-w\right)\right.\\
&\left.+\zeta\left(\zeta^2+\zeta-3\zeta w+w\right)\right)+\frac{\mathrm{sgn}\left(\zeta-\frac{v^2(1-w)w}{(1-w)(1-v)^2+w}\right)(\zeta-1)\zeta v^2w^2}{2(v-1)(v(w-1)+1)^2(\zeta+v(w-\zeta))^2}\left(5\zeta^2-6\zeta+v^2(w-\zeta)^2\right.\\
&\left.+2(2\zeta-1)v(w-\zeta)+2\right)+\frac{\zeta\left(\zeta v^2(w-\zeta)+v(2\zeta-2\zeta w+w)-1\right)}{2(v-1)\sqrt{v^2(w-\zeta)^2-2\zeta v+(4\zeta-2)vw+1}}+\frac{v^2w^2}{(v-1)^2}\\
&+\frac{\zeta}{2(v-1)^2(v(w-1)+1)^2}\left(v^4(w-1)^2\left(-\zeta+4(\zeta-2)w^2+2w\right)+v^3\left(\zeta+2(4\zeta-5)w^3\right.\right.\\
&\left.\left.+(6-8\zeta)w^2+4w-1\right)-v^2\left(\zeta+(\zeta-2)w^2-2(\zeta-2)w+1\right)+v(\zeta-2w+3)-1\right).
\end{aligned} \tag{F.100}$$

Soft-Gluon Pole Contribution

Next is the soft-gluon pole contribution given in 6.38. The partonic cross sections read

$$
\begin{aligned}
\hat{\sigma}_1^{I,\mathrm{SGP}}\left(v,w,-\tfrac{u}{\mu^2}\right) &= A_{1,1}^{I,\mathrm{SGP}}\left(v,-\tfrac{u}{\mu^2}\right)\delta(1-w) + A_{1,2}^{I,\mathrm{SGP}}(v)\,\frac{1}{(1-w)_+} + A_{1,3}^{I,\mathrm{SGP}}(v,w)\\
A_{1,1}^{I,\mathrm{SGP}}\left(v,-\tfrac{u}{\mu^2}\right) &= -\frac{\left(v^2+1\right)}{(v-1)^2}\log\left(-\frac{u}{\mu^2}(1-v)\right)+\left(\frac{1}{2v}-1\right)\log(1-v)\\
&\quad -\frac{v\left(v^2-2v+5\right)}{4(v-1)^2}+\frac{1}{2}\\
A_{1,2}^{I,\mathrm{SGP}}(v) &= -\frac{5\left(v^2+1\right)}{2(v-1)^2}\\
A_{1,3}^{I,\mathrm{SGP}}(v,w) &= \frac{v^2w^2\left(v^2-2v(w+1)+1\right)}{(v-1)^3(v(w-1)+1)^2}\log\left((1-v)^2(1-w)+w\right)\\
&\quad +\frac{1+v}{1-v}\log(v(w-1)+1)+\frac{v^2w^2\left(2vw+(v-1)^2\right)}{(v-1)^3(v(w-1)+1)^2}\log(w)\\
&\quad +\frac{\left(v\left(v\left(v^2w(w-1)^2+v\left(3(w-1)^2w-1\right)+2w^2-3w+1\right)-w+1\right)-1\right)}{(v-1)^2(v(w-1)+1)^2}\log(1-w)\\
&\quad +\frac{\left(v^2(w-1)^2-2vw-1\right)}{(v(w-1)+1)^2}\log(1-v)+\frac{5v^2w^2}{(v-1)^2}-\frac{4(v-1)}{(v(w-1)+1)^2}+\frac{v-9}{v(w-1)+1}\\
&\quad +\frac{\left(v^2-4v+5\right)(v-1)^5}{2(v-2)^4\left((v-1)^2(w-1)-w\right)^3}+\frac{\left(v^3+2v^2-17v+24\right)(v-1)^2}{2(v-2)^4\left((v-1)^2(w-1)-w\right)}\\
&\quad +\frac{\left(v^4-7v^3+23v^2-37v+26\right)(v-1)^3}{2(v-2)^4\left((v-1)^2(w-1)-w\right)^2}+\frac{\left(-3v^5-8v^4+123v^3-294v^2+206v+8\right)w}{4(v-2)^3(v-1)^2}\\
&\quad +\frac{7v^6-68v^5+287v^4-681v^3+971v^2-791v+285}{2(v-2)^4(v-1)^2}\,,
\end{aligned}
\tag{F.101}
$$

and

$$
\begin{aligned}
\hat{\sigma}_5^{I,\mathrm{SGP}}(v,w) &= \left(\frac{4}{(1-v)w(v(w-1)+1)}-\frac{v^2\left(2w^2-2w+1\right)+v(2-6w)+5}{(1-v)^2w}\right)\log(1-w)\\
&\quad -\frac{w}{v}\log(1-v)+\frac{2v^2w\left(v^2+(v-4)vw+v-2\right)}{(1-v)^5(v(w-1)+1)}\log\left(\frac{(1-v)^2(1-w)}{w}+1\right)\\
&\quad +\frac{\left(v^2-4v+5\right)(1-v)^3}{2(2-v)^4w\left(-\left(v^2(w-1)\right)+2v(w-1)+1\right)^2}+\frac{v\left(-v^3+7v^2-17v+13\right)(1-v)}{(2-v)^4w\left(-\left(v^2(w-1)\right)+2v(w-1)+1\right)}\\
&\quad +\frac{2v^4-14v^3+33v^2-22v-5}{2(2-v)^4(1-v)w}-\frac{\left(2v^5-3v^4-16v^3+31v^2-6v-2\right)w}{(2-v)^2(1-v)^3}\\
&\quad -\frac{5v^6-25v^5+27v^4+31v^3-36v^2-38v+24}{2(2-v)^3(1-v)^3}\,.
\end{aligned}
\tag{F.102}
$$

Soft-Fermion Pole Contribution

Finally, the results for the partonic cross sections of the soft-fermion pole contribution in 6.39 are shown

$$\begin{aligned}
\hat{\sigma}_{+}^{I,\mathrm{SFP}}\left(v,w,-\tfrac{u}{\mu^2}\right) &= -\frac{\left(v^2+1\right)(w-1)^2}{(v-1)^2}\log\left(-\frac{u(1-w)}{\mu^2}\right)+\frac{1}{1-v}\log(1-vw)\\
&+\frac{\left(v^2\left(-2w^2+2w-1\right)+2vw-1\right)}{(v-1)^2}\log(1-v)+\frac{vw(2-vw)}{(v-1)^2}\log(v(w-1)+1)\\
&+\left(\frac{v\left(2vw^2-2vw+v-2w+1\right)}{(v-1)^2}-\frac{2v(w-1)}{(v-1)(v(w-1)+1)^2}\right)\log\left(v^2(1-w)\right)\\
&+\frac{2v^2w^2\left(v^2(w-1)+v(w-1)+2\right)}{(v-1)^4(v(w-1)+1)^2}\log\left(\frac{(1-v)^2(1-w)}{w}+1\right)+\frac{(w-2)w}{(v-1)^2}\log(w)\\
&-\frac{2(v-1)}{(v-2)^2\left((v^2-2v)w-v^2+2v-1\right)}+\frac{-3v^4+12v^3-17v^2+16v-16}{2(v-2)^2(v-1)^2}\\
&+\frac{1}{v(w-1)+1}+\frac{v\left(v^2+v-8\right)w}{(v-2)(v-1)^2}-\frac{\left(v^2+6v-3\right)w^2}{2(v-1)^2}\\
\hat{\sigma}_{-}^{I,\mathrm{SFP}}(v,w) &= -\frac{2(v-4)v^2w^2}{(v-1)^5}\log\left(\frac{(1-v)^2(1-w)}{w}+1\right)-\frac{2v^2w^2}{(v-1)^2}\log(w)\\
&-\frac{w^2}{v}\log(1-v)-\frac{\left(v^2-4v+5\right)(v-1)^3}{2(v-2)^4\left((v-1)^2(w-1)-w\right)^2}+\frac{-2v^3+13v^2-34v+29}{2(v-2)^4(v-1)}\\
&-\frac{\left(v^3-6v^2+15v-12\right)(v-1)}{(v-2)^4\left(v^2w-v^2-2vw+2v-1\right)}+\frac{\left(v^5+7v^4-45v^3+53v^2+4v-8\right)w^2}{2(v-2)^2(v-1)^3}\\
&+\frac{\left(-2v^6+11v^5-19v^4+12v^3-17v^2+29v-8\right)w}{(v-2)^3(v-1)^3}\,.
\end{aligned}\tag{F.103}$$

F.4 γSIDIS

This part of the appendix gives the explicit formulas for the partonic cross sections that appear in the final result for the γSIDIS reaction in Eq. (6.42). The expressions are organized according to their type of pole contribution, i.e. hard pole (HP) or soft-fermion pole (SFP), by the kind of linear combination of the qgq functions ($\pm$), by the type of azimuthal spin correlation (ϕ' or ϕ^γ), and by the production channel (Compton or Interference). In total there are 16 different hard scattering coefficients listed below. Recall that these results were already obtained in a different form in Ref. [109]. In the following, the same dimensionless kinematic variables are used as in Ref. [137], defined via the relations

$$\begin{aligned}
P\cdot l &= \tfrac{1}{2}Q^2\alpha\,, & P\cdot l' &= \tfrac{1}{2}Q^2\alpha'\,,\\
l\cdot P_\gamma &= \tfrac{1}{2}Q^2\beta\,, & l'\cdot P_\gamma &= \tfrac{1}{2}Q^2\beta'\,,\\
P\cdot P_\gamma &= \tfrac{1}{2}Q^2\gamma\,, & \tilde{Q}^2 &= (1-\beta+\beta')\,Q^2\,.
\end{aligned}\tag{F.104}$$

Note that these variables are also related to x_B, $\tilde{x}_B$ as follows

$$x_B=\frac{1}{\alpha-\alpha'-\gamma}\,,\qquad \tilde{x}_B=\frac{1-\beta+\beta'}{\alpha-\alpha'}\,.\tag{F.105}$$

Using these relations, γ and $\tilde{x}_B$ can be eliminated in favor of α, α', β, β', x_B. In terms of these variables the azimuthal spin correlations have the compact form

$$\epsilon^{Pll'S}=\frac{Q^3}{2}\sqrt{\alpha\alpha'(1-\beta+\beta')}\sin(\phi_S-\phi')\,,\qquad \epsilon^{PlP_\gamma S}=\frac{Q^3}{2}\sqrt{\alpha\beta\gamma}\sin(\phi_S-\phi^\gamma)\,.\tag{F.106}$$

Moreover, there are several short-hand notations for the different denominators that will appear in the formulas below

$$D_1=1-\beta+\beta'\,,\qquad D_2=1-x_B(\alpha-\alpha')\,,\qquad D_3=1-\beta+\beta'-x_B(\alpha-\alpha')\,.\tag{F.107}$$

Hard Pole Contributions

The HP contributions for $F+G$ are given by the following partonic cross sections

$$\begin{aligned}
\hat{\sigma}^{C,\phi'}_{\mathrm{HP},+} &= -\frac{16\left(\alpha^2+(\alpha')^2\right)x_B^2}{\alpha D_1 D_3^2}\,,\\
\hat{\sigma}^{I,\phi'}_{\mathrm{HP},+} &= \frac{16\left(\alpha^2+(\alpha')^2\right)x_B^2\left(D_1\alpha'\beta' x_B+\alpha\left(\beta^2-(\beta+1)\beta'\right)x_B+D_1\beta'\right)}{\alpha\beta\beta' D_1 D_3^2}\,,\\
\hat{\sigma}^{C,\phi^\gamma}_{\mathrm{HP},+} &= \frac{16(\alpha-\alpha')\left(\alpha^2+(\alpha')^2\right)x_B^3}{\alpha D_1 D_2 D_3^2}\,,\\
\hat{\sigma}^{I,\phi^\gamma}_{\mathrm{HP},+} &= -\frac{16\left(\alpha^2+(\alpha')^2\right)x_B^3(\alpha\beta-\alpha'\beta')}{\alpha\beta\beta' D_3^2}\,.
\end{aligned}\tag{F.108}$$

The analogous results for $F-G$ have the slightly more lengthy partonic cross sections

$$\begin{aligned}
\hat{\sigma}^{C,\phi'}_{\mathrm{HP},-} &= -\frac{16}{\alpha D_1^2(1-D_2)D_3^2}\left(D_1^2+2D_1\alpha'(\beta'+1)x_B\right.\\
&\quad\left.+2x_B^2\left(\alpha^2(\beta-1)\beta-\alpha\alpha'\beta(2\beta'+1)+(\alpha')^2(\beta'+1)^2\right)\right)\,,\\
\hat{\sigma}^{I,\phi'}_{\mathrm{HP},-} &= \frac{8}{\alpha\beta\beta' D_1(1-D_2)D_3^2}\left(D_1 x_B\left(6\alpha'(\beta')^2+2\alpha\beta^2\right.\right.\\
&\quad\left.-\beta'\left(2\beta(\alpha'+\alpha)-6\alpha'+\alpha\left(\alpha\alpha' x_B^2+2\right)\right)\right)+x_B^2\left(-4\alpha^3(\beta-1)\beta^2 x_B\right.\\
&\quad-4\alpha\alpha'\beta'\left(2\beta\beta'+\beta'+\beta+\alpha'\left(3\beta\beta'+\beta'+2\beta+1\right)x_B+1\right)\\
&\quad+4(\alpha')^2\beta'(\beta'+1)(2\beta'-\beta+\alpha'(\beta'+1)x_B+2)\\
&\quad\left.+\alpha^2\left(4(\beta-1)\beta^2+\alpha'(\beta')^2 x_B+(\beta(12\beta-1)+1)\alpha'\beta' x_B\right)\right)+2D_1^2\beta'\Big)\,,\\
\hat{\sigma}^{C,\phi^\gamma}_{\mathrm{HP},-} &= -\frac{16x_B}{\alpha D_1^2 D_2(1-D_2)D_3^2}\left(2D_1(\alpha')^2(\beta'+1)x_B\right.\\
&\quad+2x_B\left(-\alpha^3(\beta-1)^2 x_B-\alpha(\alpha')^2\left((\beta')^2+2\beta\beta'+\beta'+\beta\right)x_B+(\alpha')^3(\beta'+1)^2 x_B\right.\\
&\quad\left.\left.+\alpha^2(\beta'(1-\beta)+(2\beta-1)\alpha'\beta' x_B+(\beta-1)(\beta+\beta\alpha' x_B-1))\right)+D_1^2(\alpha'-\alpha)\right)\,,\\
\hat{\sigma}^{I,\phi^\gamma}_{\mathrm{HP},-} &= \frac{16x_B}{\alpha\beta\beta' D_1(1-D_2)D_3^2}\left(\beta'\left(-\beta(\alpha'+\alpha)\left(x_B(\alpha'-\alpha+4\alpha\alpha' x_B)-D_1+D_3+2\right)\right.\right.\\
&\quad+\beta^2\left(\alpha'+2\alpha\left(\alpha x_B(3\alpha' x_B-1)+1\right)\right)+\alpha'\left(2\alpha' x_B(\alpha' x_B+1)+1\right)\Big)\\
&\quad+(\beta')^2\left(2\alpha'\left(-\beta+\alpha' x_B(-\beta+2\alpha' x_B-3\alpha\beta x_B+2)+1\right)-\alpha\beta\right)\\
&\quad\left.+\alpha'(\beta')^3\left(2\alpha' x_B(\alpha' x_B+1)+1\right)-\alpha(\beta-1)^2\beta\left(2\alpha x_B(\alpha x_B-1)+1\right)\right)\,.
\end{aligned}\tag{F.109}$$

Soft-Fermion Pole Contributions

The soft fermion pole contributions for the combination $F+G$ feature the following partonic cross sections

$$\begin{aligned}
\hat{\sigma}^{C,\phi'}_{\mathrm{SFP},+} &= \frac{16\left(\beta'(\beta'+2)+(\beta-2)\beta-2x_B\left((\beta-1)\alpha'+\alpha(\beta'+1)\right)+\left(\alpha^2+(\alpha')^2\right)x_B^2+2\right)}{\alpha D_1 D_2 D_3}\,,\\
\hat{\sigma}^{I,\phi'}_{\mathrm{SFP},+} &= -\frac{16\left(\beta'(\beta'+2)+(\beta-2)\beta-2x_B\left((\beta-1)\alpha'+\alpha(\beta'+1)\right)+\left(\alpha^2+(\alpha')^2\right)x_B^2+2\right)}{\alpha\beta' D_1 D_2}\,,\\
\hat{\sigma}^{C,\phi^\gamma}_{\mathrm{SFP},+} &= -\frac{16(\alpha-\alpha')x_B}{\alpha D_1 D_2^2 D_3}\left(\beta'(\beta'+2)+(\beta-2)\beta-2x_B\left((\beta-1)\alpha'+\alpha(\beta'+1)\right)\right.\\
&\quad\left.+\left(\alpha^2+(\alpha')^2\right)x_B^2+2\right)\,,\\
\hat{\sigma}^{I,\phi^\gamma}_{\mathrm{SFP},+} &= \frac{16x_B(\alpha\beta'-\beta\alpha')}{\alpha\beta\beta' D_1 D_2^2}\left(\beta'(\beta'+2)+(\beta-2)\beta-2x_B\left((\beta-1)\alpha'+\alpha(\beta'+1)\right)\right.\\
&\quad\left.+\left(\alpha^2+(\alpha')^2\right)x_B^2+2\right)\,.
\end{aligned}\tag{F.110}$$

And for the $F-G$ combination one finds

$$\begin{aligned}
\hat{\sigma}^{C,\phi'}_{\mathrm{SFP},-} &= \frac{16\left(x_B\left(\alpha'\left(\beta^2+(\beta'+1)^2\right)-\alpha\left((\beta'+1)^2+(\beta-2)\beta\right)\right)+D_1\left(\beta^2+(\beta'+1)^2\right)\right)}{\alpha D_1^2 D_2 D_3}\,,\\
\hat{\sigma}^{I,\phi'}_{\mathrm{SFP},-} &= -\frac{16\left(\alpha D_1\left(\beta^2+(\beta')^2\right)x_B+D_2\beta'\left(\beta^2+(\beta'+1)^2\right)\right)}{\alpha\beta\beta' D_1 D_2}\,,\\
\hat{\sigma}^{C,\phi^\gamma}_{\mathrm{SFP},-} &= \frac{16x_B}{\alpha D_1^2 D_2^2 D_3}\left(\alpha^2\left((\beta')^2+(\beta-1)^2\right)x_B-2\alpha\alpha'\left((\beta'+1)^2+(\beta-2)\beta\right)x_B\right.\\
&\quad\left.+(\alpha')^2\left(\beta^2+(\beta'+1)^2\right)x_B+D_1\alpha'\left(\beta^2+(\beta'+1)^2\right)-\alpha D_1\left((\beta')^2+(\beta-1)^2\right)\right),\\
\hat{\sigma}^{I,\phi^\gamma}_{\mathrm{SFP},-} &= \frac{16x_B\left(\alpha\beta\left((\beta')^2+(\beta-1)^2\right)-\alpha'\beta'\left(\beta^2+(\beta'+1)^2\right)\right)}{\alpha\beta\beta' D_1 D_2}\,.
\end{aligned}\tag{F.111}$$

Appendix G

Model Ansatz for the qgq Functions

This appendix provides details on the model input for the qgq functions $F^q(x,x')$ and $G^q(x,x')$ for the quark flavors $q = u, d$ that are used to perform the numerical studies in Ch. 7. Starting point is the soft-gluon pole matrix element $F^q(x,x)$. It can be related to the first TMD moment of the Sivers function $f_{1T}^{\perp(1),q}$ using (2.69), which in turn has been extracted in the literature from global data fits, in particular from SIDIS. For more information on the status of the fits, the reader is referred to the recent comprehensive review of TMDs [157]. This work makes use of an early extraction of $f_{1T}^{\perp(1),q}$, given in [148], the reason being its simple numerical implementation. This parametrization is sufficient for the purpose of the phenomenological study, namely exploring the impact of NLO effects on the single-spin observable A_{RL} in (7.5). The analysis does not aim to give cutting-edge predictions, for which one would use more recent, state-of-the-art extractions.

In Ref. [148], $f_{1T}^{\perp(1),q}$ is parameterized at a scale $\mu_0 = 1.55\,\text{GeV}$ as follows:

$$\pi\, F^q(x,x,\mu_0) = f_{1T}^{\perp(1),q}(x,\mu_0) = -\tfrac{1}{2} N^q(x)\, f_1^q(x,\mu_0)\, \sqrt{2\text{e}}\, \frac{M_1^3\, \langle k_T^2 \rangle}{M\, (M_1^2 + \langle k_T^2 \rangle)^2}\,, \tag{G.1}$$

with M the nucleon mass, the flavor-independent mass parameters $M_1 = 0.583\,\text{GeV}$ and $\langle k_T^2 \rangle = 0.25\,\text{GeV}^2$, $\text{e} = 2.7182\ldots$ the Euler constant, and $f_1^q(x,\mu_0)$ the MSTW2008 quark PDF for flavor q [59] evaluated at the scale μ_0. The flavor-dependent factor $N^q(x)$ has the form

$$N^q(x) = N^q\, x^{\alpha_q} (1-x)^{\beta_q}\, \frac{(\alpha_q + \beta_q)^{\alpha_q+\beta_q}}{\alpha_q^{\alpha_q}\, \beta_q^{\beta_q}}\,,$$

with flavor-dependent parameters N^q, α_q, β_q whose values can be found in Ref. [148] for the flavors $q = u, d, s$. However, this work will only include $q = u, d$ and the distribution functions for strange quarks s will be set to zero throughout. The SGP matrix element for negative x can be related via charge conjugation (see the discussion below (C.4)) to the first TMD moment of the antiquark Sivers function ($\bar{q} = \bar{u}, \bar{d}$),

$$\pi\, F^q(-x,-x,\mu_0) = f_{1T}^{\perp(1),\bar{q}}(x,\mu_0)\,. \tag{G.2}$$

As can be seen from Eq. (2.64), the SGP input (G.1) is already sufficient to produce predictions for the right-left asymmetry A_{RL} at LO. However, the NLO result necessitates input for F and G on their full support. Both functions are essentially unknown in the "off-diagonal" region $x \neq x'$ and have never been extracted from data (to the author's knowledge). Therefore, one has to resort to models for these correlation functions.

As a first step, "polar coordinates" are introduced via $x(r,\varphi) = r\cos\left(\varphi + \frac{\pi}{4}\right)$, $x'(r,\varphi) = r\sin\left(\varphi + \frac{\pi}{4}\right)$, with

$$\begin{aligned} r &= \sqrt{x^2 + (x')^2}\,, \\ \varphi &= \begin{cases} -\frac{\pi}{4} + \arctan(x'/x), & x \geq 0\,, x' \geq x\,, \\ \frac{3\pi}{4} + \arctan(x'/x), & x < 0\,, \\ \frac{7\pi}{4} + \arctan(x'/x), & x \geq 0\,, x' < x\,. \end{cases} \end{aligned} \tag{G.3}$$

Notice that the polar angle φ is counted from the diagonal axis $x' = x$ instead of from the x-axis.

Then, consider the qgq correlation functions as functions of r and φ, with $r \in]0, \sqrt{2}]$, $\varphi \in [0, 2\pi]$. Due to the use of polar coordinates both $F(r,\varphi)$ and $G(r,\varphi)$ are 2π-periodic in φ, that is, $F(r,\varphi) = F(r,\varphi+2\pi)$ and $G(r,\varphi) = G(r,\varphi+2\pi)$. This feature allows to express both functions as Fourier series,

$$\begin{aligned} F^q(r,\varphi) &= \sum_{n=0}^{\infty} \left[A_n^q(r)\,\cos(n\varphi) + D_n^q(r)\,\sin(n\varphi)\right], \\ G^q(r,\varphi) &= \sum_{n=0}^{\infty} \left[C_n^q(r)\,\cos(n\varphi) + B_n^q(r)\,\sin(n\varphi)\right]. \end{aligned} \tag{G.4}$$

The important symmetry constraints (C.5) of the correlation functions under $x \leftrightarrow x'$ can be conveniently implemented into the Fourier Series (G.4). In particular, it is easy to see that the symmetry of F, i.e. $F(x,x') = +F(x',x) \Leftrightarrow F(r,\varphi) = +F(r,2\pi-\varphi)$, enforces that all Fourier coefficients $D_n(r)$ vanish. Similarly, antisymmetry of G, that is, $G(x,x') = -G(x',x) \Leftrightarrow G(r,\varphi) = -G(r,2\pi-\varphi)$, means that all Fourier coefficients $C_n(r)$ also vanish.

Furthermore, one can easily implement the relation between $F(x,x)$ and $f_{1T}^{\perp(1),q}$ in Eq. (2.69) as follows,

$$\begin{aligned} F^q(r,\varphi=0) &= \frac{1}{\pi} f_{1T}^{\perp(1),q}\left(\tfrac{r}{\sqrt{2}}\right) = A_0^q(r) + A_1^q(r) + A_2^q(r) + A_3^q(r) + \ldots, \\ F^q(r,\varphi=\pi) &= \frac{1}{\pi} f_{1T}^{\perp(1),\bar{q}}\left(\tfrac{r}{\sqrt{2}}\right) = A_0^q(r) - A_1^q(r) + A_2^q(r) - A_3^q(r) + \ldots. \end{aligned}$$

These constraints can be translated into constraints for the Fourier coefficients A_0 and A_1,

$$\begin{aligned} A_0^q(r) &= \frac{1}{2\pi}\left(f_{1T}^{\perp(1),q}\left(\tfrac{r}{\sqrt{2}}\right) + f_{1T}^{\perp(1),\bar{q}}\left(\tfrac{r}{\sqrt{2}}\right)\right) - A_2^q(r) - A_4^q(r) - A_6^q(r) - \ldots, \\ A_1^q(r) &= \frac{1}{2\pi}\left(f_{1T}^{\perp(1),q}\left(\tfrac{r}{\sqrt{2}}\right) - f_{1T}^{\perp(1),\bar{q}}\left(\tfrac{r}{\sqrt{2}}\right)\right) - A_3^q(r) - A_5^q(r) - A_7^q(r) - \ldots. \end{aligned} \tag{G.5}$$

Implementing (G.5) into (G.4) yields, ($q \pm \bar{q}$ denotes the sum/difference of quark and antiquark distributions as in (G.5))

$$\begin{aligned} F^q(r,\varphi) &= \frac{1}{2\pi} f_{1T}^{\perp(1),q+\bar{q}}\left(\tfrac{r}{\sqrt{2}}\right) + \frac{1}{2\pi} f_{1T}^{\perp(1),q-\bar{q}}\left(\tfrac{r}{\sqrt{2}}\right)\cos(\varphi) \\ &\quad + \sum_{n=1}^{\infty}\left[A_{2n}^q(r)\left(\cos(2n\varphi)-1\right)\right] + \sum_{n=1}^{\infty}\left[A_{2n+1}^q(r)\left(\cos((2n+1)\varphi) - \cos(\varphi)\right)\right], \\ G^q(r,\varphi) &= \sum_{n=1}^{\infty}\left[B_n^q(r)\,\sin(n\varphi)\right]. \end{aligned} \tag{G.6}$$

Up to this point, the two Fourier expansions in (G.6) are exact and model-independent. In particular, the Fourier coefficients $A_n(r)$, $B_n(r)$ depend on $r = \sqrt{x^2 + (x')^2}$. In other words, for every Fourier component n there are two (unknown) functions $A_n(r)$, $B_n(r)$ that should ideally be fitted to experimental data. This would be an impossible task to do for all Fourier components. However, the series (G.6) are quite useful for building a parameterization that can be used as input for the numerical study of the observable A_{RL} in (7.5) at NLO. For this, some simplifying assumptions are needed.

First, Fourier series often converge quite fast on an interval $[0, 2\pi]$. Whether it does, depends of course on the series. For now, assume that keeping six free parameters for each flavor already constitutes a reasonable approximation to the exact series. To be specific, all Fourier coefficients for $n \geq 8$ in case of F and for $n \geq 7$ in case of G will be set to zero, i.e., $A_{n\geq 8}^q(r) = 0$, $B_{n\geq 7}^q(r) = 0$. If this assumption turns out to be wrong for some reason, for instance, because the explanation of experimental data may require a higher precision, one is free to add more Fourier components and truncate the series (G.6) at higher n.

The second assumption is about the functional form of the Fourier coefficients $A_n^q(r)$, $B_n^q(r)$. In a first step, they are replaced by the modified coefficients $a_n^q(r)$, $b_n^q(r)$ according to

$$\begin{aligned} A_{n=2,4,6,\ldots}^q(r) &\equiv \frac{1}{2\pi} f_{1T}^{\perp(1),q+\bar{q}}\left(\tfrac{r}{\sqrt{2}}\right) a_{n=2,4,6,\ldots}^q(r), \\ A_{n=1,3,5,\ldots}^q(r) &\equiv \frac{1}{2\pi} f_{1T}^{\perp(1),q-\bar{q}}\left(\tfrac{r}{\sqrt{2}}\right) a_{n=1,3,5,\ldots}^q(r), \\ B_n^q(r) &\equiv -\frac{1}{\pi} f_{1T}^{\perp(1),q+\bar{q}}\left(\tfrac{r}{\sqrt{2}}\right) b_n^q(r). \end{aligned} \tag{G.7}$$

The idea is that the "size" or "scale" of the qgq functions F and G is roughly set by the SGP diagonal determined by the extraction (G.1). Under this assumption, the modified coefficients $a_n(r)$, $b_n(r)$ may vary on the order of magnitude of 1, but not, say, 1000.

Third, the modified coefficients in (G.7) are approximated to be constants with respect to the radius r. Thus, replace the functions $a_n^q(r)$, $b_n^q(r)$ by their mean values $a_n^q(r) \to \langle a_n^q(r)\rangle = a_n^q$, $b_n^q(r) \to \langle b_n^q(r)\rangle = b_n^q$.

The following model ansätze result from the implementation of all assumptions:

$$\begin{aligned} F^q(r,\varphi)\Big|_{\text{model}} &= \frac{1}{2\pi} f_{1T}^{\perp(1),q+\bar{q}}\left(\tfrac{r}{\sqrt{2}}\right)\left[1+\sum_{n=1}^{3}\left[a_{2n}^q\left(\cos(2n\varphi)-1\right)\right]\right] \\ &\quad + \frac{1}{2\pi} f_{1T}^{\perp(1),q-\bar{q}}\left(\tfrac{r}{\sqrt{2}}\right)\left[\cos(\varphi)+\sum_{n=1}^{3}\left[a_{2n+1}^q\left(\cos((2n+1)\varphi)-\cos(\varphi)\right)\right]\right], \\ G^q(r,\varphi)\Big|_{\text{model}} &= -\frac{1}{\pi} f_{1T}^{\perp(1),q+\bar{q}}\left(\tfrac{r}{\sqrt{2}}\right)\sum_{n=1}^{6}\left[b_n^q\,\sin(n\varphi)\right]. \end{aligned} \tag{G.8}$$

Effectively, the models (G.8) enable a description of the functions F^q, G^q by six parameters, separately for each flavor. These parameters are collected as entries in a vector in the following way (note the specific ordering of the even and odd Fourier coefficients for F):

$$\begin{aligned} \boldsymbol{a}^q &= (a_2^q, a_4^q, a_6^q; a_3^q, a_5^q, a_7^q), \\ \boldsymbol{b}^q &= (b_1^q, b_2^q, b_3^q, b_4^q, b_5^q, b_6^q). \end{aligned} \tag{G.9}$$

It is noteworthy that no matter which values the vectors $\boldsymbol{a}^q$, $\boldsymbol{b}^q$ take, the soft-gluon pole is always provided by the extraction (G.1). It is the only constraint available from data for the functions F and G.

In order to smoothen the transition of the functions F and G at the boundaries $|x|=1$, $|x'|=1$, $|x-x'|=1$ of their support it is helpful to introduce an envelope function, for example of the following form:

$$\begin{aligned} e(x,x') &= \left(\frac{2}{1+\mathrm{e}^{50\,(x^2-1)^3}}-1\right)\left(\frac{2}{1+\mathrm{e}^{50\,((x')^2-1)^3}}-1\right)\times \\ &\quad \left(\frac{2}{1+\mathrm{e}^{50\,((x-x')^2-1)^3}}-1\right)\theta\left(1-|x|\right)\theta\left(1-|x'|\right)\theta\left(1-|x-x'|\right). \end{aligned} \tag{G.10}$$

The function $e(x,x')$ in (G.10) is approximately unity, except in the vicinity of the boundary $|x|=1$, $|x'|=1$, $|x-x'|=1$. Multiplying the function $e(x,x')$ in (G.10) with the model expressions (G.9) does not significantly alter the model but ensures smoothness of the functions F and G even at the boundary. In particular, it ensures $F(x,1)=F(1,x')=G(x,1)=G(1,x')=0$ and $(\partial_2 F)(x,1)=(\partial_1 F)(1,x')=(\partial_2 G)(x,1)=(\partial_1 G)(1,x')=0$. Therefore, the model is adapted as follows

$$F^q(r,\varphi)\Big|_{\text{model}} \to F^q(r,\varphi)\Big|_{\text{model}} e(x,x') \quad ; \quad G^q(r,\varphi)\Big|_{\text{model}} \to G^q(r,\varphi)\Big|_{\text{model}} e(x,x').$$

Constraints from Lattice QCD There exists another source of information on F from lattice QCD that one may apply here as well. One can express the second moment of the genuine twist-3 part of the DIS structure function $\bar{g}_2$, the so-called d_2^q moment, in terms of the fully integrated qgq function F^q. This feature has been discussed, for example, in [158, 159]. Interestingly, one can interpret the moment d_2 as a probe of the color Lorentz force, mediated by the strong force in the nucleon [160, 161]. The connection between d_2^q and F^q is as follows,

$$d_2^q = -\int_{-1}^{1}\mathrm{d}x\int_{-1}^{1}\mathrm{d}x'\,F^q(x,x'). \tag{G.11}$$

In Refs. [147, 162, 163, 164] the d_2 moments for up and down quarks were computed on the lattice. The values found in [147] are

$$d_2^u = -0.00365(25)\,; \quad d_2^d = 0. \tag{G.12}$$

Despite the limitations related to unphysical pion masses or renormalization schemes, these values constrain the size of the function F^q. Due to the linearity of the model (G.8) in the Fourier

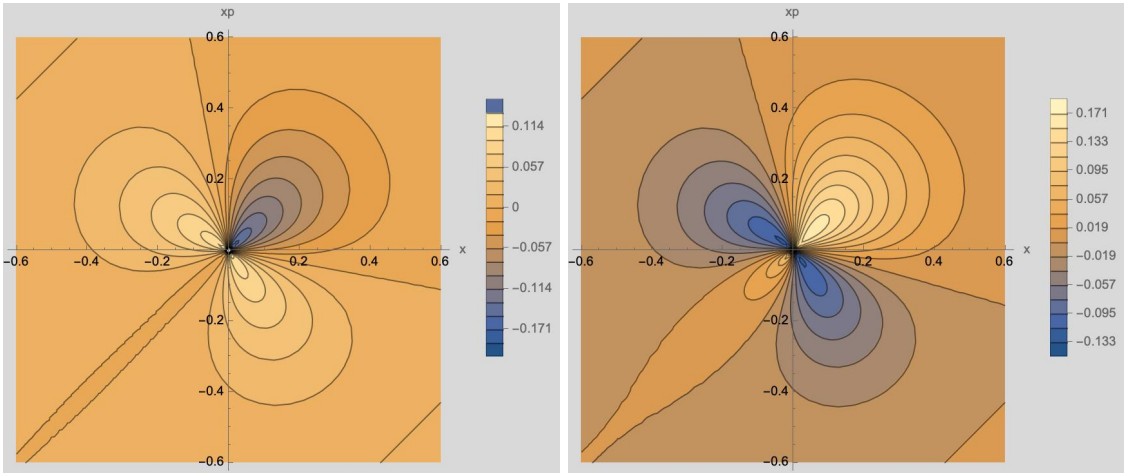

Figure G.1: Correlation functions $F^u(x,x')$ **(left)** and $F^d(x,x')$ **(right)** for Scenario 0.

coefficients a^q, it is easy to implement the lattice constraint (G.12). One simply inserts Eq. (G.8) into (G.11) to obtain

$$I_0^q + I_2^q\, a_2^q + I_4^q\, a_4^q + I_6^q\, a_6^q + I_3^q\, a_3^q + I_5^q\, a_5^q + I_7^q\, a_7^q = d_2^q\,, \tag{G.13}$$

where

$$\begin{aligned} I_0^q &\equiv -\int_{-1}^{1}\mathrm{d}x \int_{-1}^{1}\mathrm{d}x'\, F^q(r,\varphi)\Big|_{\text{model},\,\boldsymbol{a}^q=\boldsymbol{0}}\,, \\ I_i^q &\equiv -I_0^q - \int_{-1}^{1}\mathrm{d}x \int_{-1}^{1}\mathrm{d}x'\, F^q(r,\varphi)\Big|_{\text{model},\,a_i^q=1,\,a_{j\neq i}^q=0}\,. \end{aligned} \tag{G.14}$$

Solving these constraints for the Fourier coefficient a_2^q (for example) allows one to express it as a function of the remaining coefficients and thus remove one degree of freedom,

$$a_2^q = \frac{1}{I_2^q}(d_2^q - (I_0^q + I_4^q\, a_4^q + I_6^q\, a_6^q + I_3^q\, a_3^q + I_5^q\, a_5^q + I_7^q\, a_7^q))\,. \tag{G.15}$$

It must be emphasized that no constraint similar to (G.13) is known for the correlation function G.

The following three scenarios for the correlation functions based on three specific choices of Fourier coefficients (G.9) are used in the numerical analyses of Ch. 7. Each scenario is consistent with the constraint (G.11) for the moments d_2^u, d_2^d.

All scenarios are formulated in terms of the first TMD moments of the Sivers functions $f_{1T}^{\perp(1),q+\bar{q}}$ and hence, via Eq. (G.1), in terms of the unpolarized twist-2 PDFs f_1^q. The corresponding relations can strictly hold only at one scale μ_0, since the evolutions of the $f_{1T}^{\perp(1),q+\bar{q}}$ and f_1^q differ. Nevertheless, as discussed in Sec. 7, the numerical studies assume $f_{1T}^{\perp(1),q+\bar{q}}$ and f_1^q to be related in the same way at all scales, simply as a rough means of mimicking the scale evolution of the twist-3 qgq functions.

G.1 Scenario 0

The Fourier coefficients (G.9) for the first scenario are fixed as follows:

$$\begin{aligned} \boldsymbol{a}^u &= (1.1578, 0, 0; 0, 0, 0)\,, \\ \boldsymbol{a}^d &= (1.0173, 0, 0; 0, 0, 0)\,, \\ \boldsymbol{b}^u &= (0, 0, 0, 0, 0, 0)\,, \\ \boldsymbol{b}^d &= (0, 0, 0, 0, 0, 0)\,. \end{aligned} \tag{G.16}$$

This choice sets the correlation function G to zero, and provides a correlation function F that is as "levelled" as possible by utilizing only the first three Fourier components $\cos(0\varphi)$, $\cos(1\varphi)$, $\cos(2\varphi)$ in the model ansatz (G.8). Note that an additional choice $a_2^q = 0$ would violate the d_2-constraint (G.13). Scenario 0 is visualized via contour plots of F^q in Fig. G.1. NLO contributions to the asymmetry A_{RL} within this scenario are minimal in the sense that $G = 0$ and the plots in Fig. G.1 show little "structure" of F^q.

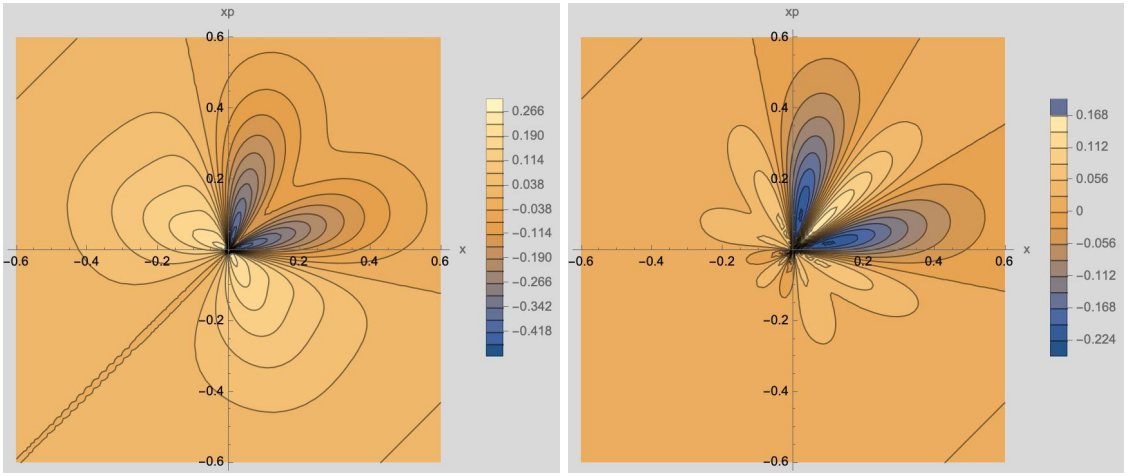

Figure G.2: Same as Fig. G.1, but for Scenario 1.

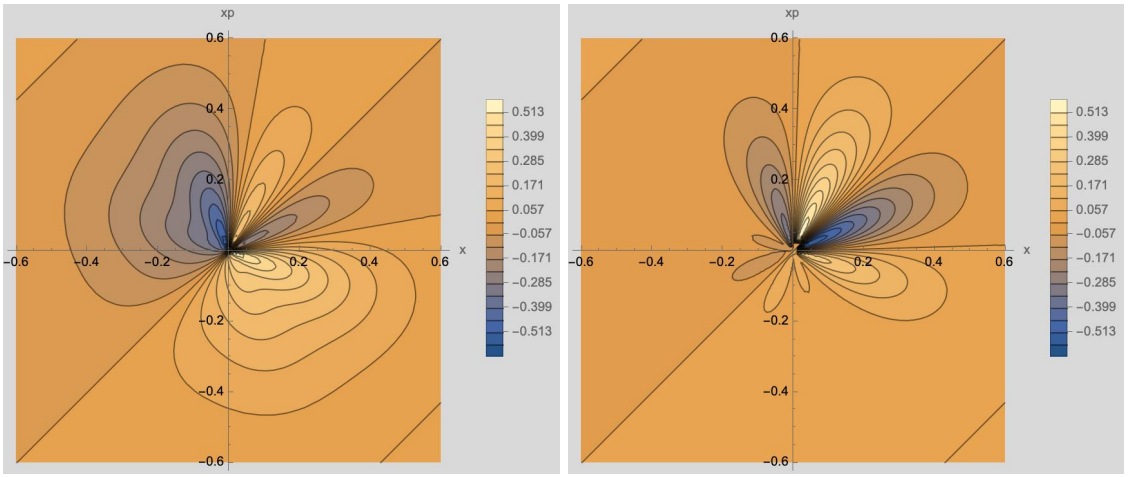

Figure G.3: Correlation functions $G^u(x,x')$ **(left)** and $G^d(x,x')$ **(right)** for Scenario 1.

G.2 Scenario 1

This scenario populates most of the Fourier coefficients (G.9) for the u- and d-quark correlation functions with relatively moderate values between -1 and 1. Doing so generates a non-vanishing correlation function G. As before, the d_2-constraint from Lattice QCD (G.14) is satisfied. This scenario is somewhat more "realistic" as far as the sizes of the correlation functions are concerned. To be specific, the Fourier coefficients in Scenario 1 are

$$\begin{aligned} \boldsymbol{a}^u &= \left(2.5308, -\tfrac{2}{3}, -\tfrac{2}{3}; -\tfrac{1}{3}, -1, -\tfrac{1}{3}\right) , \\ \boldsymbol{a}^d &= \left(-0.3429, \tfrac{2}{3}, \tfrac{2}{3}; \tfrac{1}{3}, 1, \tfrac{1}{3}\right) , \\ \boldsymbol{b}^u &= \left(-2.5308, \tfrac{1}{3}, \tfrac{2}{3}, 1, \tfrac{2}{3}, \tfrac{1}{3}\right) , \\ \boldsymbol{b}^d &= \left(0.3429, -\tfrac{1}{3}, -\tfrac{2}{3}, -1, -\tfrac{2}{3}, -\tfrac{1}{3}\right) . \end{aligned} \tag{G.17}$$

The contour plots for the resulting u- and d-quark correlation functions $F^q(x,x')$ are shown in Fig. G.2, and the corresponding correlation functions G^q for up and down quarks in Fig. G.3 shows. Note that the symmetry and antisymmetry properties of F and G under exchange $x \leftrightarrow x'$ are well visible in Figs. G.2 and G.3.

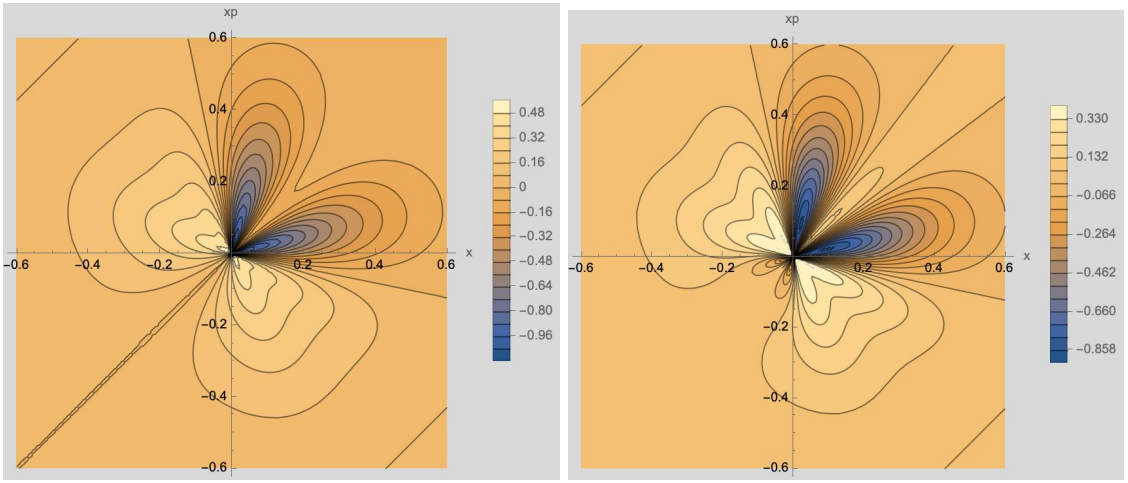

Figure G.4: Same as Fig. G.1, but for Scenario 2.

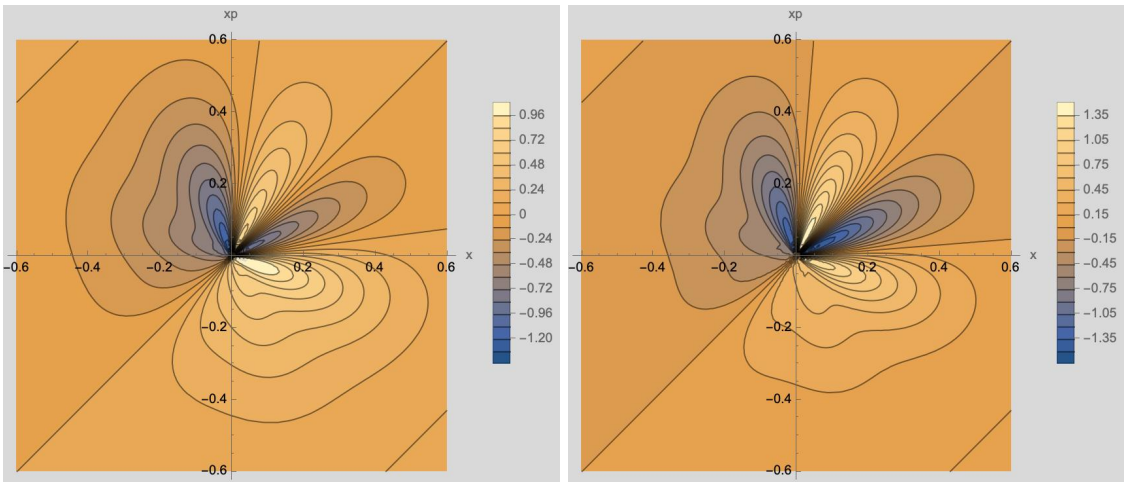

Figure G.5: Same as Fig. G.3, but for Scenario 2.

G.3 Scenario 2

Finally, Scenario 2 is similar to Scenario 1, but with three times larger Fourier coefficients in order to magnify the effects of the NLO corrections on A_{RL}. Specifically, the coefficients read

$$\begin{aligned} \boldsymbol{a}^u &= (5.2767, -2, -2; -1, -3, -1) \ , \\ \boldsymbol{a}^d &= (-3.0634, 2, 2; 1, 3, 1) \ , \\ \boldsymbol{b}^u &= (-5.2767, 1, 2, 3, 2, 1) \ , \\ \boldsymbol{b}^d &= (3.0634, -1, -2, -3, -2, -1) \ . \end{aligned} \tag{G.18}$$

As for the other two scenarios, the constraint (G.11) on d_2 by lattice QCD is satisfied also here. The resulting contour plots for the u- and d-quark correlation functions F^q are shown in Fig. G.4, while Figure G.5 presents the corresponding contour plots for G.

G.4 γSIDIS Scenarios S0 and S1

The numerical analysis for the γSIDIS process $\ell N^\uparrow \to \ell' \gamma X$ in Sec.7.4 is based on Ref. [39], which uses a different extraction of the first moment of the Sivers function $f_{1T}^{\perp(1),q}$, namely the set provided by JAM3D-22 , cf. Ref. [144]. The initial scale is then $\mu_0^2 = 2\,\mathrm{GeV}^2$, and the evolution of F^q, G^q in Eq. (G.8) is simply "inherited" from the evolution of the JAM3D-22 $f_{1T}^{\perp(1)}(x)$ extraction. Moreover, the d_2 moments for u and d quarks are chosen as $d_2^u = 0.026(4)(13), d_2^d = -0.0086(26)(146)$, taken from Ref. [163]. As a consequence, the determination of the coefficient a_2^q according to Eq. (G.15) gives a different value, even if all other coefficients a_n^q are chosen as before. This leads to the following two modified γSIDIS versions for the Scenarios 0 and 1 from before. They will be labeled

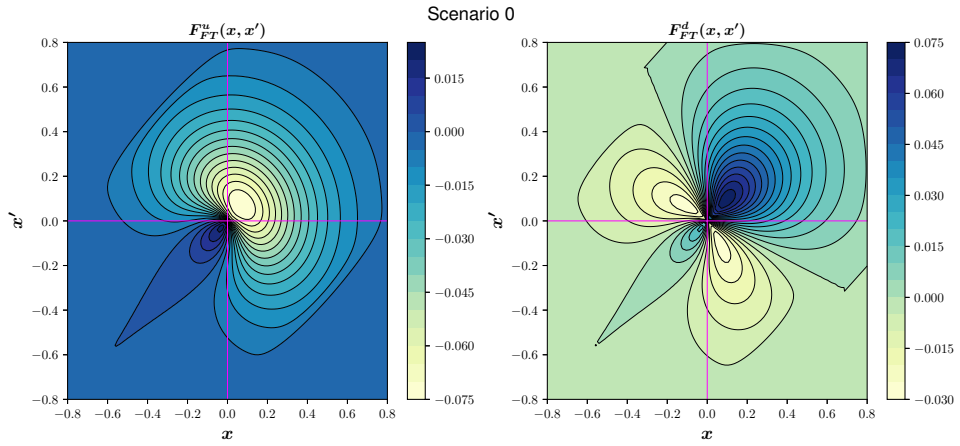

Figure G.6: F^q vs. (x, x') at a scale $\mu^2 = 4\,\mathrm{GeV}^2$ for Scenario S0 for the up quark **(left)** and down quark **(right)** in a proton. Recall that $G^q = 0$ for Scenario S0.

as "S0" and "S1", and Figs. G.6, G.7 show the resulting $F^{u,d}(x, x')$ and $G^{u,d}(x, x')$ from these two scenarios. The coefficients read explicitly

$$\begin{aligned} \boldsymbol{a}^u &= (-0.2691, 0, 0; 0, 0, 0) \\ \boldsymbol{a}^d &= (0.7822, 0, 0; 0, 0, 0) \\ \boldsymbol{b}^u &= (0, 0, 0, 0, 0, 0) \\ \boldsymbol{b}^d &= (0, 0, 0, 0, 0, 0)\,, \end{aligned} \tag{G.19}$$

for Scenario S0 and

$$\begin{aligned} \boldsymbol{a}^u &= (1.1585, -\tfrac{2}{3}, -\tfrac{2}{3}; -\tfrac{1}{3}, -1, -\tfrac{1}{3}) \\ \boldsymbol{a}^d &= (-0.6658, \tfrac{2}{3}, \tfrac{2}{3}; \tfrac{1}{3}, 1, \tfrac{1}{3}) \\ \boldsymbol{b}^u &= (-1.1585, \tfrac{1}{3}, \tfrac{2}{3}, 1, \tfrac{2}{3}, \tfrac{1}{3}) \\ \boldsymbol{b}^d &= (0.6658, -\tfrac{1}{3}, -\tfrac{2}{3}, -1, -\tfrac{2}{3}, -\tfrac{1}{3})\,, \end{aligned} \tag{G.20}$$

for Scenario S1.

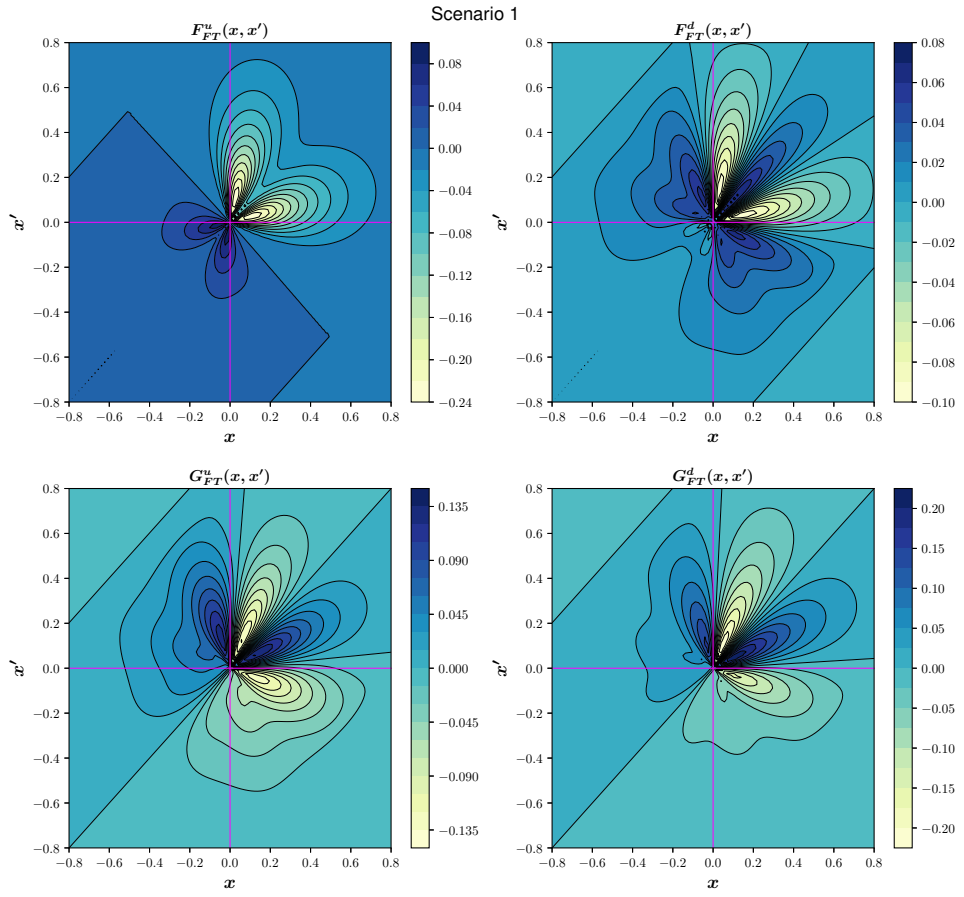

Figure G.7: F^q vs. (x, x') **(top row)** and G^q vs. (x, x') **(bottom row)** at a scale $\mu^2 = 4\,\mathrm{GeV}^2$ for Scenario S1 for the up quark **(left)** and down quark **(right)** in a proton.

List of Figures

Bibliography

[1] H. Schmidt-Böcking, L. Schmidt, H. Lüdde, W. Trageser, and T. Sauer, "The Stern-Gerlach Experiment Revisited," *The European Physical Journal H*, vol. 41, 09 2016.

[2] P. A. M. Dirac, "The Quantum Theory of the Electron," *Proceedings of the Royal Society of London. Series A, Containing Papers of a Mathematical and Physical Character*, vol. 117, no. 778, pp. 610–624, 1928.

[3] P. Dirac, *The Principles of Quantum Mechanics*. Comparative Pathobiology - Studies in the Postmodern Theory of Education, Clarendon Press, 1981.

[4] W. Pauli, *General Principles of Quantum Mechanics*. Springer-Verlag, 1980.

[5] G. F. Giudice, P. Paradisi, and M. Passera, "Testing new physics with the electron $g-2$," *Journal of High Energy Physics*, vol. 2012, nov 2012.

[6] E. Leader, "Spin in particle physics," *Camb. Monogr. Part. Phys. Nucl. Phys. Cosmol.*, vol. 15, p. 1, 2001.

[7] J. Ashman *et al.*, "A measurement of the spin asymmetry and determination of the structure function g_1 in deep inelastic muon proton scattering," *Phys. Lett.*, vol. B206, p. 364, 1988.

[8] J. Ashman *et al.*, "An investigation of the spin structure of the proton in deep inelastic scattering of polarised muons on polarised protons," *Nuclear Physics B*, vol. 328, no. 1, pp. 1–35, 1989.

[9] E. W. Hughes and R. Voss, "Spin Structure Functions," *Annual Review of Nuclear and Particle Science*, vol. 49, no. Volume 49, 1999, pp. 303–339, 1999.

[10] R. L. Jaffe and A. Manohar, "The g_1 Problem: Fact and Fantasy on the Spin of the Proton," *Nucl. Phys. B*, vol. 337, pp. 509–546, 1990.

[11] E. Leader and M. Anselmino, "A crisis in the parton model: where, oh where is the proton's spin?," *Z. Phys. C*, vol. 41, pp. 239–246, 1988.

[12] X. Ji, F. Yuan, and Y. Zhao, "What we know and what we don't know about the proton spin after 30 years," *Nature Reviews Physics*, vol. 3, 11 2020.

[13] D. L. Adams *et al.*, "Comparison of spin asymmetries and cross-sections in π^0 production by 200 GeV polarized antiprotons and protons," *Phys. Lett.*, vol. B261, pp. 201–206, 1991.

[14] K. Krueger *et al.*, "Large analyzing power in inclusive $\pi^{\pm}$ production at high x_F with a 22-GeV/c polarized proton beam," *Phys. Lett. B*, vol. 459, pp. 412–416, 1999.

[15] C. E. Allgower *et al.*, "Measurement of analyzing powers of π^+ and π^- produced on a hydrogen and a carbon target with a $22-\mathrm{GeV}/c$ incident polarized proton beam," *Phys. Rev. D*, vol. 65, p. 092008, 2002.

[16] J. Adams *et al.*, "Cross sections and transverse single-spin asymmetries in forward neutral pion production from proton collisions at $\sqrt{s} = 200$ gev," *Phys. Rev. Lett.*, vol. 92, p. 171801, 2004.

[17] S. S. Adler *et al.*, "Measurement of transverse single-spin asymmetries for mid- rapidity production of neutral pions and charged hadrons in polarized p + p collisions at $\sqrt{s} = 200$ GeV," *Phys. Rev. Lett.*, vol. 95, p. 202001, 2005.

[18] J. H. Lee and F. Videbaek, "Single spin asymmetries of identified hadrons in polarized p + p at $\sqrt{s} = 62.4$ and 200 GeV," *AIP Conf. Proc.*, vol. 915, no. 1, pp. 533–538, 2007.

[19] B. I. Abelev *et al.*, "Forward Neutral Pion Transverse Single Spin Asymmetries in p+p Collisions at $\sqrt{s} = 200$ GeV," *Phys. Rev. Lett.*, vol. 101, p. 222001, 2008.

[20] I. Arsene *et al.*, "Single Transverse Spin Asymmetries of Identified Charged Hadrons in Polarized p+p Collisions at $\sqrt{s} = 62.4$ GeV," *Phys. Rev. Lett.*, vol. 101, p. 042001, 2008.

[21] L. Adamczyk *et al.*, "Transverse Single-Spin Asymmetry and Cross-Section for π^0 and η Mesons at Large Feynman-x in Polarized $p + p$ Collisions at $\sqrt{s} = 200$ GeV," *Phys. Rev. D*, vol. 86, p. 051101, 2012.

[22] A. Adare *et al.*, "Measurement of transverse-single-spin asymmetries for midrapidity and forward-rapidity production of hadrons in polarized p+p collisions at $\sqrt{s}$ =200 and 62.4 GeV," *Phys. Rev. D*, vol. 90, no. 1, p. 012006, 2014.

[23] A. Adare *et al.*, "Cross section and transverse single-spin asymmetry of η mesons in $p^{\uparrow} + p$ collisions at $\sqrt{s} = 200$ GeV at forward rapidity," *Phys. Rev. D*, vol. 90, no. 7, p. 072008, 2014.

[24] J. Adam *et al.*, "Measurement of transverse single-spin asymmetries of π^0 and electromagnetic jets at forward rapidity in 200 and 500 GeV transversely polarized proton-proton collisions," *Phys. Rev. D*, vol. 103, no. 9, p. 092009, 2021.

[25] A. Airapetian *et al.*, "Transverse target single-spin asymmetry in inclusive electroproduction of charged pions and kaons," *Phys. Lett. B*, vol. 728, pp. 183–190, 2014.

[26] L. C. Bland *et al.*, "Cross Sections and Transverse Single-Spin Asymmetries in Forward Jet Production from Proton Collisions at $\sqrt{s} = 500$ GeV," *Phys. Lett. B*, vol. 750, pp. 660–665, 2015.

[27] U. A. Acharya *et al.*, "Probing Gluon Spin-Momentum Correlations in Transversely Polarized Protons through Midrapidity Isolated Direct Photons in $p^{\uparrow} + p$ Collisions at $\sqrt{s}$=200 GeV," *Phys. Rev. Lett.*, vol. 127, no. 16, p. 162001, 2021.

[28] A. Adare *et al.*, "Measurement of Transverse Single-Spin Asymmetries for J/ψ Production in Polarized $p + p$ Collisions at $\sqrt{s} = 200$ GeV," *Physical Review D*, vol. 82, Dec. 2010.

[29] G. L. Kane, J. Pumplin, and W. Repko, "Transverse Quark Polarization in Large P_T Reactions, e^+e^- Jets, and Leptoproduction: A Test of QCD," *Phys. Rev. Lett.*, vol. 41, p. 1689, 1978.

[30] C. Kouvaris, J.-W. Qiu, W. Vogelsang, and F. Yuan, "Single transverse-spin asymmetry in high transverse momentum pion production in pp collisions," *Phys. Rev.*, vol. D74, p. 114013, 2006.

[31] A. V. Efremov and O. V. Teryaev, "On spin effects in quantum chromodynamics," *Sov. J. Nucl. Phys.*, vol. 36, p. 140, 1982.

[32] J.-w. Qiu and G. Sterman, "Single transverse spin asymmetries," *Phys. Rev. Lett.*, vol. 67, pp. 2264–2267, 1991.

[33] Y. Koike and T. Tomita, "Soft-fermion-pole contribution to single-spin asymmetry for pion production in pp collisions," *Phys. Lett.*, vol. B675, pp. 181–189, 2009.

[34] A. Metz and D. Pitonyak, "Fragmentation contribution to the transverse single-spin asymmetry in proton-proton collisions," *Phys. Lett.*, vol. B723, pp. 365–370, 2013. [Erratum: Phys. Lett.B762,549(2016)].

[35] H. Beppu, K. Kanazawa, Y. Koike, and S. Yoshida, "Three-gluon contribution to the single spin asymmetry for light hadron production in pp collision," *Phys. Rev.*, vol. D89, no. 3, p. 034029, 2014.

[36] D. Rein, M. Schlegel, P. Tollkühn, and W. Vogelsang, "NLO corrections and factorization for transverse single-spin asymmetries," 2025.

[37] D. Rein, M. Schlegel, P. Tollkühn, and W. Vogelsang, "Transverse Nucleon Single-Spin Asymmetry for Single-Inclusive Hadron and Jet Production at NLO Accuracy," 2025.

[38] D. Rein, M. Schlegel, and W. Vogelsang, "Probing the polarized photon content of the proton in *ep* collisions at the EIC," *Phys. Rev. D*, vol. 110, p. 014041, Jul 2024.

[39] M. Harris, J. Marsh, D. Pitonyak, A. Prokudin, J. Putnam, D. Rein, and M. Schlegel, "Transverse single-spin asymmetries in γSIDIS as a direct probe of quark-gluon-quark longitudinal momentum structure," *Physics Letters B*, vol. 869, p. 139793, 2025.

[40] A. Metz, D. Pitonyak, A. Schafer, M. Schlegel, W. Vogelsang, *et al.*, "Single-spin asymmetries in inclusive deep inelastic scattering and multiparton correlations in the nucleon," *Phys.Rev.*, vol. D86, p. 094039, 2012.

[41] M. Schlegel, "Partonic description of the transverse target single-spin asymmetry in inclusive deep-inelastic scattering," *Phys.Rev.*, vol. D87, p. 034006, 2013.

[42] A. P. Chen, J. P. Ma, and G. P. Zhang, "One-Loop Corrections of Single Spin Asymmetries in Semi-Inclusive DIS," *Phys. Rev. D*, vol. 97, no. 5, p. 054003, 2018.

[43] S. Benic, Y. Hatta, H.-n. Li, and D.-J. Yang, "Single-spin asymmetries at two loops," *Phys. Rev. D*, vol. 100, no. 9, p. 094027, 2019.

[44] W. Vogelsang and F. Yuan, "Next-to-leading Order Calculation of the Single Transverse Spin Asymmetry in the Drell-Yan Process," *Phys. Rev.*, vol. D79, p. 094010, 2009.

[45] A. P. Chen, J. P. Ma, and G. P. Zhang, "One-loop corrections to single spin asymmetries at twist-3 in Drell-Yan processes," *Phys. Rev.*, vol. D95, no. 7, p. 074005, 2017.

[46] L. Gamberg, Z.-B. Kang, D. Pitonyak, M. Schlegel, and S. Yoshida, "Polarized hyperon production in single-inclusive electron-positron annihilation at next-to-leading order," *JHEP*, vol. 01, p. 111, 2019.

[47] L. Gamberg, Z.-B. Kang, A. Metz, D. Pitonyak, and A. Prokudin, "Left-right spin asymmetry in $\ell N^{\uparrow} \to hX$," *Phys.Rev.*, vol. D90, no. 7, p. 074012, 2014.

[48] S. Fitzgibbons, M. Malda, J. Marsh, D. Pitonyak, and P. Smith, "Updated numerical study of transverse single-spin asymmetries in single-inclusive pion production from lepton-nucleon collisions," *Phys. Lett. B*, vol. 852, p. 138606, 2024.

[49] G. Martinelli and G. Parisi and R. Petronzio and F. Rapuano, "The proton and neutron magnetic moments in lattice QCD," *Physics Letters B*, vol. 116, no. 6, pp. 434–436, 1982.

[50] G. Martinelli and C. Sachrajda, "A lattice study of nucleon structure," *Nuclear Physics B*, vol. 316, no. 2, pp. 355–372, 1989.

[51] H.-W. Lin, E. R. Nocera, F. Olness, and K. O. et al., "Parton distributions and lattice qcd calculations: A community white paper," *Progress in Particle and Nuclear Physics*, vol. 100, pp. 107–160, 2018.

[52] Y. Aoki, T. Blum, G. Colangelo, *et al.*, "FLAG Review 2021," *The European Physical Journal C*, vol. 82, no. 869, 2022.

[53] R. P. Feynman, "Very high-energy collisions of hadrons," *Phys. Rev. Lett.*, vol. 23, pp. 1415–1417, 1969.

[54] R. Feynman, "Photon hadron interactions." Reading, Massachusetts: W.A. Benjamin (1972).

[55] J. D. Bjorken and E. A. Paschos, "Inelastic Electron Proton and gamma Proton Scattering, and the Structure of the Nucleon," *Phys. Rev.*, vol. 185, pp. 1975–1982, 1969.

[56] J. Collins, "Foundations of perturbative QCD," *Camb. Monogr. Part. Phys. Nucl. Phys. Cosmol.*, vol. 32, pp. 1–624, 2011.

[57] X. Ji, "Parton Physics on a Euclidean Lattice," *Phys. Rev. Lett.*, vol. 110, p. 262002, 2013.

[58] B. Kriesten, A. NieMiera, W. Good, T. J. Hobbs, and H.-W. Lin, "Decoding the proton's gluonic density with lattice QCD-informed machine learning," 7 2025.

[59] A. D. Martin, W. J. Stirling, R. S. Thorne, and G. Watt, "Parton distributions for the LHC," *Eur. Phys. J. C*, vol. 63, pp. 189–285, 2009.

[60] R. D. Ball, L. Del Debbio, S. Forte, A. Guffanti, J. I. Latorre, J. Rojo, and M. Ubiali, "A first unbiased global NLO determination of parton distributions and their uncertainties," *Nucl. Phys. B*, vol. 838, pp. 136–206, 2010.

[61] S. Forte and S. Carrazza, "Parton distribution functions," 2020.

[62] D. Gross and F. Wilczek, "Ultraviolet behavior of non-abelian gauge theories," *Phys. Rev. Lett.*, vol. 30, pp. 1343–1346, 1973.

[63] H. Politzer, "Reliable perturbative results for strong interactions?," *Phys. Rev. Lett.*, vol. 30, pp. 1346–1349, 1973.

[64] S. Weinberg, "Current algebra and gauge theories. i," *Phys. Rev. D*, vol. 8, pp. 605–625, Jul 1973.

[65] L. Faddeev and V. Popov, "Feynman diagrams for the yang-mills field," *Physics Letters B*, vol. 25, no. 1, pp. 29–30, 1967.

[66] M. E. Peskin and D. V. Schroeder, *An Introduction to quantum field theory*. Reading, USA: Addison-Wesley, 1995.

[67] R. K. Ellis, W. J. Stirling, and B. R. Webber, *QCD and Collider Physics*. Cambridge Monographs on Particle Physics, Nuclear Physics and Cosmology, Cambridge University Press, 1996.

[68] G. 't Hooft and M. J. G. Veltman, "Regularization and Renormalization of Gauge Fields," *Nucl. Phys. B*, vol. 44, pp. 189–213, 1972.

[69] W. Vogelsang, "Quantenfeldtheorie 2," 2018.

[70] H. Bélusca-Maïto, A. Ilakovac, M. Mađor-Božinović, P. Kühler, and D. Stöckinger, "γ_5 in dimensional regularization – a no-compromise approach using the bmhv scheme," 2022.

[71] P. Breitenlohner and D. Maison, "Dimensional Renormalization and the Action Principle," *Commun. Math. Phys.*, vol. 52, pp. 11–38, 1977.

[72] F. Jegerlehner, "Facts of life with γ_5," *Eur. Phys. J.*, vol. C18, pp. 673–679, 2001.

[73] M. Jamin and M. E. Lautenbacher, "Tracer: Version 1.1: A mathematica package for gamma algebra in arbitrary dimensions," *Comput. Phys. Commun.*, vol. 74, pp. 265–288, 1993.

[74] J. Schwinger, "On quantum-electrodynamics and the magnetic moment of the electron," *Phys. Rev.*, vol. 73, pp. 416–417, Feb 1948.

[75] S. Laporta and E. Remiddi, "The Analytical value of the electron light-light graphs contribution to the muon (g-2) in QED," *Phys. Lett. B*, vol. 301, pp. 440–446, 1993.

[76] T. Aoyama, M. Hayakawa, T. Kinoshita, and M. Nio, "Tenth-Order QED Contribution to the Electron g-2 and an Improved Value of the Fine Structure Constant," *Phys. Rev. Lett.*, vol. 109, p. 111807, 2012.

[77] D. Hanneke, S. Fogwell, and G. Gabrielse, "New Measurement of the Electron Magnetic Moment and the Fine Structure Constant," *Phys. Rev. Lett.*, vol. 100, p. 120801, 2008.

[78] B. C. Odom, D. Hanneke, B. D'Urso, and G. Gabrielse, "New Measurement of the Electron Magnetic Moment Using a One-Electron Quantum Cyclotron," *Phys. Rev. Lett.*, vol. 97, p. 030801, 2006.

[79] D. Hanneke, S. Fogwell Hoogerheide, and G. Gabrielse, "Cavity control of a single-electron quantum cyclotron: Measuring the electron magnetic moment," *Physical Review A*, vol. 83, May 2011.

[80] P. Clade, E. de Mirandes, M. Cadoret, S. Guellati-Khelifa, C. Schwob, F. Nez, L. Julien, and F. Biraben, "Determination of the Fine Structure Constant Based on Bloch Oscillations of Ultracold Atoms in a Vertical Optical Lattice," *Phys. Rev. Lett.*, vol. 96, p. 033001, 2006.

[81] M. Cadoret, E. de Mirandes, P. Clade, S. Guellati-Khelifa, C. Schwob, F. Nez, L. Julien, and F. Biraben, "Combination of Bloch oscillations with a Ramsey-Borde interferometer: New determination of the fine structure constant," *Phys. Rev. Lett.*, vol. 101, p. 230801, 2008.

[82] R. Bouchendira, P. Clade, S. Guellati-Khelifa, F. Nez, and F. Biraben, "New determination of the fine structure constant and test of the quantum electrodynamics," *Phys. Rev. Lett.*, vol. 106, p. 080801, 2011.

[83] T. Aoyama *et al.*, "The anomalous magnetic moment of the muon in the Standard Model," *Phys. Rept.*, vol. 887, pp. 1–166, 2020.

[84] G. W. Bennett *et al.*, "Final report of the e821 muon anomalous magnetic moment measurement at bnl," *Phys. Rev. D*, vol. 73, p. 072003, Apr 2006.

[85] R. Aliberti *et al.*, "The anomalous magnetic moment of the muon in the standard model: an update," 2025.

[86] B. Abi *et al.*, "Measurement of the positive muon anomalous magnetic moment to 0.46 ppm," *Phys. Rev. Lett.*, vol. 126, p. 141801, Apr 2021.

[87] D. P. Aguillard *et al.*, "Measurement of the positive muon anomalous magnetic moment to 0.20 ppm," *Phys. Rev. Lett.*, vol. 131, p. 161802, Oct 2023.

[88] *The Muon $g-2$ Collaboration*: D. P. Aguillard *et al.*, "Measurement of the positive muon anomalous magnetic moment to 127 ppb," 2025.

[89] T. Albahri *et al.*, "Measurement of the anomalous precession frequency of the muon in the fermilab muon $g-2$ experiment," *Phys. Rev. D*, vol. 103, p. 072002, Apr 2021.

[90] T. Albahri *et al.*, "Beam dynamics corrections to the run-1 measurement of the muon anomalous magnetic moment at fermilab," Apr 2021.

[91] F. Bloch and A. Nordsieck, "Note on the Radiation Field of the electron," *Phys. Rev.*, vol. 52, pp. 54–59, 1937.

[92] D. Yennie, S. Frautschi, and H. Suura, "The infrared divergence phenomena and high-energy processes," *Annals of Physics*, vol. 13, no. 3, pp. 379–452, 1961.

[93] D. DeLaney, S. Jadach, C. Shio, G. Siopsis, and B. Ward, "Renormalization group improved exponentiation of soft gluons in qcd," *Physics Letters B*, vol. 342, no. 1, pp. 239–244, 1995.

[94] T. Kinoshita, "Mass singularities of feynman amplitudes," *Journal of Mathematical Physics*, vol. 3, pp. 650–677, 07 1962.

[95] T. D. Lee and M. Nauenberg, "Degenerate systems and mass singularities," *Phys. Rev.*, vol. 133, pp. B1549–B1562, Mar 1964.

[96] G. Sterman and S. Weinberg, "Jets from quantum chromodynamics," *Phys. Rev. Lett.*, vol. 39, pp. 1436–1439, Dec 1977.

[97] Y. L. Dokshitzer, "Calculation of the Structure Functions for Deep Inelastic Scattering and e^+e^- Annihilation by Perturbation Theory in Quantum Chromodynamics (in Russian)," *Sov. Phys. JETP*, vol. 46, pp. 641–653, 1977.

[98] V. N. Gribov and L. N. Lipatov, "Deep inelastic *ep* scattering in perturbation theory," *Sov. J. Nucl. Phys.*, vol. 15, pp. 438–450, 1972.

[99] G. Altarelli and G. Parisi, "Asymptotic freedom in parton language," *Nucl. Phys.*, vol. B126, p. 298, 1977.

[100] P. Mulders, "Transverse momentum dependence in structure functions in hard scattering processes," 2001.

[101] K. Kanazawa, Y. Koike, A. Metz, D. Pitonyak, and M. Schlegel, "Operator Constraints for Twist-3 Functions and Lorentz Invariance Properties of Twist-3 Observables," *Phys. Rev.*, vol. D93, no. 5, p. 054024, 2016.

[102] S. Meissner, "Eigenschaften von Zwei- und Drei-Parton-Korrelatoren des Nukleons," *PhD-thesis, Ruhr-University of Bochum, Germany*, 2009.

[103] J.-w. Qiu and G. Sterman, "Single transverse spin asymmetries in direct photon production," *Nucl. Phys.*, vol. B378, pp. 52–78, 1992.

[104] J.-w. Qiu and G. Sterman, "Single transverse-spin asymmetries in hadronic pion production," *Phys. Rev.*, vol. D59, p. 014004, 1999.

[105] A. Metz, M. Schlegel, and K. Goeke, "Transverse single spin asymmetries in inclusive deep-inelastic scattering," *Phys. Lett.*, vol. B643, pp. 319–324, 2006.

[106] Z.-B. Kang, A. Metz, J.-W. Qiu, and J. Zhou, "Exploring the structure of the proton through polarization observables in $lp \to \mathrm{jet}X$," *Phys. Rev. D*, vol. 84, p. 034046, 2011.

[107] K. Kanazawa, A. Metz, D. Pitonyak, and M. Schlegel, "Longitudinal-transverse double-spin asymmetries in single-inclusive leptoproduction of hadrons," *Phys.Lett.*, vol. B742, pp. 340–346, 2015.

[108] K. Kanazawa, A. Metz, D. Pitonyak, and M. Schlegel, "Single-spin asymmetries in the lepto-production of transversely polarized Lambda hyperons," *Phys.Lett.*, vol. B744, pp. 385–390, 2015.

[109] W. S. Albaltan, A. Prokudin, and M. Schlegel, "The transverse nucleon single-spin asymmetry for the semi-inclusive production of photons in lepton-nucleon scattering," *Phys. Lett. B*, vol. 804, p. 135367, 2020.

[110] Y. Koike, K. Yabe, and S. Yoshida, "Exact Relations for Twist-3 Gluon Distribution and Fragmentation Functions from Operator Identities," *Phys. Rev. D*, vol. 101, no. 5, p. 054017, 2020.

[111] Y. Koike and S. Yoshida, "Three-gluon contribution to the single spin asymmetry in Drell-Yan and direct-photon processes," *Phys. Rev.*, vol. D85, p. 034030, 2012.

[112] A. V. Efremov and O. V. Teryaev, "The transversal polarization in Quantum Chromodynamics," *Sov. J. Nucl. Phys.*, vol. 39, p. 962, 1984.

[113] A. V. Efremov and O. V. Teryaev, "Qcd asymmetry and polarized hadron structure functions," *Phys. Lett.*, vol. B150, p. 383, 1985.

[114] D. Boer, P. J. Mulders, and F. Pijlman, "Universality of T-odd effects in single spin and azimuthal asymmetries," *Nucl. Phys.*, vol. B667, pp. 201–241, 2003.

[115] T. Rogers, "Transverse moments of TMD parton densities and ultraviolet divergences," *Mod. Phys. Lett. A*, vol. 35, no. 37, p. 2030021, 2020.

[116] H. Xing and S. Yoshida, "New approach to the Sivers effect in the collinear twist-3 formalism," *Phys. Rev. D*, vol. 100, no. 5, p. 054024, 2019.

[117] V. E. Lyubovitskij, F. Wunder, and A. S. Zhevlakov, "New ideas for handling of loop and angular integrals in D-dimensions in QCD," *JHEP*, vol. 06, p. 066, 2021.

[118] W. van Neerven, "Dimensional Regularization of Mass and Infrared Singularities in Two Loop On-Shell Vertex Functions," *Nucl.Phys.*, vol. B268, p. 453, 1986.

[119] W. Beenakker, H. Kuijf, W. van Neerven, and J. Smith, "QCD Corrections to Heavy Quark Production in p anti-p Collisions," *Phys.Rev.*, vol. D40, pp. 54–82, 1989.

[120] P. Hinderer, M. Schlegel, and W. Vogelsang, "Single-Inclusive Production of Hadrons and Jets in Lepton-Nucleon Scattering at NLO," *Phys. Rev.*, vol. D92, no. 1, p. 014001, 2015. [Erratum: Phys. Rev.D93,no.11,119903(2016)].

[121] V. M. Braun, A. N. Manashov, and B. Pirnay, "Scale dependence of twist-three contributions to single spin asymmetries," *Phys. Rev. D*, vol. 80, p. 114002, 2009. [Erratum: Phys.Rev.D 86, 119902 (2012)].

[122] Z.-B. Kang and J.-W. Qiu, "Evolution of twist-3 multi-parton correlation functions relevant to single transverse-spin asymmetry," *Phys. Rev. D*, vol. 79, p. 016003, 2009.

[123] J. C. Collins and J.-w. Qiu, "A New Derivation of the Altarelli-parisi Equations," *Phys. Rev.*, vol. D39, p. 1398, 1989.

[124] A. Afanasev, M. Strikman, and C. Weiss, "Transverse target spin asymmetry in inclusive DIS with two-photon exchange," *Phys. Rev.*, vol. D77, p. 014028, 2008.

[125] Z.-B. Kang, I. Vitev, and H. Xing, "Transverse momentum-weighted Sivers asymmetry in semi-inclusive deep inelastic scattering at next-to-leading order," *Phys. Rev.*, vol. D87, no. 3, p. 034024, 2013.

[126] Y. Koike, W. Vogelsang, and F. Yuan, "On the Relation Between Mechanisms for Single-Transverse-Spin Asymmetries," *Phys. Lett. B*, vol. 659, pp. 878–884, 2008.

[127] B. Jager, M. Stratmann, and W. Vogelsang, "Single inclusive jet production in polarized pp collisions at $O(\alpha_s^3)$," *Phys. Rev. D*, vol. 70, p. 034010, 2004.

[128] B. Jager, "Photoproduction of single inclusive jets at future ep colliders in next-to-leading order QCD," *Phys. Rev. D*, vol. 78, p. 034017, 2008.

[129] A. Mukherjee and W. Vogelsang, "Jet production in (un)polarized pp collisions: dependence on jet algorithm," *Phys. Rev. D*, vol. 86, p. 094009, 2012.

[130] G. C. Blazey *et al.*, "Run II Jet Physics: Proceedings of the Run II QCD and Weak Boson Physics Workshop," 2000.

[131] S. G. Salesch, "Photoproduction of jets at HERA with open order photons up to order $\mathcal{O}(\alpha_s^2)$," master thesis, Universität Hamburg, 12 1993.

[132] M. Cacciari, G. P. Salam, and G. Soyez, "The anti-k_t jet clustering algorithm," *JHEP*, vol. 04, p. 063, 2008.

[133] P. Hinderer, M. Schlegel, and W. Vogelsang, "Double-Longitudinal Spin Asymmetry in Single-Inclusive Lepton Scattering at NLO," *Phys. Rev.*, vol. D96, no. 1, p. 014002, 2017.

[134] N. Christ and T. D. Lee, "Possible Tests of C_{st} and T_{st} Invariances in $l^{\pm} + N \to l^{\pm} + \Gamma$ and $A \to B + e^{+} + e^{-}$," *Phys. Rev.*, vol. 143, pp. 1310–1321, 1966.

[135] A. Manohar, P. Nason, G. P. Salam, and G. Zanderighi, "How bright is the proton? A precise determination of the photon parton distribution function," *Phys. Rev. Lett.*, vol. 117, no. 24, p. 242002, 2016.

[136] J. Haug and F. Wunder, "The massless non-adjacent double off-shell scalar box integral — branch cut structure and all-order epsilon expansion," *JHEP*, vol. 05, p. 059, 2023.

[137] S. J. Brodsky, J. F. Gunion, and R. L. Jaffe, "A Test for Fractionally Charged Partons from Deep Inelastic Bremsstrahlung in the Scaling Region," *Phys. Rev.*, vol. D6, p. 2487, 1972.

[138] S. Rodini, L. Rossi, and A. Vladimirov, "Numerical implementation of evolution equations for twist-3 collinear PDFs," *Eur. Phys. J. C*, vol. 84, no. 7, p. 732, 2024.

[139] D. de Florian, R. Sassot, M. Epele, R. J. Hernández-Pinto, and M. Stratmann, "Parton-to-Pion Fragmentation Reloaded," *Phys. Rev. D*, vol. 91, no. 1, p. 014035, 2015.

[140] M. Schlegel, P. Hinderer, and W. Vogelsang, "NLO K-factors for Single-Inclusive Leptoproduction of Hadrons," *PoS, QCDEV2015*, vol. 249, 2015.

[141] V. M. Braun, T. Lautenschlager, A. N. Manashov, and B. Pirnay, "Higher twist parton distributions from light-cone wave functions," *Phys. Rev. D*, vol. 83, p. 094023, 2011.

[142] M. Gluck, E. Reya, and A. Vogt, "Parton fragmentation into photons beyond the leading order," *Phys. Rev. D*, vol. 48, p. 116, 1993. [Erratum: Phys.Rev.D 51, 1427 (1995)].

[143] T.-J. Hou *et al.*, "Progress in the CTEQ-TEA NNLO global QCD analysis," 8 2019.

[144] L. Gamberg, M. Malda, J. A. Miller, D. Pitonyak, A. Prokudin, and N. Sato, "Updated QCD global analysis of single transverse-spin asymmetries: Extracting $\tilde{H}$, and the role of the Soffer bound and lattice QCD," *Phys. Rev. D*, vol. 106, no. 3, p. 034014, 2022.

[145] D. W. Duke and J. F. Owens, "Q^2 Dependent Parametrizations of Parton Distribution Functions," *Phys. Rev.*, vol. D30, pp. 49–54, 1984.

[146] M. Harris, J. Marsh, D. Pitonyak, A. Prokudin, J. Putnam, D. Rein, and M. Schlegel, "Public Google Colab Notebook for γSIDIS." `https://colab.research.google.com/github/pitonyak25/AUT_gamSIDIS_lib/blob/main/AUT_gamSIDIS_public.ipynb`.

[147] J. M. Bickerton, *Transverse Properties of Baryons using Lattice Quantum Chromodynamics*. PhD thesis, Adelaide U., 2020.

[148] M. Anselmino *et al.*, "Sivers Effect for Pion and Kaon Production in Semi- Inclusive Deep Inelastic Scattering," *Eur. Phys. J.*, vol. A39, pp. 89–100, 2009.

[149] A. Afanasev *et al.*, "Physics with Positron Beams at Jefferson Lab 12 GeV," 6 2019.

[150] J. Arrington *et al.*, "Physics with CEBAF at 12 GeV and future opportunities," *Prog. Part. Nucl. Phys.*, vol. 127, p. 103985, 2022.

[151] R. Abdul Khalek *et al.*, "Science Requirements and Detector Concepts for the Electron-Ion Collider: EIC Yellow Report," *Nucl. Phys. A*, vol. 1026, p. 122447, 2022.

[152] D. W. Sivers, "Single spin production asymmetries from the hard scattering of point - like constituents," *Phys. Rev.*, vol. D41, p. 83, 1990.

[153] D. W. Sivers, "Hard scattering scaling laws for single spin production asymmetries," *Phys. Rev.*, vol. D43, pp. 261–263, 1991.

[154] A. Metz and A. Vossen, "Parton Fragmentation Functions," *Prog. Part. Nucl. Phys.*, vol. 91, pp. 136–202, 2016.

[155] A. V. Belitsky, X. Ji, and F. Yuan, "Final state interactions and gauge invariant parton distributions," *Nucl. Phys.*, vol. B656, pp. 165–198, 2003.

[156] J. C. Collins, "Leading-twist single-transverse-spin asymmetries: Drell-yan and deep-inelastic scattering," *Phys. Lett.*, vol. B536, pp. 43–48, 2002.

[157] R. Boussarie *et al.*, "TMD Handbook," 4 2023.

[158] E. V. Shuryak and A. I. Vainshtein, "Theory of Power Corrections to Deep Inelastic Scattering in Quantum Chromodynamics. (II). Q^{-4} Effects; Polarized Target," *Nucl. Phys. B*, vol. 201, p. 141, 1982.

[159] R. L. Jaffe, "g_2-The Nucleon's Other Spin-Dependent Structure Function," *Comments Nucl. Part. Phys.*, vol. 19, no. 5, pp. 239–257, 1990.

[160] M. Burkardt, "Transverse force on quarks in deep-inelastic scattering," *Phys. Rev. D*, vol. 88, p. 114502, 2013.

[161] F. P. Aslan, M. Burkardt, and M. Schlegel, "Transverse Force Tomography," *Phys. Rev. D*, vol. 100, no. 9, p. 096021, 2019.

[162] M. Gockeler, R. Horsley, D. Pleiter, P. E. L. Rakow, A. Schafer, G. Schierholz, H. Stuben, and J. M. Zanotti, "Investigation of the second moment of the nucleon's g_1 and g_2 structure functions in two-flavor lattice QCD," *Phys. Rev. D*, vol. 72, p. 054507, 2005.

[163] S. Bürger, T. Wurm, M. Löffler, M. Göckeler, G. Bali, S. Collins, A. Schäfer, and A. Sternbeck, "Lattice results for the longitudinal spin structure and color forces on quarks in a nucleon," *Phys. Rev. D*, vol. 105, no. 5, p. 054504, 2022.

[164] J. A. Crawford, K. U. Can, R. Horsley, P. E. L. Rakow, G. Schierholz, H. Stüben, R. D. Young, and J. M. Zanotti, "Transverse Force Distributions in the Proton from Lattice QCD," *Phys. Rev. Lett.*, vol. 134, no. 7, p. 071901, 2025.

Danksagung

Ich möchte meine tief empfundene Dankbarkeit ausdrücken für alle, die mich während meiner Promotion, aber auch schon davor, unterstützt haben. Angefangen bei meinen Betreuern, die stets hilfsbereit und offen für Fragen aller Art waren. Jedes noch so kleine Detail konnte ich jeder Zeit in einer sehr konstruktiven und gewinnbringenden Weise mit ihnen diskutieren. Ich möchte mich auch bei der Arbeitsgruppe insgesamt und meinen Kollegen bedanken. Der "D7" war für mich immer ein angenehmer Arbeitsplatz und geprägt von einer positiven Atmosphäre. Besonders die gemeinsamen Reisen zu Konferenzen etc. waren nicht zuletzt wegen der guten Chemie untereinander ein absolutes Highlight meiner akademischen Laufbahn. Schließlich möchte ich mich bei Freunden und Familie bedanken, die mich immer motiviert und an mich geglaubt haben.

Selbstständigkeitserklärung

Ich erkläre hiermit, dass ich die zur Promotion eingereichte Arbeit selbständig verfasst, nur die angegebenen Quellen und Hilfsmittel benutzt und wörtlich oder inhaltlich übernommene Stellen als solche gekennzeichnet habe. Ich erkläre, dass die Leitlinien zur Sicherung guter wissenschaftlicher Praxis der Universität Tübingen (Beschluss des Senats vom 11.2.2021) beachtet wurden. Ich versichere an Eides statt, dass diese Angaben wahr sind und dass ich nichts verschwiegen habe. Mir ist bekannt, dass die falsche Abgabe einer Versicherung an Eides statt mit Freiheitsstrafe bis zu drei Jahren oder mit Geldstrafe bestraft wird.

Ort, Datum **Unterschrift**